Operation

JANGLE

NEVADA PROVING GROUNDS
OCTOBER-NOVEMBER 1952

BIOLOGICAL HAZARDS

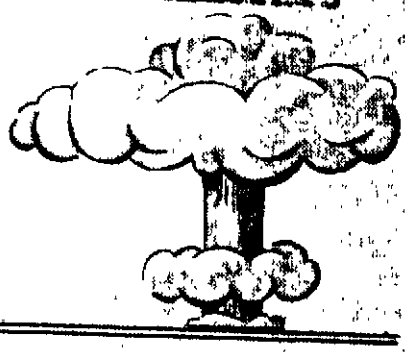

ARMED FORCES SPECIAL WEAPONS PROJECT
WASHINGTON, D.C.

CONFIDENTIAL

WT-372

This document consists of 237 plus 4 pages (counting all preliminary pages in all reports and all unnumbered blanks)

Copy 201 of 243 copies, Series B

OPERATION JANGLE

BIOLOGICAL HAZARDS

Project 2.4a Beta-Ray and Gamma-Ray Energy of Residual Contamination (WT-345)

Project 2.4b Gamma Depth Dose Measurements in Unit Density Material (WT-332)

Project 2.4c Gamma-Ray Spectrum of Residual Contamination (WT-348) Uncl.

Project 2.7 Biological Injury from Particle Inhalation (WT-396)

CONFIDENTIAL

OPERATION JANGLE

PROJECT 2.4a

BETA-RAY AND GAMMA-RAY ENERGY OF RESIDUAL CONTAMINATION

by

E. Tochilin
P. R. Howland
S. H. Fitch
R. Golden
and
J. T. Barrett

April 1952

U. S. NAVAL RADIOLOGICAL DEFENSE LABORATORY

SAN FRANCISCO 24, CALIFORNIA

PROJECT 2.4a

CONTENTS

CONTENTS (Continued)

PROJECT 2.4a

ILLUSTRATIONS

ILLUSTRATIONS (Continued)

PROJECT 2.4a

TABLES

PROJECT 2.4a

TABLES (Continued)

PROJECT 2.4a

ABSTRACT

By means of depth-dose measurements, obtained using photographic film packets, a study was made of the beta-ray energy and the ratio of beta- to gamma-ray ionization resulting from residual contamination following the surface and underground shots of Operation JANGLE. Measurements were also made of the residual gamma-ray energy.

Readings of gamma-ray energy were made with a group of modified ionization chambers and survey instruments calibrated to effective X-ray energies over a range from 65 to 1,200 kev. Field determination of effective gamma-ray energies with the modified chambers was made over a period of time from 5 to 340 hr following the surface shot, and from 5 to 97 hr following the underground shot. Readings obtained indicated the energies to vary between 84 and 140 kev for the surface shot and between 113 and 144 kev for the underground shot. Effective gamma-ray energies from the residual radiation following the surface shot were in good agreement with the energies measured following two tower shots at Operation GREENHOUSE.

To determine the effective energy of prompt gamma radiation plus base surge radiation, chambers were placed in the field prior to each shot and exposed to all radiations from time zero to approximately H + 3 hr. These measurements showed the energy to range between 430 and 565 kev for the surface shot and between 376 and 430 kev for the underground shot.

Using photographic film packets the equivalent maximum beta energy measured in close proximity to the early-time fall-out contamination for the surface shot was no greater than 1.7 Mev. This energy was an average over a period of 24 hr following the surface shot. Additional measurements of this energy at 18 in. above the contaminated ground surface gave a value of 2.0 Mev.

Equivalent maximum beta-energy measurements in close proximity to the early-time fall-out contamination for the underground shot gave a value no greater than 2.0 Mev when averaged over a period of 70 hr following the shot. Measurements at 18 in. above the contamination gave a value of 1.7 Mev.

The maximum ratio of beta-to-gamma ionization measured with film packets located in highly contaminated areas was 14 for the surface shot and 24 for the underground shot. Post-shot film packets were taken into the area following both shots and exposed to the radiation field at a distance of 18 in. above the ground. Exposures made in the highly contaminated area of the underground shot gave beta-to-gamma ratios averaging 19 to 1.

CHAPTER 1

INTRODUCTION

1.1 GENERAL

The beta and gamma radiation associated with fission-product activity are both potentially dangerous to personnel. Although the hazard from significant doses of gamma radiation has been well established, the information concerning the biological hazard resulting from beta radiation is less complete. The purpose of this study was to conduct field measurements of beta-ray energy and ionization, two factors which are directly related to the hazard to be expected from beta radiation.

Casualties from beta radiation can result from both external and internal radiation. In this report only the effects of external beta radiation are considered.

The biological effects produced by external beta radiation are superficial. In contrast to gamma radiation, beta-ray exposures are not associated with acute lethal injury. An extensive research project conducted at Oak Ridge during the war years investigated the biological effects of external beta radiation on animals. A recently published compilation of this work contains essentially all the significant data relating to the subject.[1]

1.2 OBJECTIVES

The objectives of this investigation were:

1. To determine the energy of the beta radiation at early times after the burst when personnel hazards will be greatest.

2. To determine the ratio of beta-ray to gamma-ray ionization in contaminated regions.

3. To determine the effective gamma-ray energy of the residual fission-product activity resulting from a contaminating atom bomb explosion, and to study the change in energy as a function of time.

---

[1] R. E. Zirkle, Biological Effects of External Beta Radiation, (New York: McGraw-Hill Book Co., Inc.) 1951.

4. On the basis of the above findings, to establish if regions exist where beta-ray hazard is present independent of gamma-ray hazard.

1.3 SUMMARY OF PREVIOUS EXPERIENCE

1.3.1 Beta-ray Energy of Fission-product Activity

The energy of beta radiation from fission-product activity is a factor of great importance in assessing beta-ray hazard. Since the range of beta radiation is limited, clothing will afford a certain amount of protection. The amount of protection is, however, in proportion to the energy of the incident beta rays. Normal work clothing is approximately 30 mg/sq cm thick. For a beta-ray isotope of 1 Mev maximum this thickness is sufficient to attenuate the incident ionization to one-half its initial value. In contrast, for a beta-ray isotope of 3.5 Mev maximum eight times this thickness is required to produce the same shielding effect. The higher the beta-ray energy, the greater will be the potential hazard to personnel exposed to this radiation field.

A portion of Operation GREENHOUSE Project 6.5 involved an experimental determination of the mean maximum energy of the beta particles emitted by samples of fission-product aggregate.[2] The variation of this energy with time was followed from 2 to 12 days post shot. For the period of time over which measurements were made, the beta-ray component of fission-product activity acts much like a mixture of two beta-ray isotopes having maximum energies of 0.5 and 1.5 Mev combined in such a way that each contributes equal beta-ray ionization. Such a representation is a convenient way to visualize the beta-ray characteristics of fission-product activity for the period stated.

It should be emphasized that measurements of beta-ray energy made under laboratory conditions do not necessarily represent the conditions that existed in the field. Scatter of the beta particles may considerably reduce their energy under field conditions.

1.3.2 Ratio Beta-ray to Gamma-ray Ionization

The ionization near the surface of fission-product activity is considerably higher due to beta radiation than due to gamma radiation. Measurements following the Operation GREENHOUSE test of beta- and gamma-ray ionization at the surface of plaques contaminated with fall-out

---

[2] E. Tochilin and P. R. Howland, "Interpretation of Survey-Meter Data", Operation GREENHOUSE Project 6.5, Final Report, August, 1951.

activity indicated the ratio of beta equivalent roentgen to gamma roentgen dose rate to be approximately 160.[2] Due to the limited range of the beta particles this ratio decreases markedly with increasing distance. From the data of Condit, et al., a person standing over an infinite plane of fission-product activity where beta-ray self-absorption is negligible would receive a beta-ray dose approximately twenty times the gamma-ray dose to his calves.[3] At hip height the ratio would decrease to approximately ten.

The amount of beta radiation that could be tolerated without injury to the skin is difficult to assess, since the damage is dependent upon many factors. Some of these have yet to be properly evaluated. Existing information on beta-ray casualties indicates that 1,000 rep of beta radiation could produce significant skin damage.

Reference to Knowlton's report of beta-ray casualties at Eniwetok cites one beta-ray exposure between 5,000 and 10,000 rep to the hands.[4] The exposures occurred because high-activity fission-product materials were handled directly with rubber gloves or with bare hands rather than by means of prescribed remote-handling methods. In contrast to the high localized exposure, a film badge and ionization chamber worn by the same individual indicated a total body dose of 10 roentgens.

1.3.3 Gamma-ray Energy of Fission-product Activity

Measurements of effective gamma-ray energies were made at Operation GREENHOUSE in areas contaminated with fission-product activity. The effective energy measured over a level area of barren land at distances varying from 600 to 100 yd from ground zero, ranged between 100 and 127 kev and between 83 and 120 kev following two different shots. The energy showed no significant change with time over a period of ten days. Measurements of effective gamma-ray energy were also made under laboratory conditions. The combined data indicate that for the conditions investigated the primary gamma radiation possessing an initial energy of approximately 550 kev is degraded through a process of multiple scattering to energies between 83 and 127 kev.

Other conditions are envisioned where the terrain would be considerably different. For example, contamination within a city would find activity accumulating on rooftops and other areas above the ground.

---

[3] R. I. Condit, et al., "An Estimate of the Relative Hazard of Beta and Gamma Radiation from Fission Products", USNRDL Report AD-95(H), April, 1949.

[4] N. P. Knowlton, et al., "Beta-ray Burns of Human Skin", J. Am. Med. Assn., 141 (1949), 239.

In this more complicated geometry it is conceivable that the gamma-ray energies would be different and much more dependent upon the location of measurement. The measurements made at Operation JANGLE were intended to compare the effective gamma-ray energies for a surface and an underground burst over a large area of contamination.

PROJECT 2.4a

CHAPTER 2

BETA-RAY DOSIMETRY WITH PHOTOGRAPHIC FILM

2.1 INTRODUCTION

Depth-dose curves measured through successive layers of photographic emulsion were obtained for five beta-emitting isotopes of different energies ranging from 0.50 to 3.55 Mev. Depth-dose curves obtained from film packets exposed in the field, under the conditions described in Chap. 3, were compared to the laboratory measurements. This comparison served to provide information regarding beta-ray energies encountered under field conditions.

Measurements of beta-ray ionization using photographic film were compared with similar measurements using standard ionization chamber techniques.

2.2 EXPERIMENTAL APPARATUS

All film measurements were made using dental-size film packaged in a molded rubber film holder 3/4 in. deep. The holder was filled with alternate layers of film and black paper spacers. The loaded holder, containing some sixty dental films, was covered with black paper 13.4 mg/sq cm thick. Figure 2.1 illustrates the rubber film holder, a stack of dental films, and the packaged unit.

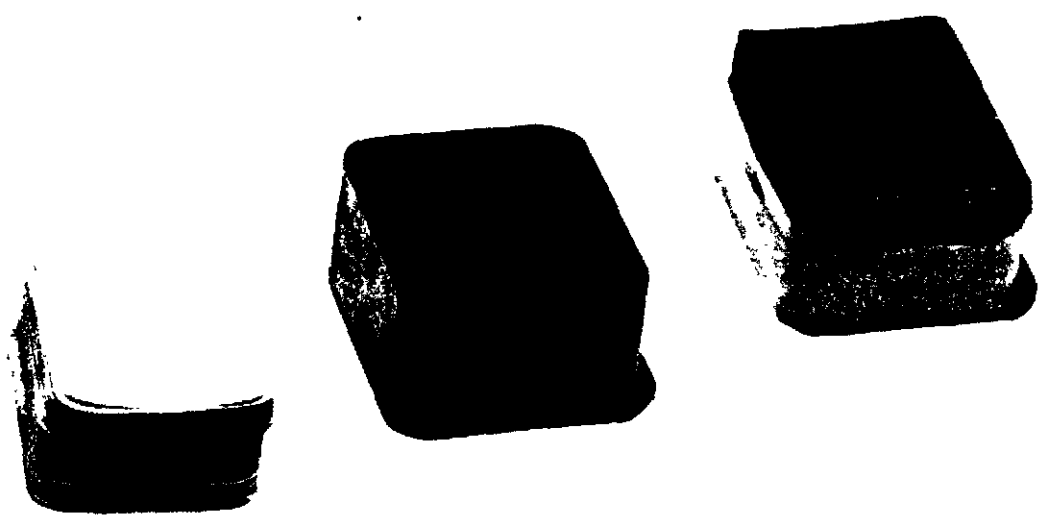

Fig. 2.1 Packaged Film Holder for Depth-dose Measurements.

Table 2.1 lists the isotopes used for the beta-ray film measurements together with the maximum energies of their beta spectra.[1] The

TABLE 2.1

Standard Beta Sources

Source	Half-life	Maximum Energy (Mev)	Filters(a) (mg/sq cm)
Ta^{182}	117 days	0.50	none
RaD plus RaE	22 yr 5 days	0.026 1.17	25
P^{32}	14 days	1.71	none
Sr^{90} plus Y^{90}	20 yr 62 hr	0.53 2.18	100
Ru^{106} plus Rh^{106}	1 yr 30 sec	0.041 2.30 (18%) and 3.55 (82%)	Flash plating of silver

(a) Used to eliminate low-energy beta components.

various films used together with their beta-ray sensitivities are shown in Table 2.2. The films were chosen to allow depth-dose measurements over a range of beta-ray intensities extending to about 20,000 rep.

TABLE 2.2

Beta-ray Sensitivity of Films Used for Depth-dose Measurements

Photographic Film	Developing Time (min)	Maximum Usable Density	Approximate Rep Dose at Maximum Density
Eastman Type K	5	6.0	6
DuPont 552 Sens.	5	3.0	10
DuPont 552 Ins.	3	6.0	70
Eastman DF-7	8	6.0	80
Eastman 5302	10	4.0	400
Eastman Translite	5	5.0	2,000
Eastman 548-O	10	4.5	20,000

1 "Nuclear Data", National Bureau of Standards Circular 499, (U.S. Government Printing Office, Washington) September 1, 1950.

Film development was carried out in Kodak Liquid X-ray Developer. The developing times used for the various emulsions at a temperature of 68°F are given in Table 2.2. No agitation was used during development. The films were fixed for 10 min in Kodak X-ray Fixer, washed for about 20 min in running water, rinsed in a water solution containing a wetting agent, and then dried. An Ansco-Sweet color densitometer, Model 11, was used to measure the density of the processed film. With this instrument it was possible to read film densities to a value of 6.0.

2.3 EXPERIMENTAL RESULTS

Characteristic curves for the various photographic emulsions exposed to radium are plotted in Figs. 2.2 and 2.3. The curves afford a comparison of the relative gamma-ray sensitivity of the different emulsions over their entire range of readable densities. The films employed to obtain the characteristic curves were developed at 68°F using the developing times listed in Table 2.2 and standard developer. Some of the Translite film was developed for 10 min in Kodak D-76 developer in order to increase its range.

The process involved in converting film exposures to depth-dose readings will be demonstrated for a film pack of DuPont 552 insensitive film exposed to a strontium 90 source at a source-to-top-film distance of 1.5 in. An exposure time was chosen so that the density of the top film would approach the maximum usable density of the film which, in this case, was 6.0. The films were developed for 3 min at a temperature of 68°F. Developed together with the depth-dose films were 5 calibration standards which were films exposed to a predetermined series of X-ray doses. When processed and read, the data from the calibration standards were plotted to obtain the characteristic curve shown in Fig. 2.4. The use of X-ray exposures as calibration standards for films exposed to beta rays will be justified later. The data from which the final depth-dose curve was obtained are given in Table 2.3. The density and net density of the processed films are given in columns 3 and 4 of the table. Net

TABLE 2.3

Depth-dose Data for DuPont 552 Insensitive Film Exposed to Sr^{90} Source

Film No.	Depth (mg/sq cm)	Density	Net Density	Relative Dose (rep)	Per Cent of Depth Dose
1	35.6	5.30	5.13	2.10	97
2	72.1	5.10	4.93	2.00	92
3	108.6	4.50	4.33	1.75	81
4	145.1	3.84	3.67	1.50	70

PROJECT 2.4a

TABLE 2.3 (Continued)

Depth-dose Data for DuPont 552 Insensitive Film Exposed to Sr^{90} Source

Film No.	Depth (mg/sq cm)	Density	Net Density	Relative Dose (rep)	Per Cent of Depth Dose
5	181.6	3.24	3.07	1.25	58
6	218.1	2.72	2.55	1.05	49
7	254.6	2.20	2.03	0.80	37
8	291.1	1.84	1.67	0.66	31
9	327.6	1.48	1.31	0.52	24
10	364.1	1.16	0.99	0.40	19
11	400.6	0.91	0.74	0.30	14
12	437.1	0.74	0.57	0.23	11
13	473.6	0.61	0.44	0.18	8.3
14	510.1	0.49	0.32	0.13	6.0
15	546.6	0.42	0.25	0.10	4.6
16	583.1	0.35	0.18	0.07	3.3
17	619.6	0.30	0.13	0.05	2.3
18	656.1	0.26	0.09	0.04	1.9
19	692.6	0.23	0.06	0.03	1.4
20	729.1	0.21	0.04	0.02	1.0
Control	-	0.17	-	-	-

density is defined as the total density minus the fog background of the control film. The characteristic curve (Fig. 2.4) allows the net density to be converted into relative ionization units. The results of this conversion are given as relative rep dose in column 5 of Table 2.3. The use of arbitrary ionization units is permissible because depth dose is calculated in terms of per cent surface dose. The relative rep dose was plotted against film depth (column 2, Table 2.3), and the curve obtained extrapolated to a surface reading. The resulting depth-dose curve, normalized to 100 per cent at the surface, is shown in Fig. 2.5. The per cent depth dose at the various film depths is tabulated in column 6 of Table 2.3.

Information required to determine how deep in a film pack any particular film is located is given in Table 2.4. The depth to the top surface of any film includes the combined thickness of the black paper cover and one black paper spacer. Only two of the films used were single-coated emulsions, namely Eastman 5302 and Eastman 548-O. In this instance the top surface of the film was the sensitive area. With the double-coated emulsions both sides of the film were blackened by radiation. The difference in the blackening on both sides is due to the amount of ionization absorbed in the cellulose acetate film base. It has been assumed that

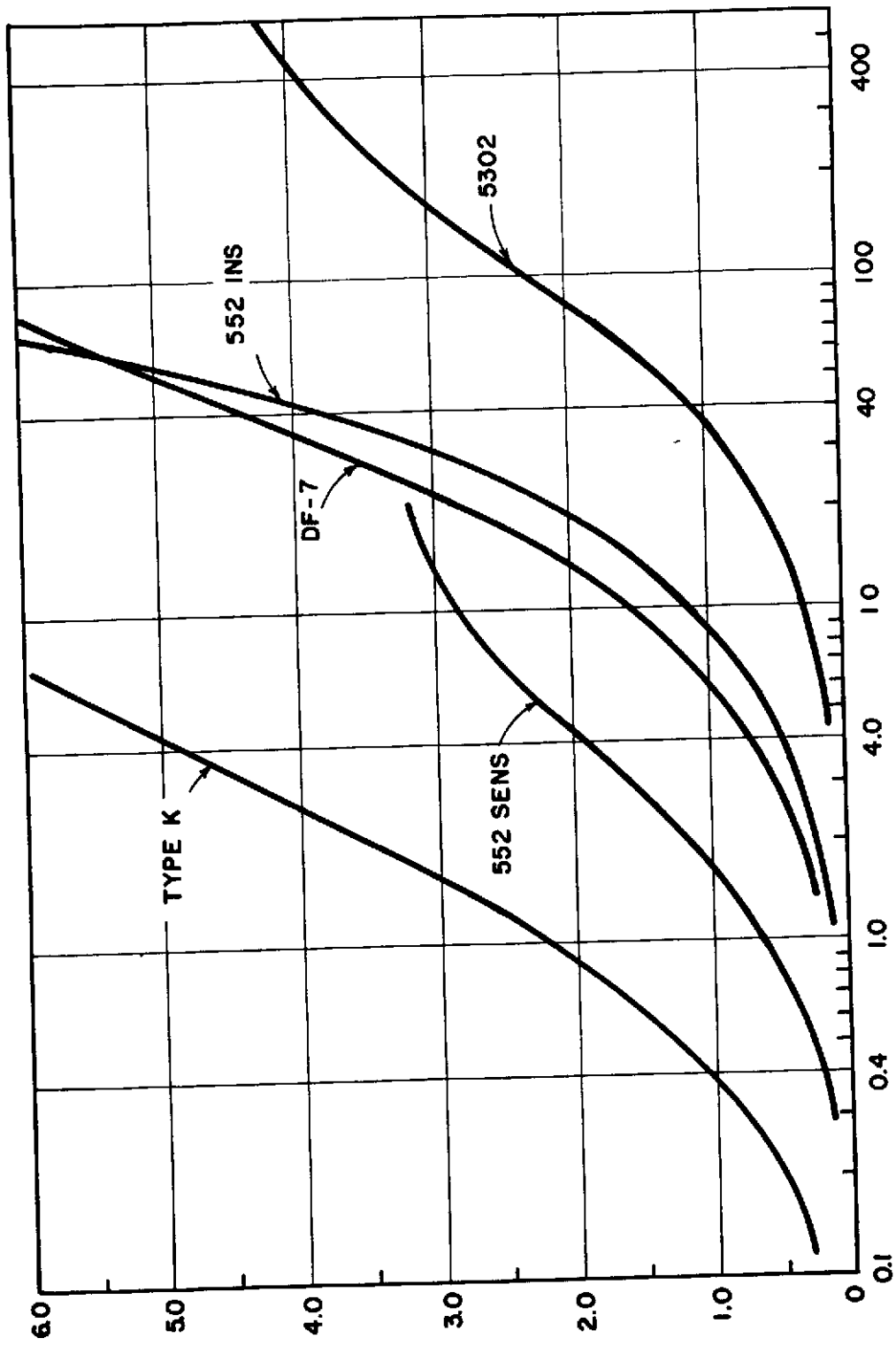

Fig. 2.2 Characteristic Curves for Du Pont 552 Films and Eastman Type K, DF-7, and 5302 Films.

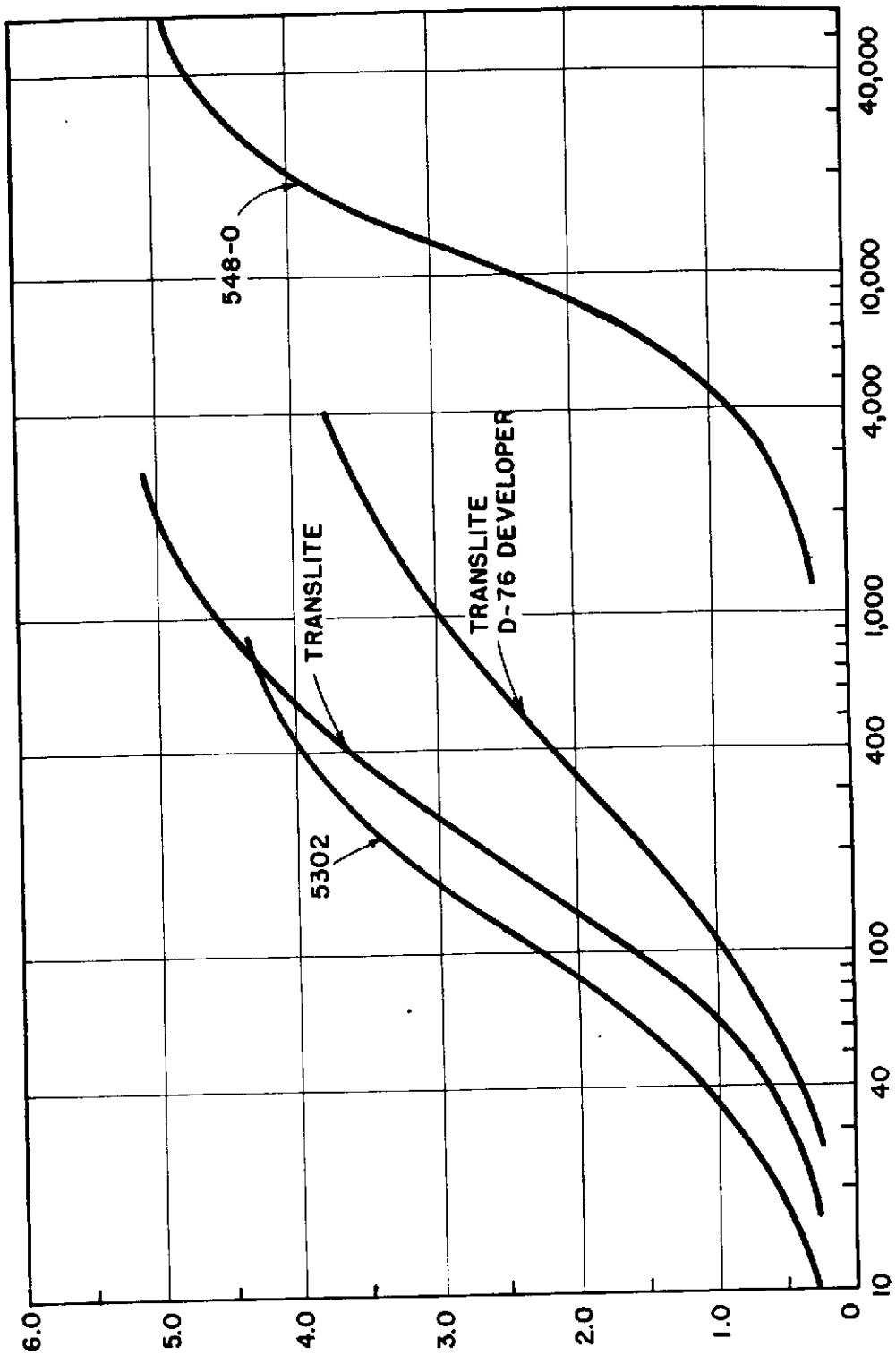

Fig. 2.3 Characteristic Curves for Eastman 5302, Translite, and 548-0 Films.

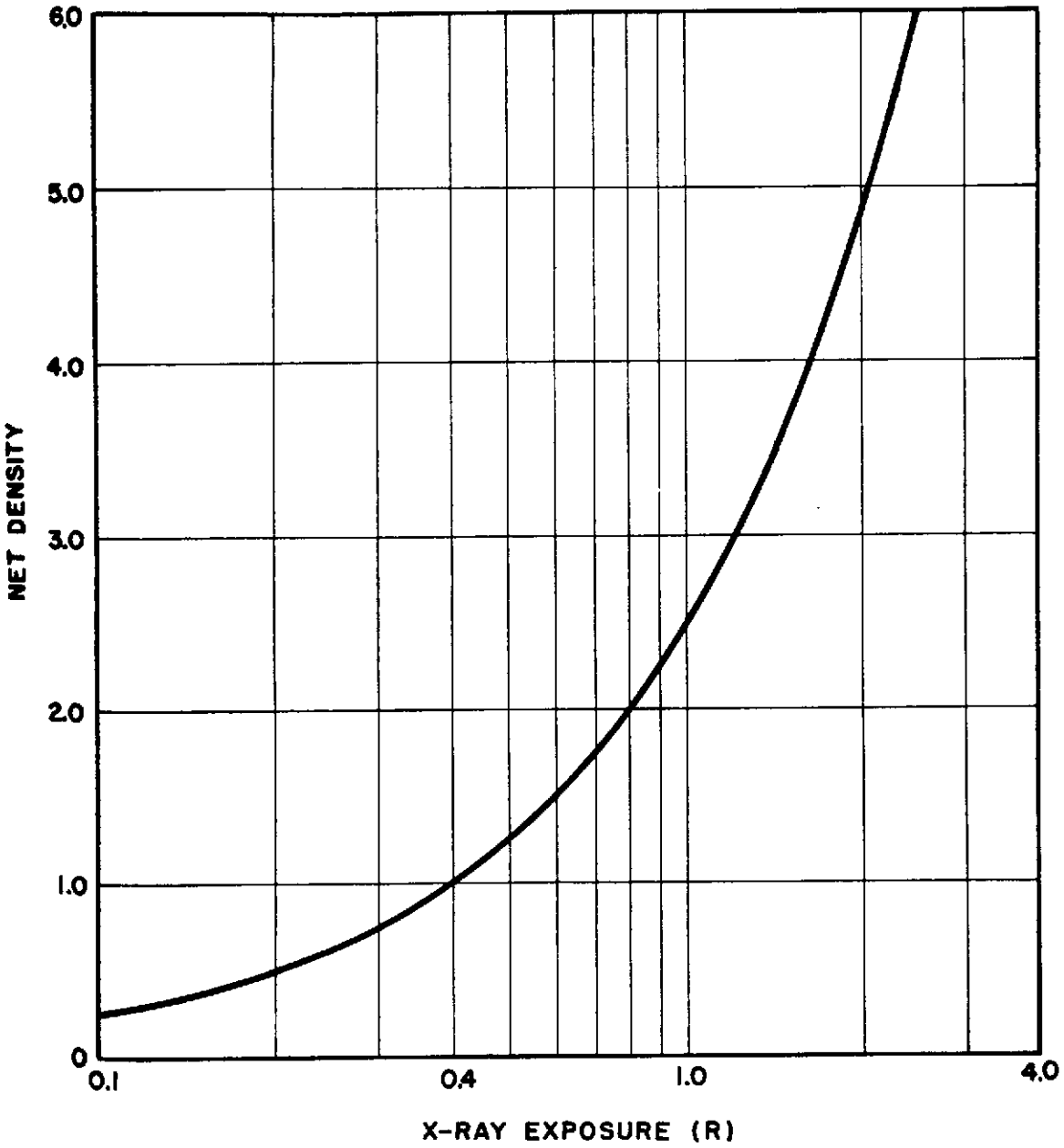

Fig. 2.4 Characteristic Curve for 552 Insensitive Film Exposed to 130-kv X rays.

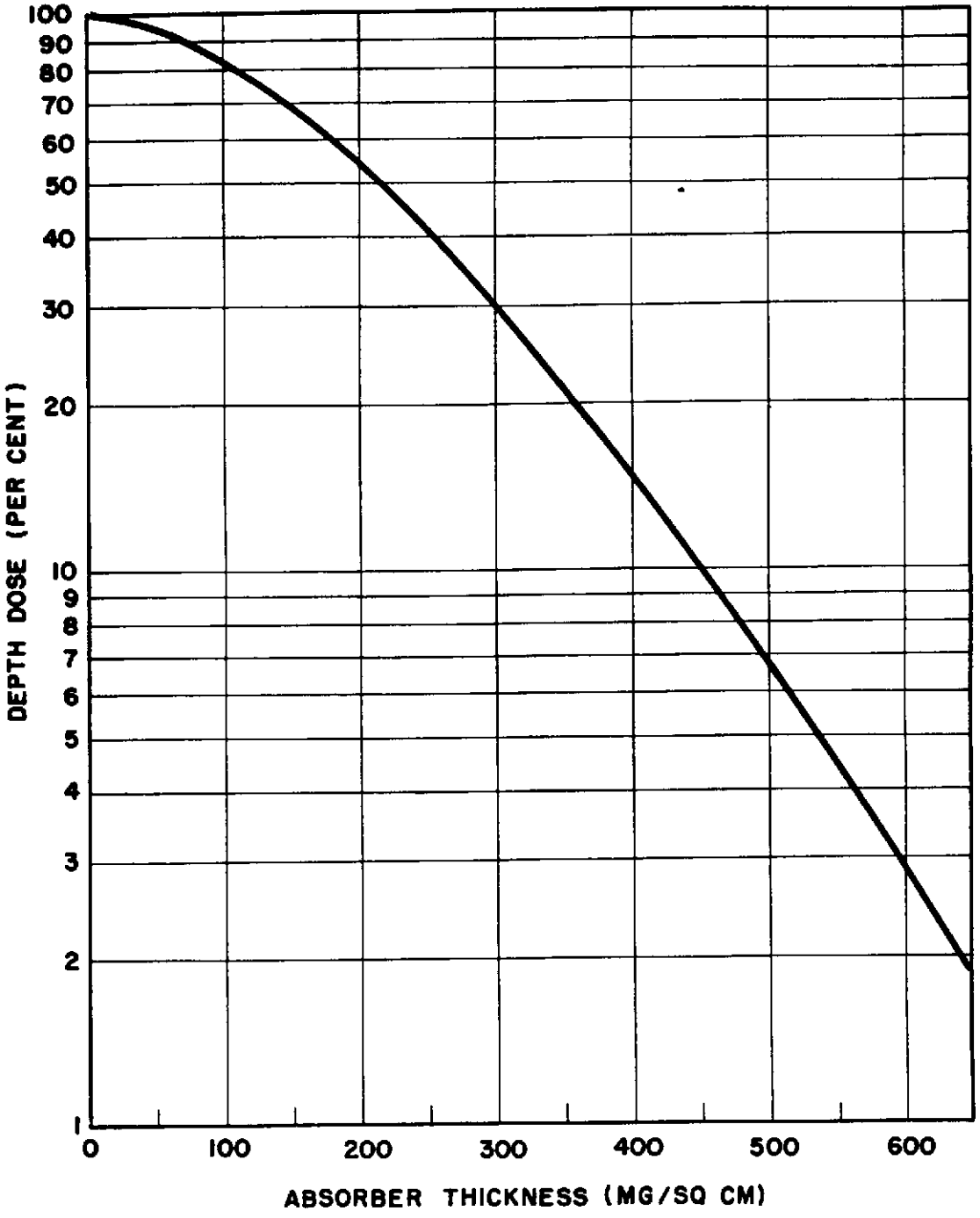

Fig. 2.5 Depth-dose Curve for 552 Insensitive Film Exposed to Sr^{90} Source.

PROJECT 2.4a

TABLE 2.4

Thickness of Films and Paper Covering

Photographic Film	Film Thickness (mg/sq cm)	Black Paper Cover (mg/sq cm)	Black Paper Spacer (mg/sq cm)	Depth to First Film (mg/sq cm)
Eastman Type K	33.6	13.4	7.9	38.1
DuPont 552 Sens.	32.0	13.4	7.9	37.3
DuPont 552 Ins.	28.6	13.4	7.9	35.6
Eastman DF-7	26.8	13.4	8.3	35.1
Eastman 5302	20.2	13.4	8.3	21.7(a)
Eastman Translite	21.6	13.4	8.3	32.5
Eastman 548-0	30.3	13.4	8.3	21.7(a)

(a) For single-coated emulsions depth is to top surface of first film.

the total blackening of such films represents the sum of two densities, and that this density occurs in the middle of the film. The depth to the sensitive area of a double-coated emulsion then becomes the depth to the top surface plus one-half the thickness of the film.

Initially all films were exposed to a strontium 90 source at a distance of 1.5 in. A comparison of the resulting depth-dose curves served to determine whether a calibration at a particular beta-ray energy could be made with one type of film rather than with all types.

Figure 2.6 shows the depth-dose curves obtained with three of the seven films used. The curves for Translite and DF-7 films represent the maximum difference obtained for any two films. The depth-dose curve for 548-0 represents an average between the two extremes. Curves for the remaining four films, if plotted, would fall between those of Translite and DF-7. The results obtained indicate that for the remaining beta-ray energies a representative depth-dose curve could be obtained with any one type of film.

Depth-dose curves were run at 1.5 in. for the remaining beta-ray sources listed in Table 2.1. Type K film was used for the tantalum 182 source while DF-7 film was used for all other exposures. Plotted in Fig. 2.7 are the depth-dose curves obtained for five different beta-ray emitting isotopes of maximum energies ranging from 0.50 to 3.55 Mev.

An effective maximum energy of 0.99 Mev has been used for RaE rather than the usual 1.17 Mev. This was done because the average

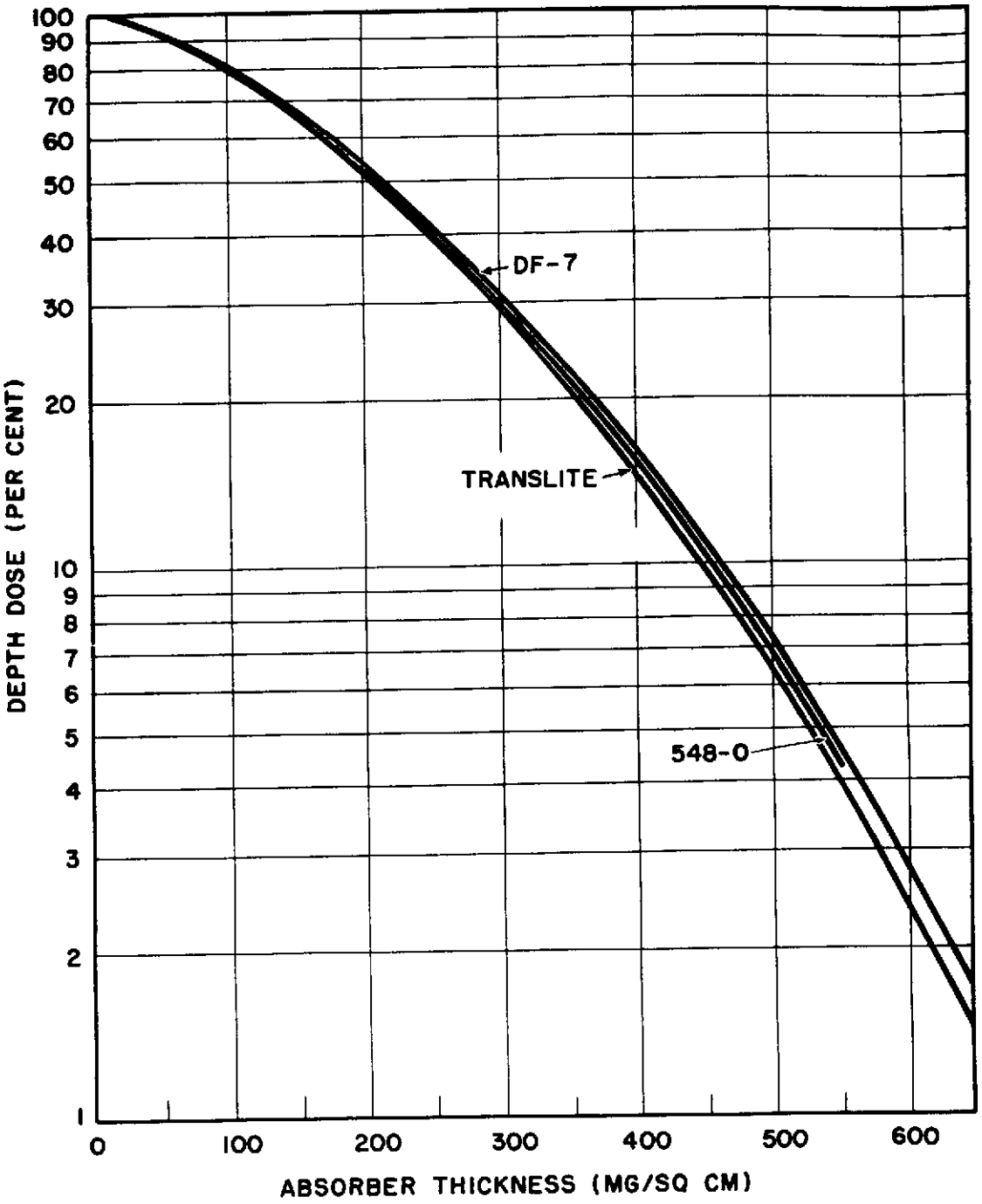

Fig. 2.6 Depth-dose Curves for 3 Films Using Sr^{90} Source.

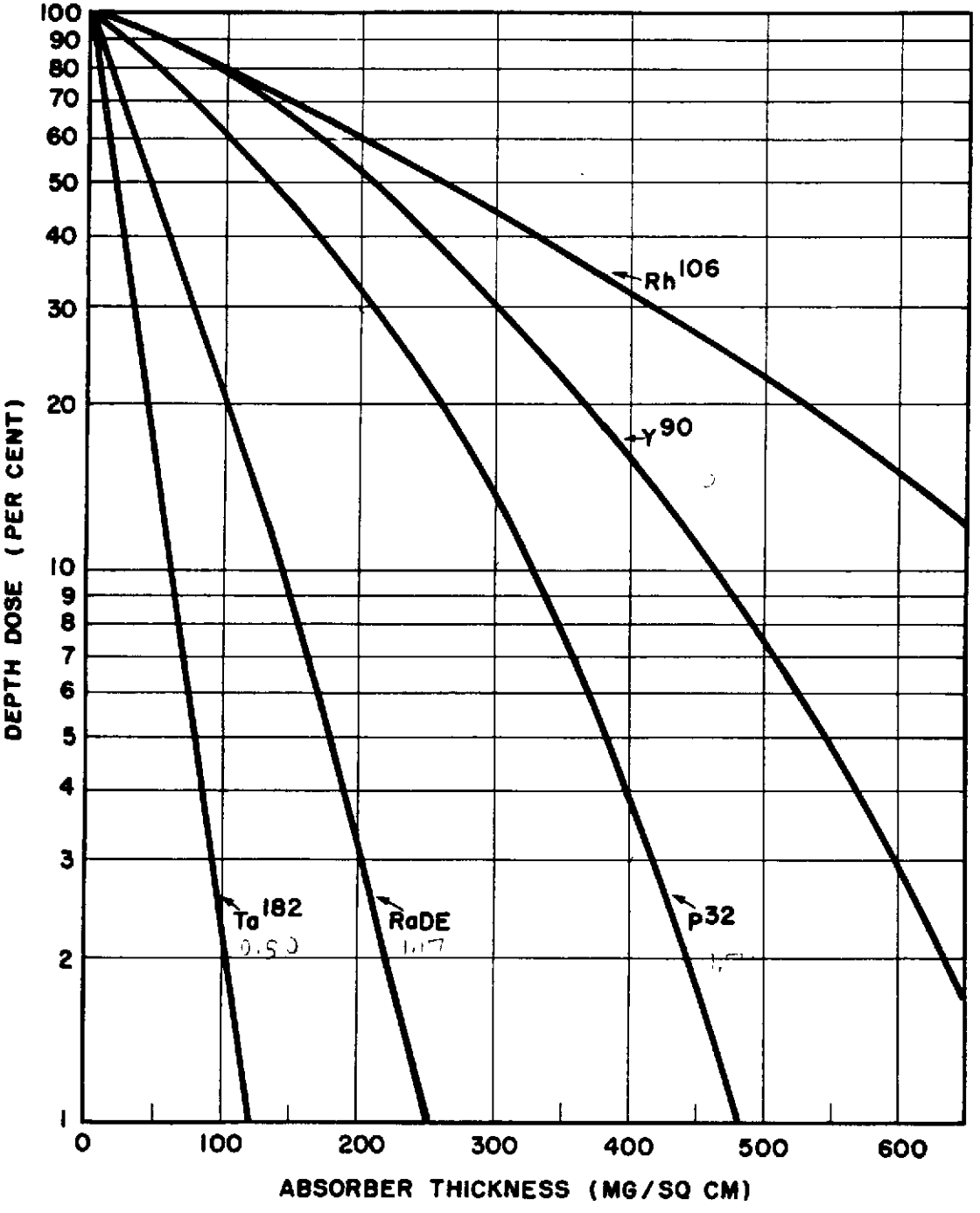

Fig. 2.7 Comparison of 5 Beta-ray Depth-dose Curves.

beta energy of RaE is 0.33 Mev or 28 per cent of the maximum.[2] If it is assumed that other standard beta emitters have average energies of 33 per cent of their maximum, then the maximum energy of RaE (1.17 Mev) can be multiplied by the ratio of 28 per cent to 33 per cent, and the resultant or "effective" maximum energy of 0.99 Mev is obtained.

The depth-dose data at a source-to-film distance of 1.5 in. were used as calibration curves to determine beta-ray energies in the fission-product field. Field-type film packets, described in Chap. 3, were exposed to fission-product activity at the same distance of 1.5 in.

The slopes of the depth-dose curves obtained from the fission-product aggregate can be compared to the slopes of the standard set of curves of Fig. 2.7. To effect an easy comparison, the family of curves in Fig. 2.8 were used. Each curve of this family is a graph of the thickness of absorber required to reduce the depth dose of the standard beta emitters to a particular percentage of its initial or zero absorber value. These percentage values run from 5 to 50 per cent as marked on the curves.

In addition to the 1.5 in. distance, depth-dose curves for the strontium 90 source were also obtained for a surface exposure and for a distance of 12 in. The three curves are shown in Fig. 2.9. The close resemblance of the curves for 1.5 in. and 12 in. indicates that no appreciable change occurs beyond the calibration distance of 1.5 in. Differences between the two curves can be attributed in part to the variation in geometry which in turn determines the amount of backscatter at any particular depth.

2.4 DISCUSSION

As seen from Fig. 2.6 the response of film to beta radiation in making depth-dose measurements is essentially independent of the type of emulsion used. By using films possessing different sensitivities to ionizing radiation depth-dose measurements can be obtained over a wide range of incident beta-ray intensities. Figures 2.2 and 2.3 illustrate the latitude in exposure made possible by using the various films listed in Table 2.2. Assuming equivalent film response to both beta- and gamma-ray ionization, this range of exposure extends from 0.1 rep to doses approximating 40,000 rep.

For purposes of personnel monitoring, the response of photographic

---

[2] L. D. Marinelli, R. F. Brinckerhoff, and G. J. Hine, "Average Energy of Beta Rays Emitted by Radioactive Isotopes", Rev. Mod. Phys., 19 (1947), 27.

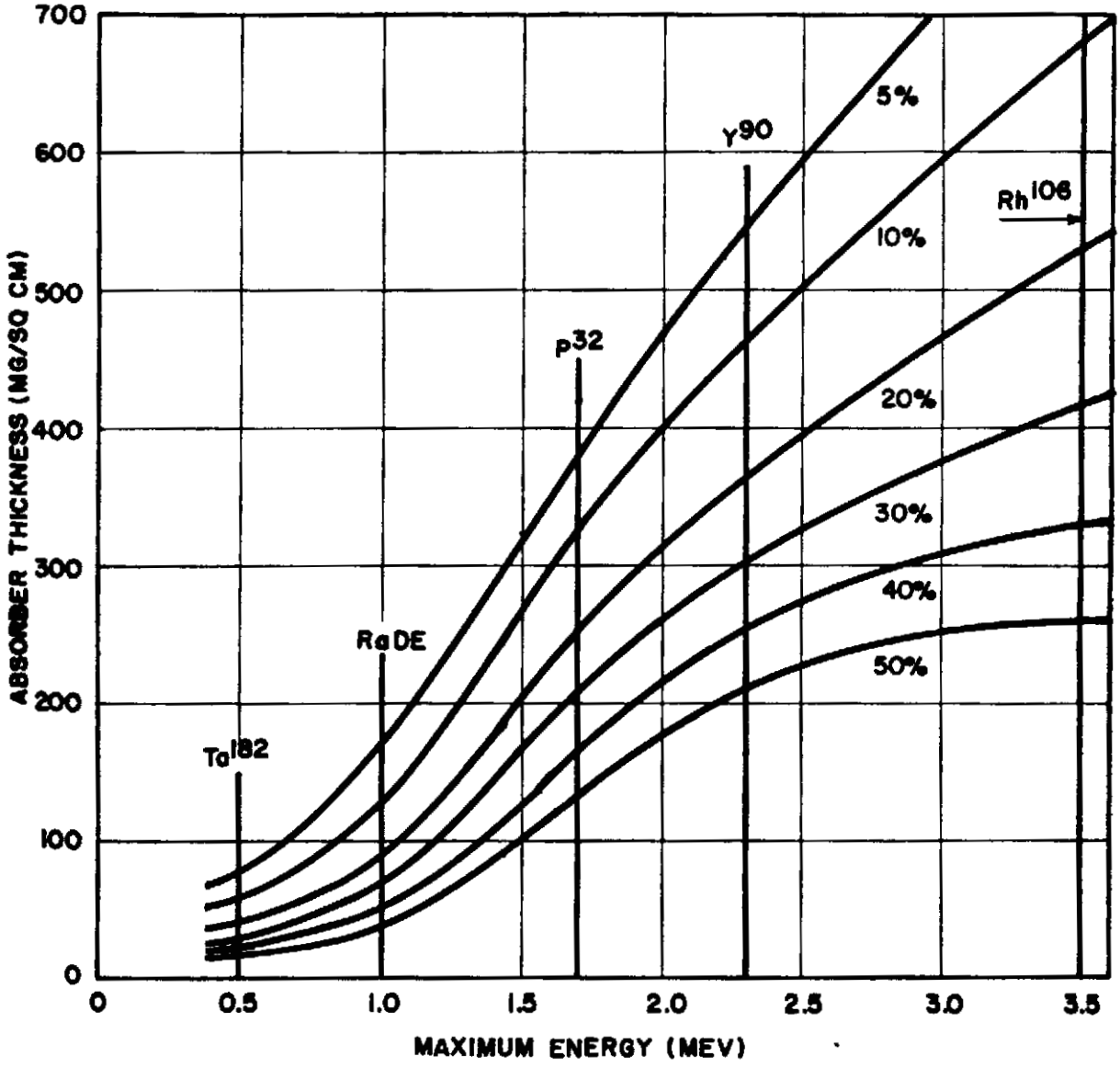

Fig. 2.8 Thickness of Absorber Required to Reduce Depth-dose of Standard Beta Emitters to a Given Percentage of Their Initial Value.

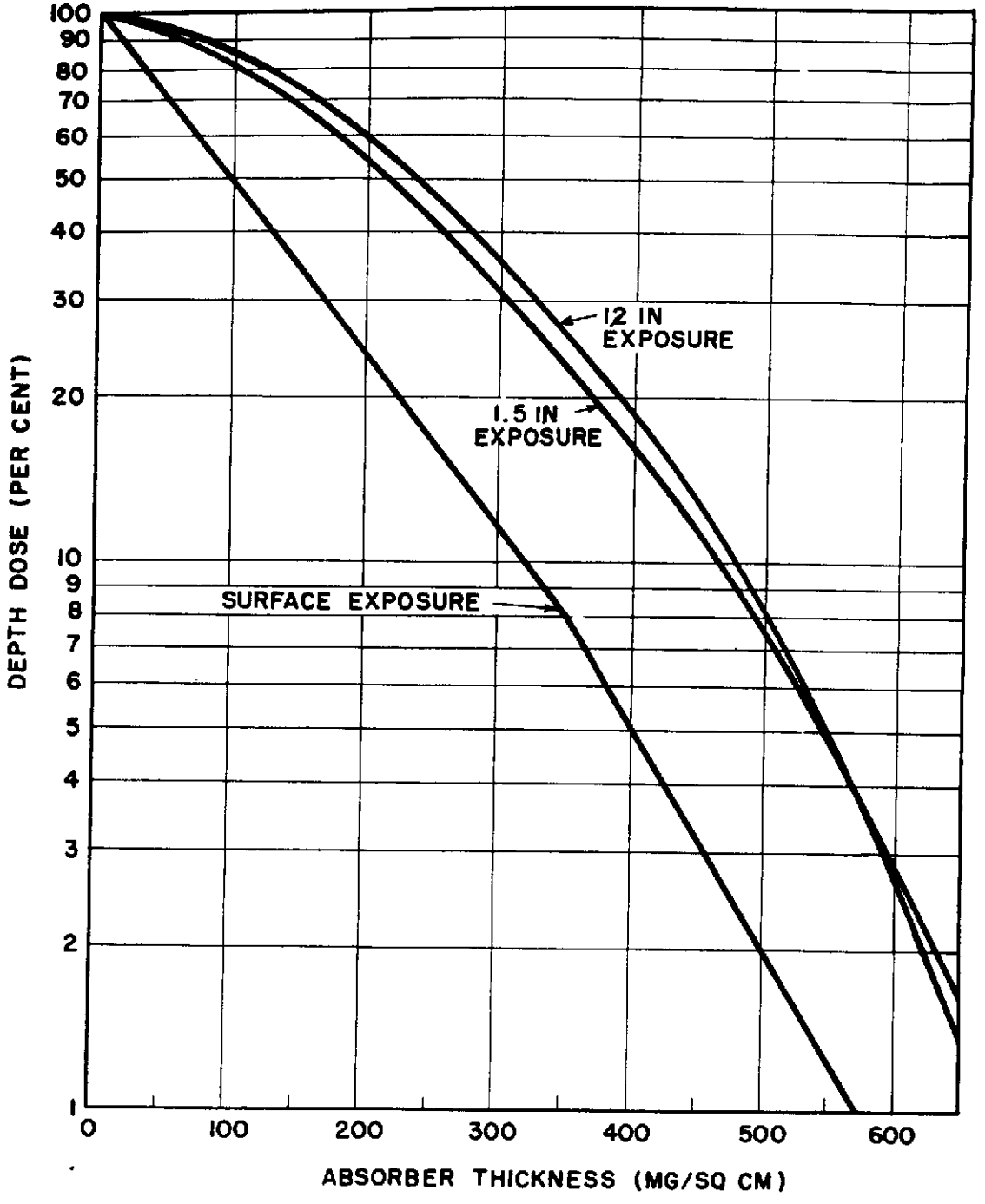

Fig. 2.9 Depth-dose Curves for Sr^{90} Source at Different Source-to-Film Distances.

film to beta-ray isotopes of maximum energies varying from 0.26 to 3.5 Mev has been investigated by E. Storm.[3] The film was found to be much less sensitive to low-energy beta radiation than to high-energy beta radiation, becoming nearly independent of energy beyond 2.5 Mev. Because all film exposures were made with the film enclosed in a dental type packet, and because the film chosen for this study was a double coated emulsion, this information is not sufficient to determine the absolute beta-ray sensitivity of film over the range indicated. The response of film to low-energy radiation is influenced in part by the absorption of beta radiation in the paper wrapper. A further decrease in film response is due to absorption in the cellulose acetate base on which the emulsion is coated, thereby affecting the amount of radiation reaching the bottom emulsion as compared to the top emulsion.

To evaluate the absolute sensitivity of film over a range of beta-ray energies would require the use of a single coated emulsion sufficiently thin so that negligible beta-ray absorption would occur. To obtain such data the response of a Eastman DF-19, a dental type film having emulsion on one side only and an emulsion thickness of 2.4 mg/cm, was investigated using beta-ray isotopes ranging in maximum energy from 0.5 to 3.55 Mev. Eastman DF-19 film has the same emulsion as Eastman DF-7, one of the films used for the beta-ray depth-dose measurements. Exposures were made in a darkroom using a source-to-film distance of 12.0 cm at which distance the outputs of the sources were calibrated by means of an extrapolation chamber.

Figure 2.10 shows the response of Eastman DF-19 film over the range

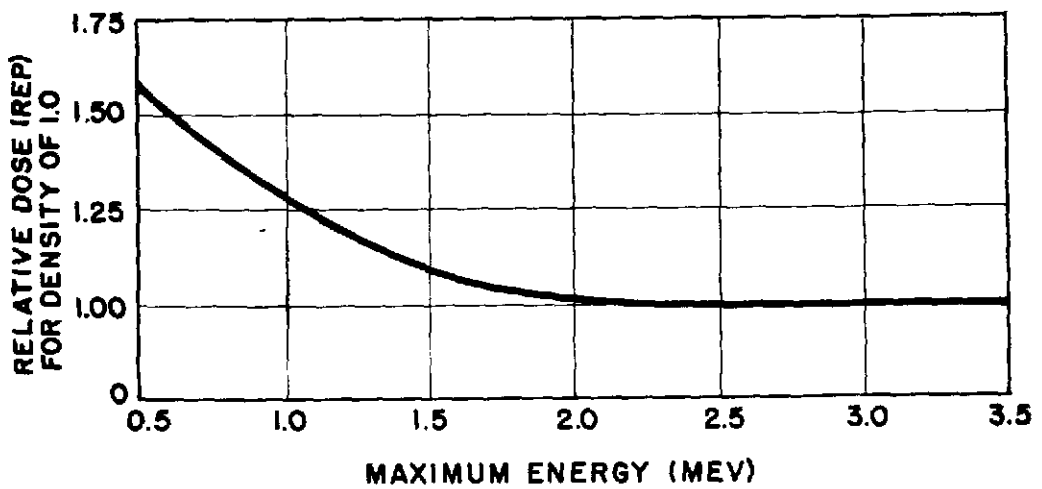

Fig. 2.10 Beta-ray Energy Response of Eastman DF-19 Film.

[3] E. Storm, "The Response of Sensitive 552 DuPont Film to Beta Radiation", Los Alamos Report 1284, August 13, 1951.

of beta-ray energies investigated. All exposures are given relative to the rep dose required to produce a density of 1.0 with the strontium 90 source (2.18 Mev). A marked decrease in film sensitivity is observed for the lower energies. To produce the same film density with a 0.5 Mev beta-ray isotope as with a 3.5 Mev beta-ray isotope required an increase in ionization exposure by a factor of 1.5. The film sensitivity is essentially constant for beta-ray energies greater than 2.0 Mev. For these energies the films are equally sensitive to both beta- and gamma-radiation. Identical film densities within five per cent were observed for a gamma-ray exposure of 1 r (using radium) as for a beta-ray exposure of 1 rep (using a strontium 90 source). On this basis the gamma-ray sensitivities assigned the various films in Figs. 2.2 and 2.3 are also their beta-ray sensitivities.

The response of photographic film to electrons has been studied by J. Fleeman and F. S. Frantz for energies ranging from 0.5 to 1.4 Mev.[4] Within these limits film response was found to be linearly proportional to the dosage received and independent of the energy of the incident electrons. R. A. Dudley has extended this study to include electrons of very low energies.[5] In this region Dudley observed that for perpendicularly incident electrons the density sensitivity of five different films is strongly dependent upon energy. The sensitivity starts at zero for zero energy, rises to a peak at approximately 0.1 Mev, and thereafter decreases to a plateau of one-third to two-thirds maximum sensitivity for energies greater than 0.5 Mev. For diffuse incidence, which is the condition when a beta-ray plaque is placed directly on film, the density sensitivity increases with energy reaching a flat maximum at 1 Mev. The initial rise between 0 and 0.1 Mev is rapid, reaching perhaps two-thirds its maximum. The numerical values cited were influenced by the emulsion thickness and the ratio of silver halide to gelatin of the various films investigated.

Because of the linear relationship of density to dosage over a wide range of beta-ray energies, it is possible to obtain quantitative depth-dose measurements using photographic films. To demonstrate this possibility, a comparison was made of ionization chamber and film techniques. Figure 2.11 illustrates the two depth-dose curves obtained using large uranium sheets in equilibrium with UX_1 and UX_2 as the radiation sources. The extrapolation chamber measurements are taken from the data of

---

[4] J. Fleeman and F. S. Frantz, Jr., "Film Dosimetry of Electrons in the Energy Range 0.5 to 1.4 Mev", Journal of Research of the National Bureau of Standards, 48 (1952), 117.

[5] R. A. Dudley, "The Measurement of Beta Radiation Dosage with Photographic Emulsions", Massachusetts Institute of Technology Ph.D. Thesis (Physics), 1951.

PROJECT 2.4a

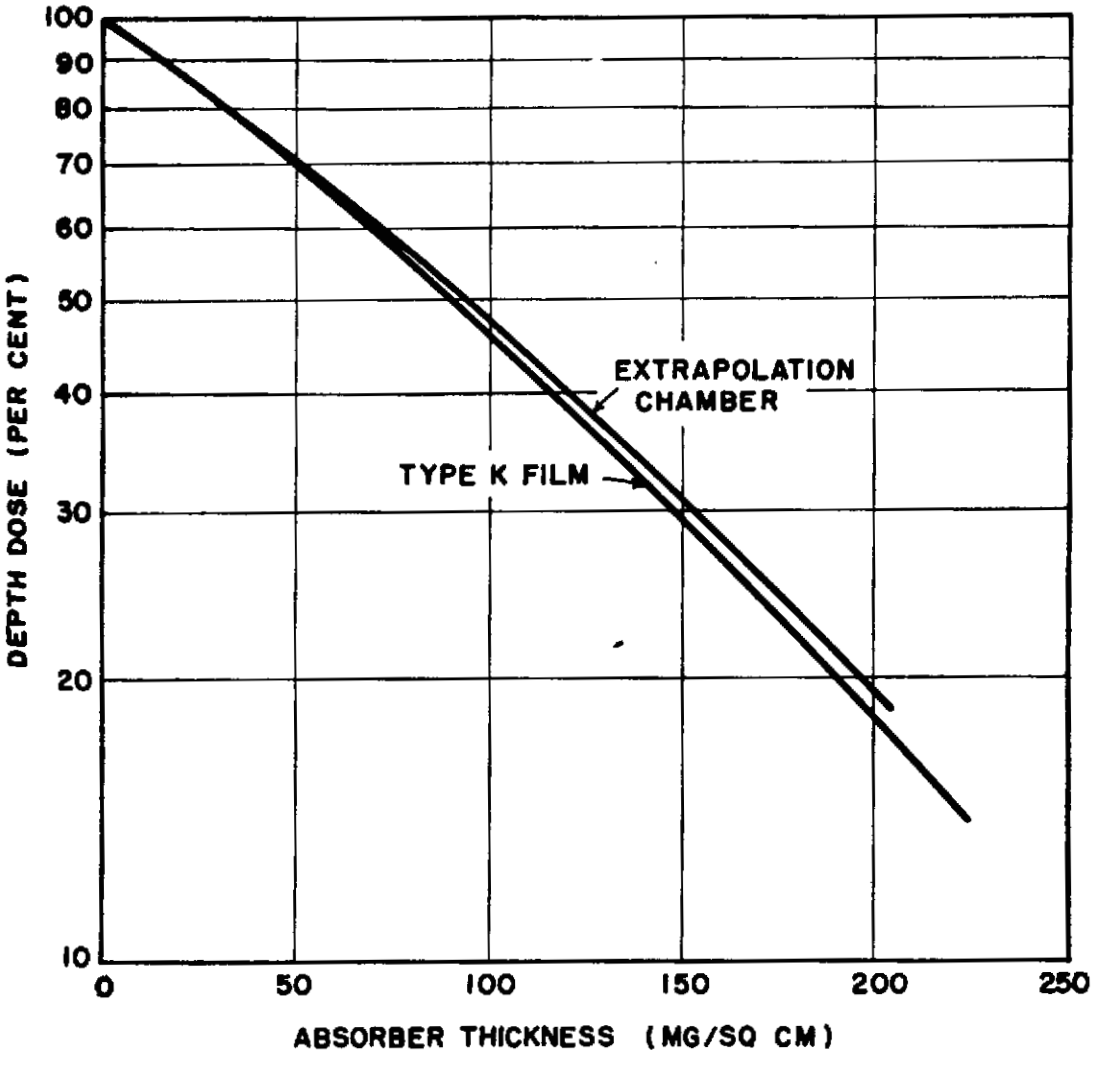

Fig. 2.11 Comparison of Extrapolation Chamber and Film Depth-dose Curves for Uranium.

H. M. Parker.[6] Cellulose acetate film was used as absorber material. For both exposures the uranium sources were covered with sufficient absorber to exclude the accompanying alpha radiation. The film depth-dose measurements with Type K X-ray film were made at the U. S. Naval Radiological Defense Laboratory (USNRDL). It is difficult to assess whether identical scattering conditions were maintained for the film and the ionization chamber measurements. For the measurements made with the uranium source, the two independent techniques compare favorably.

Figure 2.12 shows a comparison between film and extrapolation chamber measurements for a surface exposure using a type RA-1 strontium 90 beta-ray applicator supplied by Tracerlab, Inc. The depth-dose curve, obtained with an extrapolation chamber, was supplied by Tracerlab in the instruction manual included with the source. Also shown in Fig. 2.12 is a depth-dose curve from a similar source obtained by J. S. Krohmer using the extrapolation technique.[7] The Tracerlab and DF-7 film depth-dose curves are identical to a depth dose of 10 per cent. Below this value the slopes of the two curves differ. The data of Krohmer more nearly resembles the depth-dose curve obtained using the film technique than the accompanying extrapolation curve.

The satisfactory agreement between direct ionization measurements of beta radiation and a secondary type of measurement using photographic film techniques is most encouraging. The use of film offers one particular advantage in beta-ray dosimetry because, independent of its ability to measure ionization, it is capable of showing the distribution of dosage over a particular area with a resolution not attained when using other instruments. As an example, with a specially designed aperture of 0.0015 in. diameter it was possible to plot the distribution of density over a film exposed in direct contact with the surface of strontium 90 medical applicator. The applicator has an active diameter of 7.8 mm.

---

[6] H. M. Parker, "Some Physical Aspects of the Effect of Beta Radiation on Tissue", Atomic Energy Commission Declassified Document 2859, September 10, 1943.

[7] J. S. Krohmer, "Physical Measurements on Various Beta-ray Applicators", Am. J. of Roentgenol. and Radium Therapy, 66 (1951), 791.

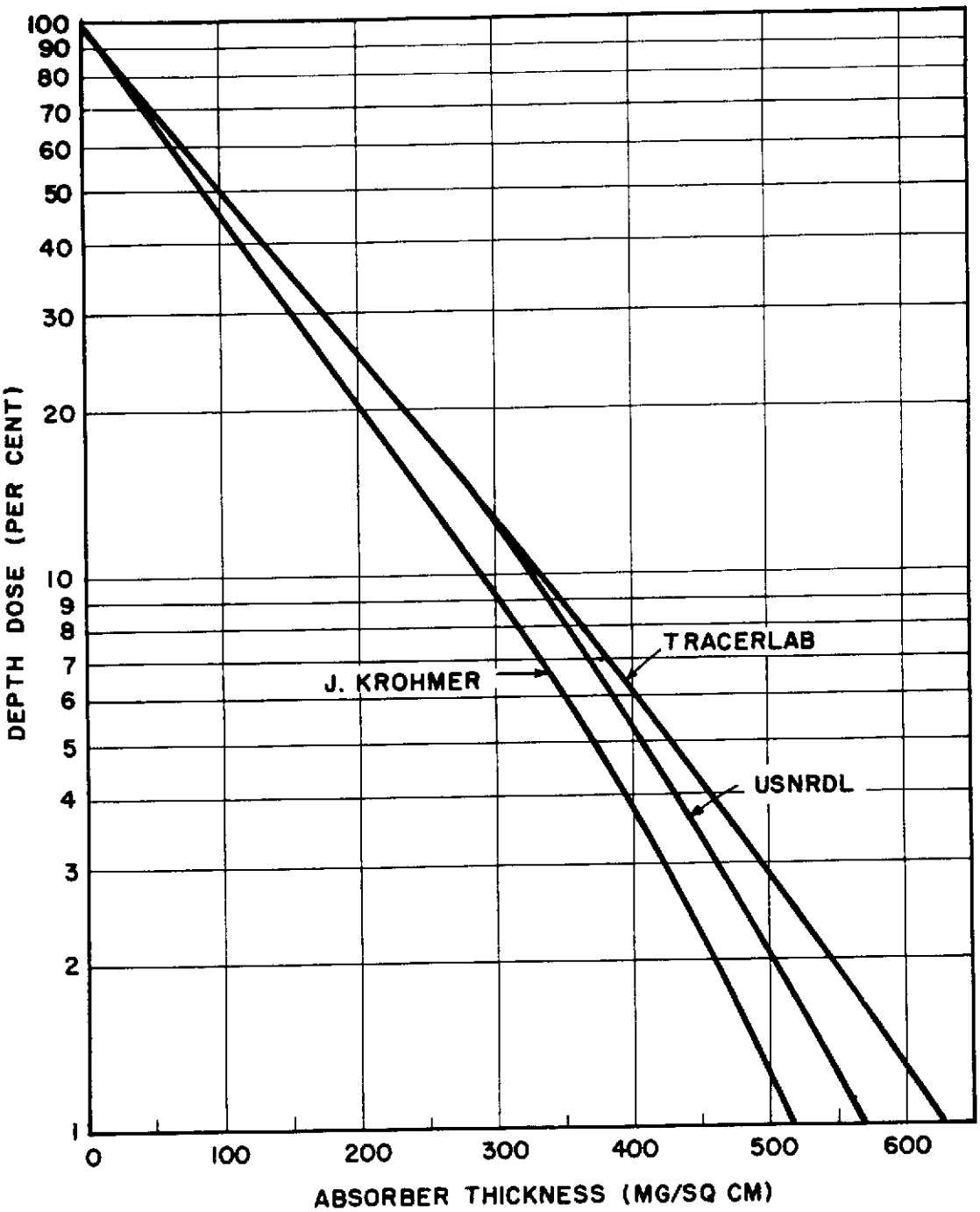

Fig. 2.12 Comparison of Extrapolation Chamber and Film Depth-dose Curves for Sr^{90} Source.

CHAPTER 3

FIELD MEASUREMENTS OF BETA-RAY ENERGIES AND BETA-RAY TO GAMMA-RAY DOSE RATIOS BY MEANS OF PHOTOGRAPHIC FILM

3.1 INTRODUCTION

The equivalent maximum energy of the composite beta-ray spectrum resulting from radioactive fall-out was measured in the field at early times following a surface and an underground burst.[1] These energy measurements were made by exposing small stacks of dental-size film to the fall-out contamination and obtaining depth-dose curves by reading the photographic density of the developed films at successive depths in the stack.[2] From these curves it was possible, further, to estimate the intensity of the beta-ray ionization relative to the gamma-ray ionization under the conditions of fall-out contamination resulting from the two types of bursts.

3.2 EXPERIMENTAL APPARATUS

Figure 2.1 illustrates one of the dental-size film packets used in the field measurements. To the left is shown a stack of some sixty dental-size films, all of the same type, prior to packaging in the 3/4-in. deep, molded-rubber film-holder. The holder is shown in the center. To the right is the completed packet covered with black, light-proof paper 13.4 mg/sq cm thick and sealed with black Texcel tape.

Figure 3.1 illustrates the manner in which four of these film packets were mounted in a Lucite holder. The holder was then covered

---

[1] The equivalent maximum energy will be defined as the energy resulting from a comparison of standard beta depth-dose curves with depth-dose curves run on fall-out contamination. The method of comparison is described later in this chapter.

[2] A depth-dose curve is a graph of the ionization produced in an absorber as a function of depth in the absorber. The ionization at any depth is plotted as a percentage of the ionization occurring at the surface of the absorber upon which the radiation is incident. The distance from the radiation source to the absorber surface upon which the radiation is incident is constant, and the distance from the radiation source to the detector (which in this case is a photographic film) varies with depth in the absorber.

Fig. 3.1 Lucite Holder Used for Mounting Film Packets

with Pliofilm 0.75 mg/sq cm thick to keep out moisture and contamination. Each packet contained film of a sensitivity differing from that of the other packets. This was to insure that at least one of the film packets would receive an exposure in the readable density range. The three individual films mounted on the front of the container were developed first and used to determine which of the four packets should be developed after exposure.

The types of emulsions, their sensitivity ranges and calibrations were described in detail in Chap. 2.

3.3 EXPERIMENTAL PROCEDURE

Two methods were used in making the field exposures. Both methods employed the film pack described in the previous section. One group of forty-six photographic film stations was set up prior to each shot. The early-time fall-out contamination which then descended upon the film container came into close proximity to the film thus giving a significant beta exposure over and above the gamma exposure. These exposures will be designated the early-time fall-out exposures.

A second group of films was brought into the contaminated area after each shot and exposed to the beta and gamma-radiation from the residual contamination that lay upon the ground. These later films were exposed in tripod holders and faced toward the ground at a height of 18 in. above the surface. This type of exposure will be designated by the term post-shot exposure.

The early-time fall-out exposures were intended primarily to give a measure of the equivalent maximum beta-ray energy of the composite beta-ray spectrum resulting from fall-out contamination. It was desired to obtain this energy measurement in as close proximity to the fall-out contamination as possible to eliminate energy changes due to air scattering and absorption and, further, to minimize self-absorption and backscatter such as would be encountered in contamination lying on the ground.

In contrast to these above measurements, the post-shot film packs were set up in tripods so as to be exposed to approximately the same beta-energy spectrum to which the trunk and limbs of a person would be exposed as he traversed an area recently contaminated as the result of a surface or underground burst.

3.3.1 Early-time Fall-out Exposures

Figure 3.2 shows the concrete containers in which the film packs, set up prior to each shot, were exposed in the field. It will be

Fig. 3.2 Concrete Container in which Film Packs were Exposed to Early-time Fall-out.

noted that the container on the right is recessed 1 1/2 in. The reason for this will be given later.

Figure 3.3 shows how a plastic covering was stretched over the film pack and concrete container prior to exposure. The cover, made of No. 3404 clear Respro plastic and 12 mg/sq cm thick, provided a surface upon which the radioactive fall-out could deposit and thus expose the photographic film underneath without directly contaminating the film packets.

With the recessed concrete container shown on the right in Fig. 3.2, the plastic cover maintained a distance of 1 1/2 in. between the fall-out contamination and the surface of the film packets. This allowed a more diffuse darkening of the stacked photographic films, and minimized the decrease in intensity due to change in distance at increasing depth in the stack. The majority of the stations contained the recessed type containers.

The container on the left in Fig. 3.2 is such that the fall-out cover is flush with the top of the film packets. This type of container is not as desirable as the recessed type since the fall-out contamination, being particulate in nature and resting very close to the film pack, may cause a spotty exposure. It is more difficult to make densitometer readings on a spotty negative than on a uniformly exposed one. However it was desirable to compare the results obtained with the two types of containers, and this was done at several stations.

A total of forty-six film stations were set up prior to the surface and the underground shots. These stations were placed along three radial lines extending away from ground zero. Figures 3.4 and 3.5 show the location of the radial lines with respect to ground zero for the two shots. Also shown are the gamma-ray dose-rate contours at one hour after each shot.[3]

The film stations were established so as to sample a respesentative area of the fall-out contamination. Figure 3.6 depicts a typical station arrangement. The locations are tabulated in Tables 3.1 and 3.2.

3.3.2 Post-shot Exposures

An additional group of film packets was brought into the contaminated area approximately 4 1/2 hr after each shot. The tripod holder in Fig. 4.12 is very similar to the ones used in exposing the

[3] These contours were provided by W. E. Strope of USNRDL.

Fig. 3.3 Plastic Cover upon which Early-time Fall-out was Deposited

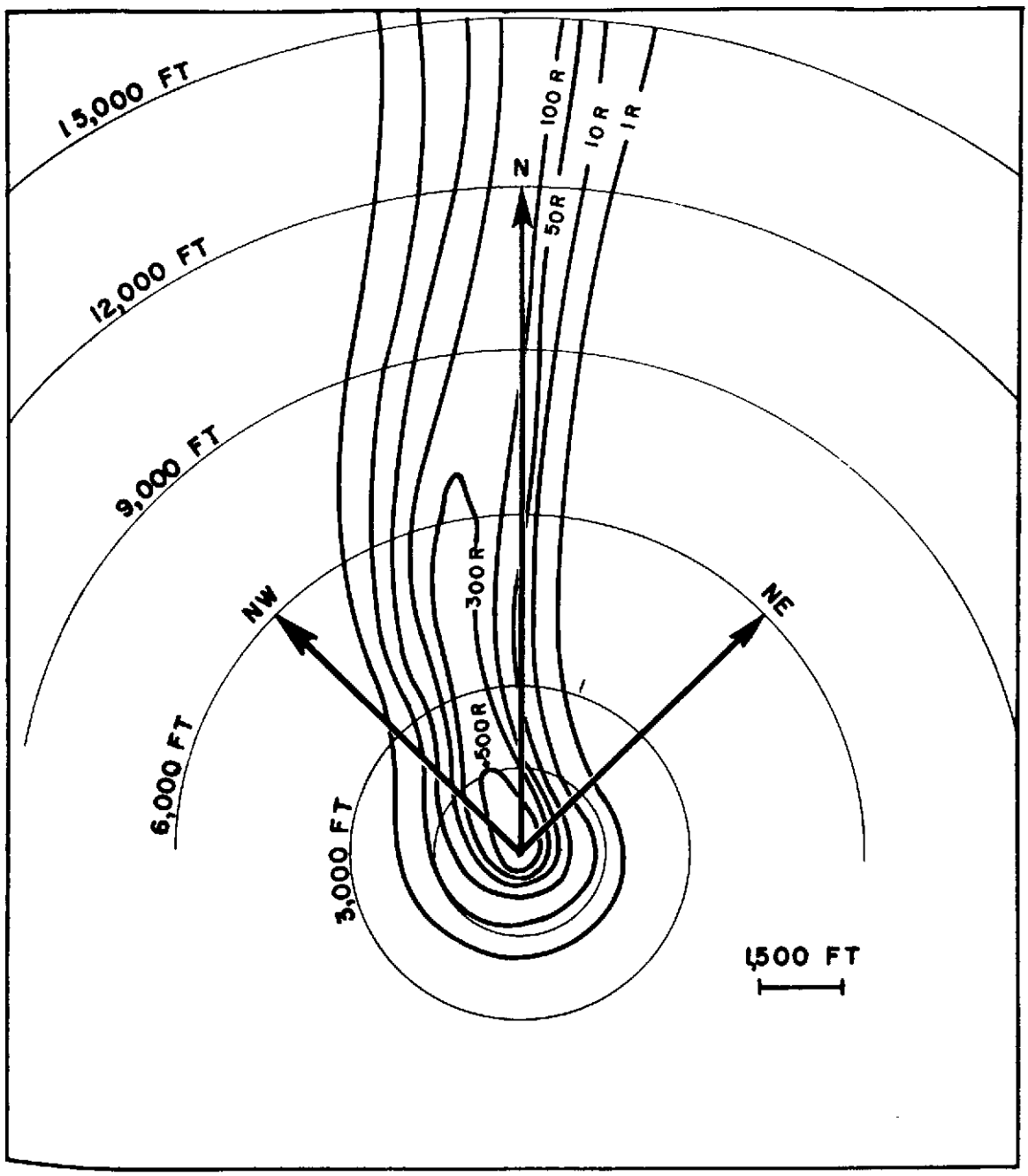

Fig. 3.4 Radial Lines Along which Early-time Fall-out Stations were Located with Respect to the Gamma-ray Dose-rate Contours Plotted at 1 hr Following the Surface Shot. Contours Given in r/hr.

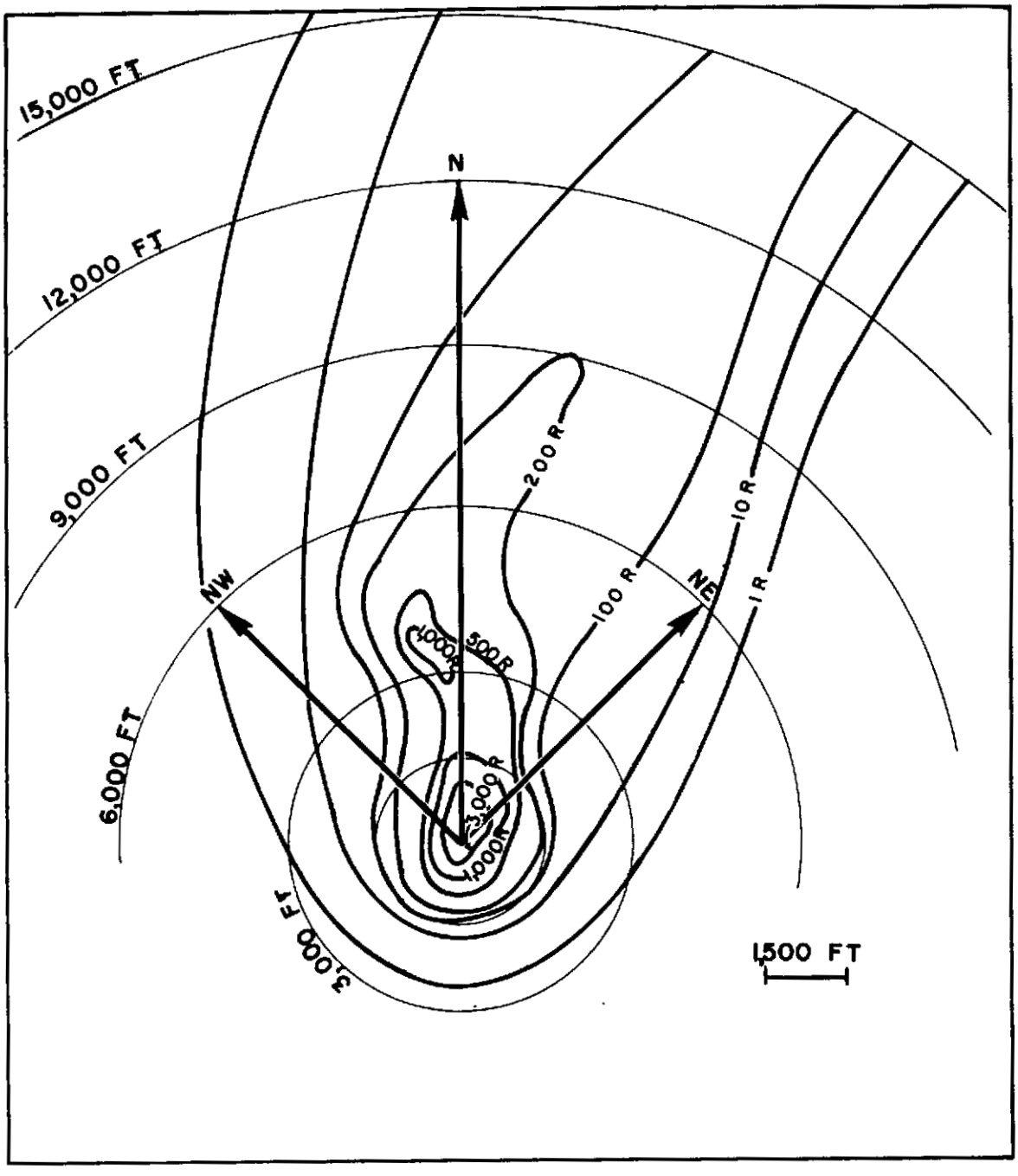

Fig. 3.5 Radial Lines Along which Early-time Fall-out Stations were Located with Respect to the Gamma-ray Dose-rate Contours Plotted at 1 hr Following the Underground Shot. Contours Given in r/hr.

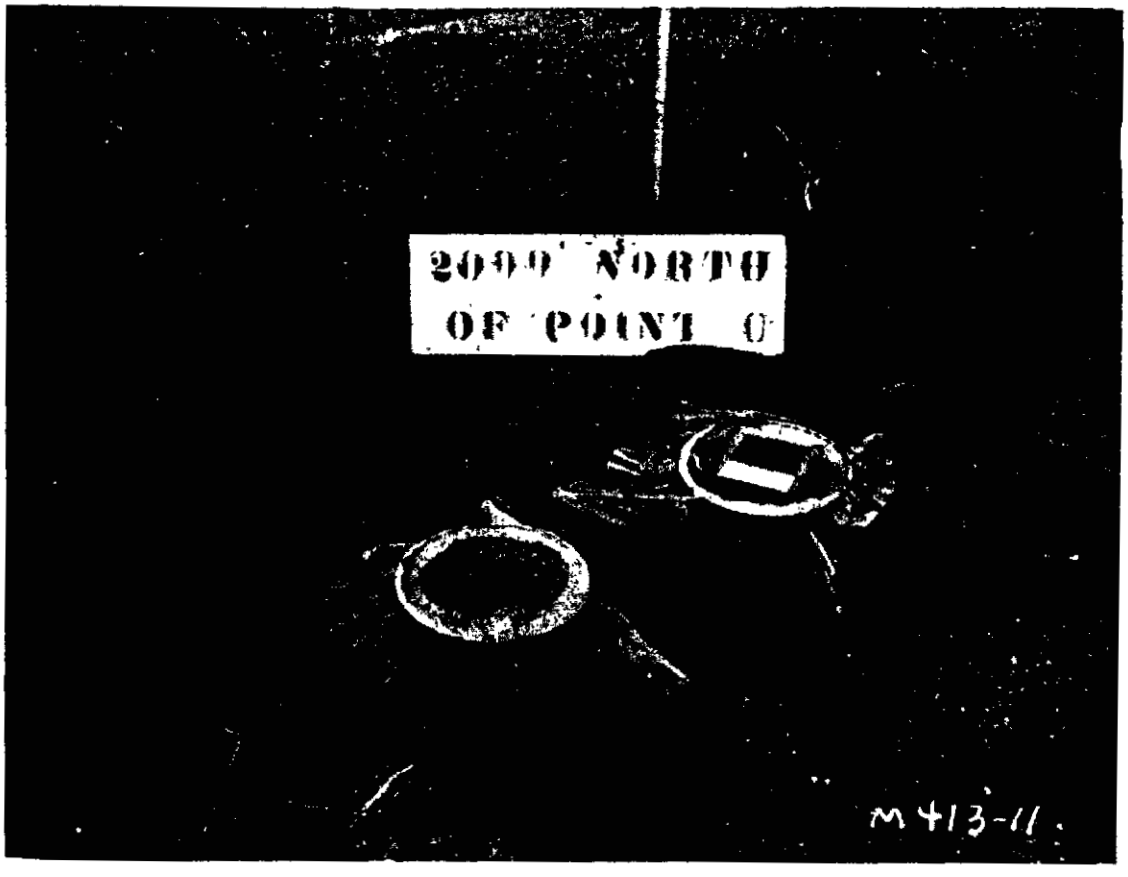

Fig. 3.6 Early-time Fall-out Station Arrangement at 2,000 ft North of the Underground Shot Zero.

post-shot film packs. The surface of the film pack faced toward the ground and was 18 in. above the surface. This arrangement simulated the exposure that might be received by an individual walking through an area contaminated with fall-out.

3.4 EXPERIMENTAL RESULTS

Examples of the beta-ray depth-dose curves obtained under field conditions by means of stacked dental film are presented below together with the tabulated data obtained from these curves.

TABLE 3.1

Location of Early-time Fall-out Stations with Respect to Ground Zero for the Surface Shot

Northwest Line			North Line			Northeast Line		
Station No.	Type(a)	Distance (ft)	Station No.	Type	Distance (ft)	Station No.	Type	Distance (ft)
1	F	1,000	14	F	1,400	34	F	1,000
2	FR	2,000	15	F	1,700	35	FR	2,000
3	R	2,300	16	FR	2,000	36	R	2,300
4	R	2,600	17	R	2,300	37	R	2,600
5	R	2,900	18	R	2,600	38	R	2,900
6	R	3,200	19	FR	2,900	39	R	3,200
7	FR	3,500	20	R	3,200	40	FR	3,500
8	R	3,800	21	R	3,500	41	R	3,800
9	R	4,100	22	FR	3,800	42	R	4,100
10	R	4,400	23	R	4,100	43	R	4,400
11	R	4,700	24	R	4,400	44	R	4,700
12	R	5,000	25	R	4,700	45	R	5,000
13	R	6,000	26	FR	5,000	46	R	6,000
			27	R	6,000			
			28	R	7,000			
			29	R	8,000			
			30	F	9,000			
			31	F	10,000			
			32	F	11,000			
			33	F	12,000			

(a) F - Flush container at this station.
R - Recessed container at this station.
FR - Flush and recessed types both at this station.

TABLE 3.2

Location of Early-time Fall-out Stations with Respect to Ground Zero for the Underground Shot

Northwest Line			North Line			Northeast Line		
Station No.	Type(a)	Distance (ft)	Station No.	Type	Distance (ft)	Station No.	Type	Distance (ft)
55	F	1,000	68	F	1,400	88	F	1,000
56	FR	2,000	69	F	1,700	89	FR	2,000
57	R	2,300	70	FR	2,000	90	R	2,300
58	R	2,600	71	R	2,300	91	R	2,600
59	R	2,900	72	R	2,600	92	R	2,900
60	R	3,200	73	FR	2,900	93	R	3,200
61	FR	3,500	74	R	3,200	94	R	3,500
62	R	3,800	75	R	3,500	95	FR	3,800
63	R	4,100	76	FR	3,800	96	R	4,100
64	R	4,400	77	R	4,100	97	R	4,400
65	R	4,700	78	R	4,400	98	R	4,700
66	R	5,000	79	R	4,700	99	R	5,000
67	R	6,000	80	FR	5,000	100	R	6,000
			81	R	6,000			
			82	R	7,000			
			83	R	8,000			
			84	F	8,000			
			85	F	10,000			
			86	F	11,000			
			87	F	12,000			

(a) F - Flush container at this station.
R - Recessed container at this station.
FR - Flush and recessed types both at this station.

3.4.1 Early-time Fall-out Exposures—Surface Shot

Figure 3.7 is a typical depth-dose curve obtained at 7,000 ft north of ground zero for the surface shot. The beta-ray curve is obtained by subtracting the gamma background from the beta-plus-gamma curve and then normalizing to 100 per cent. The curve represents an integrated exposure from zero time until 27 1/2 hr post shot.

Table 3.3 lists the equivalent maximum beta-ray energies as obtained from the depth-dose curve at each station along the north line.

TABLE 3.3

Equivalent Maximum Beta-ray Energies
Determined from Early-time Fall-out
Exposures at the Surface Shot, North Line

Distance from Ground Zero (ft)	Duration of Exposure[a] (hr)	Equivalent Maximum Beta Energy[b] (Mev)				Ratio of Beta Ionization to Gamma Ionization
		50%	30%	10%	5%	
1,400[c]	27.3	-	-	-	-	-
1,700[d]	27.3	-	-	-	-	-
2,000[d]	27.3	-	-	-	-	-
2,300[d]	27.3	-	-	-	-	-
2,600[d]	27.3	-	-	-	-	-
2,900[d]	27.4	-	-	-	-	-
3,200[d]	27.4	-	-	-	-	-
3,500	27.4	0.9	1.0	1.1	1.2	3
3,800	27.4	0.8	0.9	1.0	1.1	4
4,100	27.4	1.0	1.1	1.2	1.2	2
4,400	27.4	0.9	1.0	1.1	1.1	3
4,700	27.5	1.1	1.2	1.3	1.4	4
5,000	27.5	1.1	1.2	1.4	1.5	6
6,000	27.5	0.9	0.9	1.1	1.2	14
7,000	27.6	1.0	1.1	1.3	1.5	11
8,000	27.6	1.3	1.4	1.6	1.7	10
9,000	27.6	0.6	0.6	0.9	1.0	9
10,000	27.7	1.1	1.2	1.3	1.4	5
11,000	27.7	0.8	0.9	1.0	1.1	10
12,000	27.7	1.0	1.0	1.2	1.2	4

(a) Exposure starting at shot time.

(b) Obtained for various per cent transmissions from the depth-dose curves.

(c) Not recovered.

(d) No significant beta component at this station.

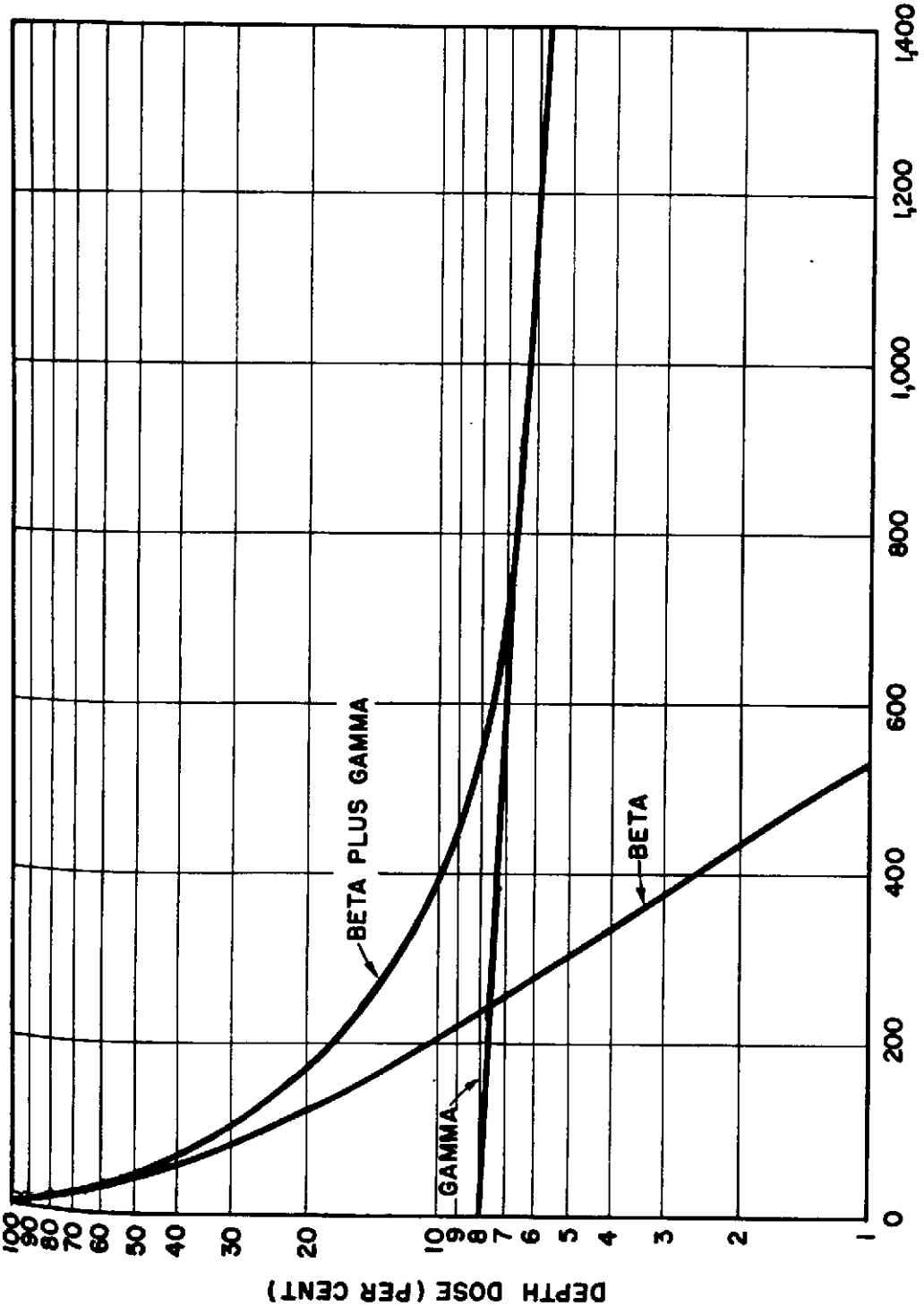

Fig. 3.7 Early-time Fall-out Depth-dose Curve Obtained at 7,000 ft North of the Surface Shot Zero.

This was the only line along which there was appreciable contamination. Reference to Fig. 2.8 in Chap. 2 will illustrate the method of obtaining these energy values. For example, using the depth-dose curve in Fig. 3.7, the amount of absorber required to reduce the beta-ray intensity to, say, 10 per cent of its initial value is determined. Then from Fig. 2.8 the equivalent maximum energy corresponding to this value of absorber is obtained from the 10 per cent curve. Similarly, for any other percentage reduction in intensity, the corresponding equivalent maximum energy value can be obtained.

In Table 3.3, energies are listed for 5, 10, 30, and 50 per cent transmission. A further treatment of this method is given in the discussion.

3.4.2 Early-time Fall-out Exposures—Underground Shot

Figure 3.8 presents a depth-dose curve taken at 4,400 ft north of ground zero for the underground shot. This curve covers an integrated exposure from time zero until 70 hr post shot.

Tables 3.4 through 3.6 list the equivalent maximum beta-ray energies as obtained from the depth-dose curves at each station.

3.4.3 Post-shot Exposures—Surface Shot

The post-shot exposures differ from the early-time fall-out exposures in that the fall-out contamination for the post-shot work was not in close proximity to the film pack, and the exposures did not start until at least 4 hr post shot. As pointed out in Section 3.3, the exposures were made at a height of 18 in. above the surface of the ground to simulate the beta-ray exposure that would be received by persons walking through an area shortly after it was contaminated with fall-out.

Figure 3.9 is a depth-dose curve obtained in this manner at 3,200 ft northwest of the surface shot. The exposure covers a 24-hr period starting at 4 1/2 hr post shot. Table 3.7 lists the equivalent maximum beta-ray energies obtained from this curve.

Adverse weather prevented the obtaining of more than a few usable exposures of this type for the surface shot.

3.4.4 Post-shot Exposures—Underground Shot

Figure 3.10 is a representative post-shot depth-dose curve obtained at 3,800 ft northwest of the underground shot. The exposure

PROJECT 2.4a

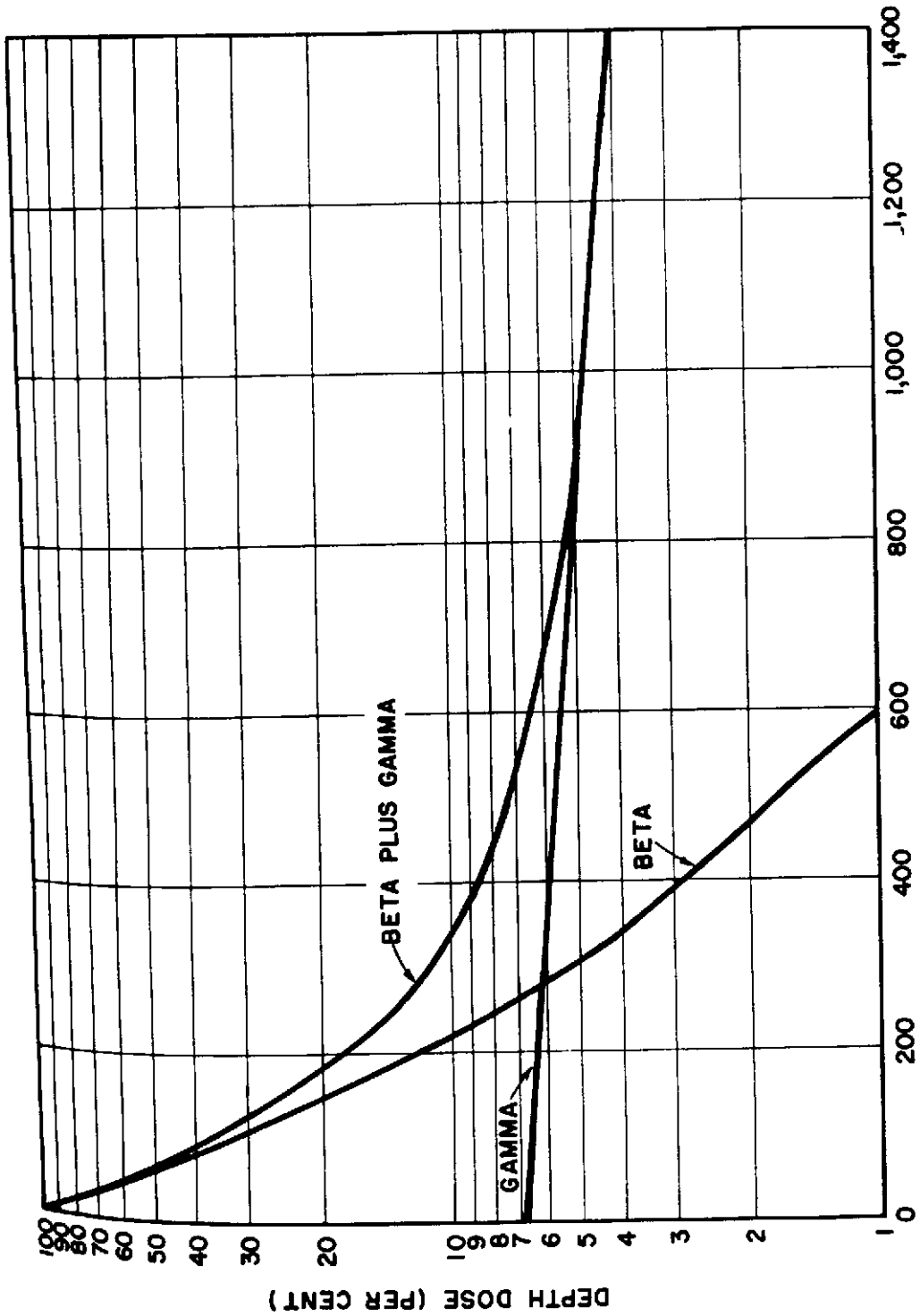

Fig. 3.8 Early-time Fall-out Depth-dose Curve Obtained at 4,400 ft North of the Underground Shot Zero.

PROJECT 2.4a

TABLE 3.4

Equivalent Maximum Beta-ray Energies Determined from Early-time Fall-out Exposures at the Underground Shot, North Line

Distance from Ground Zero (ft)	Duration of Exposure[a] (hr)	Equivalent Maximum Beta Energy[b] (Mev)				Ratio of Beta Ionization to Gamma Ionization
		50%	30%	10%	5%	
1,400[c]	70.3	-	-	-	-	-
1,700	70.2	1.4	1.5	1.7	2.0	6
2,000	70.2	1.1	1.2	1.4	1.6	14
2,300	70.2	1.2	1.3	1.5	1.6	12
2,600	70.2	1.1	1.2	1.4	1.5	20
2,900	70.2	1.3	1.4	1.7	1.9	15
3,200	70.1	1.1	1.2	1.5	1.7	15
3,500	70.1	1.1	1.2	1.4	1.5	17
3,800	70.1	1.1	1.2	1.4	1.6	15
4,100[c]	70.1	-	-	-	-	-
4,400	70.1	1.2	1.3	1.4	1.5	14
4,700[c]	70.0	-	-	-	-	-
5,000	70.0	1.1	1.2	1.4	1.6	20
6,000[c]	70.3	-	-	-	-	-
7,000[d]	70.4	-	-	-	-	-
8,000[d]	70.4	-	-	-	-	-
9,000[d]	70.5	-	-	-	-	-
10,000[d]	70.6	-	-	-	-	-
11,000	70.6	1.5	1.6	1.8	2.0	22
12,000	70.8	1.3	1.4	1.5	1.7	24

(a) Exposure starting at shot time.

(b) Obtained for various per cent transmissions from the depth-dose curves.

(c) Films not developed for technical reasons.

(d) Films overexposed.

TABLE 3.5

Equivalent Maximum Beta-ray Energies Determined from Early-time Fall-out Exposures at the Underground Shot, Northeast Line

Distance from Ground Zero (ft)	Duration of Exposure[a] (hr)	Equivalent Maximum Beta Energy[b] (Mev)				Ratio of Beta Ionization to Gamma Ionization
		50%	30%	10%	5%	
1,000[c]	-	-	-	-	-	-
2,000	23.6	1.3	1.4	1.7	2.0	13
2,300	23.6	1.1	1.2	1.4	1.5	15
2,600	23.6	1.4	1.5	1.8	2.0	4
2,900	23.7	1.3	1.4	1.6	1.7	5
3,200	23.7	1.3	1.4	1.6	1.7	6
3,500	23.7	1.2	1.3	1.5	1.6	6
3,800	23.7	1.1	1.2	1.3	1.4	5
4,100	23.7	1.2	1.2	1.3	1.4	2
4,400[d]	23.8	-	-	-	-	-
4,700[d]	23.8	-	-	-	-	-
5,000	23.8	1.2	1.4	1.5	1.7	16
6,000	23.8	1.2	1.3	1.5	1.6	17

(a) Exposure starting at time of shot.

(b) Obtained for various per cent transmissions from the depth-dose curves.

(c) Films not developed for technical reasons.

(d) No significant beta component at this station.

TABLE 3.6

Equivalent Maximum Beta-ray Energies Determined from Early-time Fall-out Exposures at the Underground Shot, Northwest Line

Distance from Ground Zero (ft)	Duration of Exposure[a] (hr)	Equivalent Maximum Beta Energy[b] (Mev)				Ratio of Beta Ionization to Gamma Ionization
		50%	30%	10%	5%	
1,000[c]	-	-	-	-	-	-
2,000	4.5	0.9	1.1	1.3	1.4	6
2,300[c]	4.6	-	-	-	-	-
2,600[c]	4.6	-	-	-	-	-
2,900	4.6	1.0	1.1	1.5	1.7	7
3,200	4.6	1.0	1.2	1.5	1.7	9
3,500	4.6	1.2	1.3	1.5	1.6	8
3,800	4.7	1.0	1.1	1.4	1.5	10
4,100	4.7	1.1	1.2	1.4	1.5	11
4,400	4.7	0.9	1.0	1.2	1.4	14
4,700	4.7	1.1	1.2	1.4	1.5	7
5,000	4.7	1.0	1.2	1.3	1.5	16
6,000[c]	4.7	-	-	-	-	-

(a) Exposure starting at shot time.

(b) Obtained for various per cent transmissions from the depth-dose curves.

(c) Films not developed for technical reasons.

TABLE 3.7

Equivalent Maximum Beta-ray Energies from the Post-shot Exposures at the Surface Shot

Distance from Ground Zero (ft)	Time between Shot and Start of Exposure (hr)	Duration of Exposure (hr)	Equivalent Maximum Beta Energy[a] (Mev)				Ratio of Beta to Gamma Ionization
			50%	30%	10%	5%	
3,200 NW	4.7	24	1.5	1.6	1.8	2.0	4
1,400 S[b]	6.2	21	-	-	-	-	-
1,200 S[b]	6.3	21	-	-	-	-	-

(a) Obtained for various per cent transmissions from the depth-dose curves.

(b) No significant beta component at this station.

PROJECT 2.4a

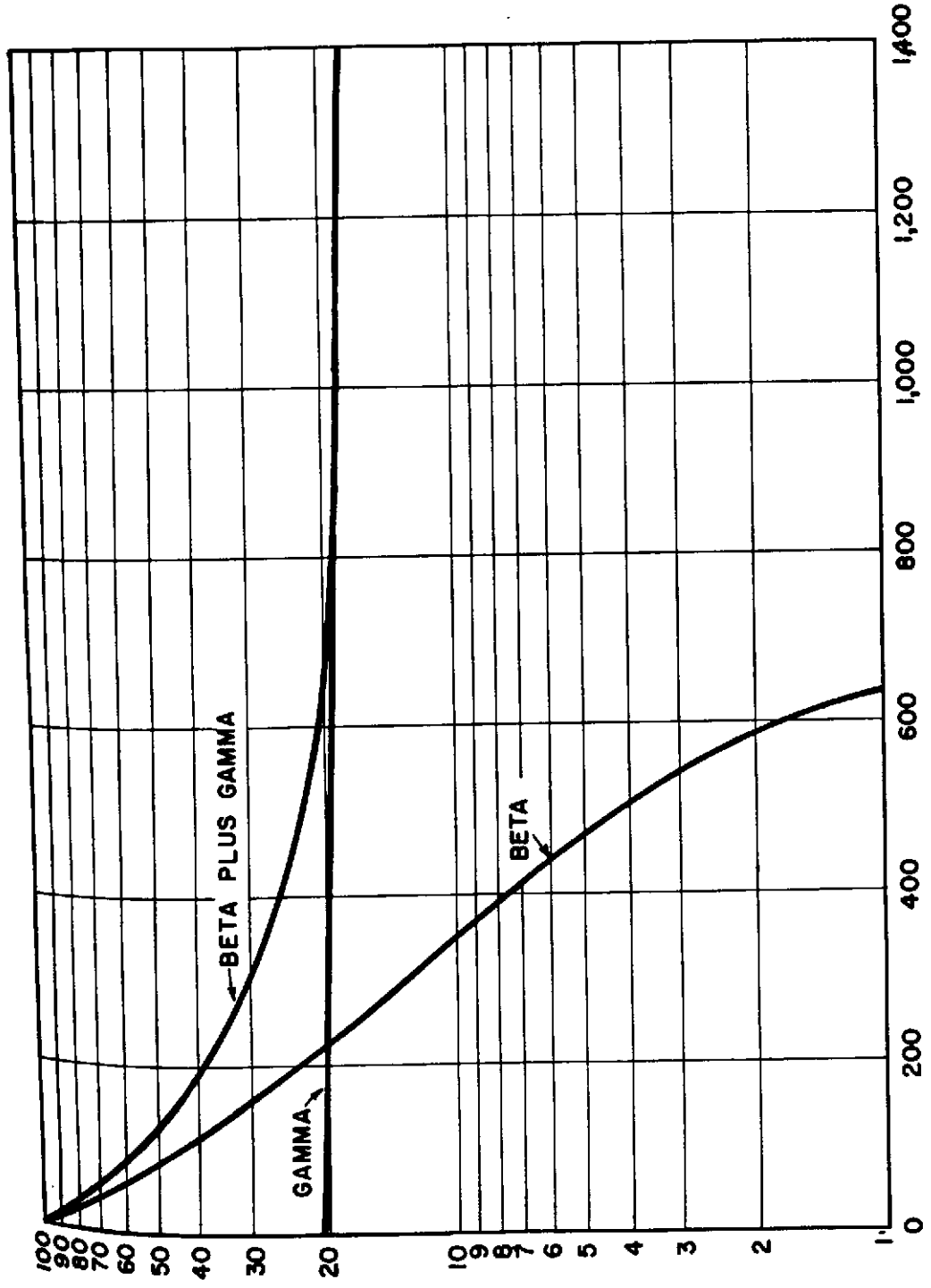

Fig. 3.9 Post-shot Depth-dose Curve Obtained at 3,200 ft Northwest of the Surface Shot Zero.

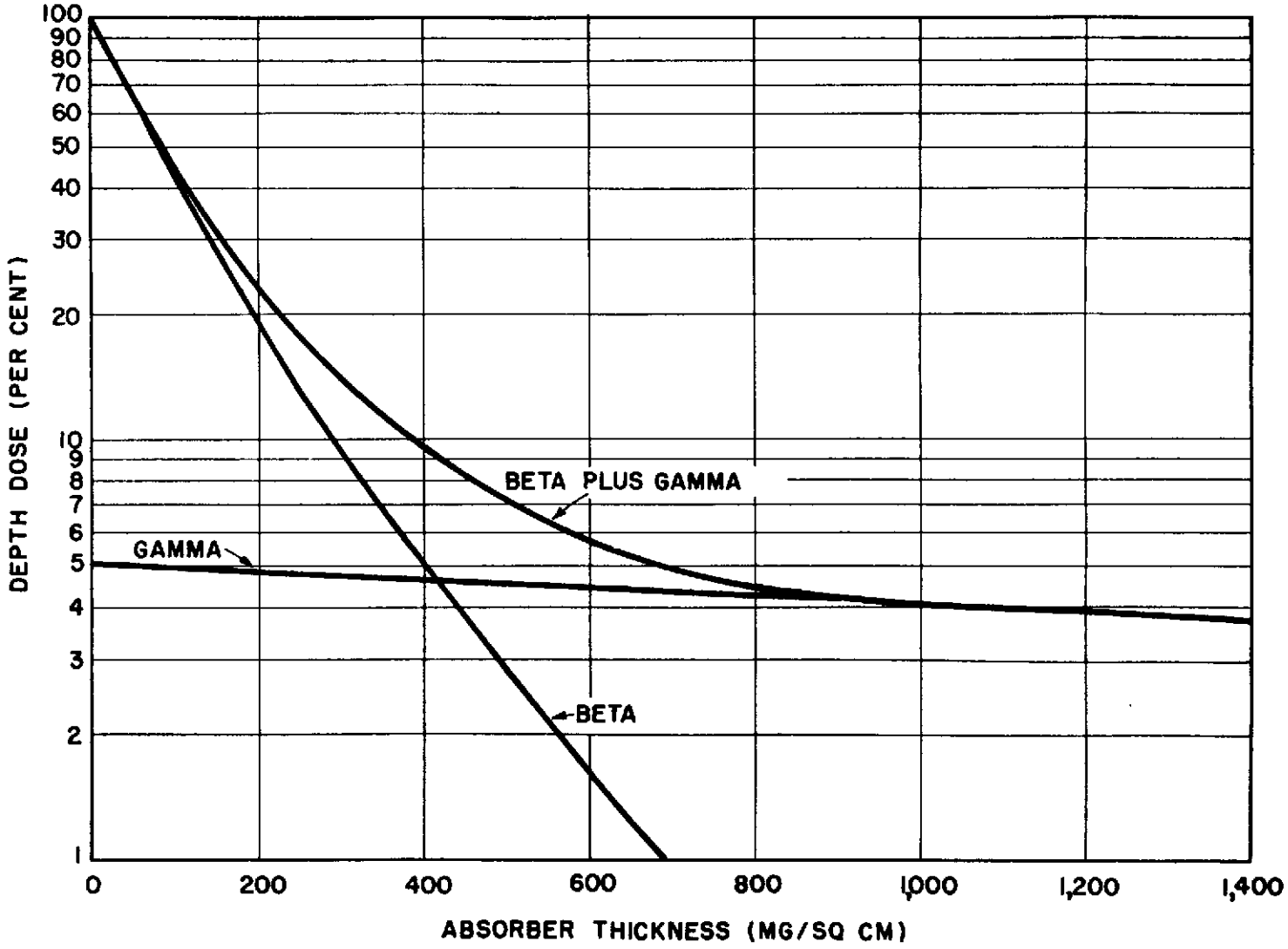

Fig. 3.10 Post-shot Depth-dose Curve Obtained at 3,800 ft Northwest of the Underground Shot Zero.

covers a 19-hr period starting at 4 1/2 hr post shot. Table 3.8 lists the equivalent maximum beta-ray energies obtained from the depth-dose curves at each station.

TABLE 3.8

Equivalent Maximum Beta-ray Energies from the Post-shot Exposures at the Underground Shot

Distance from Ground Zero (ft)	Time between Shot and Start of Exposure (hr)	Duration of Exposure (hr)	Equivalent Maximum Beta Energy(a) (Mev)				Ratio of Beta to Gamma Ionization
			50%	30%	10%	5%	
2,000 S	2.9	21.5	1.3	1.4	1.4	1.4	5
2,300 S	4.5	20	1.0	1.1	1.1	1.2	3
2,000 NW(c)	4.5	19	1.1	1.2	1.4	1.5	26
2,300 NW(c)	4.5	19	1.1	1.2	1.5	1.7	20
2,600 NW(b)	4.5	19	-	-	-	-	-
2,900 NW(c)	4.5	19	1.3	1.4	1.6	1.7	29
3,200 NW(c)	4.6	19	1.2	1.3	1.5	1.7	47
3,500 NW(c)	4.6	19	1.2	1.3	1.5	1.6	30
3,800 NW(c)	4.6	19	1.4	1.5	1.6	1.7	19
1,700 S	24	25.6	1.1	1.2	1.4	1.5	11
2,000 S	24	25.6	1.2	1.3	1.4	1.5	4
2,000 NE	24	28.5	0.9	1.0	1.2	1.4	25
2,900 NE	24	29	1.1	1.3	1.4	1.6	16
3,200 NE	24	29	1.1	1.2	1.4	1.5	16
6,000 NE	24	29	1.1	1.3	1.5	1.7	23

(a) Obtained for various per cent transmissions from the depth-dose curves.

(b) Films not developed for technical reasons.

(c) Contaminated by fission-product dust.

3.5 DISCUSSION

A comparison of the depth dose curves and beta-to-gamma ratios obtained with films exposed in a flush-type container as compared to films exposed in the recessed container at a depth of 1.5 in. shows them to be almost identical. Except in two instances where badly spotted films were obtained, there was uniform film blackening over the entire surface of the films exposed in the flush-type containers, thus indicating that the contamination was very evenly distributed over the

areas investigated. In Tables 3.1 and 3.2 the stations at which both the flush and the recessed film containers were located are noted. For these locations the equivalent maximum beta-ray energies and beta-to-gamma ratios given in Tables 3.3 through 3.6 are for the films exposed in the recessed type containers only.

3.5.1 Equivalent Maximum Beta-ray Energy

The beta-ray spectrum emitted by an aggregate of fission products is a composite spectrum. It is composed of a continuous beta-ray spectrum for each beta-emitting isotope of the aggregate. In order to assign a biologically significant maximum energy to this composite fission-product spectrum, beta-ray depth-dose curves obtained with fission-product contamination were compared with beta-ray depth-dose curves obtained with standard isotopes emitting a single continuous beta-ray spectrum. For such isotopes considerable data are known concerning their biological effects.[4] Using the method of comparison described in Chaps. 2 and 3 it is found that no unique maximum energy can be assigned the composite fission-product spectrum, but rather a series of energies must be given corresponding to the particular depths in the depth-dose curve at which the energy values are obtained.

If a depth-dose curve were to be run on a single isotope of unknown maximum energy in order to determine its maximum energy by this method, it would be found that the energies obtained for various percentage reductions in initial intensity would agree very closely.

The fact that no unique maximum beta-ray energy can be assigned to the composite beta-ray spectrum of fission products by this method indicates that a knowledge of the shape of the beta-ray spectral distribution curve for an aggregate of fission-product contamination is needed.

The fact that the sensitivity of photographic emulsions to unit beta dose decreases with decreasing energy of the beta particles below 2 Mev introduces an error in the beta-ray energy determinations. The magnitude of the energy dependence is pointed out in Sec. 3.5.2. As the low-energy beta particles of the fission-product beta-ray spectrum are absorbed with increasing depth of penetration in the film packet the film will be more sensitive to the remaining beta particles of higher energy and the resultant depth-dose curve will be distorted in proportion to the energy dependence of the film and the relative proportion of low-energy beta particles to high-energy beta particles. The net result will

[4] R. E. Zirkle, Effects of External Beta Radiation, (New York: McGraw-Hill Book Company, Inc., 1951).

be to make the depth-dose curve appear to fall off more slowly with increasing absorber than it actually does. This fact makes the measured beta-ray energy values appear somewhat greater than they are. The magnitude of this error is not known since a spectral distribution of the composite fission-product beta-ray spectrum would be needed in order to determine this correction. As a result no attempt has been made to correct the measured energy values for this error. In any case, the energies as presented in Tables 3.3 through 3.8 would be lower if the correction could be made.

In lieu of a spectral distribution curve, some idea of the biological significance of the depth-dose curves can be gained when it is realized that even for a transmission of 10 per cent the equivalent maximum energies obtained are somewhat less than the maximum energy of the beta particles from P^{32}. By far the greatest amount of information concerning the biological effect of beta rays is known for P^{32}. Low-Beer has done work in this field, although the results are not immediately applicable without due consideration for the fact that his exposures extended over long periods of time, whereas most beta-ray burns from fission-product contamination would occur in much shorter times.[5]

3.5.2 Ratio of Beta-ray to Gamma-ray Ionization

Tables 3.3 through 3.8 list the beta-to-gamma ionization ratios obtained at the various stations.

Reference to Figs. 3.7, 3.8, 3.9, and 3.10, which give four representative depth-dose curves for the surface and underground shots, shows that the curves could be resolved into their individual beta- and gamma-ray components. The curves were plotted assuming the film to be equally sensitive to both beta- and gamma-radiation, that is, assuming the same density would be obtained for either a rep of beta or a roentgen of gamma radiation. Reference to Fig. 2.10 shows that for beta-ray isotopes having maximum beta-ray energies of greater than 2 Mev the sensitivity remains constant. A comparison between a 1 r gamma-ray exposure from radium and a 1 rep beta exposure from a strontium 90 beta-ray source (2.18 Mev maximum) shows that the same photographic density is obtained. For beta-ray spectra with maximum energies of less than 2 Mev the sensitivity of film to unit beta dose decreases with energy. The sensitivity of Eastman DF-19 film (single coated DF-7 film) at 1 Mev maximum energy is about 35 per cent less than at 2 Mev. For films with a thinner emulsion the energy dependence would be less. The fact that this energy dependence exists could increase the beta-to-gamma

[5] B. V. A. Low-Beer, "External Therapeutic Use of Radioactive Phosphorus", Radiology, 47 (1946), 213.

ionization ratios measured with DF-7 film by a factor as great as 1.35. It is not likely that the ratios could be in error by this much since a considerable portion of the composite fission-product beta-ray spectrum had components with maximum energies greater than 1 Mev. However, without a knowledge of the spectral distribution of the fission-product beta-ray spectrum it is not possible to make an exact correction to the measured beta-ray ionization. Since no data were available concerning the fission-product beta-ray spectrum no correction was attempted.

Due to the marked energy dependence of photographic film to X- or gamma-ray energies below 200 kev a further adjustment of the measured gamma-ray ionization was required. To determine this energy dependence of the films, a calibration over a range of effective X- and gamma-ray energies was carried out.

The effective energy of the residual fission-product gamma radiation to which the post-shot film packs were exposed was determined from the data obtained in Chap. 4. This information, together with the energy-dependence calibration for the various films, was used to determine the correction required to convert the measured gamma-ray dose to its proper value.

In contrast to the post-shot film pack measurements, the gamma-ray dose measurements obtained with the early-time fall-out films are correct in that the effective energy of the incident gamma radiation is greater than 200 kev and thus beyond the energy-dependence-region. That this is true can be seen from Chap. 4 where data on the effective energy of the early gamma plus cloud and early fall-out gamma radiation indicate it to be well above 200 kev. Laboratory measurements on the effective energy of the gamma radiation resulting from fission-product contamination taken at Operation GREENHOUSE were also in accord with these measurements. A further comparison between the total gamma-ray dose measured with the early-time fall-out film packs and the National Bureau of Standards (NBS) film dosimeters showed reasonable agreement. Since the NBS film dosimeters were designed to minimize the response to radiation below an effective energy of 200 kev this agreement would indicate that no correction to the measured gamma-ray dose was required.

Of the entire group of scanning packs placed in the field following the underground shot, seven were found to be contaminated. These packs were located along the NW line at distances ranging from 2,000 to 3,800 ft from ground zero. Reference to Table 3.8 indicates that the ratios obtained at these stations were exceedingly high. It is felt that the ratios obtained with the packs located along the NW line may not actually indicate the beta-to-gamma ratio obtained 18 in. above the ground. Instead, the ionization produced could result from both the ground below and from fission-product contamination deposited on the surface of the film packs, a condition which would tend to increase the values obtained. For this reason an average beta-to-gamma ratio will be

considered rather than the maximum ratio observed.

From Table 3.8 the average ratio of beta-ray ionization for the underground post-shot exposures is approximately 19. It is of interest to see what this average ratio for the scanning packs would be when extrapolated to 1.5 in., the distance from contamination of the fall-out packs. Beta- and gamma-dose rate data measured as a function of height above the contaminated ground surface allowed the ratio at 18 in. to be extrapolated to a corresponding ratio at 1.5 in. This extrapolation gave a value of greater than 100 at 1.5 in. It can be seen from Tables 3.4 through 3.6 that none of the early-time fall-out measurements made at a distance of 1.5 in. gave a ratio in excess of 24. Were both the scanning and the fall-out packs exposed to exactly the same type of radiation, this difference would not exist.

The fall-out packs, in addition to the ionization received from the residual fission products, were further subjected to early gamma and cloud gamma radiation. On this basis the gamma-ray dose received from these two effects was at least four times greater than the subsequent gamma-ray dose received from the residual contamination deposited in the vicinity of the film packs. Thus, for the early-time fall-out packs, even though the beta-to-gamma ratio from the residual contamination could produce a beta-to-gamma dose of approximately 100, the radiation from the early gamma plus cloud gamma reduced the ratios obtained to no larger than 24 to 1 over the periods involved.

CHAPTER 4

FIELD DETERMINATION OF EFFECTIVE GAMMA-RAY ENERGY

4.1 INTRODUCTION

Energy-dependent ionization chambers were constructed and calibrated for field measurements of the energies of the early and the residual gamma radiations. These chambers were exposed to both the surface and the underground shot and provided data on the variation of residual gamma-ray energy with time and distance. Energy-dependent survey meters were also constructed and calibrated to provide a means of determining gamma-ray energies over a large area of contamination.

4.2 EXPERIMENTAL APPARATUS

The energy-dependent chambers were constructed by the Landsverk Electrometer Co. These were modified Model L-66, 2-r personnel dosimeters and Model L-50, 100-r personnel dosimeters. The Landsverk Model L-60 low-range charge-reader was modified so that it could be used with the 100-r chambers. This allowed all chambers to be read with one charging unit. Because the proper size condenser was not available for the high-range scale of the charge-reader, the Model L-50 dosimeter gave a full scale reading of 90 r. Half the 90-r chambers were actually used as 30-r chambers by reading them on the low scale of the modified charge-reader. Thus three ranges of chambers were available: 2 r, 30 r, and 90 r.

Each of the three types of chambers was divided into four groups, three of which were modified to serve as energy-dependent chambers by lining the central electrode with various metals, and one of which was unmodified. Copper and tin foils 0.0015 in. thick and lead foil 0.003 in. thick were used as the lining materials for the three modified groups. In addition, there were constructed four aluminum-lined 2-r chambers with a foil thickness of 0.001 in. In the 30-r and 90-r modified chambers the tolerance between the inner and outer electrodes was maintained at 0.005 in. and in the 2-r chambers at 0.060 in. The various metallic foils were cemented to the central electrodes at the USNRDL and returned to Landsverk for assembly. The charge-reader and a typical chamber are illustrated in Fig. 4.1.

The foils used in the aluminum- copper- and tin-lined chambers were the thinnest that could be easily obtained. For these chambers the foil thickness was not critical; however, it was desired to minimize any

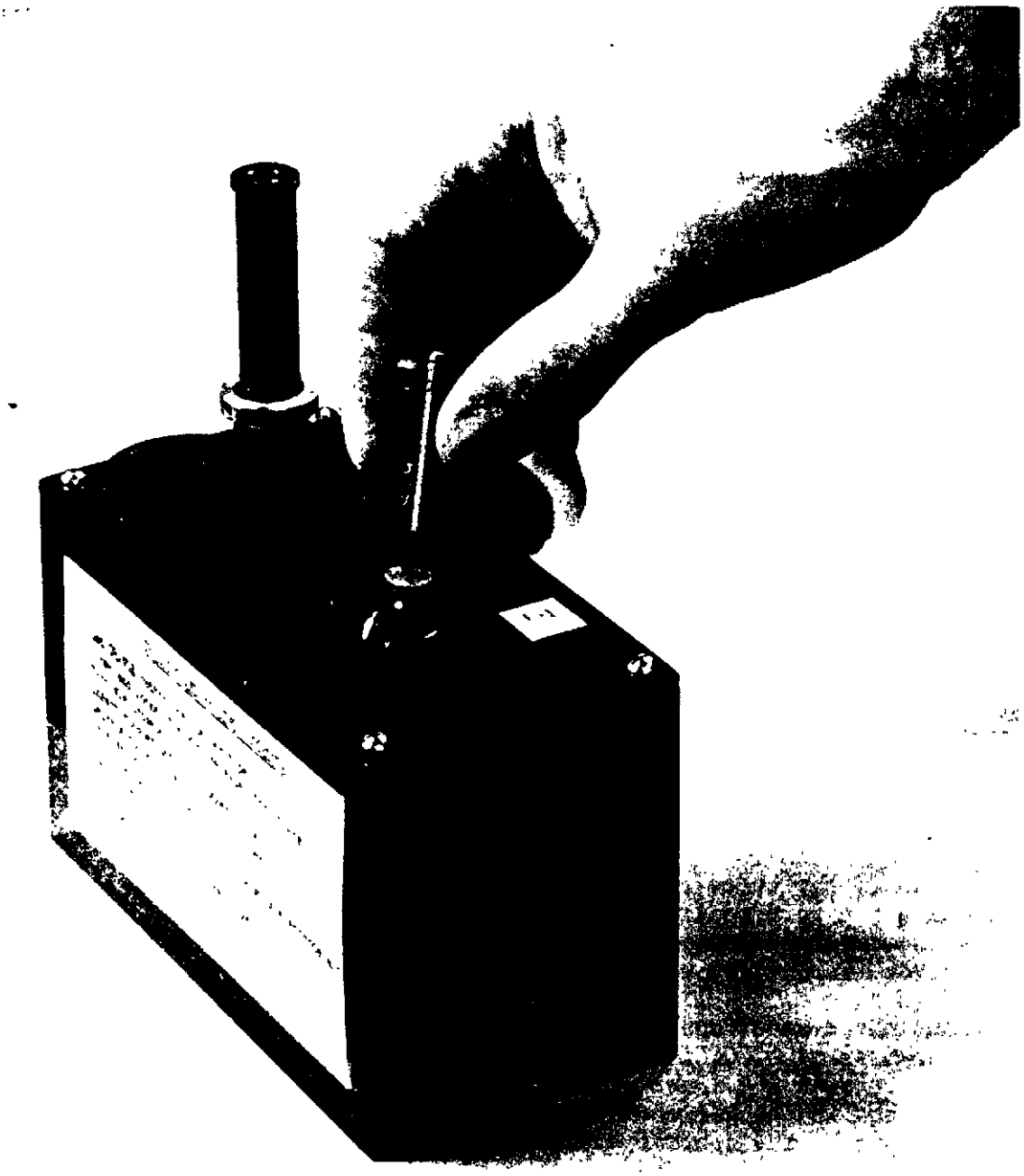

Fig. 4.1 Landsverk Ionization Chamber and Charge-reader.

absorption of low-energy gamma rays that might occur in the foil itself. Preliminary calibrations with lead-lined chambers indicated that a lining thicker than 0.001 in. would be required if these chambers were to produce significant ratios up to 1.25 Mev. On the basis of several tests a lead foil 0.003 in. thick was chosen.

Energy-dependent survey meters were made from Tracerlab type SU-1E "Cutie Pies", as shown in Fig. 4.2. These instruments were easily modified by providing them with a group of lined chambers which could be interchanged with the conventional unlined ones; linings were of 0.0015 in. copper and tin foils, 0.003 in. lead foil, and 0.001 in. aluminum foil. Fig. 4.3 shows the SU-1E instrument and its associated chambers.

4.3 EXPERIMENTAL PROCEDURE

4.3.1 Laboratory Calibration

Both the chambers and the survey instruments were calibrated by exposure to X rays and gamma rays. In this method of calibration, developed by Clarkson and Mayneord, the ratio of ionization produced in two chambers having different wall materials determines the energy of the incident radiation.[1] The chambers were calibrated by exposing lined and unlined groups to X- and gamma-radiation of known effective energy and determining the ratio between the two readings. Thirty chambers in a Lucite tray were exposed at one time as illustrated in Fig. 4.4. The calibration was carried out in this manner in order to duplicate exposure conditions in the field where a Lucite tray and supporting stand were used to position the chambers. Table 4.1 lists the radiation sources, added filtration, and effective energy of each calibration point. Plotted in Fig. 4.5 are the experimental ratios of aluminum- copper- tin- and lead-lined chamber readings to unlined 2-r chamber readings over the energies investigated. Previous experimental data obtained with similar chambers at Operation GREENHOUSE indicated that there was no need to extend the calibration below 65 kev. An identical calibration was also carried out for the 30-r and 90-r chambers except that there was no aluminum-lined chambers in this range.

A representative group of 2-r chambers were also calibrated by NBS. Exposures were made to heavily filtered X-rays of effective energies ranging from 25 to 840 kev. Gamma rays from cobalt 60 were used to obtain an additional calibration point at 1,200 kev. Table 4.2 lists the exposure conditions for the NBS calibration while Fig. 4.6 gives the experimental data obtained with the four groups of chambers.

---

[1] J. R. Clarkson and W. V. Mayneord, "The Quality of High Voltage Radiations, Part II", Brit. J. of Radiology, 12 (1939), 168.

Fig. 4.2 Tracerlab Type SU-1E Portable Survey Instrument in Operating Position.

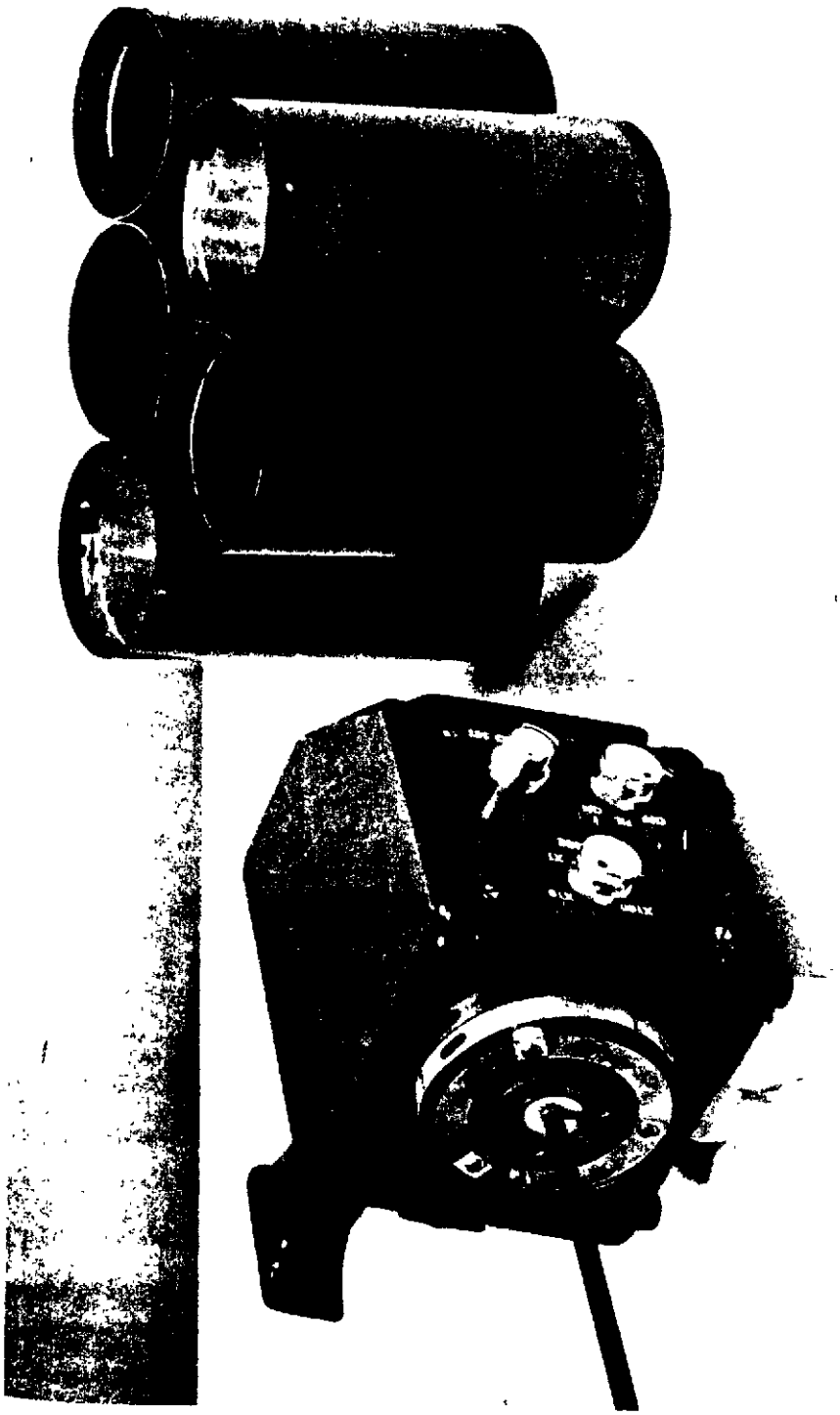

Fig. 4.3 SU-1E Instrument and Associated Chambers.

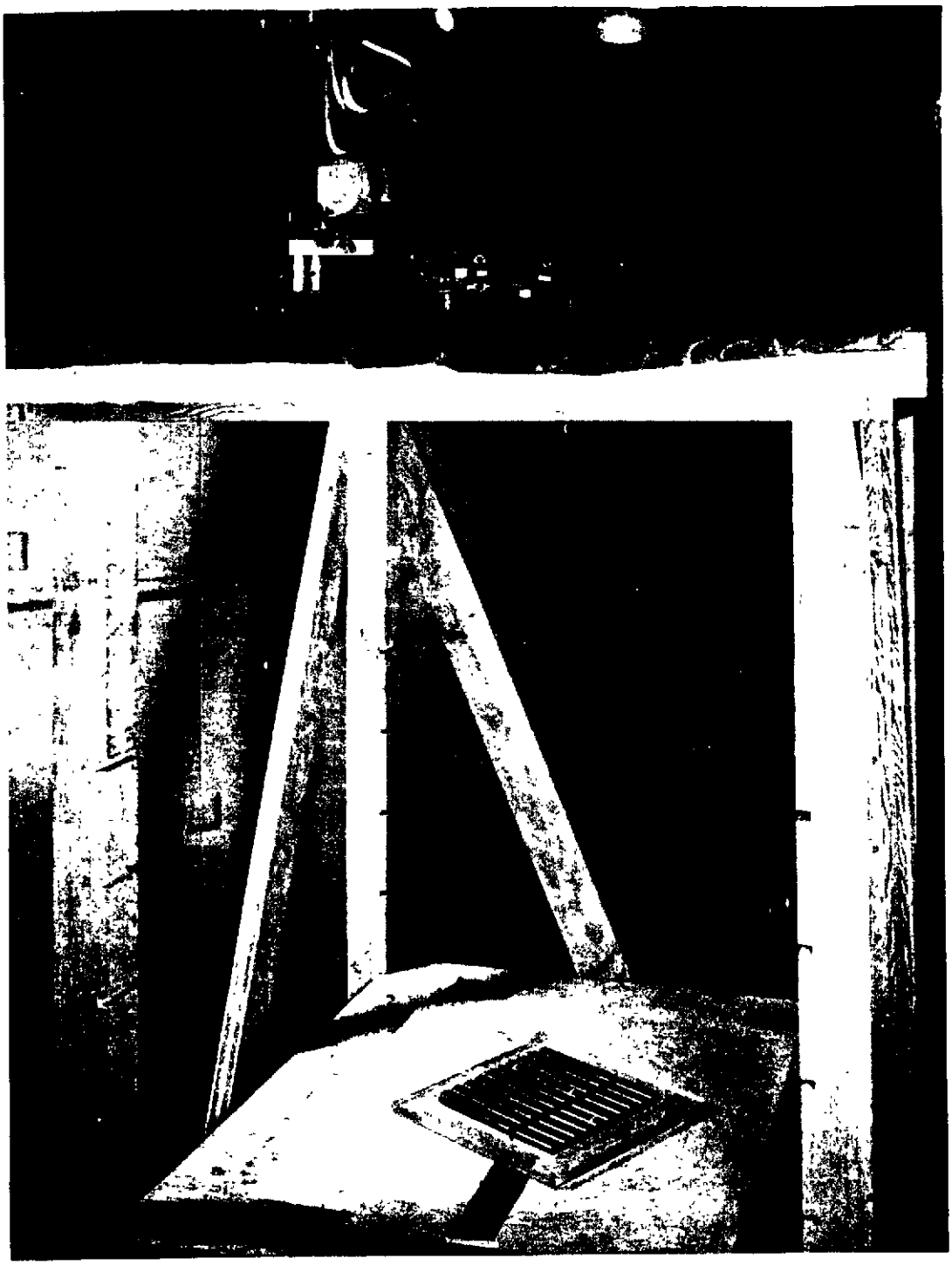

Fig. 4.4 Method of Calibrating Ionization Chambers by Exposure to X Rays.

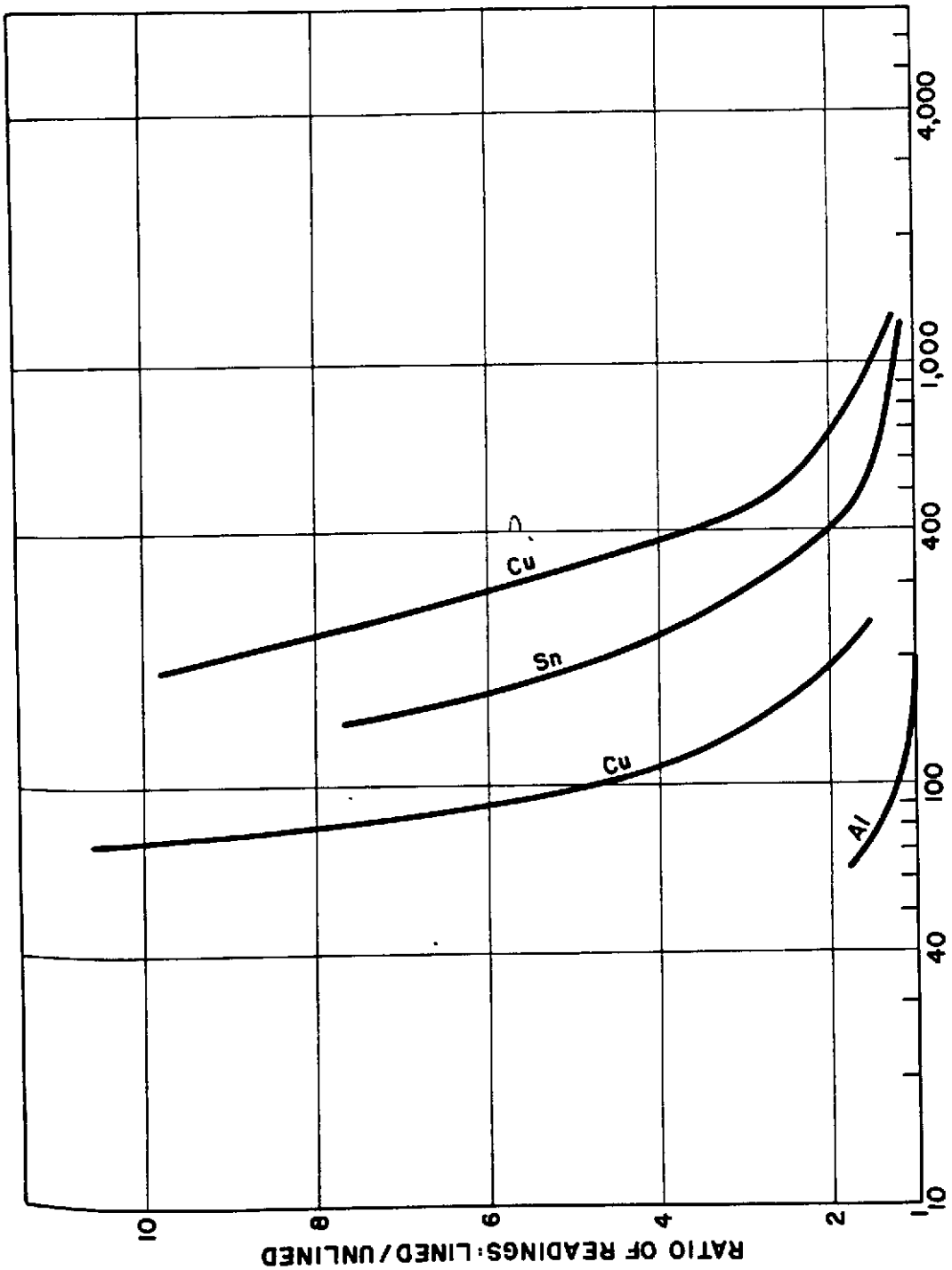

Fig. 4.5 USNRDL Calibration Curve for 2-r Ionization Chambers.

TABLE 4.1

USNRDL Calibration Points for Energy-dependent Chambers

Source	Tube Potential (kv)	Filter (mm)	Half-value Layer (mm)	Effective Energy (Mev)
Co^{60}	-	-	-	1.25
1000-kv X-ray(a)	1,000	18.8 Pb	7.68 Pb	0.860
1000-kv X-ray(a)	1,000	-	3.44 Pb	0.450
1000-kv X-ray	1,000	-	2.30 Pb	0.350
400-kv X-ray	400	6.0 Cu	4.9 Cu	0.198
250-kv X-ray	250	6.0 Cu	3.68 Cu	0.149
250-kv X-ray	220	3.28 Cu	2.51 Cu	0.119
250-kv X-ray	200	2.0 Cu	1.73 Cu	0.098
250-kv X-ray	170	0.7 Cu	0.75 Cu	0.074
250-kv X-ray	150	0.42 Cu	0.59 Cu	0.065

(a) Transmission targets; all others are reflection targets.

TABLE 4.2

NBS Calibration Points for Energy-dependent Chambers

Source	Tube Potential (kv)	Filter (mm)	Effective Energy (Mev)
Co^{60}	-	-	1.200
1000-kv X-ray	1,000	45.4 Pb	0.840
1000-kv X-ray	700	14.0 Pb	0.510
250-kv X-ray	250	3.30 Pb + 14.7 Cu	0.225
250-kv X-ray	200	1.65 Pb + 9.74 Cu	0.180
250-kv X-ray	150	14.70 Cu	0.130
250-kv X-ray	100	4.99 Cu	0.086
250-kv X-ray	80	2.54 Cu	0.068
250-kv X-ray	60	0.90 Cu + 4.03 Al	0.050
250-kv X-ray	40	0.11 Cu + 4.03 Al	0.032
250-kv X-ray	30	2.00 Al	0.025

PROJECT 2.4a

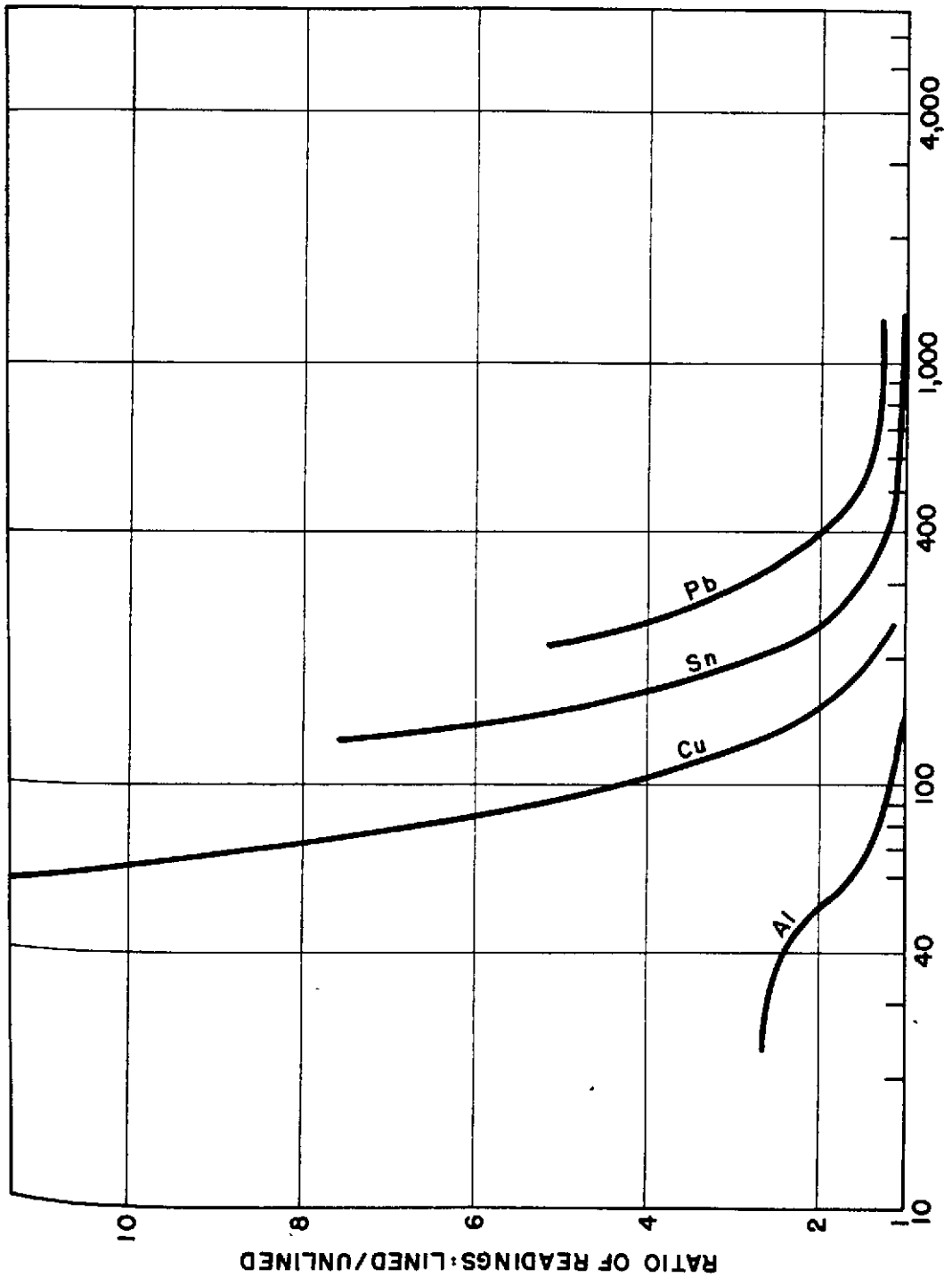

Fig. 4.6 NBS Calibration Curve for 2-r Ionization Chambers.

The NBS calibration curves are for single chambers exposed in air under conditions of negligible scattering and represent an absolute calibration for the chambers involved. More detailed information regarding the NBS calibration may be obtained by reference to a similar study by F. H. Attix.[2,3]

The survey instruments were calibrated in a similar manner except that lined and unlined instruments were exposed to the radiation successively rather than simultaneously. Calibrations were made with filtered X rays having effective energies from 88 to 212 kev. Figures 4.8 and 4.8 illustrate the method of shielded exposure to the 250-kv set. Radium and cobalt 60 provided calibrating radiation of higher energy to which the instruments were exposed by the device shown in Fig. 4.9. Table 4.3 lists the calibration points.

TABLE 4.3

Calibration Points for Energy-dependent Survey Instruments

Source	Tube Potential (kv)	Filter (mm)	Half-value Layer (mm)	Effective Energy (Mev)
Co^{60}	-	-	-	1.25
Radium	-	-	-	0.8
250-kv X-ray	250	8.1 Pb	0.805 Pb	0.212
250-kv X-ray	200	5.4 Pb	0.50 Pb	0.177
250-kv X-ray	150	28 Cu	2.8 Cu	0.125
250-kv X-ray	100	11 Cu	1.2 Cu	0.088

4.3.2 Field Measurements

To determine the effective energy of early gamma radiation plus cloud and early fall-out gamma radiation, selected groups of chambers were placed in the field prior to each shot and exposed to all radiations from time zero to approximately H + 3 hr. For both the surface shot and the underground shot, eight exposure stations were established along a radial line south of ground zero. Each station consisted of

---

[2] F. H. Attix, "Calibration Study of Five Modified 1-r Argonne Type Ionization Chambers for U. S. Naval Radiological Defense Laboratory", National Bureau of Standards Report 1325, November, 1951.

[3] E. Tochilin and P. R. Howland, "Interpretation of Survey-meter Data", Operation GREENHOUSE, Project 6.5, August, 1951.

PROJECT 2.4a

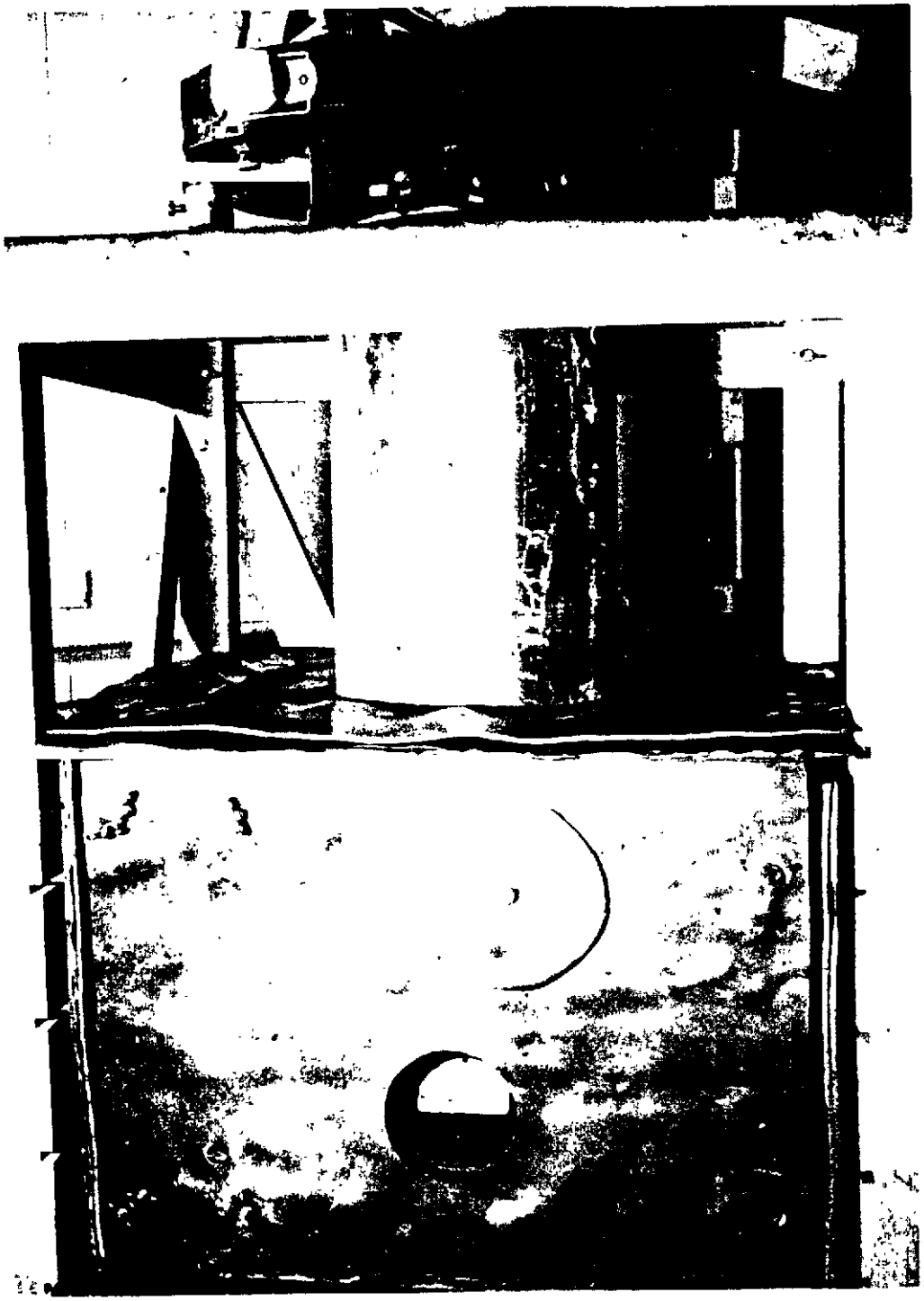

Fig. 4.7 Method of Calibrating Survey Instrument by Shielded Exposure to X Rays; Meter Seen through Hole in Shield Door.

Fig. 4.8 Method of Calibrating Survey Instrument by Shielded Exposure to X Rays; Interior of Shield with Instrument in Calibrating Position.

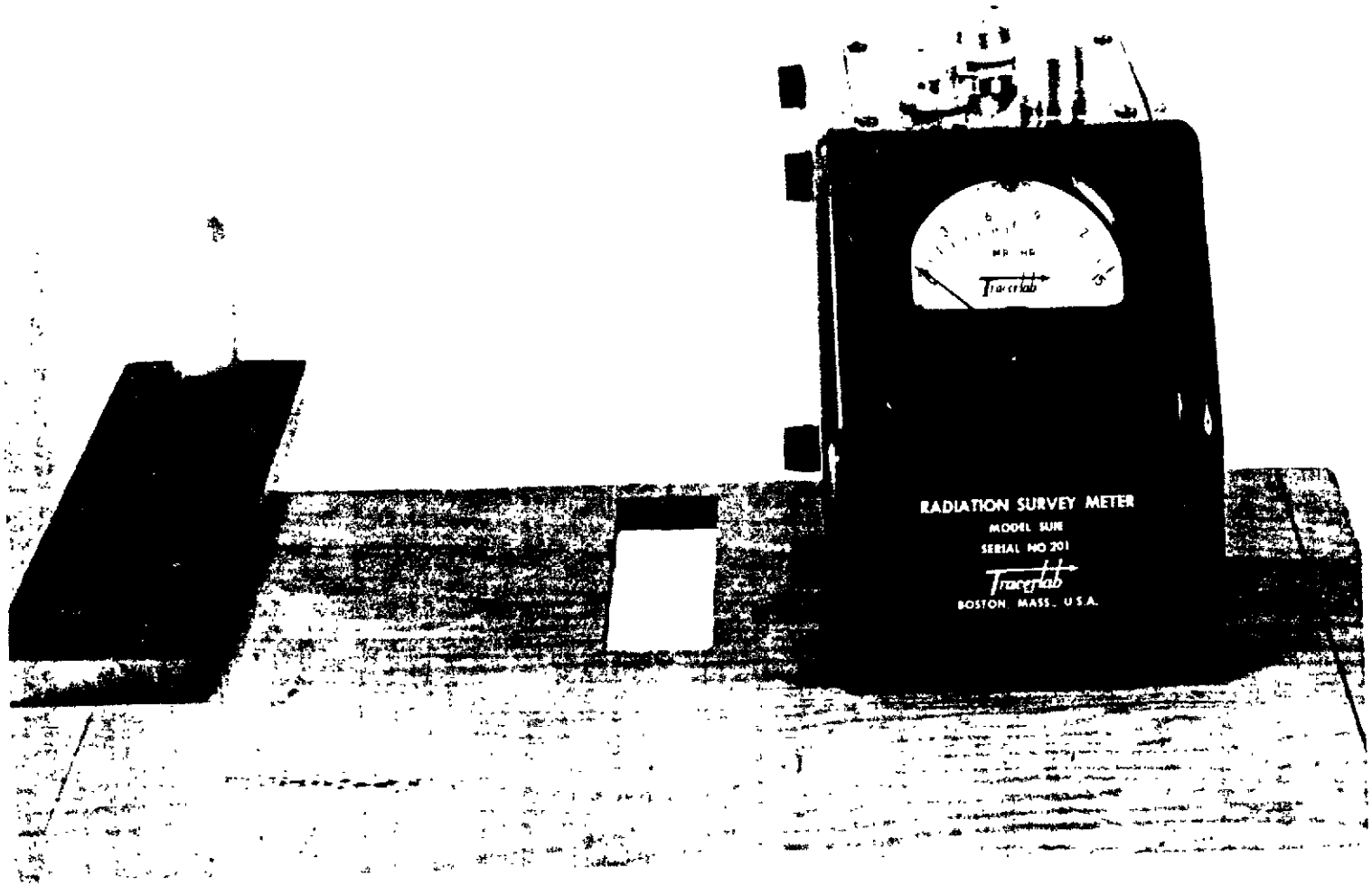

Fig. 4.9 Method of Calibrating Survey Instruments by Exposure to Radium and Cobalt 60.

twelve chambers housed in a drilled Lucite block, 2 3/4 x 2 1/4 x 1 3/4 in. which was suspended by springs at the center of a 40 x 40 x 40 in. wooden box. The block and its chambers are illustrated in Fig. 4.10. The wooden box was fastened to the ground with wire and stakes to prevent movement with the shock wave. Most of the chambers were recovered and read as soon as personnel were admitted to the area after the shot. The data on the surface shot and on the underground shot are presented in Tables 4.4 and 4.5 respectively. Many of the chambers yielded no ratios because of

TABLE 4.4

Chamber Measurements on Prompt Radiation, Surface Shot

Distance South of Ground Zero (ft)	Dose (r)	Chamber Range (r)	Chamber Lining	Ratio: Lined/Unlined	Effective Energy (kev)
3,600	26.4	90	Cu	1.71	220
		90	Sn	2.22	338
		90	Pb	2.74	430
4,200	11.2	90	Cu	1.43	>250
		90	Sn	1.93	390
		90	Pb	2.14	565
		30	Cu	1.70	>250
		30	Sn	2.30	350
		30	Pb	2.42	490
4,800	5.4	90	Cu	1.43	>250
		90	Sn	1.86	410
		90	Pb	2.14	565
		30	Cu	1.80	250
		30	Sn	2.00	410
		30	Pb	2.20	540
6,000	0.9	2	Cu	1.33	>250
		2	Sn	2.00	417
7,200	0.2	2	Cu	1.37	>250
		2	Sn	2.00	418
		2	Pb	2.63	525

off-scale readings. For this reason no data were obtained at stations closer than 3,600 ft for either shot. One group of chambers, located at 600 ft south for the underground shot, was never recovered because of the intense residual radiation at that station.

Measurements on the effective gamma-ray energy of the residual fission-product activity began five hours post shot and were

PROJECT 2.4a

TABLE 4.5

Chamber Measurements on Prompt Radiation, Underground Shot

Distance South of Ground Zero (ft)	Dose (r)	Chamber Range (r)	Chamber Lining	Ratio: Lined/Unlined	Effective Energy (kev)
3,600	35.8	90	Cu	1.8	210
4,200	15.7	90	Cu	1.57	> 250
		90	Sn	2.54	298
4,800	8.2	90	Cu	1.71	220
		90	Sn	2.71	281
		90	Pb	3.15	376
		30	Cu	1.54	> 250
		30	Sn	2.44	310
		30	Pb	2.72	430

made every day for two weeks. Selected groups of chambers were exposed in the field after each shot. Each exposure unit consisted of twelve chambers, a Lucite tray and a 30-in. tripod, as shown in Figs. 4.11 and 4.12. These tripods were stationed about ground zero on south, northwest and northeast lines for the surface shot; and on a south line for the underground shot. Exposures were made to residual radiation for 1 to 170 hr depending on field intensity at the station and the range of the chambers used there. The field intensities varied from 3 to over 5,000 mr/hr. The chambers were charged in a radiation-free area and taken to an appropriate radiation field. After exposure the chambers were removed again to a radiation-free area, read, and recharged for another exposure. The results of chamber measurements on the surface and the underground shots are presented in Tables 4.6 and 4.7, respectively.

The energy-dependent survey instruments were used in the field in conjunction with the ionization chambers. A lined and an unlined survey instrument were supported at chest height in a field of appropriate intensity, and the readings recorded. The lined instrument was then replaced by one with a different type lining and the reading again taken keeping the reading on the unlined instrument unchanged. Each instrument with a different metallic lining was thus used with the same unlined instrument.

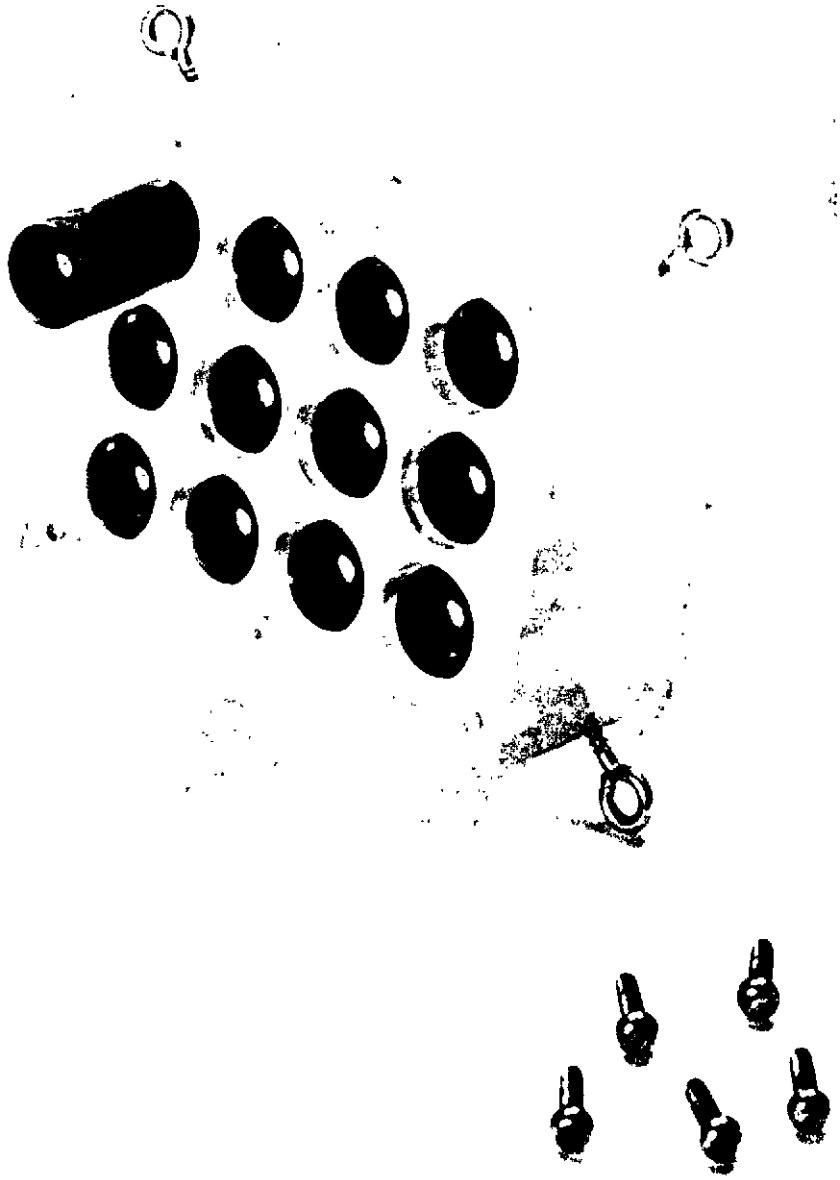

Fig. 4.10 Support Block and Ionization Chambers for Exposure to Prompt Gamma Radiation.

Fig. 4.11 Lucite Exposure Tray with Ionization Chambers.

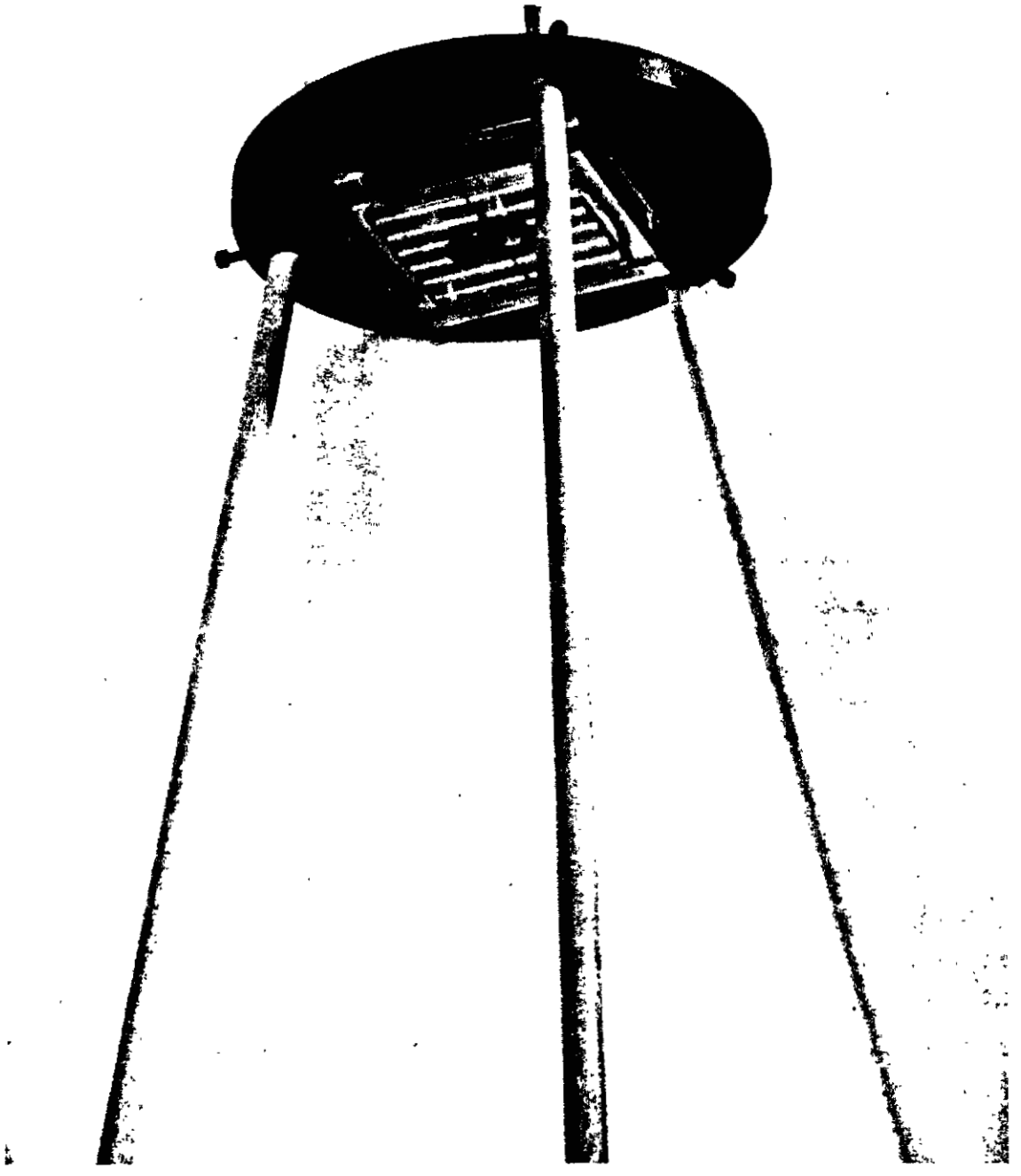

Fig. 4.12 Chambers and Tray in Tripod for Exposure to Residual Radiation.

TABLE 4.6

Chamber Measurements on Residual Radiation, Surface Shot

Distance from Ground Zero (ft)	Time Chamber Placed in Field after Shot (hr)	Total Exposure Time (hr)	Total Dose (r)	Chamber Range (r)	Chamber Lining	Ratio: Lined/Unlined	Effective Energy (kev)
2,000 S	5.02	21.32	0.57	2 2	Al Cu	1.07 3.15	140 134
2,000 S	5.02	21.32	0.57	2 2	Al Cu	1.18 3.25	105 130
2,000 S	5.02	21.32	0.57	2	Cu	3.19	132
1,100 S	5.15	44.52	12.01	90 90	Cu Sn	3.48 6.69	126 143
1,100 S	5.15	21.08	8.64	30	Cu	3.60	116
1,600 S	27.55	22.17	0.45	2 2	Al Cu	1.35 4.30	86 113
1,600 S	27.55	22.17	0.46	2	Cu	4.37	113
2,000 S	27.27	46.68	0.22	2 2	Al Cu	1.2 4.33	103 113
2,000 S	27.27	22.30	0.12	2 2 2	Cu Sn Pb	4.45 10.71 11.5	111 - -
2,000 NE	27.93	21.43	0.43	2 2	Al Cu	1.00 4.01	- 117
2,000 NE	27.93	21.43	0.35	2	Cu	4.40	112
2,400 NW	51.87	3.73	0.57	2	Al	1.03	>140
1,300 NE	50.80	3.78	0.37	2	Cu	5.07	105
1,015 S	51.35	3.65	0.38	2	Al	1.37	85
1,100 S	51.28	3.72	0.33	2	Cu	5.27	103
1,800 NE	54.85	18.40	0.32	2	Cu	4.32	113
1,600 S	55.27	19.63	0.13	2 2	Al Cu	1.25 6.06	96 97
1,500 S	55.32	18.58	0.23	2	Cu	5.59	100
3,200 NW	55.90	19.13	0.34	2	Cu	5.02	105

TABLE 4.6 (Continued)

Chamber Measurements on Residual Radiation, Surface Shot

Distance from Ground Zero (ft)	Time Chamber Placed in Field after Shot (hr)	Total Exposure Time (hr)	Total Dose (r)	Chamber Range (r)	Chamber Lining	Ratio: Lined/Unlined	Effective Energy (kev)
650 S	74.57	24.50	7.38	90	Cu	5.29	85
2,300 NW	75.48	23.43	1.64	30 30	Cu Sn	6.23 12.9	87 -
2,500 NW	75.42	3.17	0.20	2 2	Al Cu	1.18 5.17	105 104
1,100 NE	73.63	26.72	2.04	30	Cu	6.81	83
1,050 S	74.45	3.67	0.22	2 2	Al Cu	1.30 5.69	90 99
1,270 NE	73.55	4.05	0.21	2	Cu	5.99	97
1,100 S	74.43	3.68	0.17	2 2	Al Cu	1.33 6.07	87 92
2,000 S	74.33	24.87	0.02	2 2	Cu Sn	9.00 21.00	- -
1,700 NE	77.85	22.6	0.12	2	Cu	6.20	95
1,450 S	78.42	20.72	0.16	2 2	Al Cu	1.38 6.57	84 93
1,500 S	78.45	20.70	0.14	2 2 2	Al Cu Sn	1.14 5.41 1.28	113 102 -
3,200 NW	79.03	19.08	0.20	2 2	Al Cu	1.27 5.63	93 100
2,000 S	99.73	170.73	0.20	2 2	Al Cu	1.18 3.7	109 122
1,750 S	99.82	100.6	0.15	2 2	Al Cu	1.29 5.66	93 100
700 S	99.97	100.45	7.09	90	Cu	5.34	85
1,100 S	99.92	100.50	2.22	30	Cu	5.32	93
2,160 NE	100.88	99.20	0.12	2 2	Cu Sn	5.22 12.9	103 -

TABLE 4.6 (Continued)

Chamber Measurements on Residual Radiation, Surface Shot

Distance from Ground Zero (ft)	Time Chamber Placed in Field after Shot (hr)	Total Exposure Time (hr)	Total Dose (r)	Chamber Range (r)	Chamber Lining	Ratio: Lined/Unlined	Effective Energy (kev)
2,160 NE	100.88	99.20	0.13	2 2	Al Cu	1.12 5.26	120 103
1,250 NE	100.98	99.10	2.61	30	Cu	5.7	90
1,100 NE	101.03	122.75	5.77	90	Cu	4.59	92
1,100 S	226.2	21.9	0.18	2 2	Al Cu	1.09 5.86	130 98
1,200 S	226.32	21.95	0.11	2 2	Al Cu	1.00 5.64	>140 100
415 S	248.15	22.25	8.58	90 90	Cu Sn	3.15 6.28	115 147
1,100 S	248.83	22.35	0.29	2	Cu	3.82	120
300 S	270.93	18.23	10.7	90 90	Cu Sn	3.33 6.82	110 140
975 S	270.85	18.40	0.22	2 2	Al Cu	1.25 5.01	96 105
400 S	270.32	1.02	0.33	2	Cu	4.0	117
- (a)	270.35	0.98	4.19	30 30	Cu Sn	3.12 6.18	130 160
450 S	271.58	17.62	3.18	30 30	Cu Sn	4.22 8.72	104 -
200 S	289.15	25.38	16.60	90	Cu	3.11	115
900 S	289.13	25.47	0.26	2	Cu	5.56	101
1,100 S	314.45	47.13	0.22	2 2	Al Cu	1.43 4.77	80 108
450 S	314.48	23.10	3.29	30 30	Cu Sn	3.73 7.31	113 150

(a) Crater lip.

PROJECT 2.4a

TABLE 4.6 (Continued)

Chamber Measurements on Residual Radiation, Surface Shot

Distance from Ground Zero (ft)	Time Chamber Placed in Field after Shot (hr)	Total Exposure Time (hr)	Total Dose (r)	Chamber Range (r)	Chamber Lining	Ratio: Lined/Unlined	Effective Energy (kev)
200 S	314.53	23.03	14.0	90 90	Cu Sn	2.77 5.81	127 156
900 S	314.80	22.80	0.20	2	Cu	5.22	103
750 S	340.33	21.25	0.29	2	Cu	4.84	107
400 S	340.68	20.87	4.54	30 30	Cu Sn	3.73 6.32	113 158
150 S	340.72	20.82	12.7	90 90	Cu Sn	2.75 5.47	128 163

TABLE 4.7

Chamber Measurements on Residual Radiation, Underground Shot

Distance South of Ground Zero (ft)	Time Chamber Placed in Field after Shot (hr)	Total Exposure Time (hr)	Total Dose (r)	Chamber Range (r)	Chamber Lining	Ratio: Lined/Unlined	Effective Energy (kev)
2,300	4.48	18.23	2.28	90 90	Cu Sn	2.67 5.67	132 159
1,815	23.98	23.08	3.09	30 30	Cu Sn	3.65 6.61	115 155
1,780	24.00	22.97	5.63	90 90	Cu Sn	2.9 5.70	121 158
1,100	46.92	1.15	4.81	30 30	Cu Sn	2.99 5.12	137 173

PROJECT 2.4a

TABLE 4.7 (Continued)

Chamber Measurements on Residual Radiation, Underground Shot

Distance South of Ground Zero (ft)	Time Chamber Placed in Field after Shot (hr)	Total Exposure Time (hr)	Total Dose (r)	Chamber Range (r)	Chamber Lining	Ratio: Lined/Unlined	Effective Energy (kev)
1,750	46.83	1.20	0.354	2	Cu	2.82	144
1,000	46.92	2.50	14.7	90 90	Cu Sn	2.75 4.81	128 178
1,690	49.33	21.57	9.62	90 90	Cu Sn	2.56 4.43	137 190
1,780	49.27	21.65	2.60	30 30	Cu Sn	3.71 6.74	113 154
5,100	49.13	21.83	0.27	2	Cu	4.1	116
5,100	70.72	24.5	0.27	2	Cu	4.02	117
1,715	70.88	24.28	4.16	30 30	Cu Sn	2.91 4.88	140 178
1,690	70.90	47.05	12.9	90 90	Cu Sn	2.55 4.27	138 195
1,520	72.83	23.08	13.1	90 90	Cu Sn	2.47 4.62	142 183
1,750	95.1	1.90	0.199	2 2	Cu Sn	3.1 7.08	134 157
1,100	95.17	1.83	2.9	30 30	Cu Sn	3.03 6.00	135 160
850	95.17	1.83	8.93	90 90	Cu Sn	2.76 5.40	127 164
2,750	96.92	21.08	0.24	2 2	Cu Sn	3.3 7.67	129 150
1,700	96.95	21.02	3.57	30 30	Cu Sn	3.08 4.96	133 176
1,230	96.98	20.12	11.1	90 90	Cu Sn	3.01 5.88	118 155

PROJECT 2.4a

For the surface burst, measurements were taken about ground zero on south, northeast and northwest lines at distances from 700 to 3,200 ft beginning five hours post shot. Measurements on the contamination from the underground burst were taken on a south line at distances from 1,800 to 3,000 ft beginning five hours post shot. The results of these readings are presented in Tables 4.8 and 4.9.

TABLE 4.8

Survey Instrument Measurements on Residual Radiation, Surface Shot

Distance from Ground Zero (ft)	Time of Measurement after Shot (hr)	Field Intensity (mr/hr)	Chamber Lining	Ratio: Lined/ Unlined	Effective Energy (kev)
2,000 S	5.25	87	Cu Sn Pb	2.87 6.21 9.20	169 197 250
2,400 S	5.32	35	Cu Sn Pb	3.43 5.72 8.58	157 200 264
3,000 S	5.35	10.2	Cu Sn Pb	2.45 5.78 8.13	176 200 275
2,600 NE	28.17	8.5	Al	1.18	>140
2,600 NE	28.17	8.9	Cu Sn	3.94 8.1	149 187
2,600 NE	28.17	9	Al Cu Sn	1.2 4.0 8.22	>140 148 187
3,200 NW	79.08	2.3	Al Cu Sn	1.3 5.57 10.9	113 124 172
2,550 NW	79.16	9.7	Al Cu Sn	1.29 4.95 10.2	116 132 176
700 S	100.0	2	Al Cu	1.48 6.45	93 112
700 S	100.0	1.5	Al Cu	1.6 7.27	85 103

PROJECT 2.4a

TABLE 4.8 (Continued)

Survey Instrument Measurements on Residual Radiation,
Surface Shot

Distance from Ground Zero (ft)	Time of Measurement after Shot (hr)	Field Intensity (mr/hr)	Chamber Lining	Ratio: Lined/ Unlined	Effective Energy (kev)
1,100 NE	101.08	14.2	Al Cu	1.34 5.7	106 123
1,100 NE	101.08	11.5	Al Cu Sn	1.30 5.65 11.1	115 124 171
250 S	270.92	10.4	Al	1.27	120
250 S	270.92	9.0	Al	1.23	130

TABLE 4.9

Survey Instrument Measurements on Residual Radiation,
Underground Shot

Distance South of Ground Zero (ft)	Time of Measurement after Shot (hr)	Field Intensity (mr/hr)	Chamber Lining	Ratio: Lined/ Unlined	Effective Energy (kev)
2,300 2,300	4.5 4.5	4.3 3.1	Cu Cu	3.45 4.17	157 145
3,000	4.62	15	Al Cu Sn	1.00 3.26 6.87	>140 160 193
3,000	4.62	13.5	Al Cu Sn	1.04 3.48 7.11	>140 156 192
2,350	22.60	10.1	Al Cu Sn	1.26 3.66 7.43	122 153 190
2,350	22.60	8.8	Al Cu Sn	1.23 4.09 8.07	130 147 188

TABLE 4.9 (Continued)

Survey Instrument Measurements on Residual Radiation, Underground Shot

Distance South of Ground Zero (ft)	Time of Measurement after Shot (hr)	Field Intensity (mr/hr)	Chamber Lining	Ratio: Lined/ Unlined	Effective Energy (kev)
2,700	22.82	6.0	Al Cu Sn	1.23 3.67 7.66	130 153 189
2,700	22.82	6.5	Al Sn	1.19 7.09	>140 192
2,700	22.82	6.2	Cu	3.71	153
1,820	24.25	28	Al Cu	1.29 4.07	115 146
1,820	24.25	20	Al Cu	1.30 4.60	113 138

Measurements with both the chambers and the survey instruments were carried out in such a way as to obtain the best data for determining how the effective energy of the residual gamma radiation varies with locality and with time after shot.

4.4 DISCUSSION

The NBS calibration of Landsverk 2-r chambers, given in Table 4.2, differs in several respects from the USNRDL calibration shown in Table 4.1. The NBS calibration points are for heavily filtered X-ray beams. The resulting X-ray spectrum is narrow and approaches the idealized calibration condition of using a single-energy gamma-ray isotope. Furthermore, chambers were exposed individually, thus minimizing any scattering that could take place. Such conditions allow absolute calibration of the individual chambers involved.

Using the 250-kv X-ray unit (the calibration points for which are given in Table 4.1) a series of measurements was made with individually-exposed aluminum- and copper-lined chambers, and compared with the NBS calibration. For effective energies from 65 to 149 kev the calibration data are identical. Although the USNRDL calibration points are for a comparatively broad spectrum they are in complete agreement with the NBS

narrow-beam calibration. The exposures made with the 400-kv and 1,000-kv X-ray units (Table 4.1) utilized a beam subjected to little or no filtration, thus giving a very broad spectrum. Differences between the USNRDL and NBS calibration curves for tin- and lead-lined chambers (Figs. 4.5 and 4.6) are primarily due to large differences in the spectral distribution of the X-ray beams used for calibration.

Throughout the report the USNRDL calibration curves were used, because this calibration was carried out in Lucite containers to duplicate exposure conditions in the field, and because experimental observations indicated that a broad energy spectrum would be encountered in the field.

4.4.1 Prompt Radiation

Measurements of the effective gamma-ray energy from combined early-gamma plus cloud and early fall-out gamma radiation were made using the energy-dependent ionization chambers. The data for the surface shot, presented in Table 4.4, show that the effective gamma-ray energy measured at the various stations is dependent upon the type of chamber used. At 4,200 ft south of ground zero the average of two readings for various chambers gave effective energies of greater than 250 kev for the copper chambers, 379 kev for the tin-lined chambers, and 528 kev for the lead-lined chambers. The discrepancy among the three readings immediately raises the question as to which, if any, can be considered valid. To answer this question requires some knowledge of the practical limitations of the different types of chambers involved.

A study of Fig. 4.5, the representative calibration curve for the 2-r chambers, shows that each type of metal-lined chamber is designed for use over a limited energy spectrum. For example, using the copper-lined chamber, energies can be determined to values not greater than 250 kev. For any gamma-ray spectrum containing maximum energies no greater than 250 kev, copper-lined and air-wall chambers would be used. However, consider the same chambers exposed to an unfiltered beam of X rays from a million-volt machine. With no filtration the spectrum is sufficiently broad so that a portion extends below 250 kev. This part of the spectrum will produce a greater ionization in the copper chamber than in the air-wall chamber. The spectrum above 250 kev will produce equal ionization per unit volume in each chamber and contribute nothing to the ionization ratio. Thus, the chamber pair is blind to much of the spectrum and indicates an effective energy only of that portion of the spectrum to which it is sensitive. For linings of elements possessing higher atomic numbers this sensitivity is extended toward higher energies. A lead-chamber pair exposed to the same million-volt X-ray beam will "see" a more representative portion of the gamma-ray spectrum than will the copper-chamber pair.

A consideration of the probable spectrum of the radiation resulting from the combined prompt gamma radiation and the fission-product cloud would indicate a rather broad spectrum with a maximum energy extending above one Mev. On this basis the readings obtained with the lead-chamber pair using the USNRDL broad-spectrum calibration would be most representative of the gamma-ray effective energy. From Table 4.4, using the data obtained at 4,200 and 4,800 ft where two comparative readings are available, the effective energy from the combined prompt gamma radiation and fission-product cloud following the surface shot is between 490 and 565 kev.

Measurements of the prompt radiation from the underground shot are given in Table 4.5. Readings using the lead-chamber pair were made only at a distance of 4,860 ft south of ground zero. Effective energies ranging from 376 to 430 kev were obtained. These energies are significantly lower than those obtained at identical distances following the surface shot.

4.4.2 Residual Radiation Measured by Ionization Chambers

The effective energies obtained for the residual radiation following the surface shot are presented in Table 4.6. Readings were obtained primarily with aluminum- and copper-lined chambers. Intermittent readings were also taken with the tin-lined chambers. The agreement between energies read with the aluminum- and copper-lined chambers was excellent. A comparison indicates the following maximum and minimum values were obtained: 140 to 84 kev with the aluminum-lined chambers and 134 to 90 kev with the copper-lined chambers. The few readings obtained with the tin-lined chambers were approximately 30 kev higher than readings made at the same time with copper-lined chambers.

No uniform variation of effective energy with location or time is apparent from measurements with the ionization chambers. The combined effects of time and distance versus energy is illustrated for the surface shot in the three dimensional diagram given in Fig. 4.13 which clearly shows that the highest energies were observed close to the crater and at early times. At other localities and times the energies were less and varied from place to place in a virtually random manner.

The values for the surface shot contamination compared favorably with effective energies obtained for two tower shots at Operation GREENHOUSE for which the energies obtained with similar aluminum-lined and copper-lined chambers ranged between 83 and 127 kev.[4]

---

[4] E. Tochilin and P. R. Howland, op. cit.

PROJECT 2.4a

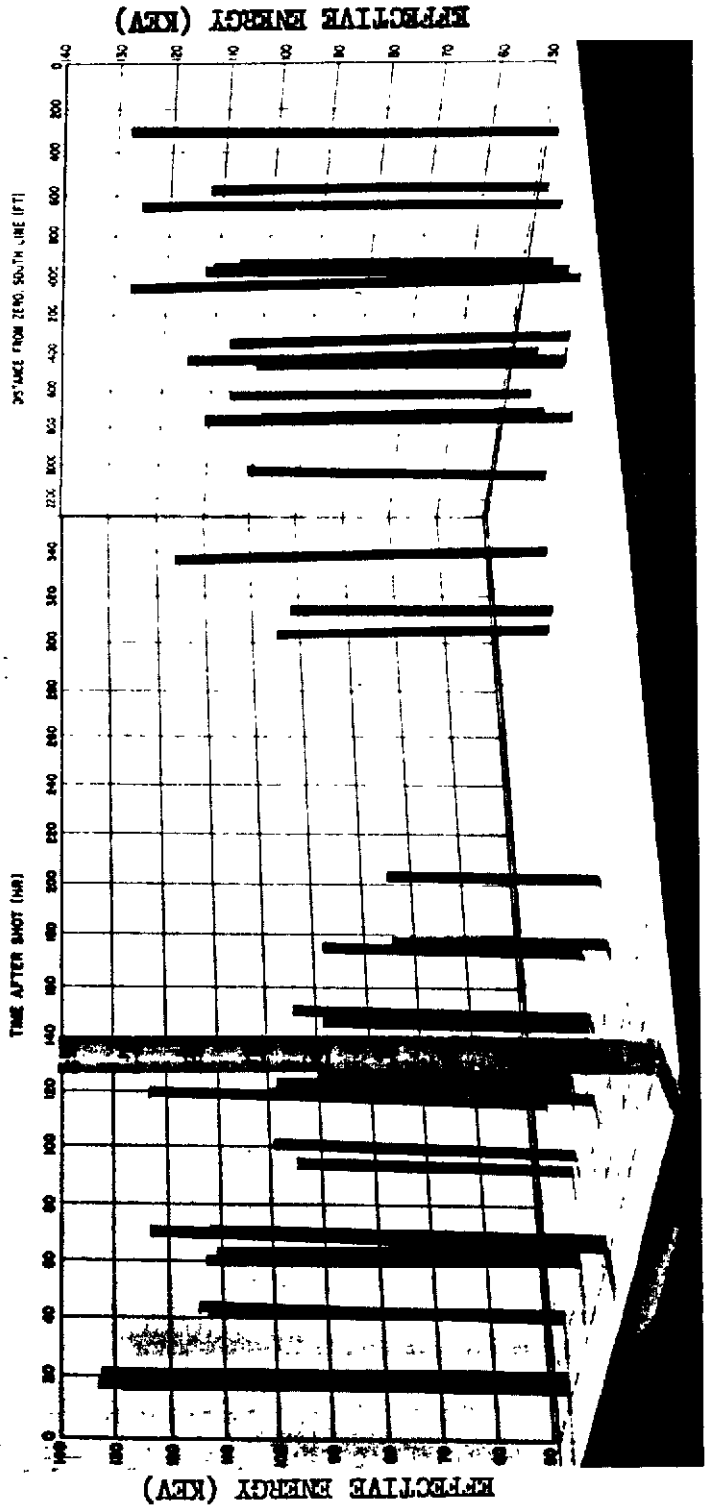

Fig. 4.13 Three Dimensional Map of Time, Distance, and Energy for the Surface Shot Contamination.

The residual gamma-ray effective energies obtained following the underground shot were measured with copper- and tin-lined chambers. A tabulation of all data obtained is presented in Table 4.7. No readings were made with the aluminum-lined chambers because of the high dose rates involved. Aluminum-lined chambers were available only in the 2-r group. The energies measured with copper-lined chambers ranged between 113 and 144 kev as compared to values between 154 and 195 kev obtained with the tin-lined chambers.

The residual effective energies associated with the underground shot were generally higher and more uniform than those for the surface shot. The underground burst produced a circular area of fine dust at a radius of approximately 1,750 ft from ground zero. Within this circle the radiation energy was distinctly higher than outside. Using the copper-lined chambers the radiation energy averaged 140 kev inside compared to 115 kev outside the circular area. Using the tin-lined chambers no differences in energy could be detected in the two regions.

Previously it was pointed out that valid measurements of effective energy could be made with the copper-lined chambers only if the gamma-ray spectrum did not extend to energies significantly above 250 kev. Similarly, aluminum-lined chambers will not read correctly if the energies encountered are above 150 kev. The close agreement between the readings obtained with both the aluminum-lined and copper-lined chambers strongly indicates that the gamma-ray spectrum as seen in the field contains no significant components of radiation possessing energies greater than 150 or 200 kev. This conclusion is supported by similar work performed by the Brookhaven group who obtained gamma-ray spectrum data in the field with a crystal spectrometer.[5] The tin-lined chamber readings are high because they are not able to resolve properly the low-energy portion of the spectrum. Although not shown in Fig. 4.5 the energy versus ratio curve for the tin-lined chambers bends over, and for energies below 60 kev becomes double-valued. Thus, when measuring any component of gamma radiation below 60 kev, the tin-lined chambers read high.

4.4.3 Residual Radiation Measured by Survey Instruments

The residual gamma-ray energy following both the surface and the underground shot was also measured using the modified type *SU-1E* survey instruments. Figure 4.14 shows, for the surface shot, the change in effective energy as a function of time. This curve was plotted from

[5] W. Bernstein, R. L. Chase, and J. B. H. Kuper, "Gamma-ray Spectrum Measurements of Residual Radiation", Operation JANGLE, Project 2.4c, April, 1952.

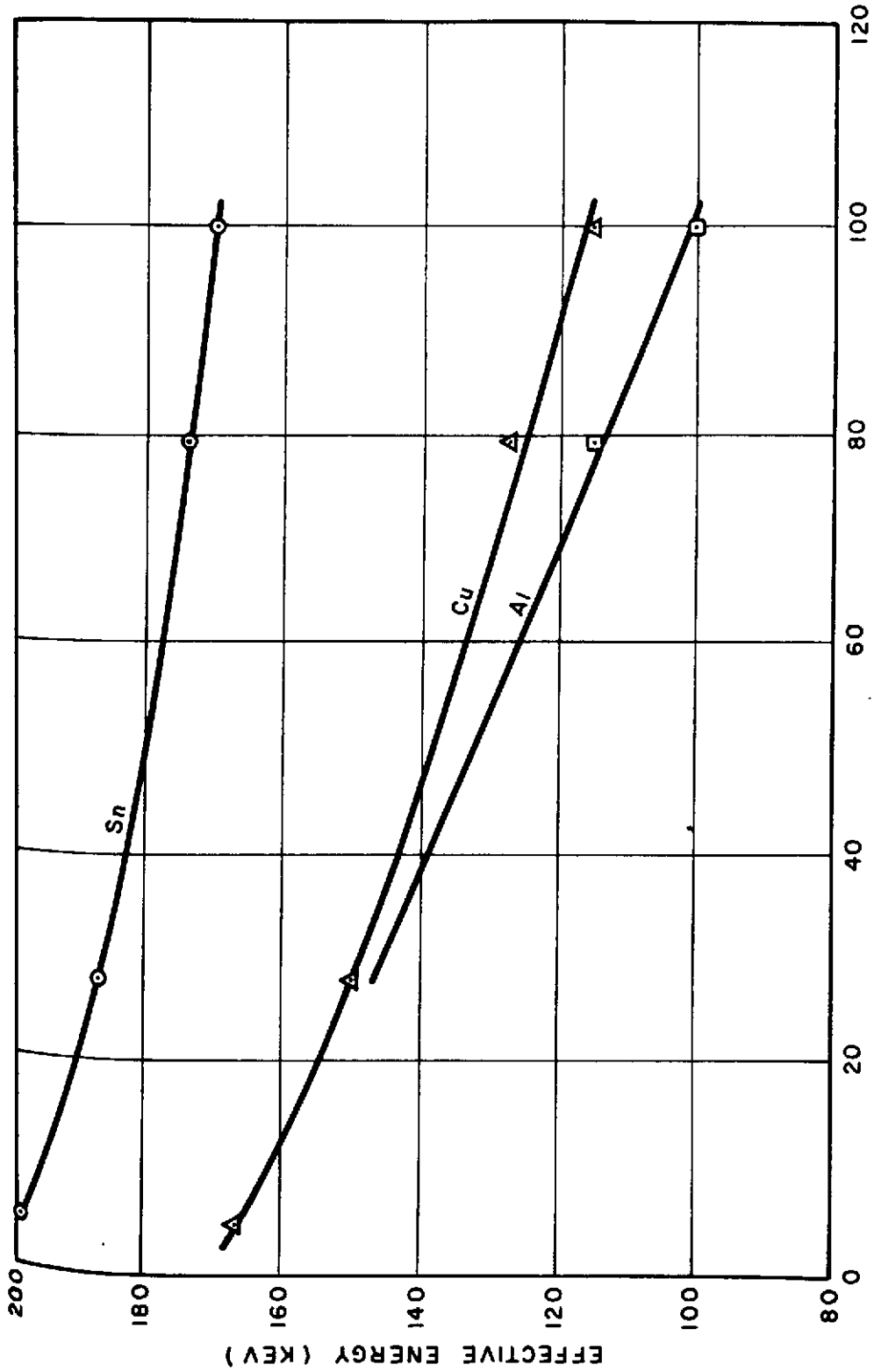

Fig. 4.14 Variation with Time of Residual Radiation Energy for the Surface Shot as Determined by Survey Instruments.

the data in Table 4.8, which tabulates all readings made with the survey instruments. As with the ionization chambers, measurements were made with aluminum-, copper- and tin-lined chambers. Significant is the high value of the energy observed at 5 hr compared to the other points. This large value was not evident with the ionization chambers placed in the field at the same time, possibly because they were exposed for an elapsed time of 21 hr before being read. The readings obtained with the aluminum- and copper-lined survey instruments are in general agreement with readings made at similar times and locations with the aluminum- and copper-lined ionization chambers. As already mentioned, these chambers will read correctly whereas the tin-lined chambers read high.

Effective gamma-ray energies measured with energy-dependent survey instruments following the underground shot are listed in Table 4.9. Readings were obtained only at 4.5 and 23 hr because at this time all operating personnel had received the maximum permissible dose for the operation. At 4.5 hr post shot the effective energy for the underground shot, like the surface shot, was high, averaging 158 kev with the copper-lined chambers.

Except for the readings made at 5 hr post shot, there is good agreement between survey meter measurements and ionization chamber measurements of effective gamma-ray energy. For this reason, the field measurements presented in the abstract and discussed in Chap. 5 (Conclusions) have been restricted to the measurements of gamma-ray energy made with the modified ionization chambers.

CHAPTER 5

CONCLUSIONS

5.1 CONCLUSIONS

The important properties of beta- and gamma-radiation fields arising from fission-product contamination can be summarized as follows:

5.1.1 Effective Gamma-ray Energy

1. The effective gamma-ray energy measured at times ranging from 5 to 340 hr following the surface shot, and at distances varying between 3,200 and 150 yd from ground zero, ranged between 84 and 140 kev.

2. The highest energies were observed in the vicinity of the crater and also at early times following the burst. At other localities and times the energies were less and varied in a random manner.

3. The effective energies for the surface shot were similar to those obtained for two tower shots at Operation GREENHOUSE, where the energies ranged between 83 and 127 kev.

4. The effective gamma-ray energy measured at times ranging from 5 to 97 hr following the underground shot, and at distances varying between 2,300 and 850 yd from ground zero, ranged between 113 and 144 kev.

5. The underground burst produced a circular area of fine dust about ground zero at a radius of approximately 1,700 ft. Within this circle the energy was distinctly higher, averaging 140 kev, as compared to 115 kev outside the circular area. The difference in energy within the two areas is due to geometry rather than any change in chemical composition of the fission products.

6. The effective energy of the combined early gamma plus cloud and early fall-out gamma radiation following the surface shot ranged between 430 and 565 kev.

7. The effective energy of the combined early gamma plus cloud and early fall-out gamma radiation following the underground shot ranged from 376 to 430 kev.

5.1.2 Equivalent Maximum Beta Energies

1. The equivalent maximum beta energy as determined from film pack measurements on early-time fall-out contamination was no greater than 1.7 Mev when averaged over an exposure period from time zero until 24 hr following the surface shot.

2. For the underground shot the equivalent maximum beta energy of the early-time fall-out contamination was no greater than 2.0 Mev when averaged over an exposure period from time zero until 70 hr following the shot.

3. Since the beta energies presented for these two shots are averaged over the time intervals involved, somewhat higher equivalent maximum energies are to be expected within the first hour post shot. Other considerations indicate the energy within the first hour would not be much greater than 2 Mev.

4. A single post-shot measurement of the equivalent maximum beta energy at a height of 18 in. above the contaminated ground surface gave a value of 2.0 Mev for the surface shot. This exposure covered a 24-hr period starting at 4.5 hr post shot.

5. A series of post-shot measurements at a height of 18 in. gave an equivalent maximum beta energy of 1.7 Mev for the underground shot.

5.1.3 Beta-to-gamma Ratio

1. The ratio of beta-ray to gamma-ray ionization on the surface of film packets located from 3,500 to 12,000 ft north of ground zero ranged from 2 to 14 for the surface shot. No significant ratios were observed closer than 3,500 ft. The ratios are for an integrated exposure from time zero until 27.5 hr post shot.

2. The ratio of beta-ray to gamma-ray ionization on the surface of film packets located from 1,700 to 5,000 ft north of ground zero ranged from 6 to 20 for the underground shot. From 6,000 to 10,000 ft all films were overexposed. At 11,000 and 12,000 ft the two farthest locations at which films were placed, ratios of 22 and 24 were measured. The ratios are for an integrated exposure from time zero until 70 hr post shot.

3. The ratio of beta-ray to gamma-ray ionization made at a height of 18 in. above the ground following the surface shot and at 3,200 ft northwest of ground zero was 4. Due to adverse weather conditions this was the only exposure made.

4. The ratio of beta-ray to gamma-ray ionization made at a height of 18 in. above the ground at various locations following the underground shot averaged 19.

5. Extrapolating the beta-to-gamma ratio obtained from the post-shot packets at the underground shot to a distance of 1.5 in. gave a ratio of approximately 100 to 1. This is in contrast to a maximum ratio of 24 to 1 measured at the same distance by means of the fall-out packets. The difference exists because the fall-out packets were subjected to components of gamma radiation arising from the early-gamma plus cloud-gamma radiation which contributed no simultaneous beta radiation. Thus, even in the most highly contaminated areas of the underground shot, the fall-out film packets saw a component of gamma radiation which was 4 times greater than the gamma radiation received from the fission products deposited over the films.

OPERATION JANGLE

PROJECT 2.4b

GAMMA DEPTH DOSE MEASUREMENT IN UNIT-DENSITY MATERIAL

by

FRANCIS W. CHAMBERS, JR.

and

STAFF

of

THE NAVAL MEDICAL RESEARCH INSTITUTE

May 1952

Naval Medical Research Institute

National Naval Medical Center

Bethesda 14, Maryland

ACKNOWLEDGMENTS

Active participation in these field tests involved the following personnel: R. Sharp, ENS (MSC) USN; J. T. Istock, HMC, USN; and P. E. Thompson, HMC, USN.

Assisting in the preparation of equipment and pre- and post-test calibration were the following personnel of the Radiation Technology Division, Naval Medical Research Institute: J. E. Morgan, CDR (MSC) USN; and C. R. Biles, HMC, USN.

The assistance of other institutions has also been of value: D. T. O'Connor and his radiology group at the Naval Ordnance Laboratory, White Oak, Maryland, by permitting use of the 2- and 10-Mev General Electric X-ray units; Adair Morrison of the National Research Council of Canada made available a high-intensity source of Co^{60}; and John S. Laughlin of the Department of Radiology, University of Illinois, permitted calibration experiments with the 22-Mev Allis-Chalmers betatron.

Without the courtesies and cooperation of these various individuals and institutions, data in this report would have been seriously limited in scope and accuracy.

PROJECT 2.4b

CONTENTS

PROJECT 2.4b

ILLUSTRATIONS

TABLES

PROJECT 2.4b

ABSTRACT

Field measurements of biologically significant characteristics of gamma radiation from nuclear detonation tests for this operation are presented. Depth-dose measurements in media of approximately unit density were made, using ionization chambers of high electrical saturation and essentially flat wave-length response and DT-60 (phosphate glass) detectors which also had an essentially flat wave-length response.

Transmission curves at several distances for a 1.2-Kilotonnage surface burst and a 1.2 Kilotonnage underground burst indicate a constant value of radiation quality within the limits considered except where excessive fall-out was present. The limits were chosen to include the dose range near absolute probable lethality.

Comparative evaluation of depth-dose readings with various simulated sources indicate that a satisfactory laboratory equivalent to the initial gamma component of bomb radiation is offered by the 10-Mev betatron at the Naval Ordnance Laboratory, White Oak, Maryland.

CHAPTER 1

INTRODUCTION

1.1 OBJECTIVE

The objective of this experiment was to determine the dose arising from the initial radiation and the residual radiation up to approximately two hours after detonation at various depths in approximately unit density material, to measure the equilibrium dose at various upwind distances and to investigate the possibility of reproducing in the laboratory, the effective energy of a surface and underground nuclear detonation.

1.2 HISTORICAL BACKGROUND

Since the time that it became evident that ionizing radiation influenced living tissue, clinical radiologists and radiation physicists have been working to improve the techniques employed in evaluating the biological effects of radiation. An excellent paper by Quimby[1] gives a history of this valuable work.

It was realized very early that the distribution of gamma and X radiation in tissue depended upon the quality (wave length) of the radiation as well as the quantity. Investigators immediately began to look for a means of measuring the amount of radiation received at various depths in the body. It was not practical to measure the depth doses directly in the patient, so a substitute had to be found. Since tissue consists predominantly of water, it was decided that measurements could be made at various depths in a water bath and that the values would be approximately the same as if they were made in the tissue itself. This water bath came to be known as a phantom. It was not always convenient to use water for depth dose measurements; so the suitability of other substances was investigated and it was found that several materials could be used if their density and atomic number approximated that of water. Spiers[2] has presented a rather comprehensive analysis of the characteristics of some materials commonly used in phantoms for radiation measurement.

---

[1] Edith H. Quimby, Sc.D., "The History of Dosimetry in Roentgen Therapy", The American Journal of Roentgenology and Radium Therapy, LIV, No. 6, Dec 1945, 686-703.

[2] F. W. Spiers, "Materials for Depth Dose Measurement", Brit. J. Radiol., 16:90, 1943.

The use of suitable detectors and phantom materials has made it possible to estimate what effect various quantities and qualities of radiations will have at different depths in the body.

1.3 BASIC PRINCIPLES INVOLVED

When a monochromatic beam of gamma or X radiation interacts with a scattering medium, there will be quanta present of varying wave lengths due to the Compton effect. Individual quanta will have been scattered in traversing the medium, so the single wave length will have gradually disappeared and been replaced by a broad band of wave lengths extending away on the long wave-length side of the primary radiation. Since as a general rule the primary beam itself is not monochromatic, the spectral distribution at various points within the medium becomes even more complex.

When this complex spectral distribution is superimposed on the scattering phenomena, filtration effects, which tend to eliminate the longer wave lengths from both the primary and secondary radiation, are also introduced. The two sets of phenomena are acting in opposite directions so far as a resultant effective wave-length change is concerned; therefore, it is possible that a measurement of the quality of the primary beam would give little indication of the nature of the radiation within the scattering mass. Even an absorption curve in approximately unit-density material does not supply the radiologists and radiation physicist with the information he must have to evaluate the dose at various depths in the body, since it does not take into consideration the contribution of secondary scatter from what underlying tissue might exist.

It has, therefore, been the practice in radiology, whenever the quality of a beam of radiation is unknown, to place ionization chambers throughout a unit-density phantom which is irradiated under conditions similar to those used for the patient. These ionization chambers measure the amount of ionization taking place at the various locations in which they were placed. This information permits the radiologist and radiation physicist to calculate the dose received by various parts of the body and to evaluate the effects that might be produced.

CHAPTER 2

MATERIALS AND METHODS

2.1 GENERAL

Spherical lucite phantoms containing three types of detector, ionization chambers, film, and glass, were used for this project.

2.2 SPHERICAL PHANTOMS

2.2.1 Information Obtained from the Spheres

From the data obtained, it should be possible to calculate the absorption coefficient for broad-beam conditions in approximately unit-density material and to determine the equilibrium wall-thickness dose. At equilibrium wall thickness a ratio between the number of X-ray photons and secondary electrons is established and this ratio will remain constant as the primary beam is attenuated by further wall material.

2.2.2 Design of the Spheres

The spherical phantoms (Figs. 2.1 and 2.2) were so designed that the detectors in them could measure the integrated dose in approximately 4π geometry; however, the resultant geometry would depend upon the design of the detectors. The ionization chambers would record approximately a 4π field. This would not be true of the film and glass. It was necessary to add material for supports, so in the case of all spheres a constant value of six per cent of the surface was used for this purpose. The spheres were made of lucite and each had a central cavity of 5-cm diameter in which to place the detectors. The wall thicknesses surrounding this cavity were 0.6, 1.0, 1.6, 3, 5, 9, and 17.5 cm.

2.2.3 Detectors Used in the Spheres

Ionization chambers, film, and phosphate glass were used as detectors in the spheres.

A Sievert type ionization chamber was found to be the most suitable for use in this experiment. It is 5 millimeters in diameter and 20 millimeters long. A charge of 540 volts produces a voltage gradient of approximately 11,000 volts per centimeter. The

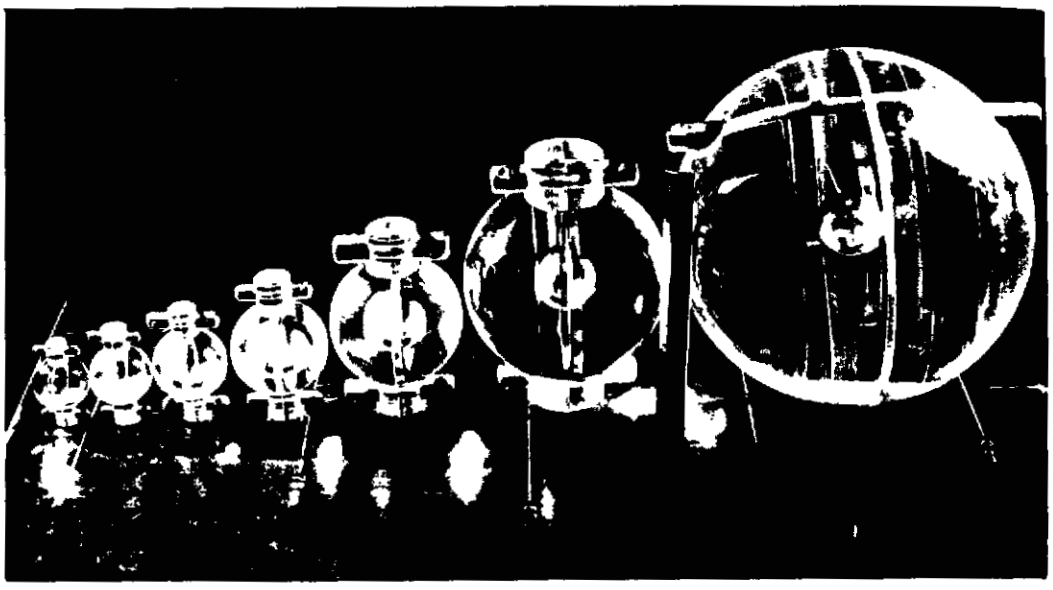

Fig. 2.1 Set of Seven Lucite Spheres

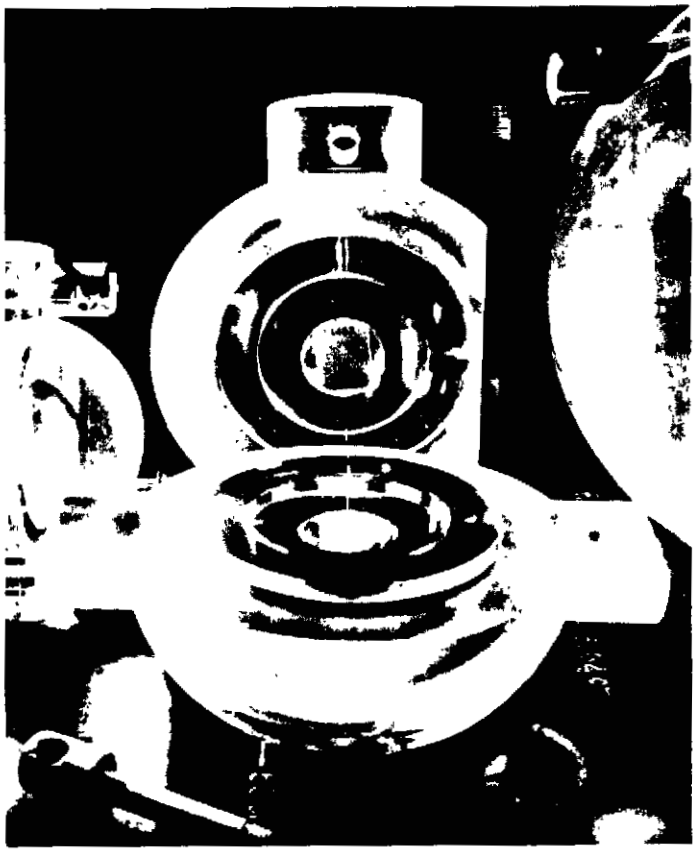

Fig. 2.2 Disassembled Sphere Showing Film Pack in Central Cavity

practical working range is from 50 to 650 r, the limits being set by the electrometer. The average leakage is less than one per cent in 24 hours. Under conditions of saturation voltage and equilibrium wall thickness the chamber is in good agreement with a 100 r Victoreen chamber from 100 Kev to approximately 5 Mev.

Navy Department Bureau of Ships DT-60 Radiac Detectors were used which contained phosphor glass. These detectors are enclosed in a case which reduces their energy dependence to approximately 20 per cent from 80 Kev to 1.2 Mev. The 10 to 600 r range of the detector is limited by the present reader and not the detector itself; therefore, the range could be extended, if desired, by designing a new reader.

Unshielded Adlux film was also used which was energy dependent; therefore, it could not be used for absorption measurements.

2.2.4 Control Studies

The spheres were used in pre- and post-test control studies to evaluate the response of the three detectors to various energies in approximately unit-density material. Calibration exposures were made from 50 to 800 r with various X-ray and betatron voltages between 200 KVP and 22 Mev, having effective energies of approximately 100 Kev, 400 Kev, 700 Kev, 1 Mev, 5 Mev, and 10 Mev, and also with a large Co^{60} gamma source. In this series each of the three types of detector was exposed, both individually and in conjunction with the other two, in each thickness of sphere.

2.2.5 Method of Exposing Spheres

The seven spheres of varying wall thickness were suspended about two feet from the ground on an "A" frame in such a manner that there would be the least chance of their shadowing each other (Fig. 2.3).

Five stations were used in each shot, a station being an "A" frame containing the seven spheres of varying wall thickness. For the surface shot, the stations extended along a line slightly south of west and were placed at A (750 yd), B (850 yd), C (950 yd), D (1,050 yd), and E (1,169 yd). For the underground shot, the stations extended along a line 10 degrees south of west and were placed at A (500 yd), B (600 yd), C (700 yd), D (800 yd), and E (1,000 yd).

2.3 SWINE PHANTOMS

Swine phantoms were placed at the same locations as the spheres.

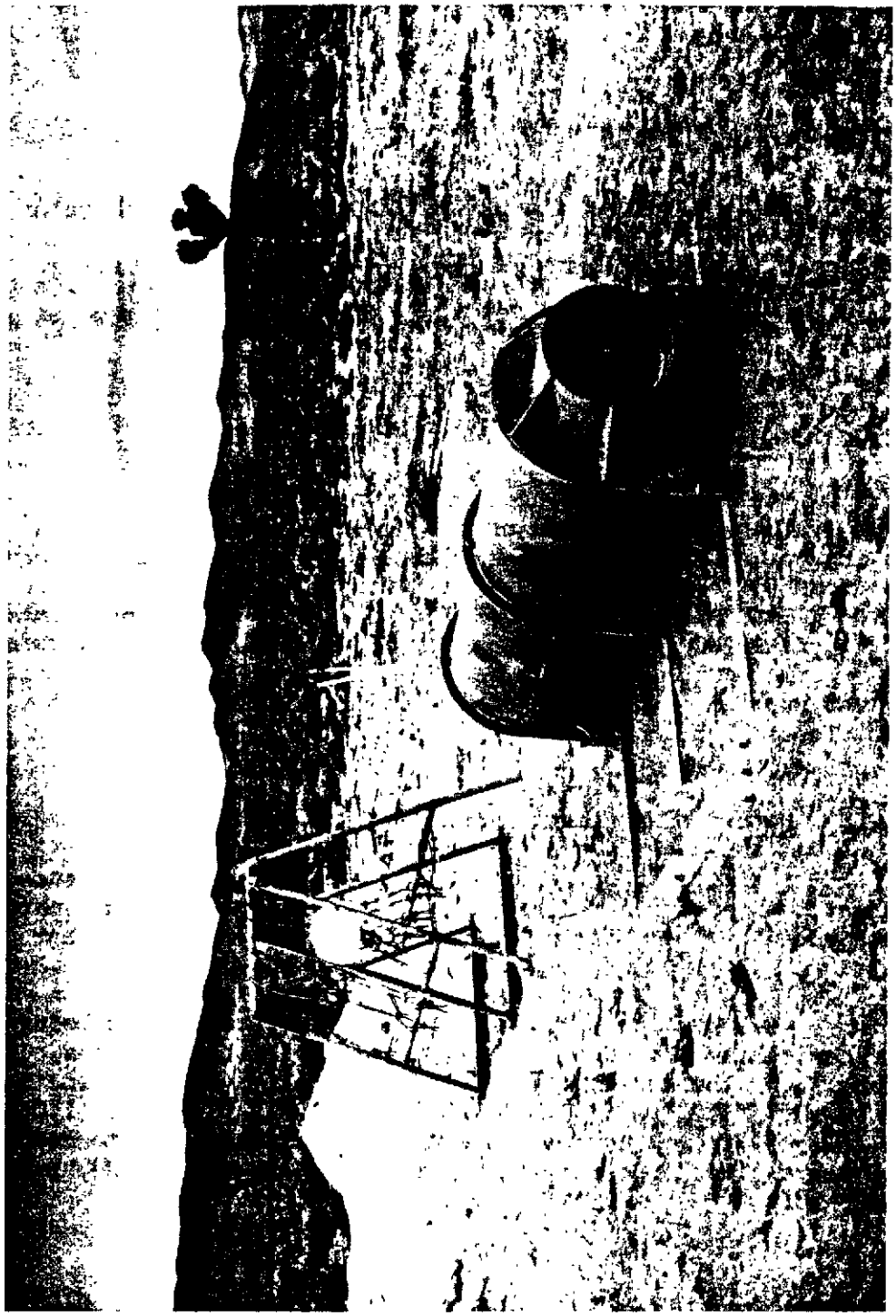

Fig 2.3 Station as Set in Field Ready for Detonation

PROJECT 2.4b

Each swine phantom (Fig. 2.4) was made up of a laminated cylinder of $\frac{1}{4}$-in. masonite 36-cm long and 36-cm in diameter, capped with laminated hemispheres of 18-cm radius, making the over-all length of the phantom 72 cm.

Although it was realized, after control studies had been made, that the films to be used were not a very satisfactory type of detector for depth-dose measurements, it was decided that they would supply some information of value for future use. Film packs were accordingly distributed throughout each swine phantom (Fig. 2.5).

PROJECT 2.4b

Fig. 2.5 Arrangement of Film Packs in Various Layers of Masonite Swine Phantom

Fig. 2.4 Swine Phantom on Auxiliary Assembly Stand

CHAPTER 3

RESULTS

3.1 GENERAL

Dosage measurements made in the lucite spheres, and based on ionization-chamber readings, appear to be the most reliable. This was also found to be true with the GREENHOUSE and BUSTER data. The DT-60 (phosphate glass) detectors, where used, were in fair agreement with the ionization chambers. The energy dependent characteristics of the film made it impossible to use it for the evaluation of depth-dose measurements with acceptable accuracy. However, the film data did prove to be of considerable value in confirming the slope obtained with ionization chambers in the dose versus distance curves. When a suitable X-ray generator is made available, the necessary control studies can be carried out to permit accurate evaluation of all film and glass data in terms of depth-dose response.

3.2 LUCITE SPHERES

Five stations, each of which incorporated a set of seven lucite spheres containing ionization chambers and film, were set up for the surface and underground shots. DT-60 detectors were also used when available and placed in the spheres. All detectors were recovered following detonation of the weapons.

The data obtained have been tabulated in Table 3.1. These data have been plotted in Fig. 3.1. The following information can be obtained from these curves: the absorption coefficient in lucite and air, the equilibrium wall thickness in lucite, and the dose at five distances from point of detonation. One station was omitted from the data on the underground shot because it could not be recovered at the same time as the other stations due to excessive fall-out.

The absorption coefficient for broad-beam conditions may be obtained in the following manner:

Since $$I_2 = I_1 e^{-\mu x} \qquad (3.1)$$

$$\mu = \frac{\text{Ln } I_1 - \text{Ln } I_2}{x} .$$

TABLE 3.1

Per Cent Equilibrium Dose in Lucite Spheres of Varying Wall Thickness

Shot	Yd	5.0 cm		9.0 cm		17.5 cm	
		Ionization Chamber	DT-60 (Phos.Glass)	Ionization Chamber	DT-60 (Phos.Glass)	Ionization Chamber	DT-60 (Phos.Glass)
Surface	750	92.7		86.4		69.4	
	850	92.5		87.7		65.8	
	950	88.7		82.6		60.9	
	1,050	91.3		85.5		65.2	
Underground	600*		89.1		79.5		58.0
	700*	91.7	90.6	80.2	77.3	55.6	59.3
	800	91.4		80.8		63.6	
	1,000	92.7		80.7		67.0	
Average		91.6% ± 3%		83.4% ± 5%		65.3% ± 6%	

* Data questionable due to excessive fall-out.

CHAPTER 3

RESULTS

3.1 GENERAL

Dosage measurements made in the lucite spheres, and based on ionization-chamber readings, appear to be the most reliable. This was also found to be true with the GREENHOUSE and BUSTER data. The DT-60 (phosphate glass) detectors, where used, were in fair agreement with the ionization chambers. The energy dependent characteristics of the film made it impossible to use it for the evaluation of depth-dose measurements with acceptable accuracy. However, the film data did prove to be of considerable value in confirming the slope obtained with ionization chambers in the dose versus distance curves. When a suitable X-ray generator is made available, the necessary control studies can be carried out to permit accurate evaluation of all film and glass data in terms of depth-dose response.

3.2 LUCITE SPHERES

Five stations, each of which incorporated a set of seven lucite spheres containing ionization chambers and film, were set up for the surface and underground shots. DT-60 detectors were also used when available and placed in the spheres. All detectors were recovered following detonation of the weapons.

The data obtained have been tabulated in Table 3.1. These data have been plotted in Fig. 3.1. The following information can be obtained from these curves: the absorption coefficient in lucite and air, the equilibrium wall thickness in lucite, and the dose at five distances from point of detonation. One station was omitted from the data on the underground shot because it could not be recovered at the same time as the other stations due to excessive fall-out.

The absorption coefficient for broad-beam conditions may be obtained in the following manner:

Since $$I_2 = I_1 e^{-\mu x} \qquad (3.1)$$

$$\mu = \frac{\text{Ln } I_1 - \text{Ln } I_2}{x} .$$

TABLE 3.1

Per Cent Equilibrium Dose in Lucite Spheres of Varying Wall Thickness

Shot	Yd	5.0 cm		9.0 cm		17.5 cm	
		Ionization Chamber	DT-60 (Phos.Glass)	Ionization Chamber	DT-60 (Phos.Glass)	Ionization Chamber	DT-60 (Phos.Glass)
Surface	750	92.7		86.4		69.4	
	850	92.5		87.7		65.8	
	950	88.7		82.6		60.9	
	1,050	91.3		85.5		65.2	
Underground	600*		89.1		79.5		58.0
	700*	91.7	90.6	80.2	77.3	55.6	59.3
	800	91.4		80.8		63.6	
	1,000	92.7		80.7		67.0	
Average		91.6% ± 3%		83.4% ± 5%		65.3% ± 6%	

* Data questionable due to excessive fall-out.

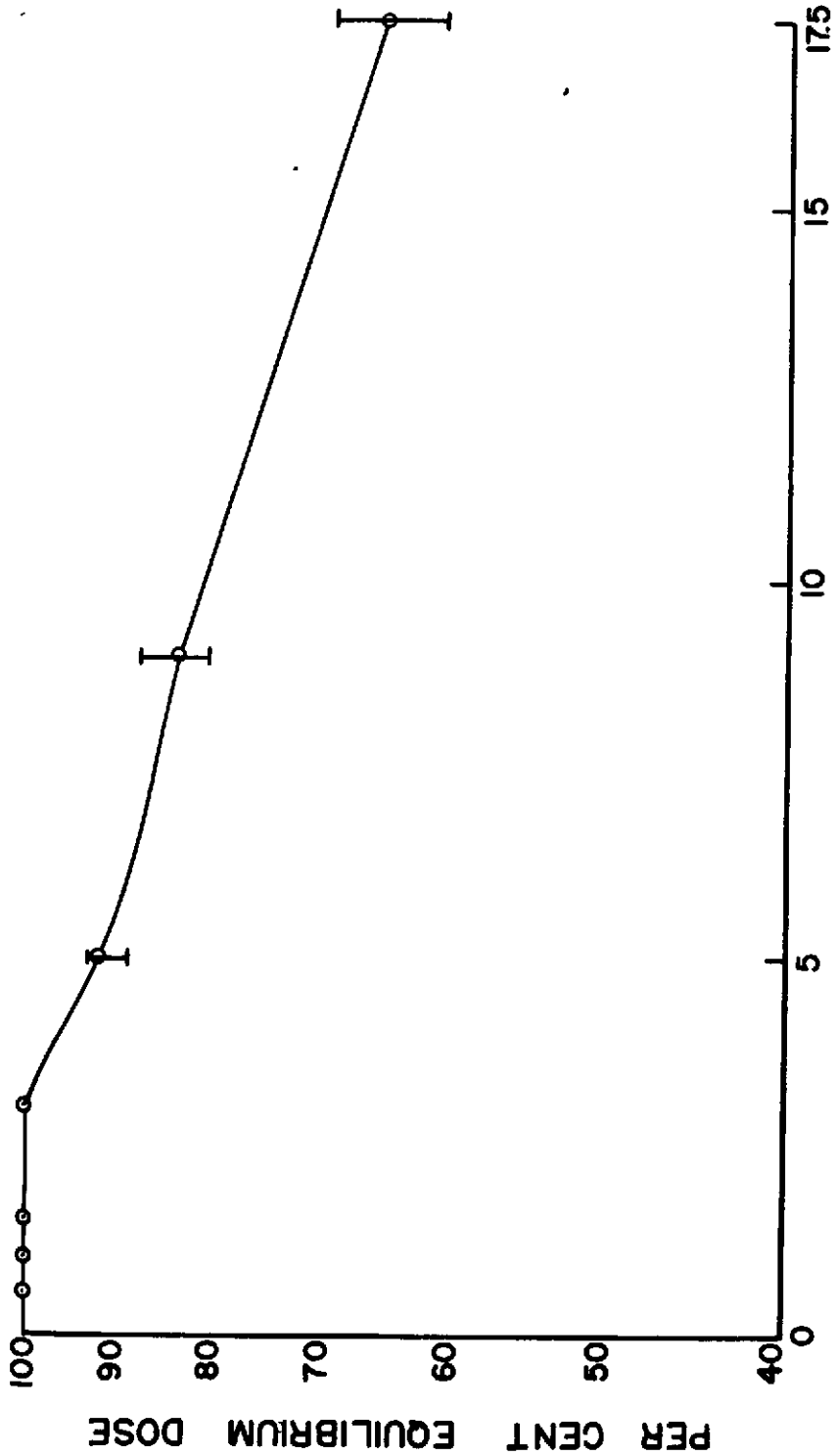

Fig. 3.1 Composite Curve of Per Cent Equilibrium Dose versus Wall Thickness of Lucite Spheres

From Table 3.1

$$I_1 = 83.4$$

$$I_2 = 65.3$$

$$x = 8.5 \text{ cm} .$$

Substituting in Eq. 3.2

$$\mu = \frac{4.42365 - 4.17899}{8.5}$$

$$\mu = \frac{0.24466}{8.5}$$

$$\mu = 0.028784 \text{ cm}^{-1}$$

The mean-free path in lucite is:

$$\lambda = \frac{1}{\mu} = \frac{1}{0.028784} = 34.74 \text{ cm} .$$

3.3 EQUILIBRIUM WALL THICKNESS

The equilibrium wall thickness for the initial gamma radiation of the nuclear weapon appears to be between 2.5 and 3 cm of lucite. The experimental error would have to be reduced to more definitely establish this value.

3.4 EQUILIBRIUM DOSE VERSUS DISTANCE CURVE

The equilibrium dose versus distance curves for the surface and underground shots are shown in Figs. 3.2 and 3.2a.

3.5 rd^2 VERSUS d CURVE

Since the rd^2 versus d plot is also used, it would be well to use it here.

$$r = \frac{r_0 e^{-\mu d}}{d^{\,1<n<2}} \qquad (3.3)$$

PROJECT 2.4b

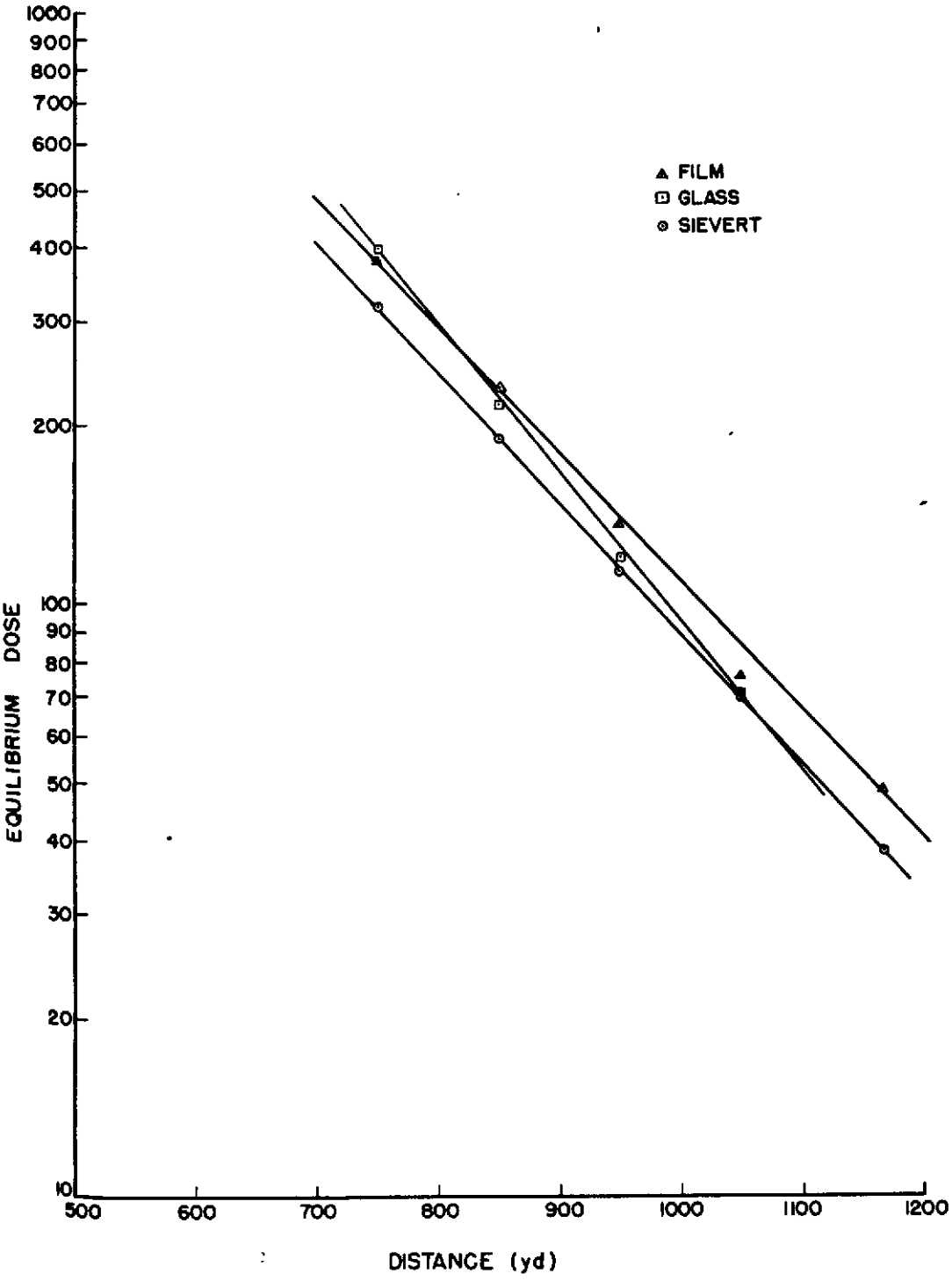

Fig. 3.2 Dose versus Distance Plot

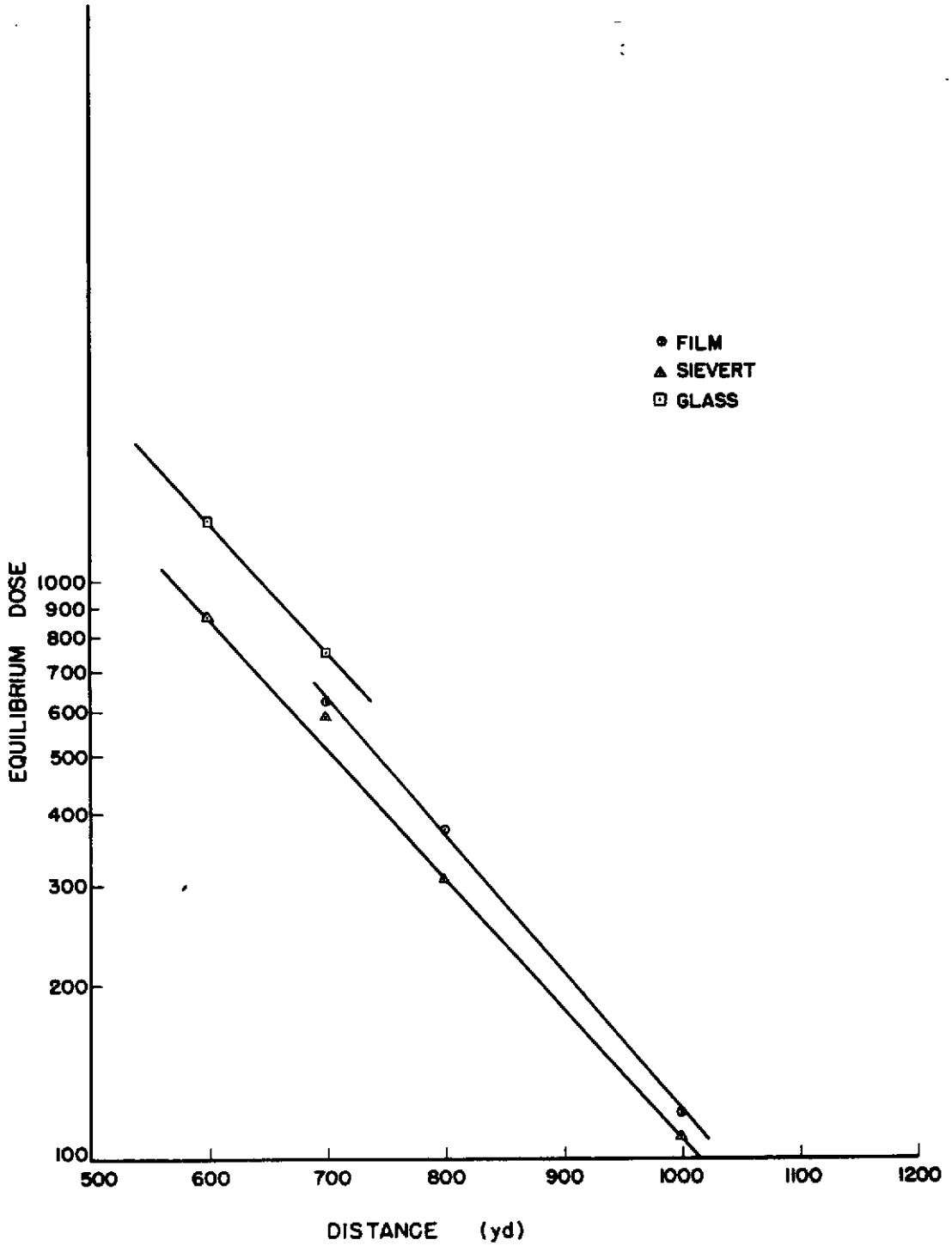

Fig. 3.2a Dose versus Distance Plot

where r in roentgens can be determined experimentally at a distance d.

Assuming (1) that there is little change in the absorption coefficient and (2) that n is approximately 2 over that range of distances in which we are interested; also substituting λ for $\frac{1}{\mu}$ where λ is the mean-free path in (3.3)

$$r = \frac{r_0 e^{-\frac{d}{\lambda}}}{d^2} \qquad (3.\ )$$

$$rd^2 = r_0 e^{-\frac{d}{\lambda}} \qquad (3.5)$$

$$\ln rd^2 = \ln r_0 - \frac{d}{\lambda} \ln e \qquad (3.6)$$

The rd^2 versus d curves for the surface and underground shots are shown in Fig. 3.3.

3.6 REPRODUCTION OF THE GAMMA-RAY EFFECTS OF THE BOMB IN THE LABORATORY

Several sources of radiation were used in attempting to reproduce the effects of the bomb in the laboratory. The spheres, with ionization chambers in them, were exposed to a 2-Mev General Electric industrial X-ray generator, a high-intensity source of Co^{60}, a 10-Mev General Electric betatron and a 22-Mev Allis-Chalmers betatron. The results are shown in Fig. 3.4. The curve marked Comp. in Fig. 3.4 is the data obtained from the nuclear detonations.

From these curves it is apparent that the 10-Mev betatron, used without added filtration, most accurately duplicates in absorption characteristics the bomb radiation. Spectral analyses of the 10-Mev betatron at the Naval Ordnance Laboratory, White Oak, Maryland, have been made by the National Bureau of Standards.[3,4]

---

[3] P. K. S. Wang and M. Wiener, "Spectral analysis of 10 Mev Betatron Radiation by Nuclear Emulsion", Physical Rev., Vol. 76, No. 11, 1724-1725, Dec 1, 1949.

[4] J. W. Motz, X-ray Section, National Bureau of Standards, Personal Communication, May 12, 1952.

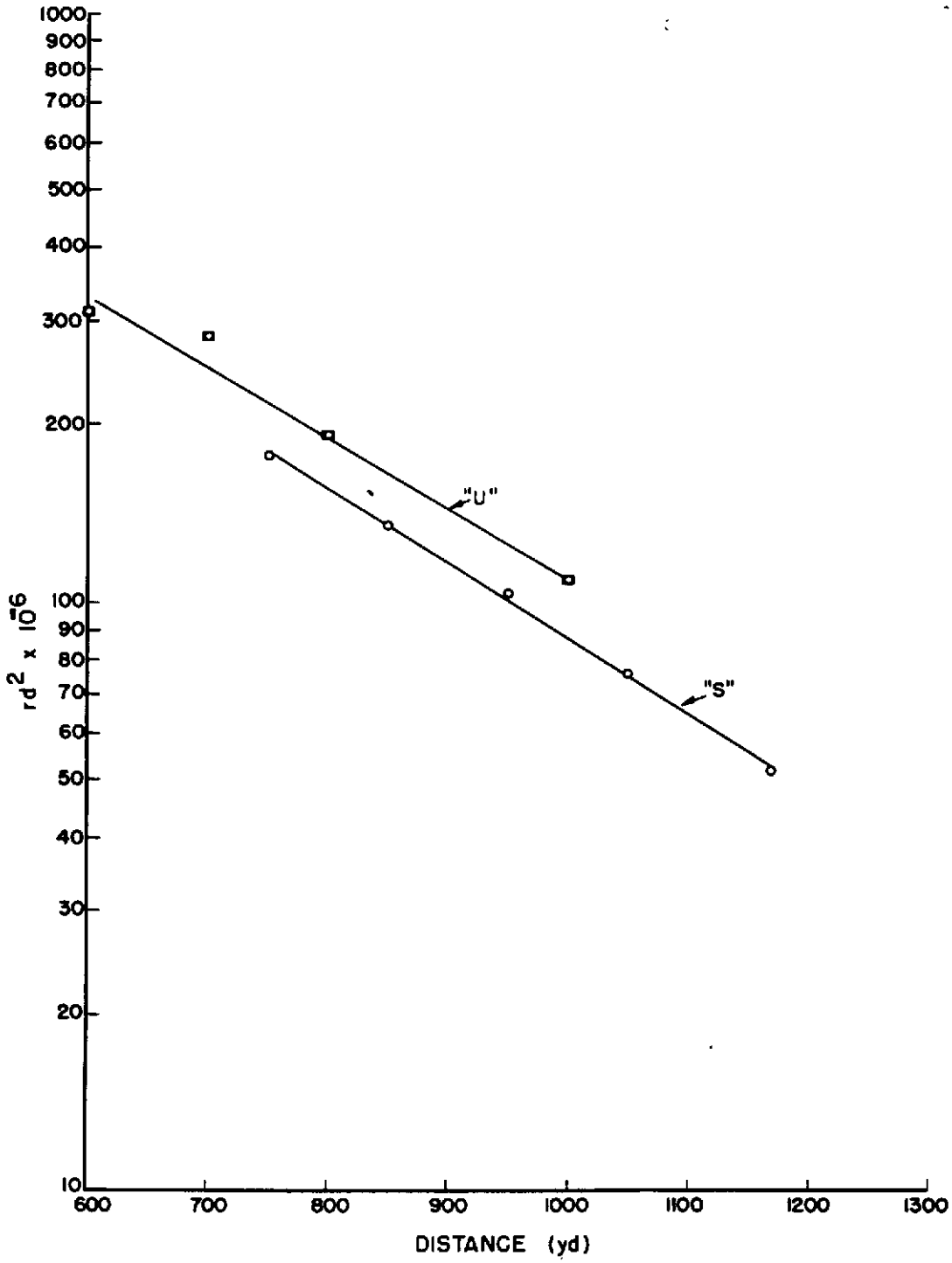

Fig. 3.3 rd^2 versus d Plot

PROJECT 2.4b

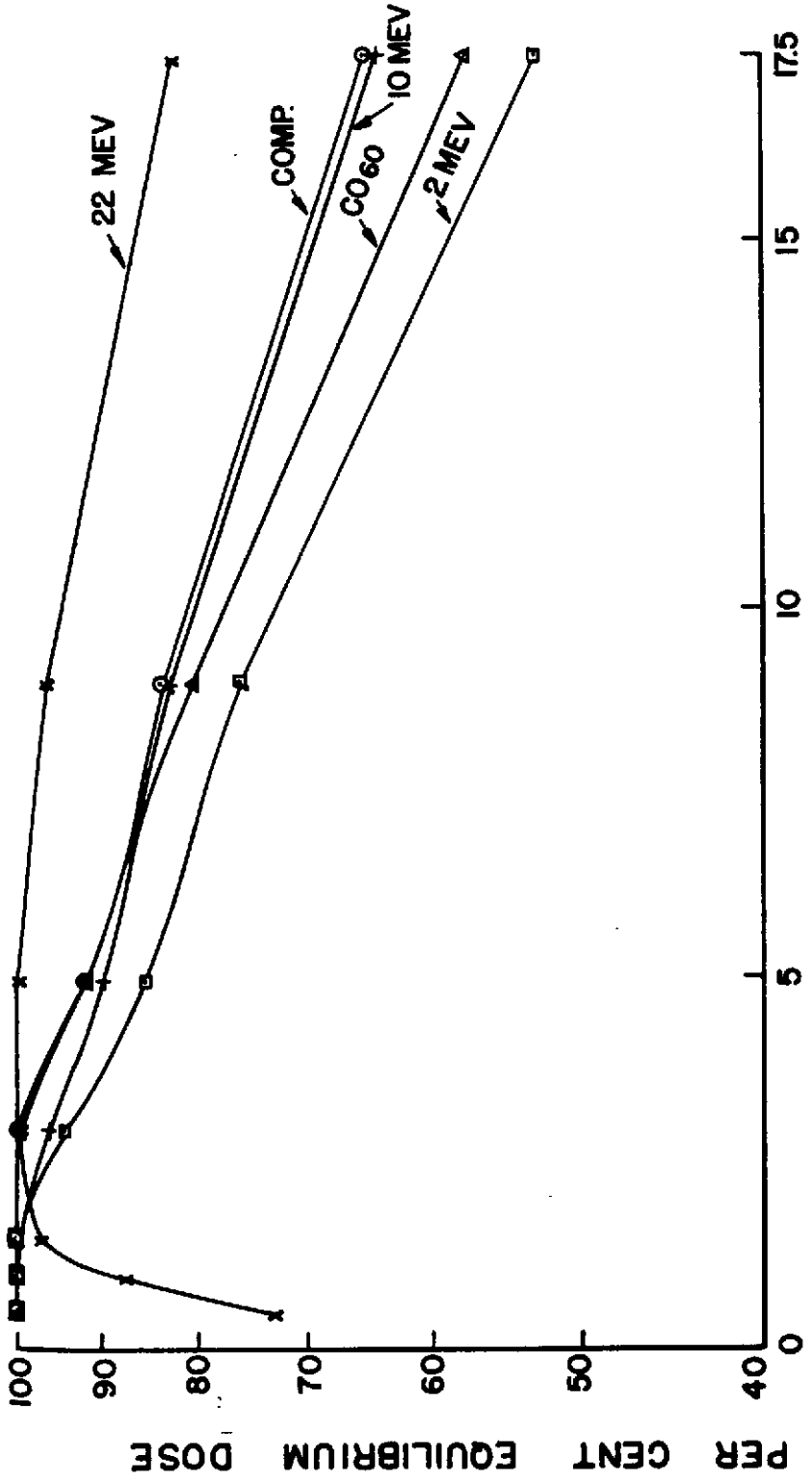

Fig. 3.4 Comparison Curve of Various Energies

3.7 SAMPLE OF DATA OBTAINED FROM STATION B OF THE SURFACE SHOT

Jangle Surface Shot

Station B ~~Distance 850 yd~~ Pressure 27.85 in. Temperature 32° F Correction Factor 1.018

Sphere Wall Thickness cm	Chamber No.	Dose Roentgens	Average Dose Corrected Roentgens	% Equilibrium Dose
17.5	A-12	119		
	B-12	122	123	65.8
	B-13	122		
9.0	A-13	166		
	A-14	158	164	87.7
	B-14	160		
5.0	A-17	169		
	B-15	172	173	92.5
	B-16	170		
3.0	A-18	184		
	A-19	183		
	B-17	174		
1.6	A-23	213*		
	B-18	183		
	B-19	189	187	
1.0	A-24	184		
	A-28	172		
	B-20	178		
0.6	A-29	193		
	B-21	194		
	B-22	192		

* This reading was not used as the chamber was suspected of losing some of its charge before the detonation.

CHAPTER 4

DISCUSSION

4.1 GENERAL

This experiment was designed to obtain depth-dose curves in approximately unit-density material for a surface and an underground nuclear detonation in order that they might be compared with those obtained at other tests of nuclear weapons.

The data from this experiment do not appear to be in as close agreement as that obtained at GREENHOUSE. This is probably due to the fact that dust presented a problem in using the ionization chambers at the Nevada Test Site which did not exist at GREENHOUSE. Attempts were made to build a dust-free laboratory, but it was found when the blower system was disassembled that considerable dust had passed through the filters. Although it would be desirable to reduce the experimental error, the question could be raised whether or not it would change any conclusions that might be drawn from a biomedical standpoint. In the case of a heterogeneous population, it is very doubtful if there would be any significance in the fact that the dose at a 17.5 cm depth was 61 r or 69 r rather than 65 r.

There are indications that there might possibly be some change in energy with distance; however, the change appears to be so small (within the limits of biomedical interest) that it is masked by the experimental error of our data.

It is apparent from Table 3.1 that the relative per cent transmission as determined by the DT-60's and ionization chambers are in good agreement. This is probably due to the removal of the energy dependent characteristics of the glass by the DT-60 case. The dose versus distance curves for an energy independent film, glass, and ionization chamber are yet in need of resolution.

It is also apparent that excessive fall-out introduced longer wave-length components which reduced the effective energy at any location where it occurred; however, outside of the fall-out area there was no significant change in the depth-dose curves from those at GREENHOUSE or BUSTER.

CHAPTER 5

CONCLUSIONS

5.1 GENERAL

1. The type of ionization chamber used in the spheres proved to be satisfactory for measuring the high intensity radiation emitted by the bomb within the limits of their range.

2. The depth-dose effects of the bomb can be reproduced in the laboratory by using an X-ray generator producing a beam with characteristics similar to that of the General Electric 10-Mev betatron at the Naval Ordnance Laboratory, White Oak, Maryland. The spectral distribution of this machine may be obtained from the National Bureau of Standards. (See page 15)

3. The curves showing dose versus distance on a semilog plot for the two shots were essentially straight lines and can be assumed to be linear in the LD_{0-100} range which is of interest to a biomedical program.

4. The curves showing rd^2 versus d where r is roentgens and d is distance for the two shots could be drawn as straight parallel lines.

5. The energy of the radiation at the distances of interest from a biomedical standpoint was approximately the same for the two shots. This energy was also approximately the same as that obtained at GREENHOUSE and BUSTER (Fig. 5.1).

6. The data from this experiment is very limited with regard to the contribution from the radiation due to excessive fall-out. Where excessive fall-out did occur around the stations that could be recovered, the effective energy appeared to be lower than that where it did not exist.

PROJECT 2.4b

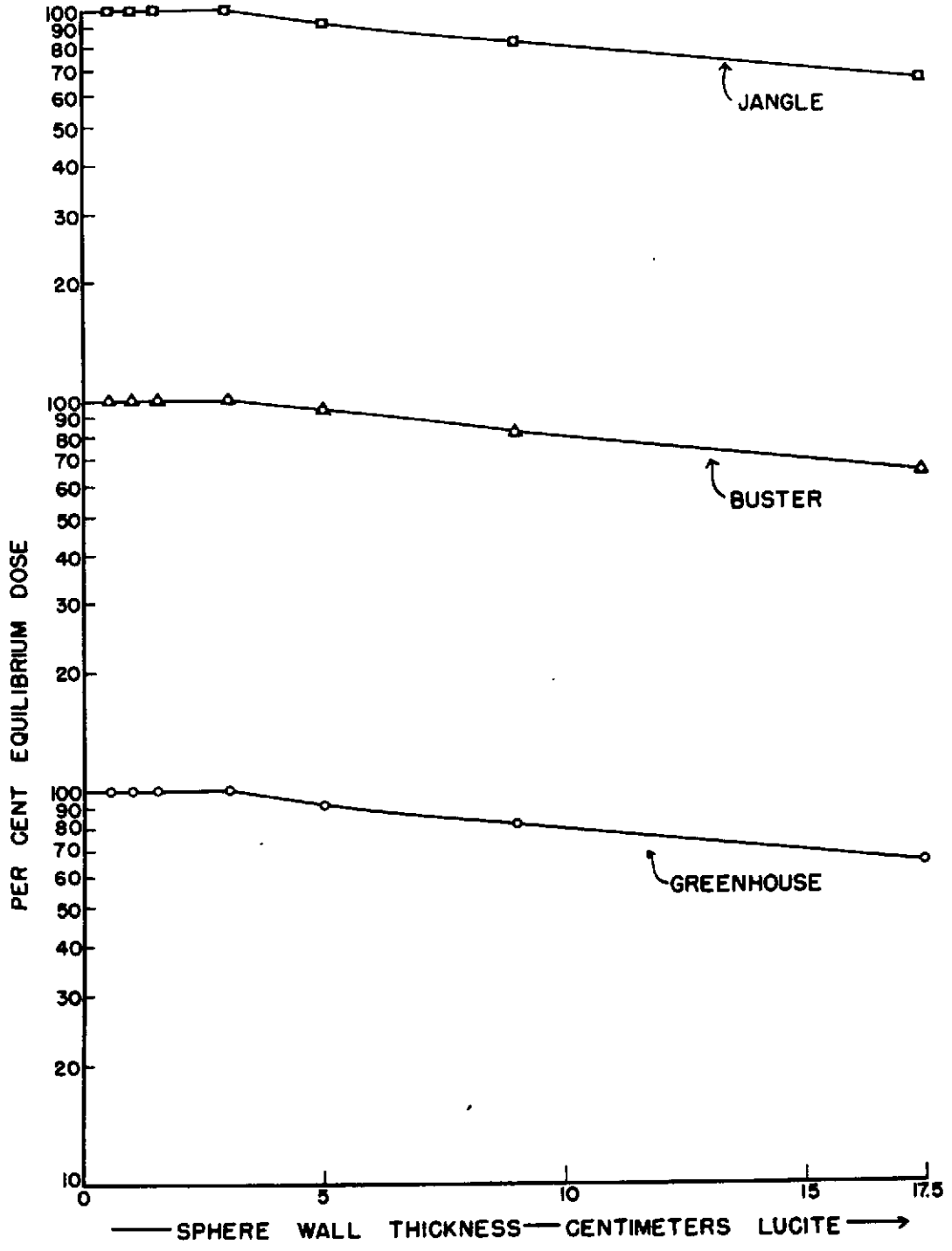

Fig. 5.1 Comparison of Per Cent Equilibrium Dose versus Wall Thickness of Lucite for JANGLE, BUSTER, and GREENHOUSE

CHAPTER 6

RECOMMENDATIONS

6.1 RECOMMENDATIONS FOR FUTURE EXPERIMENTS

A more complete absorption curve in approximately unit-density material should be obtained by increasing the number and wall thickness of the spheres.

It would also be desirable to obtain depth-dose measurements in approximately unit-density material for the radiation due to fall-out.

6.2 RECOMMENDATIONS FOR DEVELOPMENT OF EQUIPMENT

The limited number of ionization chambers used gave reliable data. It would, therefore, seem advisable to investigate the possibility of expanding their maximum range and mass producing them.

OPERATION JANGLE

PROJECT 2.4c

GAMMA RAY SPECTRUM MEASUREMENTS OF RESIDUAL RADIATION

by

W. Bernstein
R.L. Chase
J.B.H. Kuper

June 24, 1952

Brookhaven National Laboratory
Upton, N.Y.

PROJECT 2.4c

ACKNOWLEDGEMENTS

Numerous members of the Brookhaven Laboratory staff, in addition to Seymour Rankowitz, the assistant project officer, contributed to the project, especially H. McChesney, Jr., A.W. Schardt, John Garfield, E.H. Foster, Stanley MacCormack, F. Heemsoth, Marshall Bull, M. Slavin and D. Clareus.

PROJECT 2.4c

ILLUSTRATIONS

TABLES

CONTENTS

PROJECT 2.4c

ABSTRACT

Knowledge of the spectral distribution of gamma radiation in the residual contamination from a low altitude burst is of importance in the design of radiation measuring equipment and protective measurements generally. In the case of a strong extended source large amounts of degraded radiation can be expected.

In this project an attempt was made to determine the gamma ray spectrum in the field, using scintillation spectrometer techniques. Recovery time of the sweep circuits restricted observations to the fringe areas well removed from the crater.

Because of instrumental difficulties and lack of experience under field conditions, no worth while information was secured from the surface shot, but at least two good sets of data were obtained from the underground shot. These indicated an overwhelming preponderance of gamma rays in the energy region below 200 kev. It is felt that this result has demonstrated the possibilities of the method and indicates the desirability of further work with improved apparatus.

GAMMA RAY SPECTRUM MEASUREMENTS OF RESIDUAL RADIATION

1.1 OBJECTIVE

The objective of this project was to determine as well as possible the shape of the gamma ray spectrum of the residual contamination after a surface or subsurface burst. Particular attention was paid to obtaining information about the high energy tail of the distribution and the softer components (less than 200 kev) in the degraded radiation which are biologically quite effective.

1.2 HISTORICAL AND THEORETICAL

Previous attempts at measuring the spectrum of the gamma radiation from the residual contamination after an atomic explosion have employed indirect methods to arrive at an "effective voltage" for the radiation. Unfortunately this information is of limited value unless the spread of the distribution is known as well. Since it is apparent that relatively large amounts of low energy degraded radiation from "sky shine" will be present, it is important to take this spectrum region into consideration when designing radiation measuring equipment and personnel protective measures.

At present it is difficult, if not impossible, to calculate the degraded spectrum to be expected from even a monochromatic source. Therefore, direct measurement in the field seems to offer the only possibility of obtaining this information in sufficient detail. The methods of scintillation counter spectrometry employing pulse height analysis appear to be the most attractive from the standpoint of speed and portability. Unfortunately this method has serious limitations when dealing with an extended spectrum. As is well-known, gamma ray photons of a given energy incident on a crystal may give a group of large pulses arising from photoelectric absorption, a broad distribution of Compton recoils and, finally, a very large number of small pulses arising from back scatter, electrons which lose only a portion of their energy in the crystal, and similar effects. The presence of this low energy tail in the distribution makes it necessary to study the low energy part of the spectrum separately, making measurements with and without absorbers of suitable material and thickness. The high energy end of the spectrum can best be investigated with a rather large crystal of sodium iodide (containing thallium activator). For the low energy portion a thin sodium iodide crystal is employed, taking measurements with and without suitable absorbers. Some information about the shape of the intermediate energy portion of the spectrum may be inferred with a large anthracene crystal which would show very little photoelectric effect in comparison to the

Compton effect. A sodium iodide crystal would give confusing results in this intermediate energy range because of the presence of both photoelectric and Compton processes whose relative importance is energy dependent.

In field measurements of this sort the complications of a multichannel electronic pulse height analyzer seem quite unnecessary, so it was decided to employ a simpler photographic method. This method has now been developed to the point where it is capable of results equivalent to a 50 channel pulse height analyzer.

1.3 INSTRUMENTATION

In order to collect the required data in a reasonable amount of time without overexposing the personnel involved, a scintillation spectrometer was constructed. The instrument includes a group of three photo-multiplier tubes with associated scintillating crystals and stabilized high voltage supply, a pulse amplifier and pulse height analyzer based on the gray wedge technique. Figure 1 is a block diagram of the instrumentation components.

The pulses from the spectrometer amplifier are stretched by a pulse stretcher to give a constant amplitude for a time as long as the oscilloscope sweep. The stretched pulses are amplified again, and displayed on the screen of the oscilloscope. The oscilloscope is operated on a triggered sweep so that each event appears as a horizontal line whose height is proportional to the energy of the event. The distribution is then photographed through a gray wedge mounted on the oscilloscope face (Figure 2).

The three scintillation counters with their associated photomultiplier tubes were mounted in a single pickup probe housing, which could be operated with up to 20 feet of cable (Figure 3). The balance of the equipment was mounted in a 3/4 ton 4 x 4 truck (weapons carrier, Figure 4). A gasoline driven alternator (Homelite Model 23A115) was mounted on the front bumper of the truck (Figure 5). A Sorenson voltage regulator, Model 500-S, was employed.

In order to obtain sufficient stability of calibration for field work, it was necessary to use a system with a well stabilized gain. Most critical is the photomultiplier tube power supply which furnished up to 1500 volts at 150 x 10^{-6} amps. and was carefully stabilized to 0.1 percent (Figure 6). The voltages applied to the three 5819 photomultiplier tubes were individually adjusted for optimum operation. A selector switch permits rapid change from one photomultiplier to another. The pulse amplifier, in addition to having constant gain and linearity, must be free of overload difficulties if the low energy end of the spectrum is to be

examined. A specially designed pulse amplifier[1] was used which does not permit large pulses from the high energy gamma rays to displace the baseline when small pulses are being examined. Figure 7 is a circuit diagram of the amplifier and pulse stretcher.

A Tektronix Model 511A oscilloscope was modified (Figure 8) with the following considerations in mind: The spot intensity and focus should be constant, independent of counting rate; the sweep should be blanked outside the wedge dimensions to eliminate extraneous background light; the vertical deflection amplifier should be linear for a vertical deflection of at least two inches.

The equipment, as constructed, had one serious drawback which was not properly corrected until after the tests. No adequate provision was made to prevent baseline shifts with changes in counting rate.[2] As a result there were marked errors in reading the zero energy reference in many of the pictures.

The oscilloscope sweep duration was adjusted to 5×10^{-6} sec. This value is a compromise between two conflicting requirements. The sweep must not be so long that there is an appreciable probability that many pulses will be separated by less than the sweep duration. At the same time, the sweep should be long enough that enough light for a picture will be collected in a reasonable time.

Since the density of an absorbing medium varies inversely with the logarithm of the transmission, a filter or wedge with a linearly increasing density has a logarithmically decreasing transmission. When the oscilloscope distribution is observed through such a filter, and contour lines of equal integrated light energy are plotted, the distance of these lines along the wedge is proportional to the logarithm of the number of times the sweep has appeared at that amplitude, provided the sweep intensity is constant. When photographed, these contour lines then appear as isodensity lines on the film. Changes in the exposure time merely move the height of these isodensity lines up or down on the film. Printing on high contrast paper makes easier the selection of the isodensity line which is read. The advantage of this method over other photographic methods is that the intensity reading is not dependent upon the film characteristics, with the exception of reciprocity failure.

1 R.L. Chase and W.A. Higinbotham, Rev. Sci. Inst. 23, 34 (Jan. 1952).

2 An improved pulse stretcher and oscilloscope will be described in a forthcoming publication. W. Bernstein and R.L. Chase, "A Gray Wedge Pulse Height Analyzer" - in preparation, to be submitted to Rev. Sci. Inst.

The gray wedge was constructed by grinding a rectangular piece of neutral density filter glass (2" x 3" x 0.2") with an initial density of one, into a linearly tapered wedge, with a sharp edge along one of the 2" edges. This was cemented to a mating piece of clear glass to make a more rugged assembly and to reduce refraction effects (Figure 9). The intensity range of this wedge is 10 - 1, and is calibrated by photographing regularly recurrent, uniform pulses at different rates for the same exposure times.

There are certain requirements which determine the selection of the film which can be used. Fairly high contrast and small grain size are necessary to simplify the determination of the isodensity line, and the speed should be as high as possible consistent with these factors. The long time reciprocity failure law(3) is well approximated by the expression $E = It^p$. We have used Kodak spectroscopic type IV F film for which $p = .72$, because of its high contrast and small grain size. The camera is a standard 35 mm type (DuMont 296) mounted on the oscilloscope by a stovepipe. The isodensity line is selected by enlarging and printing on Kodalith paper. The transition may be read easily by eye because of the high contrast. If intensity comparison between different picture is desired, all conditions affecting the developing and printing must be constant.

Three crystals were used to examine the gamma ray energy distribution. A small (1 cm x 1 cm x 0.2 cm) NaI-Tl crystal was used in the 0 - 0.2 Mev region; a 2 cm x 1.5 cm x 1.5 cm anthracene crystal was used in the 0.3 Mev - 1.0 Mev region, and a large (3 cm dia. x 2 cm high) NaI-Tl crystal was used above 1 Mev. The crystals were all mounted as shown in Figure 10. The NaI-Tl crystal mounts were evacuated and then filled with Argon to prevent tarnishing of the crystal. All the crystal were cemented to the pyrex window with Gelva 2.5 resin to provide optica contact and prevent movement of the crystals. The crystal mounts were taped to the 5819 photomultipliers, and Nujol was used to provide optical contact between the window and the tube. It was not necessary to select photomultipliers for high resolution since this is a minor factor with a continuous distribution. Magnetic shields surrounded the tubes t eliminate changes in performance with orientation. The light-tight shields were made of bakelite to decrease scattering and absorption of low energy events. The high energy crystal was surrounded in addition by 1/8" of lead to reduce the number of low energy events reaching the crystal.

The crystals were calibrated before each set of data was taken. The low energy crystal was calibrated with In^{114} (192 kev and 25 kev) b adjusting the high voltage on the tube so that the 192 kev line appear at the end of the picture. The operating conditions of the intermediat

3 C.E.K. Mees, "Theory of the Photographic Process", MacMillan, 1948, pgs. 236 ff.

range anthracene crystal were set so that the Compton edge of a Co^{60} source appeared at the end of the picture. The high energy NaI-Tl crystal was also calibrated with Co^{60} by adjusting the high voltage so that the combined Compton edge and photoelectric lines appeared about 1/5 of the distance from the low energy end of the picture, thus giving an energy range of about 0 - 4 Mev.

1.4 ANALYSIS OF DATA

Since high energy events produce a marked excess of small pulses in a small crystal, it was necessary to use absorber techniques to separate the true low energy events from the distribution produced by the higher energies. A tin absorber, with a transmission of 10 percent at 100 kev, was selected for this purpose. Figure 11 is a plot of the total absorption[4] of the tin absorber in the 0 - 200 kev range. The differences between the data with and without the absorber, corrected by the absorber efficiency, gives the true distribution of low energy events.

The absorption properties of the crystals must be considered in analyzing the data. In the low energy region (NaI-Tl crystal) the photoelectric effect is predominant, and the contribution of the Compton scattered events is neglected. Also, the range of the secondary electrons produced in the crystal is small compared to the dimensions of the crystal. Therefore, the observed pulse height is proportional to the total gamma ray energy. It was further assumed that it was valid to calculate the crystal efficiency from the thickness of the crystal, because of the poor geometry for horizontal events. Figure 12 is a plot of the total absorption curve for this crystal. This was calculated only for the iodine component since the sodium contribution is small at this energy.

Certain assumptions must be made when analyzing the data from the intermediate energy anthracene crystal. Since the Compton effect is predominant in this crystal, the photoelectric contribution was neglected. It was then assumed that the response of the crystal to a monoenergetic gamma ray in this energy range could be approximated by a rectangle. Figure 13 shows an experimental curve (obtained with a sliding single channel analyzer) of a Cs^{137} source and the approximate rectangle. The number of counts in the rectangle is given by the area divided by the channel width. If the experimental distribution is considered as the sum of a group of such rectangles corresponding to different energy gamma rays, then the intensity in any energy interval is the product of the derivative of the experimental curve in the interval and the average energy of the interval. It is further assumed that the area of a given rectangle is proportional to the total absorption of the crystal at

[4] L. Costrell, Nat. Bureau of Standards, private communication.

that energy. Figure 14 is a plot of the total absorption curve for this anthracene crystal.

The analysis of the region above 1 Mev is complicated by the increasing importance of the pair production peak with increasing energy. However, no information was found above 1 Mev and it was not necessary to develop a procedure for the interpretation of this region.

1.5 OPERATION

The equipment was driven to a number of contaminated locations at times ranging from .2 hours to 4 days after each of the two shots. Table 1 and the map of the area (Figure 15) show the locations visited and the times in hours after the shots.

A number of difficulties arose during the course of the experiment, due partly to equipment failure and partly to lack of experience in its operation. Much of the data collected after the surface shot cannot be considered reliable because the zero energy point on the energy axis was not located with sufficient care. Unfortunately the operator was not aware of this until after the films were developed.

Other causes of data loss were:

1) Failure of a cathode ray tube in the oscilloscope.

2) Vibration due to driving over rough roads caused a camera lens to shake loose, spoiling one roll of film.

3) Poor guesses at exposure times.

Table 1 shows the data that have so far been analyzed in detail. In addition, that data which is considered sufficiently reliable for further analysis is so indicated.

1.6 REDUCTION OF DATA

In the low energy region photographs taken with and without absorber for the same exposure time are plotted on a linear scale. The curve taken with absorber is subtracted from the curve without absorber. The resulting curve is then corrected for the variable crystal and absorber efficiency. Figure 16 is a typical photograph of the low energy distribution taken without the tin absorber. Figure 17 shows one set of plotted experimental data. The energy scale is established from the In^{114} calibration photograph. A serious error is introduced in the picture interpretation because of a poorly marked and changing zero. This

results in some uncertainty as to the location of the 50 - 60 kev peak, but has a large effect near 200 kev where the error is multiplied by the crystal and absorber efficiency corrections. The error is estimated to be ±50 percent above 100 kev and about ±10 percent in peak position.

Figure 18 is a typical photograph of the pulses from the intermediate energy anthracene crystal. Figure 19 is a plot of one set of data from the intermediate energy crystal and shows linear plots of the experimental data, the observed gamma ray distribution, and the distribution corrected for crystal efficiency. Since almost all the pictures taken in this region were underexposed, it is difficult to locate the energy at which the intensity falls off again. However, it is reasonable to place this point at about 900 kev from some of the data available.

Since the low and intermediate energy data do not overlap, it was necessary to normalize the two curves in the following manner: The number of quanta per energy interval for anthracene is given by:

$$N(E)dE_A = \frac{dh_A}{dE} \cdot E_A \frac{dE}{\Delta E_A} \cdot \frac{\epsilon_A G_A}{t_A^p}$$

The number of quanta per energy interval for NaI-Tl is given by:

$$N(E)dE_N = h_N \frac{dE}{\Delta E_N} \cdot \frac{\epsilon_N G_N}{t_N^p}$$

Where $\frac{dh_A}{dE} E_A \epsilon_A$ = number of quanta at any energy for the anthracene crystal obtained from Figure 11.

ΔE = effective channel width where $\Delta E_A = 5\Delta E_N$ because the channel width is changed with energy scale change

G_A = geometry[5] for anthracene which is 1/4.5 for a centimeter cube times 1/6 for one face of this cube

5 The geometry corrections for both crystals are derived in the following manner. It is desirable to normalize the information to the number of quanta absorbed per cm^2 per unit time. The radiation in the case of both crystals is assumed to be isotropic. Since the volume of the anthracene crystal used is 4.5 cm^3 it is necessary to use a geometrical factor of 1/4.5 to reduce it to a one centimeter cube. This must then be divided by a geometrical factor of 6 to give the radiation that entered one of the 6 surfaces of the one cm cube. In the case of the NaI-Tl crystal, the subtraction procedure measured only the radiation crossing the 1 cm^2 face.

G_N = geometry[5] for NaI-Tl which is 1 for a 1 cm^2 area

ϵ_A and ϵ_N = efficiency

t_A^p and t_N^p = exposure times for the respective photographs corrected for reciprocity failure

h_N = height of NaI curve

The ratio of the number of events at a given energy in anthracene to those in NaI-Tl is given by

$$\frac{N(E)dE_A}{N(E)dE_N} = \frac{\frac{dh_A}{dE} \cdot E_A \frac{dE}{\Delta E_A} \frac{\epsilon_A G_A}{t_A^p}}{h_N \frac{dE}{\Delta E_N} \frac{\epsilon_N G_N}{t_N^p}}$$

$$\frac{N(E)dE_A}{N(E)dE_N} = \frac{\frac{dh_A}{dE} E_A \frac{\epsilon_A}{t_A^p}}{5 \cdot 4.5 \cdot 6\, h_N \frac{\epsilon_N}{t_N^p}}$$

Therefore, it is possible to obtain a scale factor for selected points on both curves. A check of the approximations was obtained by measuring the 30 kev Cs^{137} X-ray with the NaI-Tl crystal and the 670 kev gamma ray with the anthracene. The calculated conversion coefficient is in good agreement with the listed value.(6) No useful data was obtained above 1 Mev.

Figure 20 is a composite plot of the two curves normalized in this fashion for two locations at distances of 8,000 and 11,000 feet, at 48 and 96 hours after the underground shot. Most of the radiation is concentrated below 200 kev with a peak at about 55 kev. The higher energy radiation appears to be peaked at about 1 Mev. It was extremely difficult to detect any major changes in the curves with location or orientation of the detector. Direct radiation from the crater would not reach the instruments at these locations, hence the observed

6. Nuclear Data, National Bureau of Standards #499, Sept. 1, 1950.

radiation was mostly scattered and from fallout, with possibly some direct radiation from the crater lip area.

Figure 21 is a plot of the gamma ray spectrum expressed as energy flux (number times energy) versus energy. Figure 22 is a plot of the gamma ray spectrum as relative number of roentgens at any energy versus energy. This was calculated from the curve of energy flux to produce 1 roentgen versus energy given by Siri.[7]

In an attempt to confirm this conclusion an experiment was performed using the BNL Chemistry Department 2 million volt electron Van de Graaff as a point source and observing radiation scattered from the wooden building roof and sky. Since there is a considerable amount of lead around the target, only hard gammas will escape to be scattered. The detector is shielded from the direct primary radiation by a concrete wall.

Figure 23 is the actual experimental photograph of the scattered radiation from the Van de Graaff, obtained with a 2 decade gray wedge. Figure 24 is a photograph of the spectrum of the In^{114} source showing the 192 kev gamma ray and the 25 kev X-ray. The resolution of the In^{114} photoline agrees with that obtained with a single channel pulse height analyzer. Figure 25 is a plot of the Van de Graaff scattered radiation obtained in a manner similar to that previously described, using In^{114} as the calibration source. Here again, one obtains the 70 kev scattered radiation.

1.7 CONCLUSIONS AND RECOMMENDATIONS

It is evident that it is possible to make gamma ray spectrum measurements in the field, using scintillation counter techniques, improved as a result of the present experiences.

At moderately large distances from the crater most of the radiation is degraded by scattering. This is particularly true in the present instance where direct radiation from the crater was blocked and only the lip and fallout could contribute direct radiation. The radiation is practically isotropic.

The area over which scattered radiation may be appreciable is very large and hence in some situations large numbers of personnel may be exposed.

7 W. Siri, "Isotopic Tracers and Nuclear Radiation," McGraw-Hill, 1949, Pg. 411.

The predominant energy in the scattered radiation (or "sky shine") seems to lie in the 50 to 100 kev region, where many types of radiation measuring instruments exhibit strong energy dependence or even cut off.

Moderate amounts of shielding (on all sides, not just on the side toward the source) can effect a considerable reduction in the radiation dose received by personnel in the regions exposed to sky shine.

Further work in the field with apparatus improved on the basis of the present experiences is necessary to establish the spectrum in more detail, and to obtain more information on the variation of the intensity of the scattered radiation with distance and time. This should be done with personnel thoroughly familiar with the problems of scintillation spectrometry.

It is felt that a panel truck or other closed vehicle would be preferable to the open truck.

Experiments using anthracene crystals and expressing the results in terms of the energy absorbed in the organic crystals (rather than in quanta per unit area and time) might be more directly useful and easier to interpret.

TABLE 1

Location and Time of Experimental Photographs

Time (hrs)	Location (See Fig. 15)	Distance from Zero (ft)	Radiation Level mr/hr	Data Analyzed	Low Energy Data Can Be Analyzed	Intermediate Energy Data Can Be Analyzed	Unsatisfactory Data
			Surface Shot				
S + 2 1/2	12	4000	10	-	X	-	1, 2
S + 3	A	3000	60	-	-	-	1, 2
S + 4	B	1500	40	-	-	X	1
S + 5 1/2	A	3000	20	-	-	-	1, 2
S + 29	A	3000	2	-	-	-	1, 2
S + 52	6	2000	10	-	-	-	1
S + 53	C	1200	100	-	-	-	1, 2
S + 55	2	2000	100	-	-	X	1
			Underground Shot				
U + 2	111	4000	80	-	-	X	1, 3
U + 26	128	11000	450	-	X	X	-
U + 28	111	4000	42	-	X	X	-
U + 48	128	11000	230	X	-	-	-
U + 48 1/2	124	8000	180	-	X	X	-
U + 49	115	4000	90	-	X	-	2
U + 50	107	3000	110	-	X	-	-
U + 96	128	11000	90	X	-	-	-
U + 96 1/2	124	8000	85	X	-	-	-
U + 97	115	4000	50	-	X	-	2
U + 98	107	3000	?	-	X	?	2

Explanation of unsatisfactory data

1. Poor zero
2. Anthracene picture underexposed
3. Oscilloscope power supply trouble

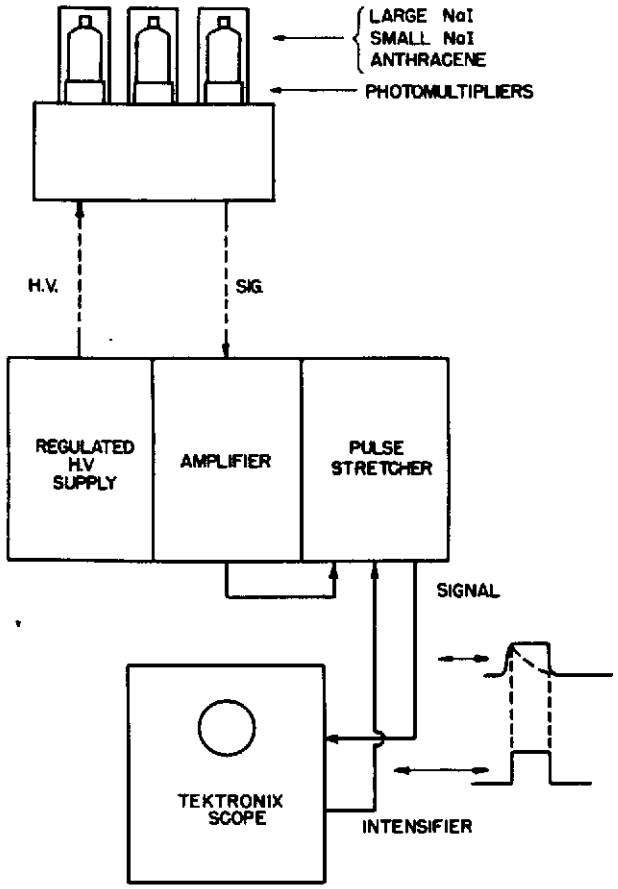

Fig. 1. Block Diagram of Photographic Scintillation Spectrometer

PROJECT 2.4c

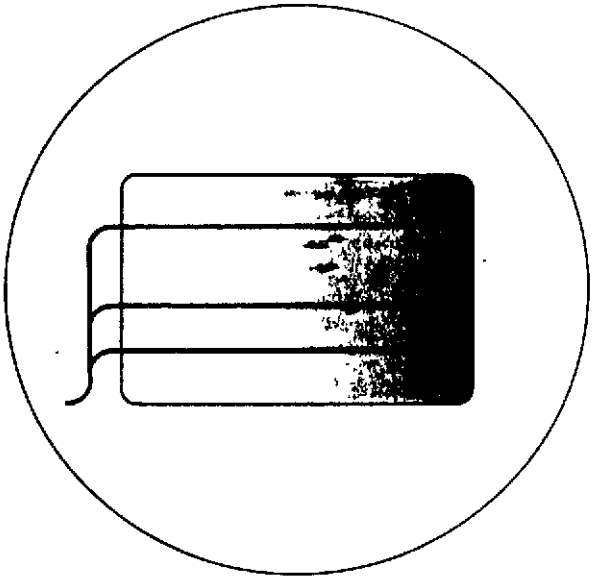

Fig. 2. Stretched Pulses Observed through the Gray Wedge

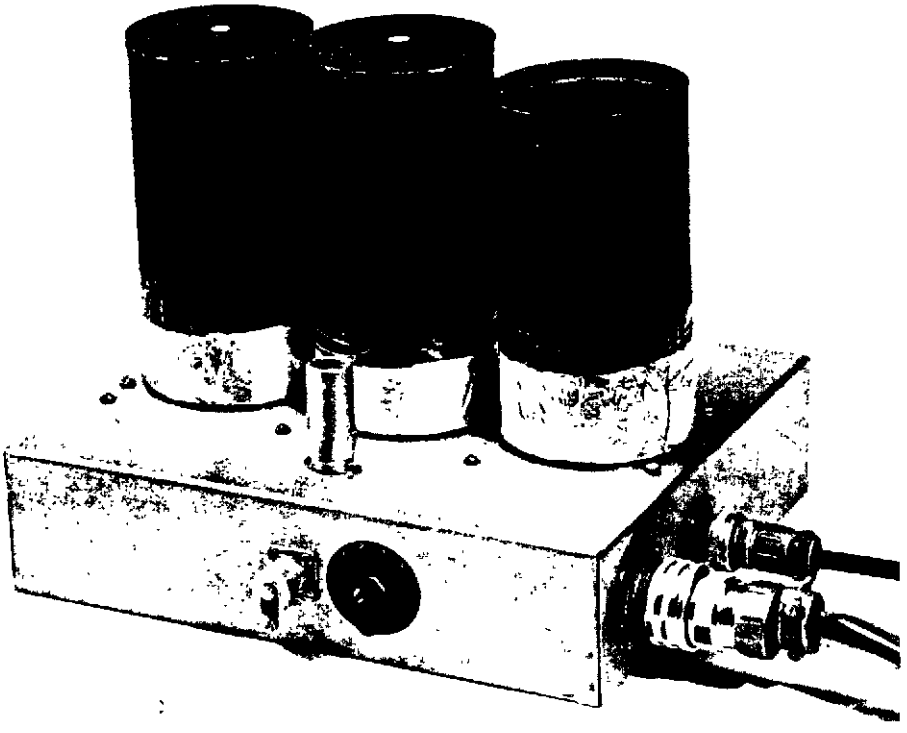

Fig. 3. Scintillation Counter Assembly

PROJECT 2.4c

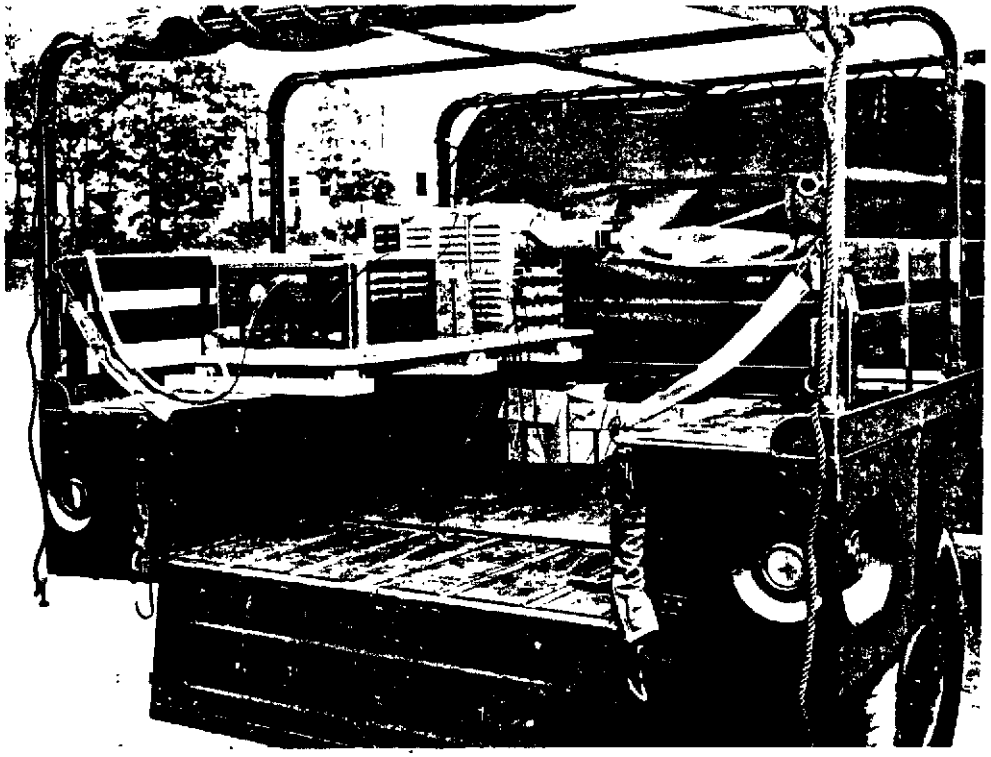

Fig. 4. Arrangement of Equipment in the Truck

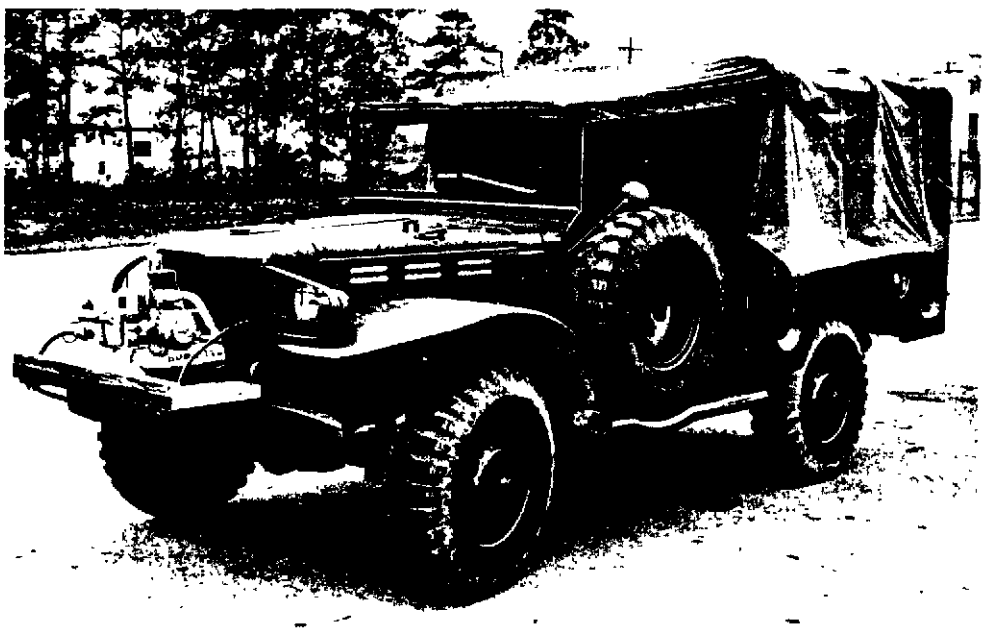

Fig. 5. Truck, Showing Generator

PROJECT 2.4c

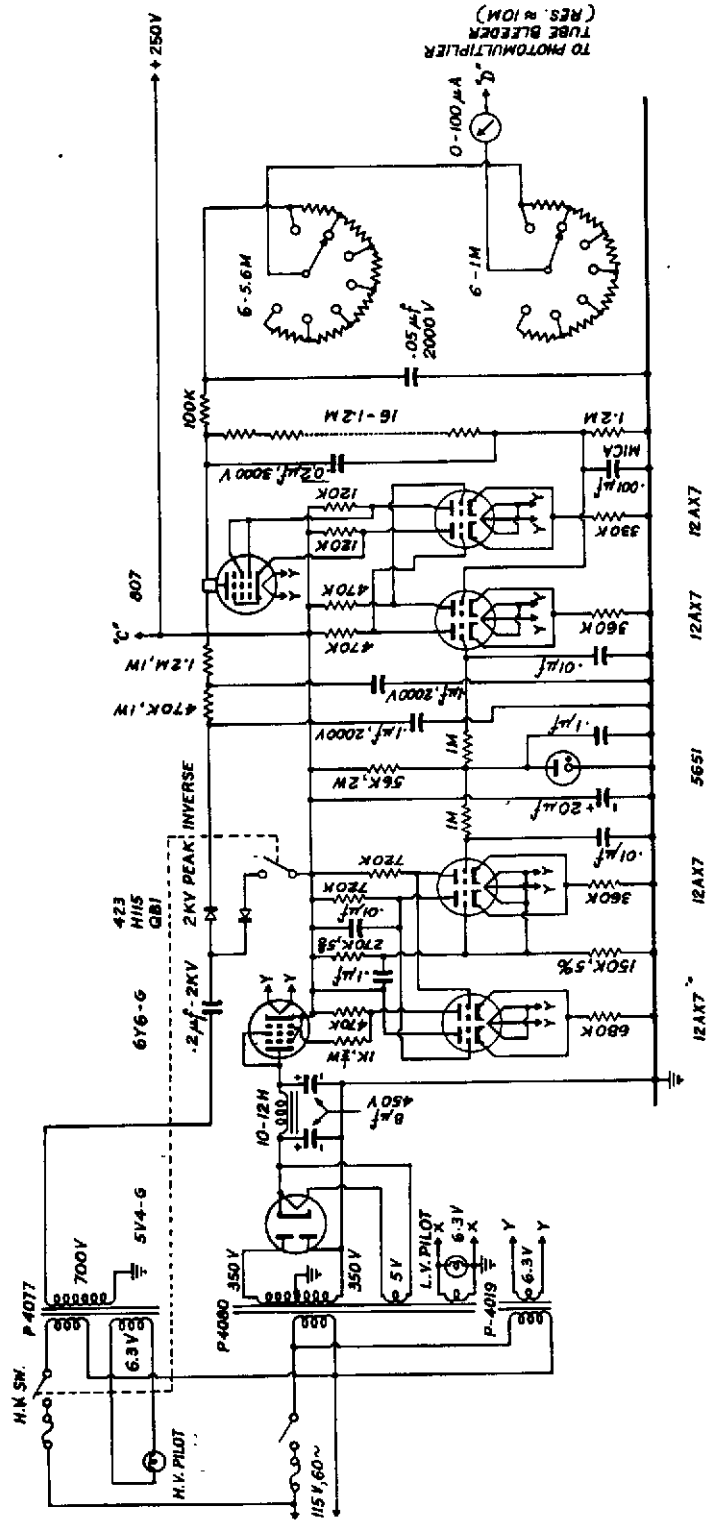

Fig. 6. Circuit Diagram of H.V. Supply

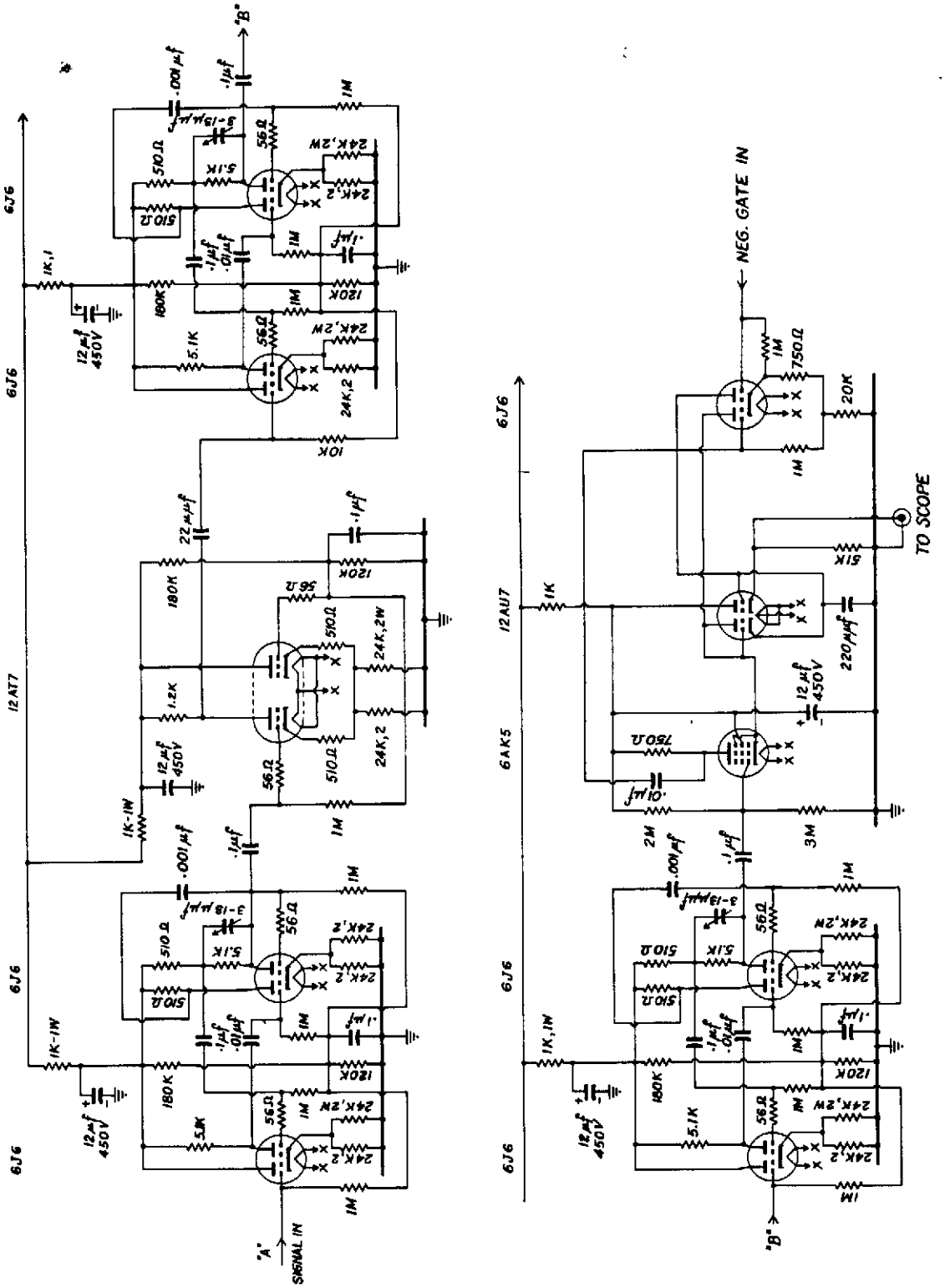

Fig. 7. Circuit Diagram of Amplifier and Stretcher

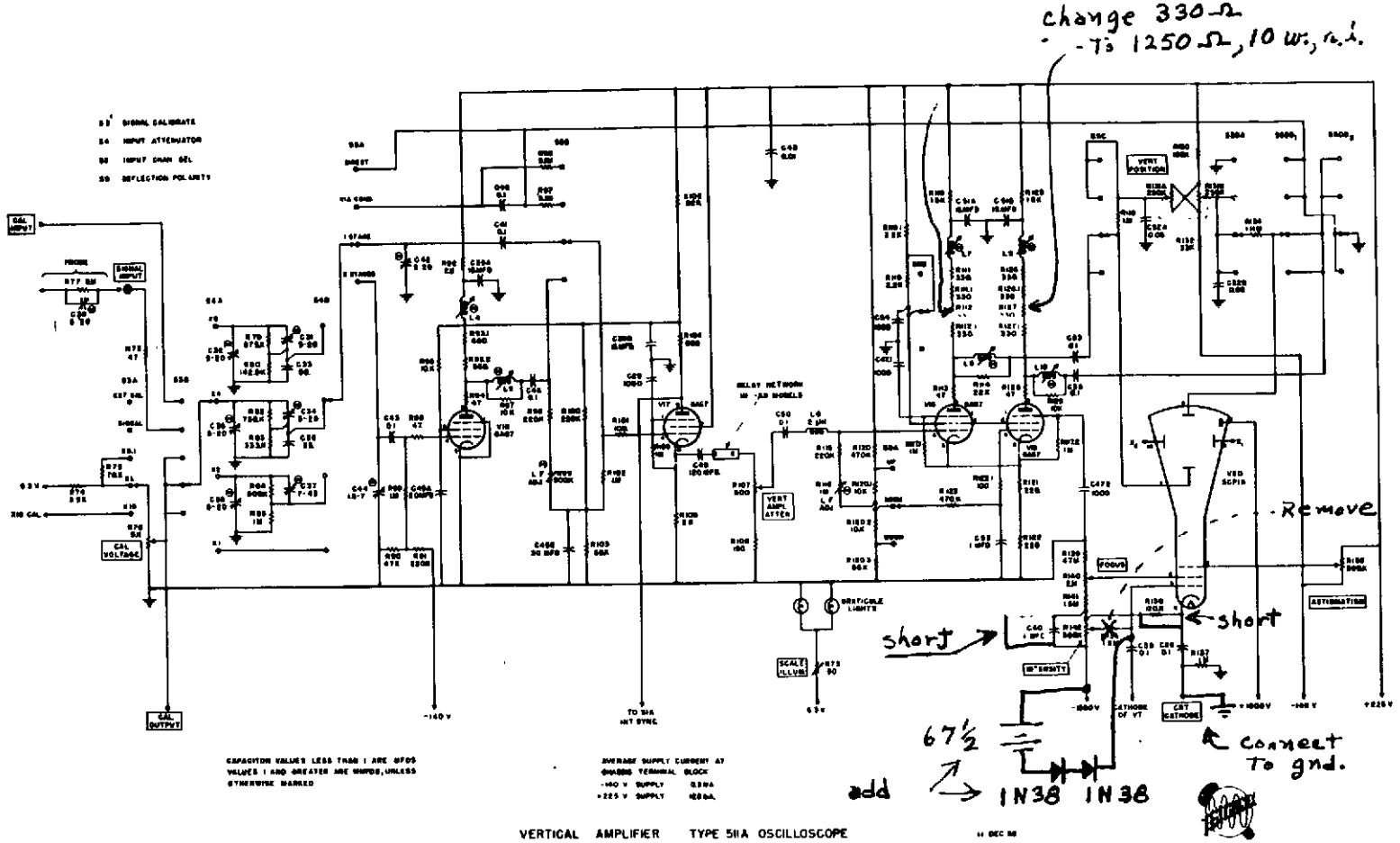

Fig. 8a. Modification of the Tektronix Oscilloscope

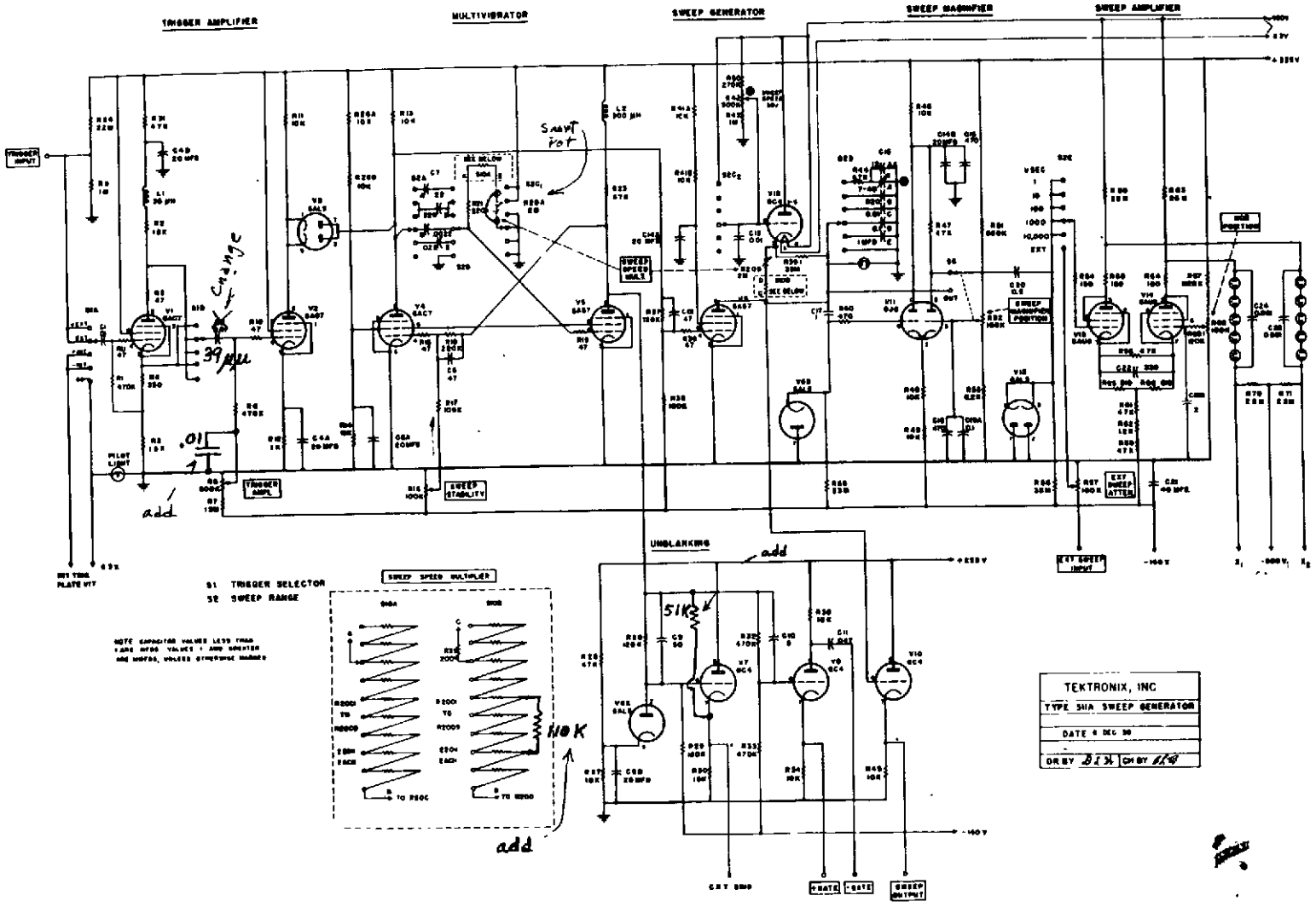

Fig. 8b. Modification of the Tektronix Oscilloscope

PROJECT 2.4c

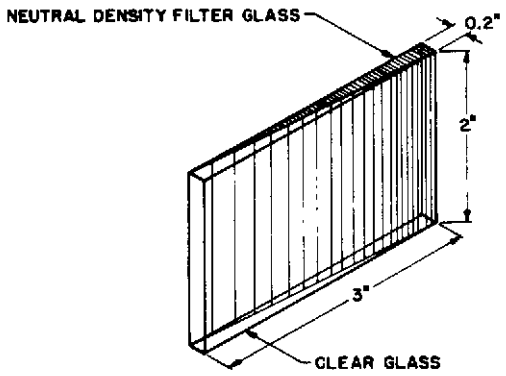

Fig. 9. Detail of the Gray Wedge

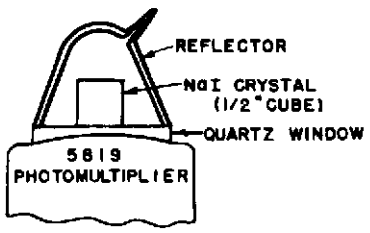

Fig. 10. Crystal Mounting

PROJECT 2.4c

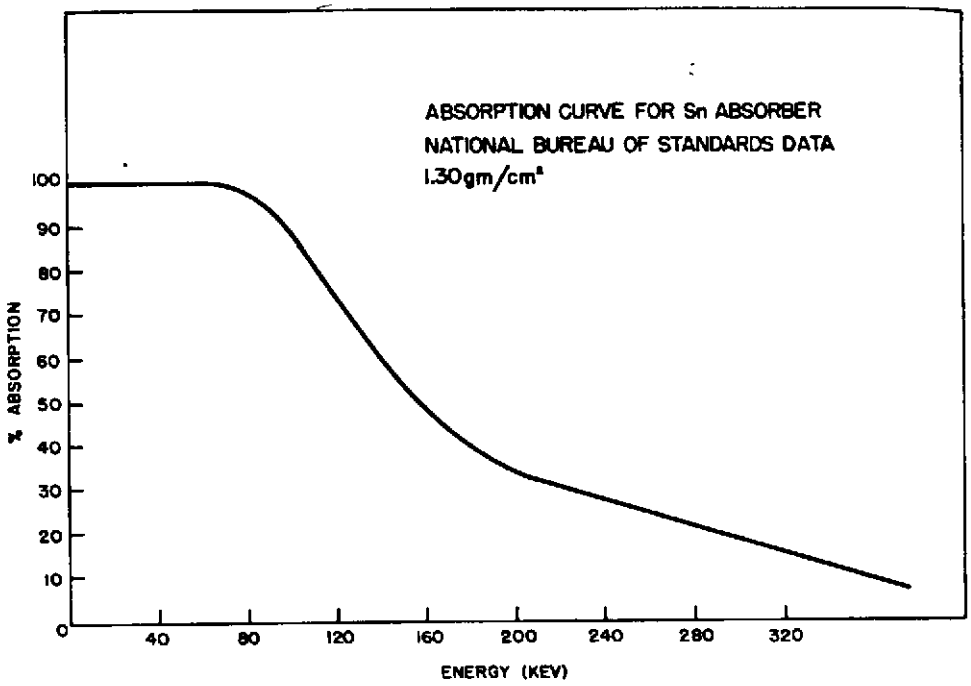

Fig. 11. Total Absorption Curve for Tin Absorber

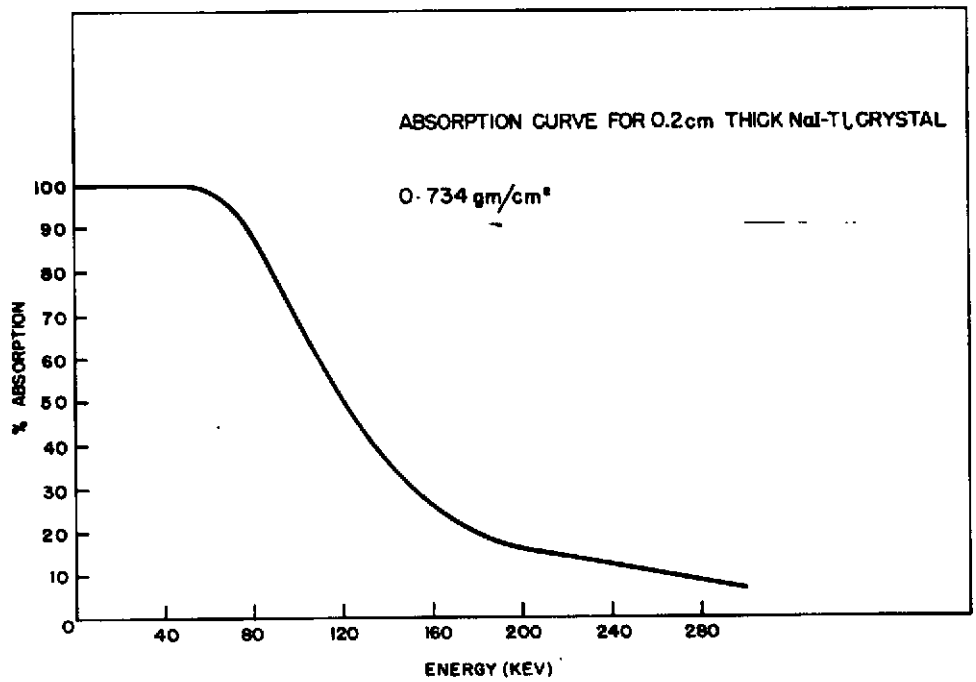

Fig. 12. Total Absorption Curve for Low Energy NaI-Tl Crystal

PROJECT 2.4c

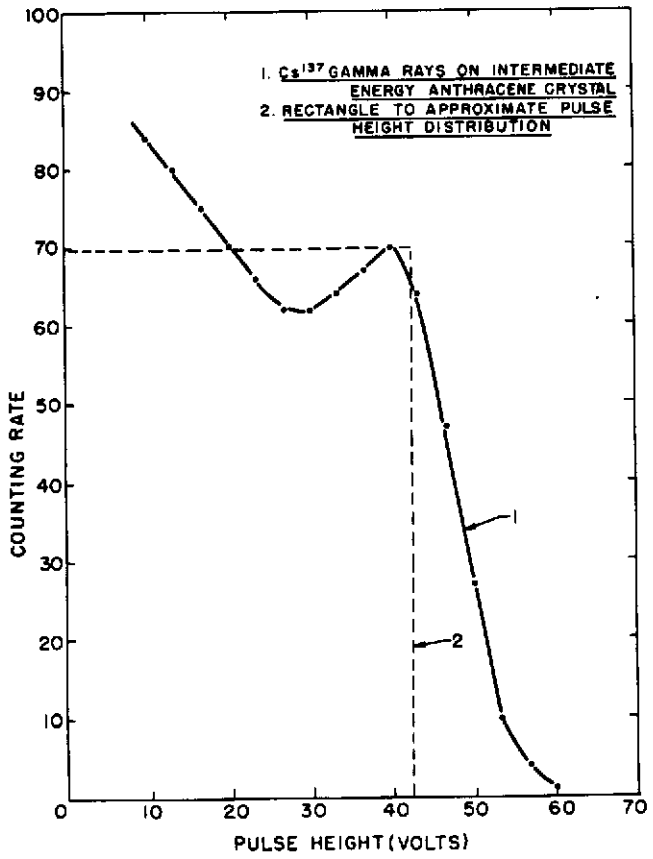

Fig. 13. Approximate Representation of Gamma Ray Spectrum with Anthracene Crystal

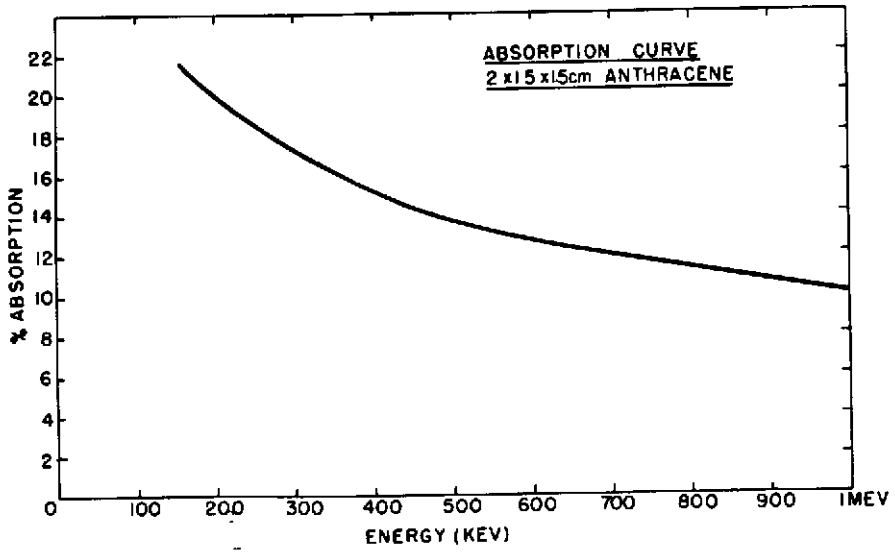

Fig. 14. Total Absorption Curve for Anthracene Crystal

PROJECT 2.4c

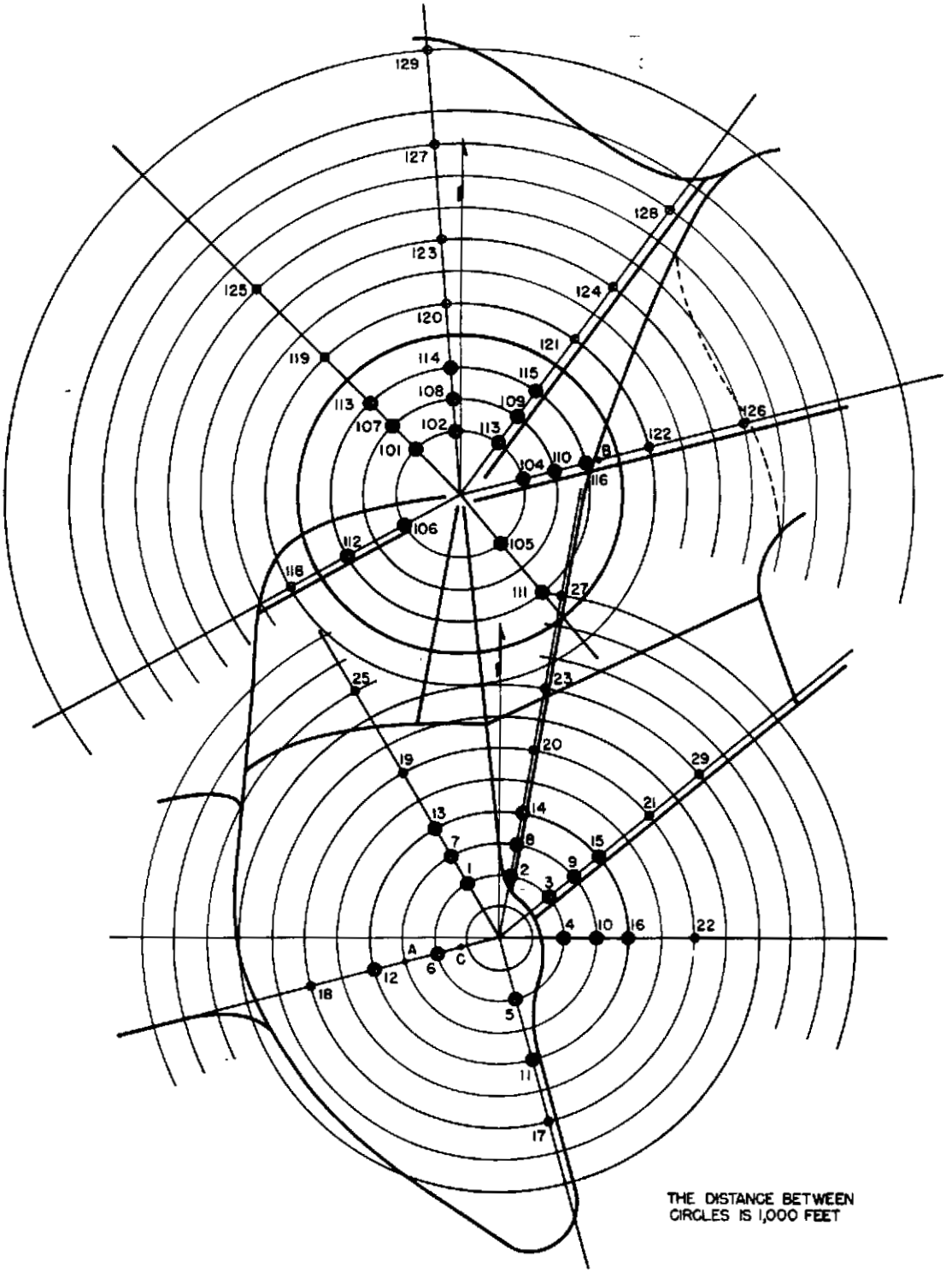

Fig. 15. Map of Test Area

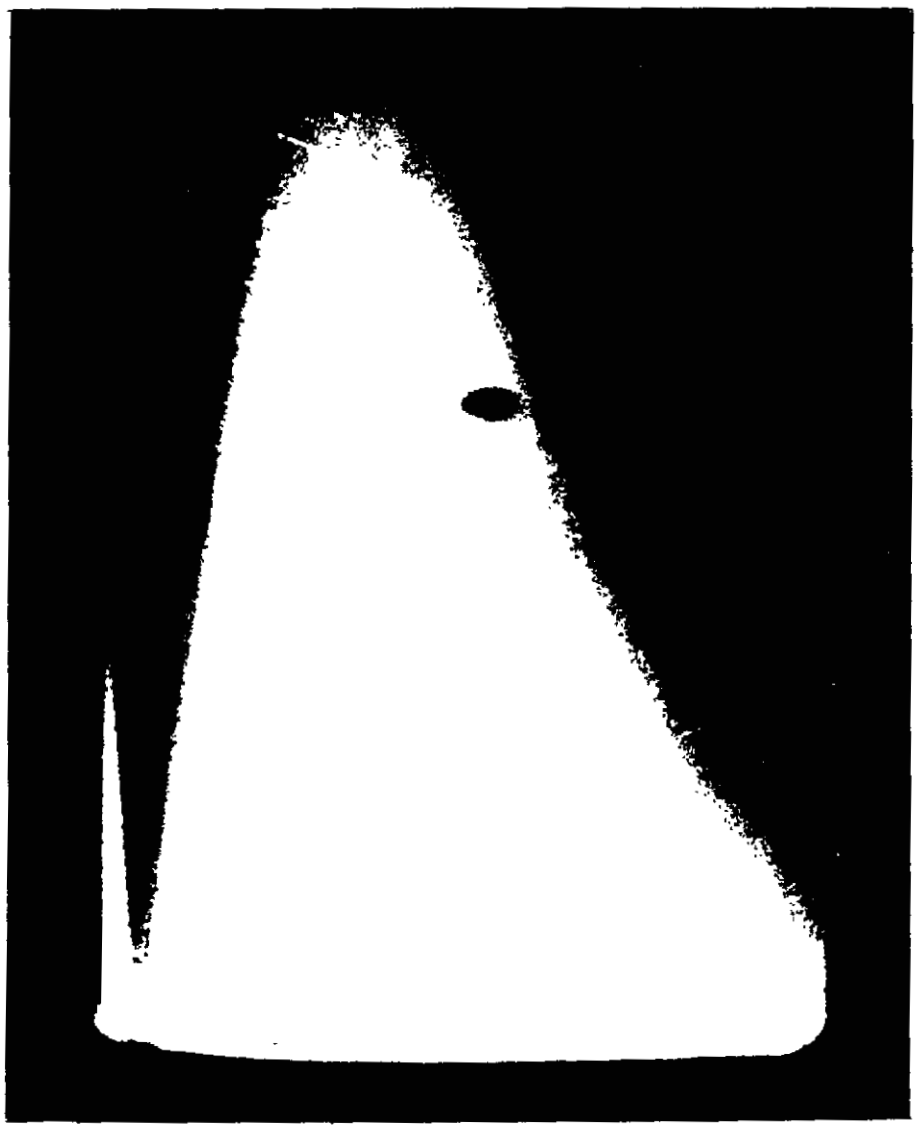

Fig. 16. Sample Pulse Distribution from Low Energy Crystal

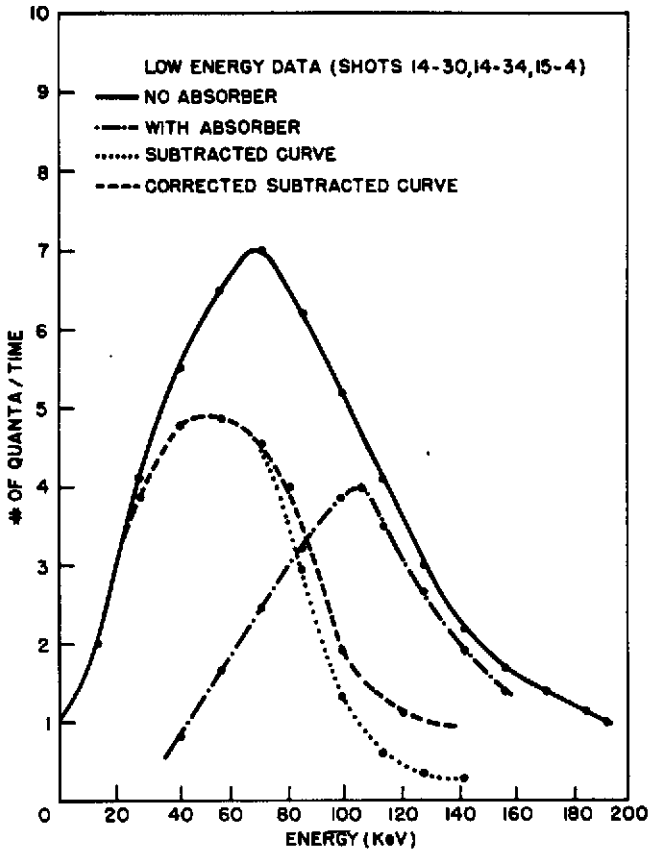

Fig. 17. Data Obtained from Low Energy Crystal

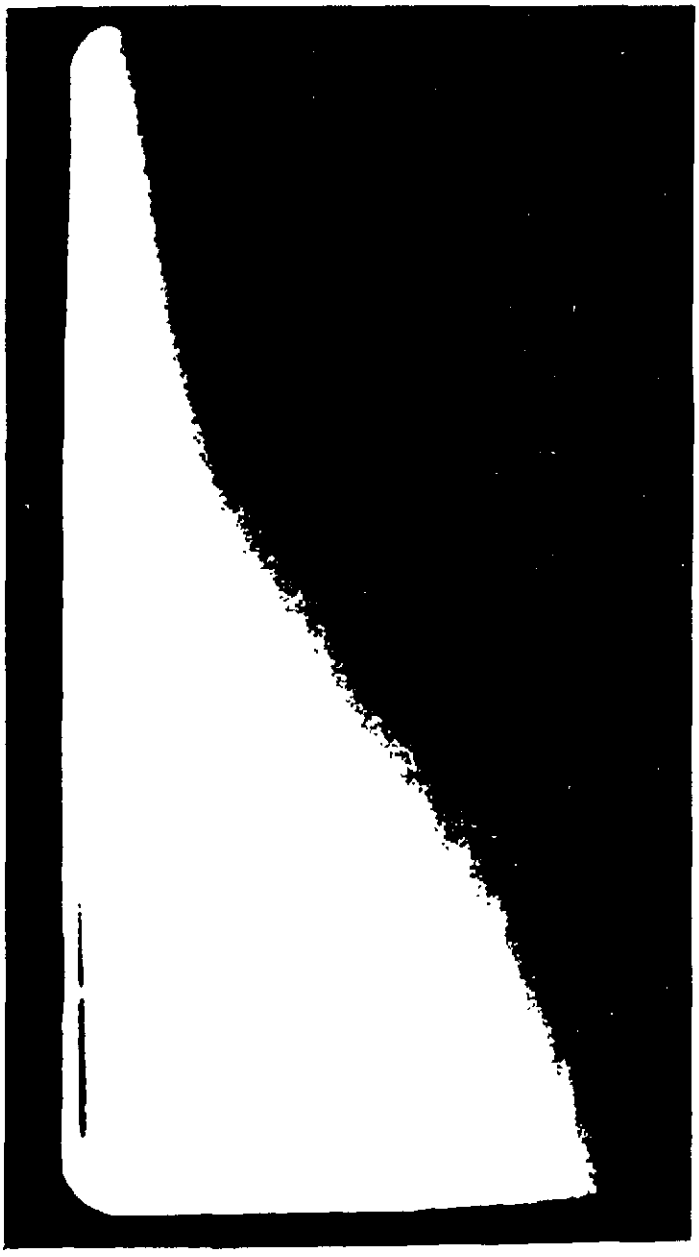

Fig. 18. Sample Pulse Distribution from Intermediate Energy Crystal

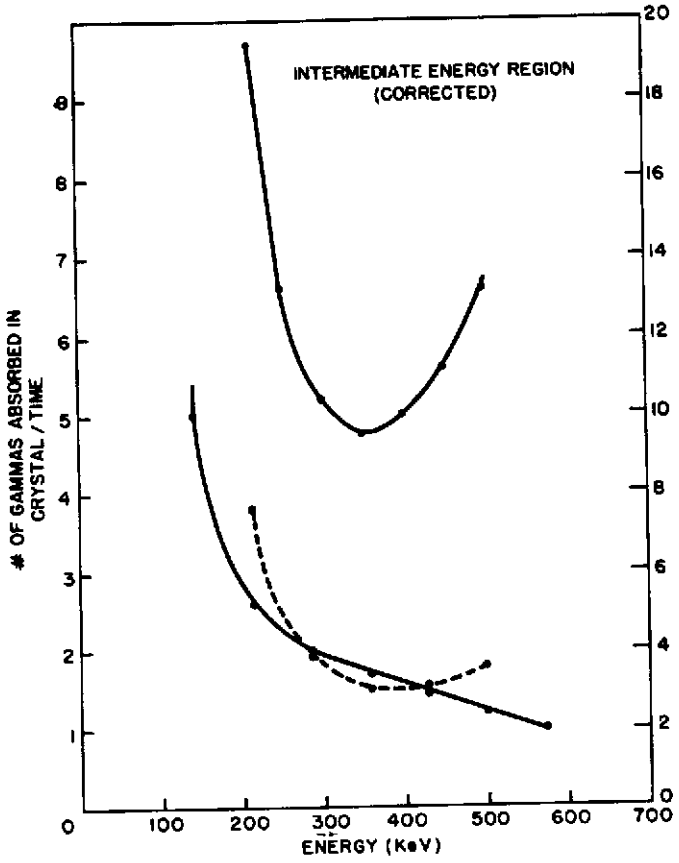

Fig. 19. Intermediate Energy Data

PROJECT 2.4c

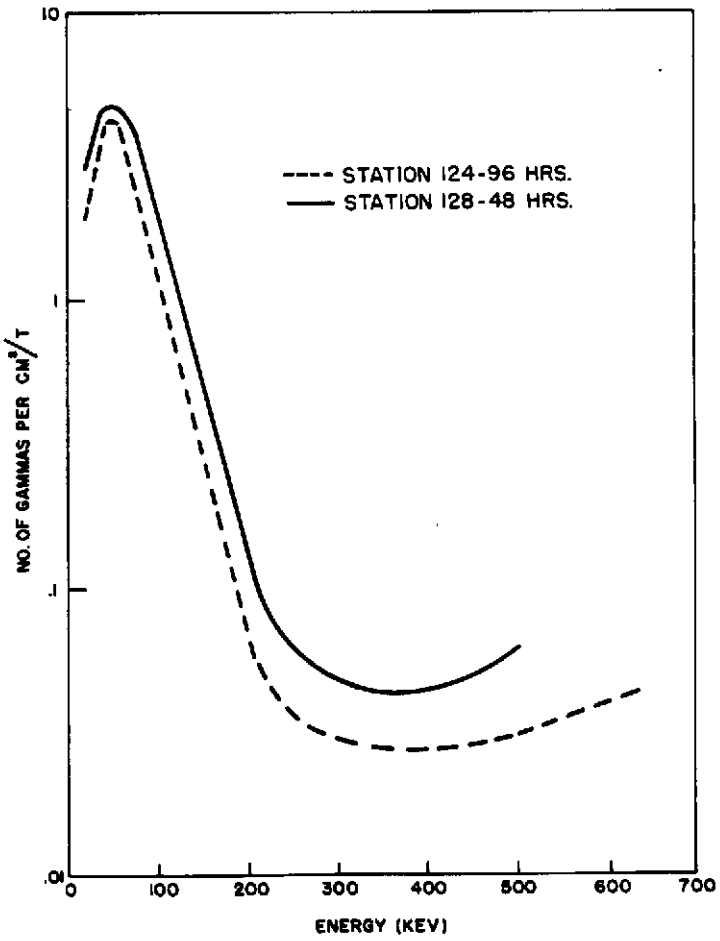

Fig. 20. Composite Curve of Low and Intermediate Energy Regions

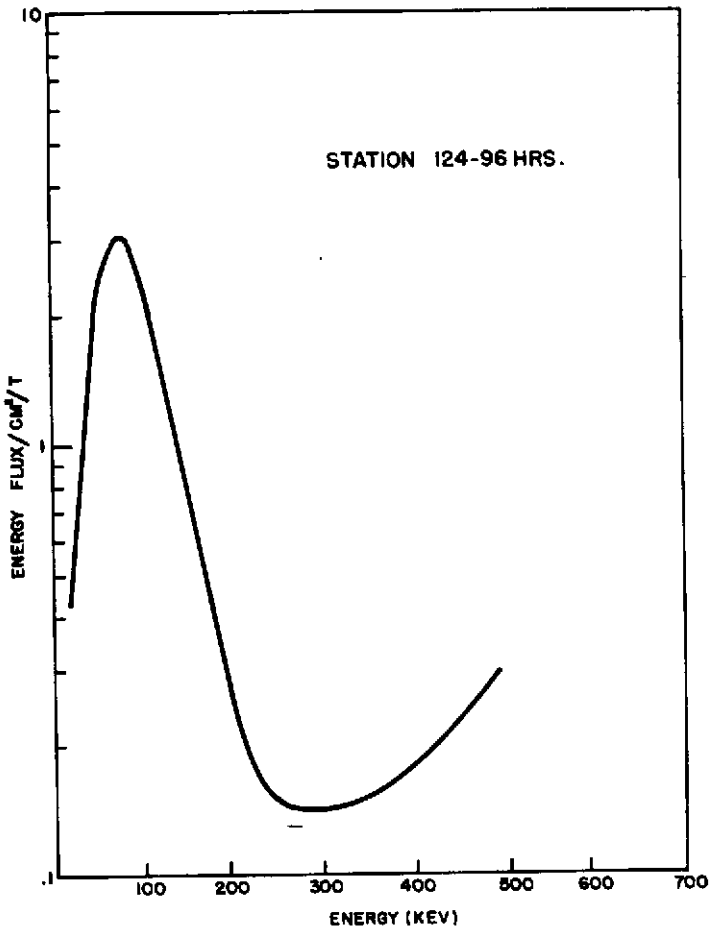

Fig. 21. Gamma Ray Distribution Plotted as Energy Flux vs. Energy

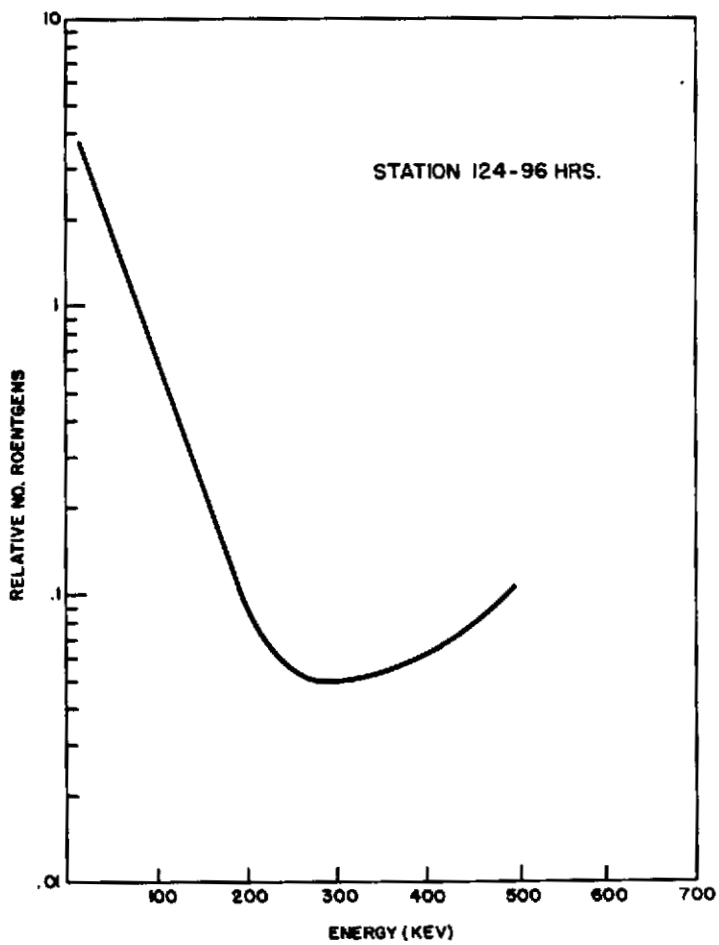

Fig. 22. Gamma Ray Distribution Plotted as Relative Number of Roentgens vs. Energy

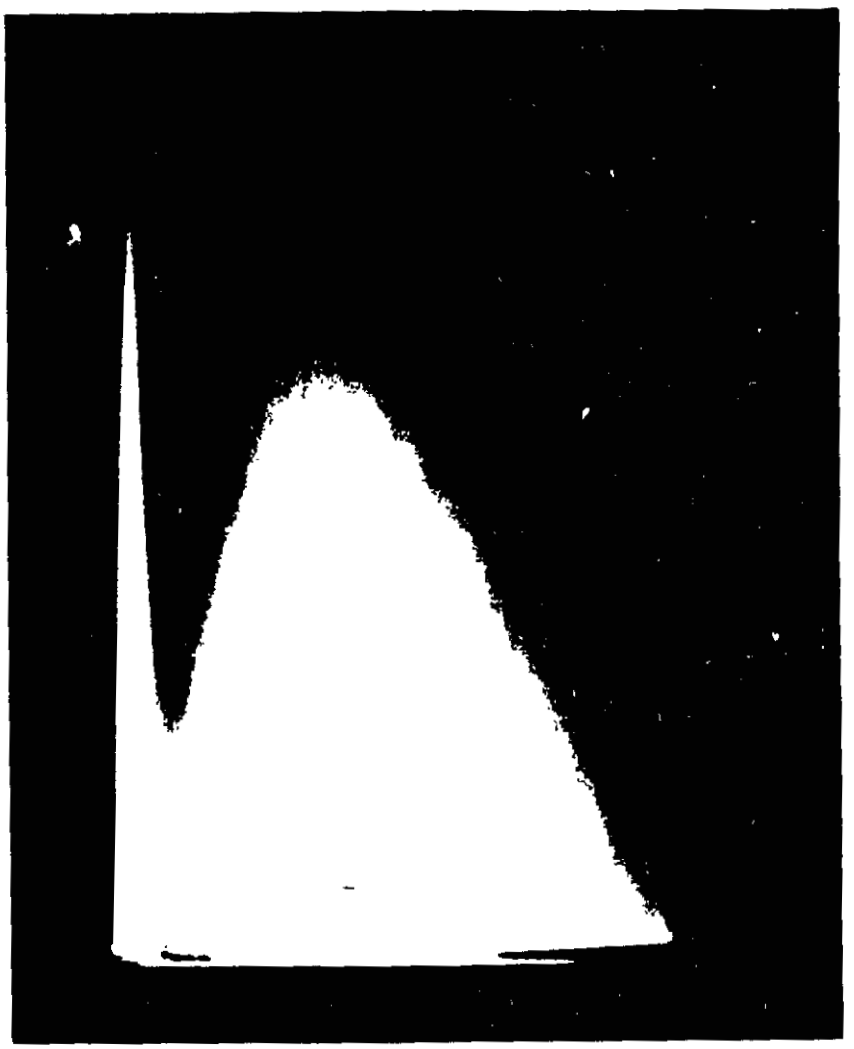

Fig. 23. Van de Graaff Scattered Radiation
(Exp. Photo)

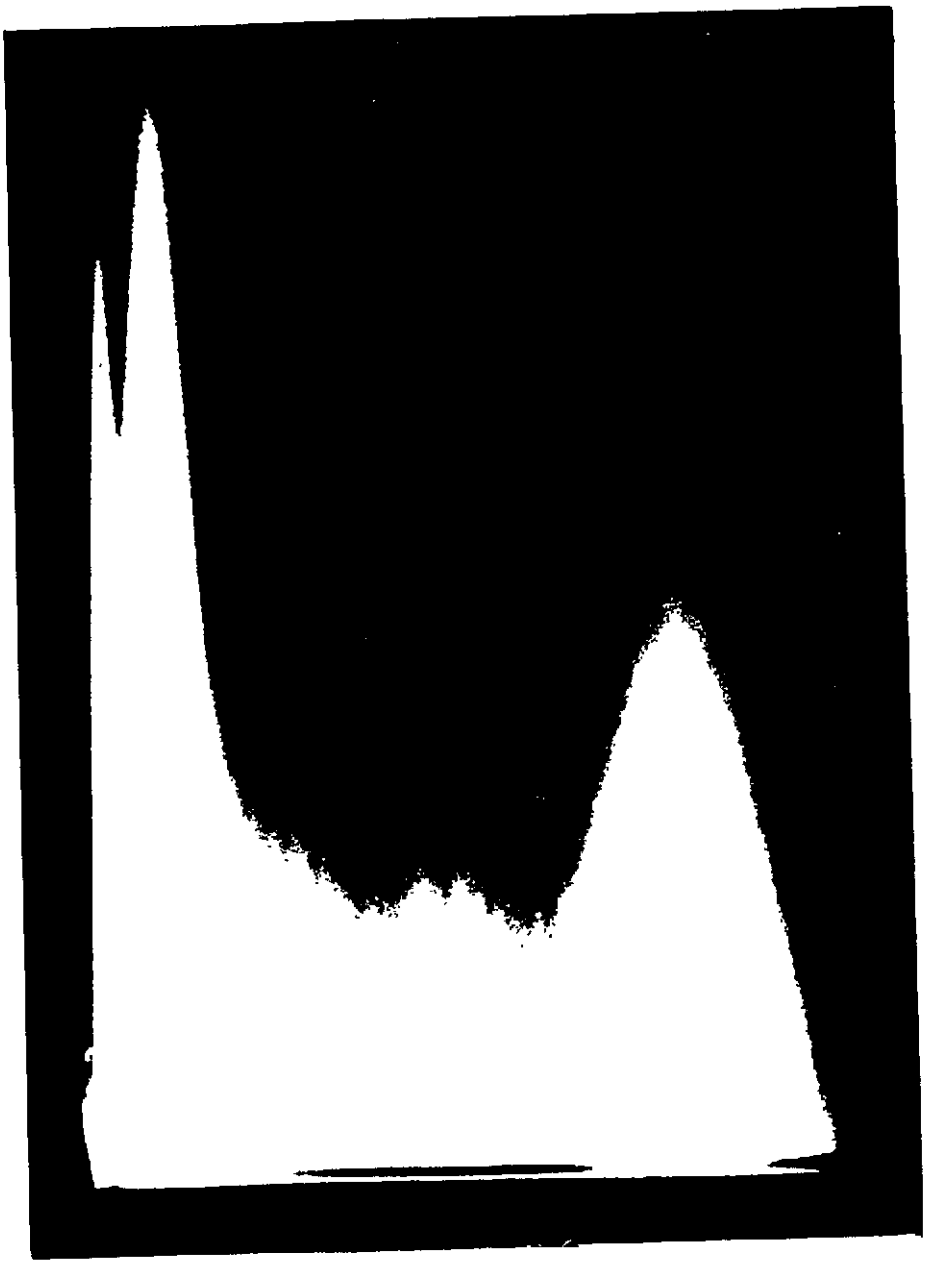

Fig. 24. In^{114} Calibration Photograph

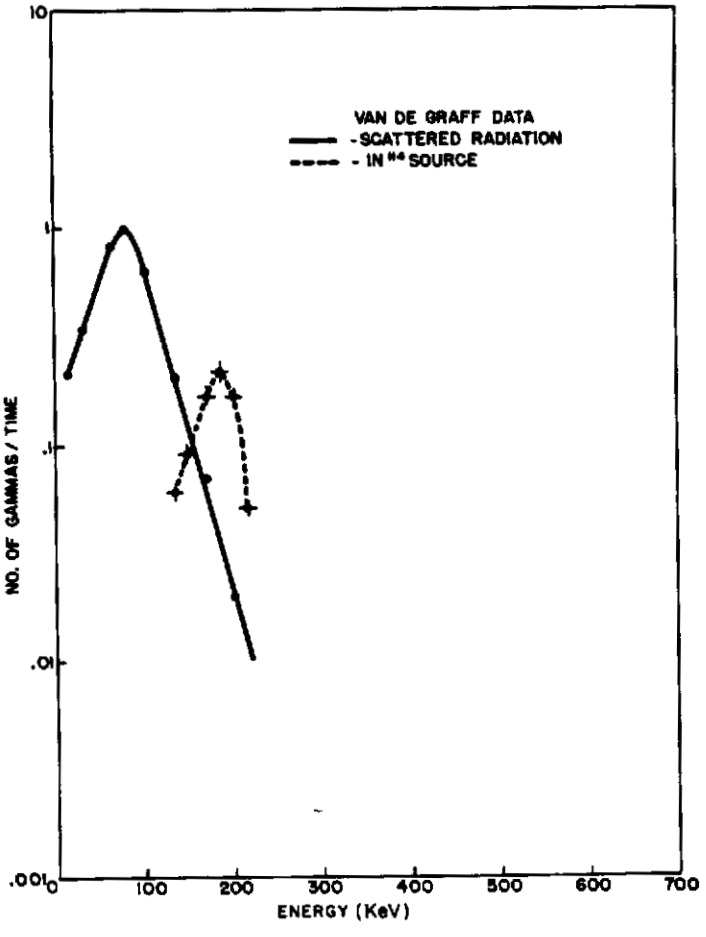

Fig. 25. Van de Graaff Scattered Radiation and In^{114} Source

OPERATION JANGLE

PROJECT 2.7

BIOLOGICAL INJURY FROM PARTICLE INHALATION

By

FALCONER SMITH
D. W. BODDY
MARVIN GOLDMAN

June 18, 1952

Laboratory of Physical Biology

National Institute of Arthritis and Metabolic Diseases

National Institutes of Health

Public Health Service - Federal Security Agency

Bethesda, Maryland

ACKNOWLEDGMENTS

The assistance and cooperation of all the participants made possible the completion of this project. In particular the guidance of Dr. Howard L. Andrews, Director of Program 2 was invaluable. Appreciation is expressed to Lt. Col. Martell and his staff in the AFSWP for their cooperation in providing additional help at critical times.

Assays of radioactivity in tissue samples and radiochemistry were done by Dr. C. R. Maxwell and his staff. Sincere appreciation is expressed for this valuable contribution.

Appreciation is also expressed to Mr. Kenneth Bradshaw whose care of the animals and their quarters, both at Bethesda and at the Test Site, was a most important contribution.

The assistance in fiscal matters given by Mr. G. A. Brandner and in the procurement of supplies by Mr. Lynn Neff of NIH was sincerely appreciated.

Film dosimetry of animal exposure stations conducted by the personnel of the Evans Signal Laboratory, was much appreciated.

PROJECT 2.7

CONTENTS

PROJECT 2.7

ILLUSTRATIONS

PROJECT 2.7

ILLUSTRATIONS (Continued)

[redacted]
Security Information

PROJECT 2.7

TABLES

PROJECT 2.7

ABSTRACT

Mongrel dogs and sheep were exposed at 2500, 5000, and 8000 feet from surface and underground zero. The purpose of the exposure was to assess the hazard due to inhalation of the dust associated with surface and underground atomic detonations; and to compare the internal and external doses obtained in the exposed test animals.

Animals were sacrificed at from H + 10 to H + 24 hours, and at D + 2, D + 4, D + 9, and D + 70 days. Dry ashed homogenates of lung, liver, spleen, kidney, blood, bone, urine and gut contents were assayed for radioactivity. Representative pieces of soft tissues were fixed by a freezing dehydration method for the preparation of autoradiographs. Samples of bone were wet ashed and assayed for their radioactivity.

Radioactivity in tissues taken from animals exposed during the surface shot was extremely low and total body amounts of radioactive materials found at the time of sacrifice were estimated to range between 0.06 μc and 2.13 μc. Total body activity for animals exposed during the underground test ranged between 2.22 μc and 31.1 μc. Integrated internal dosage due to β emission ranged from 0.10 rep to 0.43 rep. Dosage for dog lungs due to β emission ranged between 0.25 and 7.03 rep and between 0.19 and 8.83 rep for sheep lungs. Tissue radioactivity had fallen below limits of detection in all animals by D + 9 following the underground shot. Embryonic tissues and associated fluids contained just detectable activity.

Three types of radioactive particles were detected in autoradiographs of lung tissue. One of these particles was a pure α emitter of 5 mev energy and was probably Pu^{239}. A second type of active particle emitted α and β particles while a third was a pure β emitter of indeterminate energy. Autoradiographs of soft tissue other than lungs showed no blackening. A few bone samples contained sufficient activity to cause some blackening on Ilford plates after 29 days of exposure. No evidence of α activity could be detected in bone samples. Radiochemical analysis of the femurs strongly indicated that their activity was due to Ba^{140} and Sr^{90}.

Amounts of activity taken up by the combined action of inhalation and ingestion in animals exposed to the dust associated with either type of detonation were not physiologically significant. The mixture of materials thus taken up was undetectable in tissues of animals sacrificed 4 days after the surface shot and 9 days after the underground shot. It is calculated that the underground detonation of a 20 KT weapon would not result in a short term inhalation and ingestion hazard to dogs and sheep exposed under conditions comparable with those prevailing during the JANGLE underground test.

CHAPTER 1

INTRODUCTION

1.1 OBJECTIVES

Objectives of the study of the biological injury from particle inhalation, project 2.7, are as follows:

1. To estimate the inhalation hazard associated with the two types of detonations in Operation JANGLE.
2. To determine the relationship between internal radiation dose and external dose in order to evaluate their relative importance in the two types of detonations.
3. To estimate the inhalation hazard from similar detonations of greater yield.

1.2 HISTORICAL AND THEORETICAL CONSIDERATIONS

Under laboratory conditions an evaluation of the hazards resulting from inhalation of radioactive dusts requires that certain fundamental data be available. Not all of these data are obtainable under field conditions. Retention of particulate matter by the lungs is a function of particle size; respiratory pattern, including the rates of flow of air into and out of the lungs; the respiratory rates; and particle concentration in the inhaled air.

Particle size markedly influences depth of penetration and therefore lung retention of the active materials. Van Wijk demonstrated that 25% of 0.2 μ particles were removed by breathing compared to 80% removal of 2 μ particles. Depth of penetration increases with decreasing particle size as shown by Hatch but particles under 0.5 μ in diameter, tend to be flushed out in the exhaled air. Particles 0.5 μ to 5 μ in diameter, assuming no aggregation are more likely to reach the alveoli and be retained in the lung than are either larger or smaller particles. Dygbert demonstrated that intratracheal injection of suspensions of U_3O_8 particles having a size range of 0.2 μ to 10 μ gave a physiological response that varied inversely with the particle size.

From the foregoing evidence it has been assumed in this study that the inhaled particles of physiological significance lie in a size range between 0.2 μ and 5 μ, particle size measurement in the inhaled air

under field conditions being impractical. Particles larger in diameter than 5 μ would not have reached the alveoli in the exposed animals while those below 0.2 μ would be expected to have been flushed out during the exhalation phase of the respiratory cycle.

It is obvious that the duration of exposure to dusts of high concentration will appreciably influence the amount of particulate matter taken into the lungs. Acute exposure of 5 to 30 minutes to suspensions containing P^{32} tagged bacterial spores 0.5 μ to 1.5 μ in diameter were shown by Taplin to result in significant contamination of the lung parenchyma for as long as 72 hours. The exposure of the animals in both the surface and the underground tests of Operation JANGLE are considered of an acute nature the duration of which is about 30 minutes.

The respiratory rates and patterns of the exposed animals during this interval of time had to be taken as average for the species, since no data were obtained on these factors during the test. With human subjects, and flow rates between 60 and 18 liters per minute, Landahl found that retention values were larger at larger flow rates but that even at the lowest flow rates the maximum retention occurred with particles 0.25 μ to 0.55 μ in diameter. Ventilation volumes for the animals during the exposure period will be assumed to be those which have appeared in the literature (see studies by Morgan, Grodins, Comroe and Gardner for dogs; Kibler and Lee for sheep). Dogs, weighing between 8 kg and 15 kg respire at the mean rate of 18 respirations per minute and have an average minute volume of 4 liters. Ventilation volumes in sheep vary widely but may be taken to average 20 liters per minute (range 13 to 25 liters). Respiratory rates per minute for sheep fluctuate between 35 and 44 at 3° to 23°C. Employing these data the total volumes of air passing into the lungs of the dogs and sheep during the 30-minute exposure are calculated to be 120 liters and 600 liters respectively.

Only about 60% of the particulate matter of 5 μ diameter and below is retained in the respiratory tract. Hatch presents data showing that over-all lung retention of particles of less than 1 μ to about 4 μ range between 50% and 70%. Brown, in reviewing several studies, found lung retention to be about 55% for 1 μ particles and about 30% for 5 μ particles.

Calculation of total theoretical uptake by the test animals during a 30-minute exposure following the underground test may be made, using data derived from air-borne particle studies.[1] Median diameter of gross samples in three hour collections on thermal precipitators was 0.22 μ. The radioactive particles of the range 0.5 μ to 8 μ in such samples

1. The authors are grateful to Mr. I. G. Popoff, Technical Coordinator N.R.D.L., for the data used in these calculations.

were found[1] to have a median diameter of 1.4 μ after autoradiographic and optical examination. For the three hour collection period the average mass concentration for 0.5 μ to 8 μ radioactive particles was calculated to be 0.013 μ gm per liter. An 8 kg dog, breathing at the rate of 18 times per minute and exposed to this concentration of material for 30 minutes following the underground detonation (omitting consideration of matter less than 0.5 μ) could have accumulated within its lungs a maximum of 0.93 μ gm. In a similar exposure a 45 kg sheep could have obtained 5.8 μ gm of radioactive particulate matter 0.5 μ to 8 μ in diameter.

From the three-hour collection data the concentration at H + 1 hour of air-borne radioactivity carried by particles in the 0.5-8 μ range is about 100 μc per μ gm. Data from the final report in project 2.5a-2 show that a maximum of 4-6% of the total activity is carried on particles below 20 μ in diameter. Of this amount approximately 1% is carried on particles of less than 1 μ diameter. In addition differential fall-out data obtained in project 2.5a-2 indicate that periods of high concentration of short duration occurred at various stations and therefore the reported concentrations of activity are only approximate. Furthermore the average specific activity of dust particles from collector samples at 10 hours, although constant up to about 3.5 μ in diameter, dropped markedly and remained low in particles up to about 9 μ in diameter.[2] Assuming 1.5 μc per liter as an average value for the particulate matter taken up and retained by both sheep and dogs at the end of 30 minutes, theoretical total uptake of activity for an 8 kg dog would be 180 μc (0.022 μc/gm) and 900 μc (0.020 μc/gm) for a 45 kg ewe. This amount of activity is of the order of 10 to 100 times higher than the total activity determined from measurements of radioactivity in animals exposed during the underground test as will be indicated later, in a discussion of the results.

1. Samples from 2.5a stations 108 and 120.
2. The authors are grateful to Lt. Col. Charles Robbins (project 2.5a) for these data.

CHAPTER 2

TEST RESULTS

2.1 EXTERNAL GAMMA DOSAGE, MORTALITY AND SACRIFICE TIMES FOR ANIMALS EXPOSED DURING THE SURFACE AND UNDERGROUND TESTS

2.1.1 External Gamma Dosage - Surface Test

Tables 2.1 and 2.2 present a schematic arrangement of the layout of the animal exposure stations (12 ewes, 15 dogs) during the surface test and permit a comparison to be made between the location of the stations on their respective arcs and total external radiation dosage received during the exposure. Animal exposure procedures are discussed in Appendix A. Animal stations for the surface test were spaced at intervals of 175, 300 and 400 feet for the 2500, 5000 and 8000 foot arcs respectively. Standard foxholes[1] located along a line 45° east of North at 2500 and 5000 feet from surface zero were constructed. Four animals (2 dogs and 2 ewes) were placed in the foxholes at 2500 feet while 3 animals (1 dog and 2 ewes) were in foxholes at 5000 feet.

National Bureau of Standards film dosimeters placed in pairs within 10 feet of surface animal stations and inside the foxhole stations showed that gamma dosage was less than 10 r at all positions on the 5000 and 8000 foot arcs. Animals exposed at the surface stations at 2500 feet received doses ranging from 265 r on the east end to a maximum of 300 r near the center of the arc. Animals exposed in foxhole positions at 2500 feet received external doses ranging about 3.5% of the dosage received by adjacent surface exposed animals. Table 2.2 gives the distribution of the gamma dose measurements within the foxholes and shows that the dosage at the region of the animals' bodies was less than 10 r at both 2500 feet and 5000 feet.

2.1.2 External Gamma Dosage - Underground Test

Twenty ewes and 23 dogs were exposed to the underground detonation. Tables 2.3 and 2.4 present a schematic plan of the layout for animal stations used during this test. Animals which had been exposed at 5000 feet and 8000 feet from surface zero and which had not been sacrificed were reused for the underground test because gamma doses received during the prior exposure were negligible and radioactive contamination was found to be below significance. Late changes in the layout and number of stations made it impossible to instrument all

1. See Appendix A for dimensions of foxholes.

PROJECT 2.7

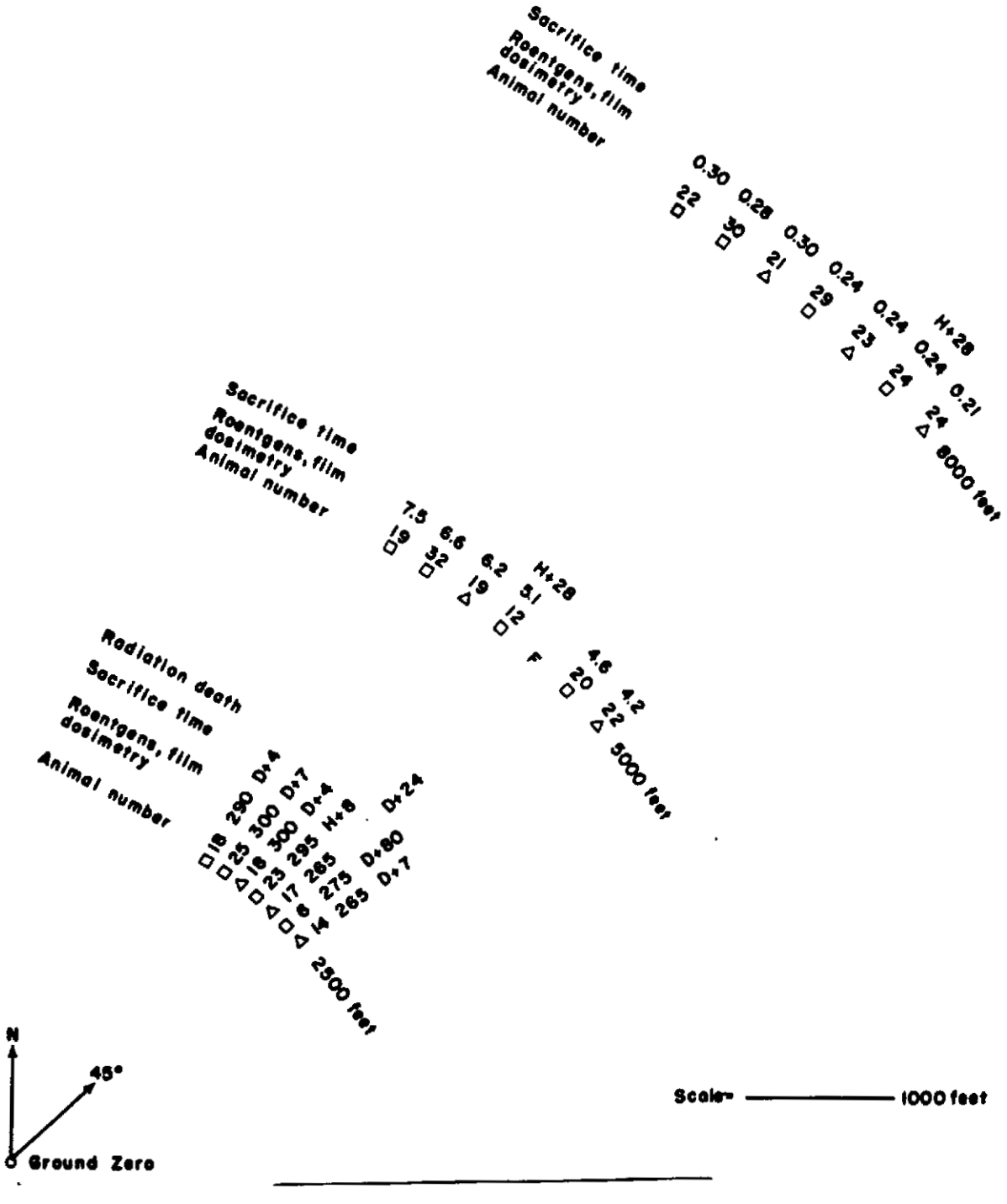

Table 2.1. Animal Exposure Stations, Surface Test; △ Sheep, □ Dogs, F Indicates Foxhole Positions

PROJECT 2.7

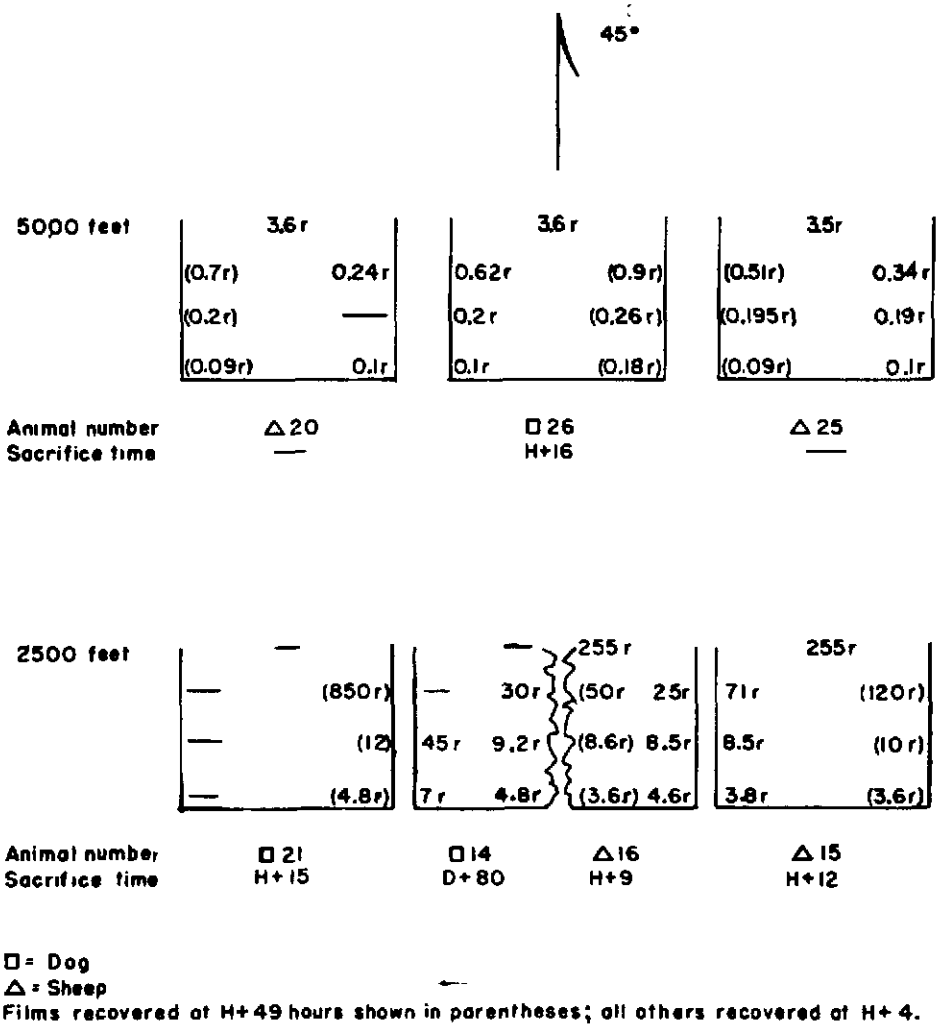

Table 2.2. Foxhole Dosimetry, Surface Test

stations with film dosimeters. Independent measurements made with Polaroid self-developing papers[1] attached at the back of each animal showed that those stations not otherwise instrumented received doses in excess of 400 r. Total external dose was estimated from 6 hour and 24 hour total dose data of project 2.1a[2] for the animal exposure stations which were not metered by film packets and these doses are

1. Polaroid Corporation, Cambridge, Mass., paper designation-DT-65-/PD.
2. L. Costrell, Operation JANGLE, Project 2.1a; Gamma radiation as a function of Time and Distance; National Bureau of Standards, 1952.

shown in parentheses in Table 2.3. Data from 2.1a station No. 123 indicate a 24 hour dose of 360 r while at station No. 124 the total dose was 702 r at 6 hours. An interpolation of the 24 hour total dose

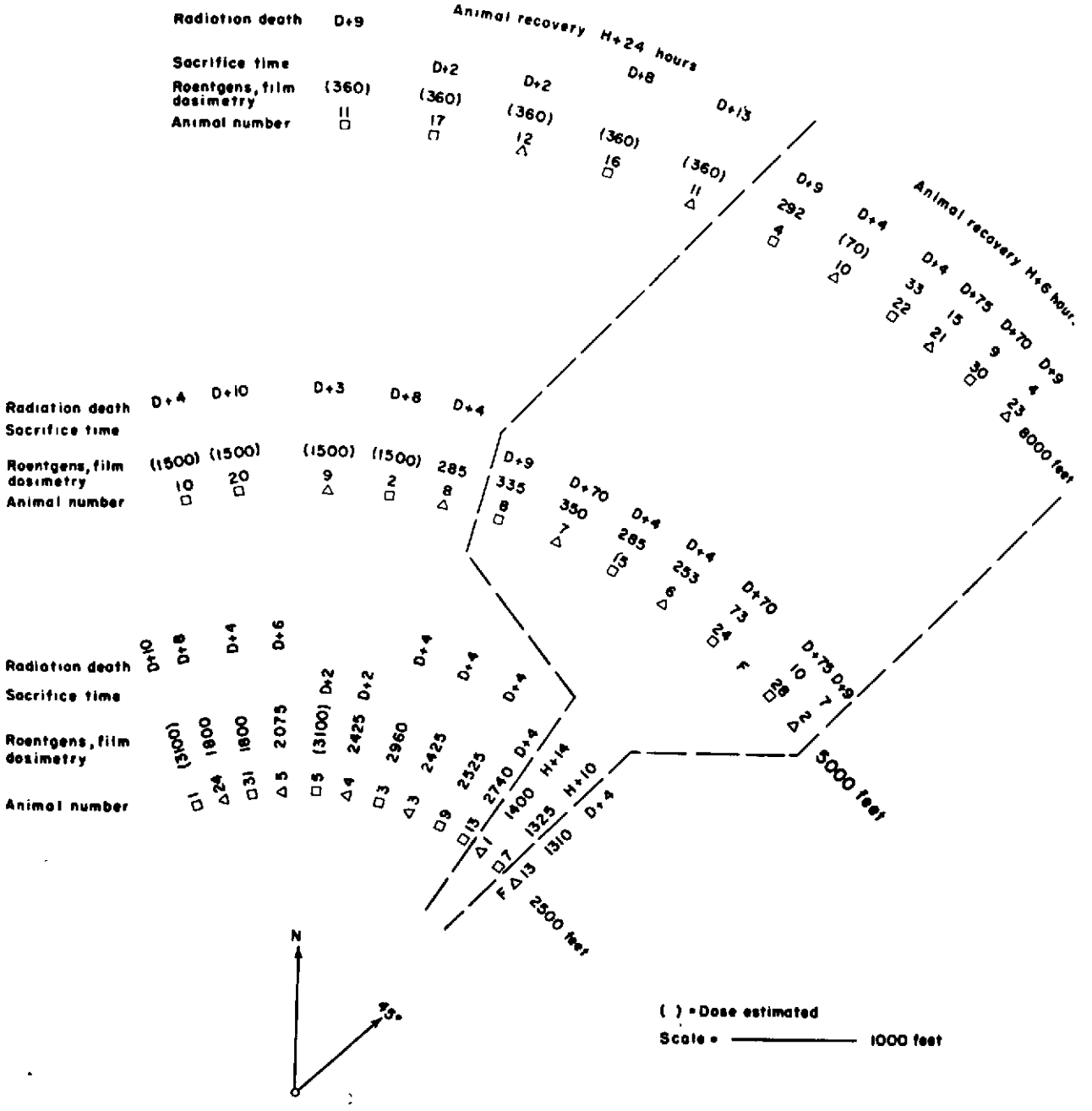

Table 2.3. Animal Exposure Stations, Underground Test; △ Sheep, □ Dogs, F indicates Foxhole Positions

PROJECT 2.7

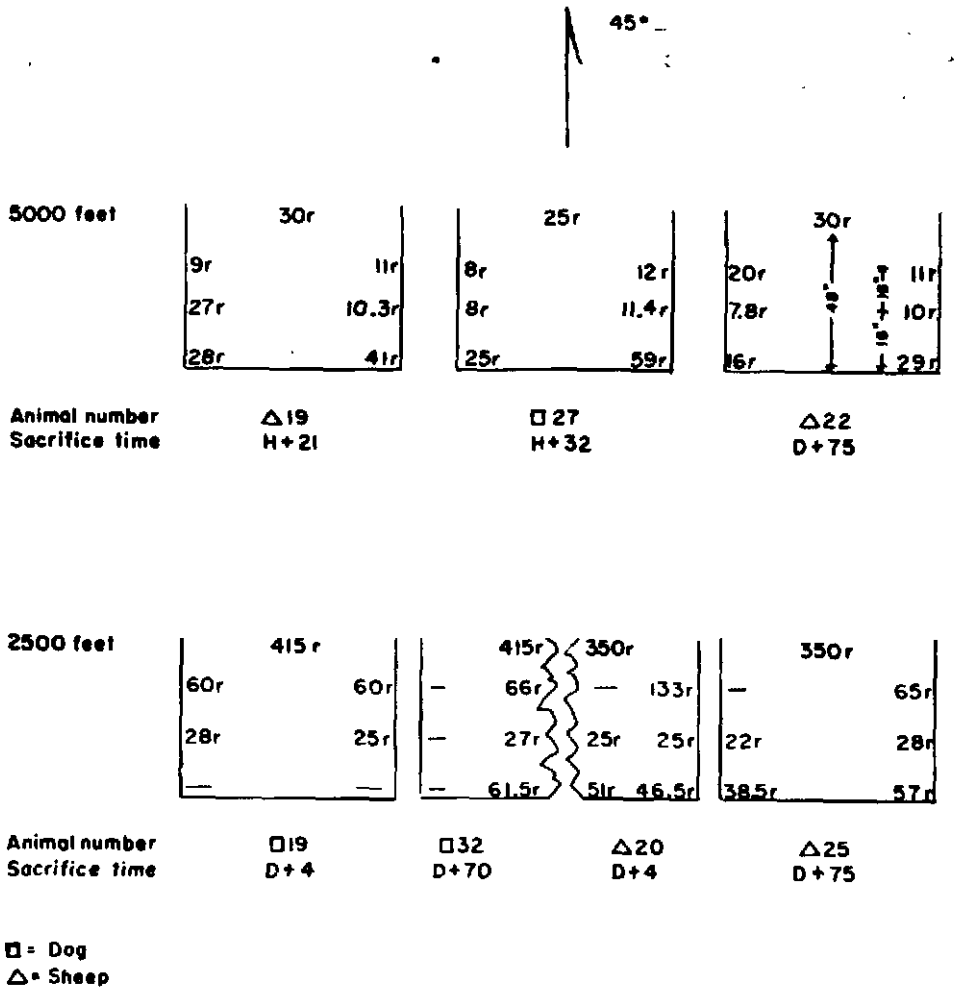

Table 2.4. Foxhole Dosimetry, Underground Test, Symbols as in Table 2.3

data from 2.1a stations No. 120 and No. 114 indicate that the animals toward the north end of the 5000 foot arc may have received about 1500 r. This estimate results in a large difference in dose between dog No. 2 and ewe No. 8. However, the 10 hour, 1000 r contour falls approximately between these two exposure stations. It is suspected that the film dose given in Table 2.3 for ewe No. 8 and dog No. 8 are too low. A similar discrepancy occurs at the north end of the 2500 foot arc in which the last animal received a dose of the order of 3100 r as determined from an interpolation of the results obtained at 2.1a stations No. 102 and No. 108. It is therefore suggested that the doses determined by film dosimetry for dog No. 31 and ewe No. 5 are too low since they are clearly inconsistent with the measurements made in project 2.1a.

External gamma dosages were generaly higher for corresponding stations in the underground test than they were in the surface test. Maximum doses from film measurements for surface exposed animals at 2500 feet ranged from 1800 r near the north end of the arc, 2960 r about the center to 1310 r on the east. Doses ranged between 7 r and 350 r along the 5000 foot arc and between 4 r and 292 r on the 8000 foot arc. Film dosimeters were recovered simultaneously with the animals and recovery was completed for all animals by H + 24 hours. Foxhole exposed animals at 2500 feet received only about 4% of the dose received by adjacent surface exposed animals. At 5000 feet the dosage fell off steeply towards the south at about the 45° line so that surface and foxhole animals appeared to receive nearly similar doses.

2.1.3 Mortality of Animals Exposed During the Surface and Underground Tests

Sacrifice of animals at intervals following exposure in both the surface and the underground test prevented accurate calculation of percent mortality. Table 2.5 summarizes the mortality which resulted from radiation in both tests. Animals that survived to D + 70

TABLE 2.5

Mortality and Sacrifice of Surface Exposed Animals During the Surface and Underground Tests

Distance from Ground Zero in Feet	Sheep				Dogs			
	Sacrifice Before D + 10	Sacrifice at D + 10	Died	MST[a] Days	Sacrifice Before D + 10	Sacrifice D + 70 and 75	Died	MST[a] Days
2500[b]	2	0	1	24	3	1	0	-
5000[b]	0	0	0	-	1	0	0	-
8000[b]	0	0	0	-	1	0	0	-
Total	2	0	1		5	1	0	
2500[c]	2	0	4	5	3	0	4	5.5
5000[c]	1	1	3	3.3	2	2	3	7.4
8000[c]	3	1	1	13	3	1	2	8.5
Total	6	2	8		8	3	9	

a. Mean Survival Time in Days of Animals Which Died of Radiation Injury.
b. Surface Test.
c. Underground Test.

are considered as survivors. Only one animal (ewe No. 17) died following exposure during the surface test, while 8 ewes and 9 dogs died of radiation injury following the underground test. Radiation deaths in this test were more numerous among the animals exposed at 2500 feet than at 5000 or 8000 feet because of the high gamma dosages. Similarly mean time to death was somewhat less in the animals exposed at 2500 feet than in those exposed at 5000 and 8000 feet. Nine of 12 surface exposed dogs had died by D + 10 while 8 of 10 ewes had died by D + 13. No foxhole exposed animals died of radiation injury. All of the animals that died following exposure presented terminal symptoms characteristic of radiation injury. No evidence of blast or thermal burn injury appeared in any of the animals autopsied. At the time of sacrifice of ewe No. 7 (D + 70) lesions were found on the skin between the ears. Since this injury had not been observed prior to D + 40 or 50 days, the injury was considered to have resulted from local irradiation produced by an accumulation of fission products which had been trapped on the skin. At D + 70 a survey meter (G-M type) indicated activity of the order of 11 mr/hr at the site of the injury while at the same time a dose rate of 0.5 mr/hr was measured near the animal's hindquarters. Figure 2.1 illustrates the characteristic appearance of the ewes just prior to their death from radiation injury. Both sheep and dogs refused food shortly after exposure and diarrhea appeared by D + 2 in nearly all cases in which the total dosage had been greater than 100 r.

Tables 2.6 and 2.7 present data showing weight changes in exposed dogs and sheep following the underground test. Percentage weight loss in surface exposed animals tended to be greater with higher total body doses, and the dogs generally suffered a greater percent weight loss than the sheep. Foxhole exposed animals showed weight gains or only negligible losses. Neither food nor water were provided the animals during exposure, and although animals were not weighed immediately after their exposure, only small weight differences occurred in the early sacrificed animals. It is assumed, therefore, that the exposure and deprivation were associated with unimportant weight changes.

2.2 EVALUATION OF INTERNAL HAZARD RESULTING FROM EXPOSURE DURING THE SURFACE AND UNDERGROUND DETONATION

2.2.1 Estimation of Internal Radioactivity Following the Surface Test

Activity was so low in all of the tissues studied from all animals sacrificed, irrespective of their location during the contaminating exposure, that no counting data are considered statistically significant. Table 2.8 summarizes the data obtained and the values given are corrected for decay to the sacrifice time for each animal.

Several assumptions were made in order to calculate total

PROJECT 2.7

TABLE 2.6

Weight Changes in Dogs Exposed in the Underground Test

Group[a]	Dog No.	Wt. in Kg. on Day Exposed	Wt. in Kg. at Day of Radiation Death	Wt. in Kg. at Day of Sacrifice	Day of Death	Day of Sacrifice	Gain or Loss, Kg.	% Change in Wt.	External Dose in r[b]
1	16	16.32	12.24		D + 8		-4.08	-25	(360)
	11	15.19	13.15		D + 13		-2.04	-13	(360)
	17	7.25		6.57		D + 2	-0.68	- 9.5	(360)
	22	7.25		5.89		D + 4	-1.36	-18	33
	4	14.05		13.5		D + 9	-0.55	- 3	292
	30	9.97				D + 70			
2	10	12.01	9.75		D + 4		-2.26	-18.8	(1500)
	2	10.9	7.9		D + 8		-3	-27.5	(1500)
	20	12.92	9.52		D + 10		-3.4	-26.3	(1500)
	15	12.92		11.79		D + 4	-1.13	- 8.7	285
	8	9.29		9.07		D + 9	-0.22	- 2	335
	24	8.16		7.93		D + 70	-0.23	- 2.8	73
	28	11.56		12.25		D + 75	+0.69	+ 5.9	10
3	27	11.56		10.2		H + 32	-1.36	-11.7	
4	31	11.32	8.16		D + 4		-3.16	-27.9	1800
	3	9.06	7.25		D + 4		-1.81	-20	2960
	9	9.07	7.25		D + 4		-1.82	-21	2525
	1	12.2	9.5		D + 10		-2.7	-22.1	(3100)
	7	8.16				H + 10			1325
	5	8.16		6.80		D + 2	-1.36	-17	(3100)
	13	12.92		10.88		D + 4	-2.04	-15.8	2740
5	32	5.89		7.9		D + 75	+2.19	+37.2	
	19	7.25		6.8		D + 4	-0.45	- 6.2	

a. Groups designated as follows:
   1. 8000 foot, surface exposed
   2. 5000 foot, surface exposed
   3. 5000 foot, foxhole exposed
   4. 2500 foot, surface exposed
   5. 2500 foot, foxhole exposed

b. Dose given in parentheses is estimated.

PROJECT 2.7

TABLE 2.7

Weight Changes in Ewes Exposed in the Underground Test

Group[a]	Ewe No.	Wt. in Kg. on Day Exposed	Wt. in Kg. at Day of Radiation Death	Wt. in Kg. at Day of Sacrifice	Day of Death	Day of Sacrifice	Gain or Loss, Kg.	% Change in Wt.	External Dose in r[c]
1	11	46.7	Missing		D + 13				(360)
	12	59.8		52.1		D + 2	- 7.7	-13	(360)
	10[b]	45.3		40		D + 4	- 5.3	-11.7	(70)
	23[b]	49.6		53.9		D + 9	+ 4.3	+ 8	4
	21[b]	36.7		47.6		D + 75	+10.9	+23	15
2	9	49.4	44		D + 3		- 5.4	-11	(1500)
	8	45.3	Missing		D + 4				285
	6[b]	45.3	40.3		D + 4		- 5	-11	253
	2[b]	40.3		38.5		D + 9	- 1.8	- 4.4	7
	7[b]	59.8		65.3		D + 70	+ 5.5	+ 8.2	350
3	19[b]	44.9		52.6		H + 21	+ 7.7	+17.1	
	22[b]	53.5		74.8		D + 75	+21.3	+40	
4	4[b]	44.4		42.2		D + 2	- 2.2	- 5	2425
	3	39	29		D + 4		-10	-25.6	2425
	5	56.2	45.8		D + 6		- 8.4	-14.9	2075
	24	60.2	51.7		D + 8		- 8.5	-14.1	1800
	1[b]	42.2		42.2		H + 14	-	-	1400
	13	53.5		49.4		D + 4	- 4.1	- 7.6	1310
5	20[b]	44.4		39		D + 4	- 5.4	-12.1	
	25	50.7		63		D + 75	+12.3	+21.5	

a. Groups designated as follows:
   1. 8000 foot, surface exposed
   2. 5000 foot, surface exposed
   3. 5000 foot, foxhole exposed
   4. 2500 foot, surface exposed
   5. 2500 foot, foxhole exposed

b. Pregnant an estimated 2-3 months at the time of exposure.

c. Dose given in parentheses is estimated.

Figure 2.1. Ewe No. 8 at D + 3, One Day Prior to Radiation Death Following a Dose of 285 r

radioactive contamination which was present in the animals at the time of their sacrifice. None of the preparations contained sufficient activity to enable decay curves to be made. It was necessary to assume that the distribution of fission products inhaled and ingested corresponded with that which was found for crater and lip earth samples. This assumption seems reasonable in view of the fact that it was found that highly active samples of gut contents and certain tissues taken from animals exposed in the underground test gave decay curves whose slopes fitted reasonably well when compared to similar portions of earth sample decay curves.

Data on tissue samples given in Table 2.8 are subject to a large error because the counting rate was low for all samples and 10 minute counts only were obtained. It is considered worthwhile, however, to present the data with the foregoing reservations to enable a comparison to be made between the surface and underground types of contaminating detonations with respect to their relative internal hazard.

Radioactive contamination for the whole animal was estimated from the counts made upon small samples of lung, kidney, liver, spleen, and blood by multiplying the total weight of the animal by the mean for the samples counted. This procedure presupposes that the musculature of each animal contained an amount of radioactive contamination which was equal to the mean for those organs which were

TABLE 2.8

Estimation of Total Internal Contamination at Sacrifice Time in Animals Exposed at the Surface and in Foxholes During the Surface Test

Group[a]	Animal[b] No.	Time of Sacrifice	Wt. in Gms.	Tissue	d/min/gm	d/min[c]	µc at time of Sacrifice	µc in % of total at Sacrifice Time
1	Dog 29	H+28	7,710	Total body	15.3	1.2×10^5	0.054	100
			72	Lung	35.4	2.5×10^3	0.0012	4.0
				Gut cont.[d]	15.7			
2	Dog 12	H+28	12,240	Total body	28.64	3.5×10^5	0.16	
			85	Lung	0			
				Gut cont.	57.8			
3	Dog 26	H+16	9,520	Total body	23.7	2.3×10^5	0.10	100
			82	Lung	26.3	2.3×10^3	0.0010	1
4	Dog 23	H+ 8	11,330	Total body	202.98	2.3×10^6	1.03	100
			105	Lung	324.4	3.4×10^4	0.0153	1.5
				Gut cont.	36.1			
	Dog 18	D+ 4	88	Lung	44.1	3.8×10^2	0.0002	
				Gut cont.	.0			
	Ewe 18	D+ 4	67,100	Total body	30.3	2.03×10^6	0.915	100
			659	Lung	34.8	2.3×10^4	0.010	1.1
				Gut cont.	22.5			

a. Groups designated as follows:
   1. 8000 foot, surface exposed
   2. 5000 foot, surface exposed
   3. 5000 foot, foxhole exposed
   4. 2500 foot, surface exposed

b. See Tables 2.1 and 2.2 for location of animal stations.

c. Total body weight X mean d/min/gm for all tissues counted.

d. Mean values per gram of contents of stomach, small intestine and large intestine.

PROJECT 2.7

TABLE 2.8 (Continued)

Estimation of Total Internal Contamination at Sacrifice Time in Animals Exposed at the Surface and in Foxholes During the Surface Test

Group[a]	Animal[b] No.	Time of Sacrifice	Wt. in Gms.	Tissue	d/min/gm	d/min[c]	µc at time of Sacrifice	µc in % of total at Sacrifice Time
5	Ewe 15	H+12	41,500	Total body	61.34	2.5×10^6	1.120	100
			625	Lung	93.50	5.84×10^4	0.02	1.8
				Gut cont.[d]	427			
	Dog 21	H+15	12,670	Total body	35.2	4.45×10^6	0.200	100
			131	Lung	45.1	5.9×10^3	0.0026	1.4
	Ewe 16	H+ 9	33,300	Total body	146.1	4.86×10^6	2.18	100
			557	Lung	163.1	9.08×10^4	0.041	1.8
				Gut cont.	177.1			

a. Groups designated as follows:
   5. 2500 foot, foxhole exposed
b. See Tables 2.1 and 2.2 for location of animal stations.
c. Total body weight X mean d/min/gm for all tissues counted.
d. Mean values per gram of contents of stomach, small intestine and large intestine.

studied. The contribution of the gut contents to the total internal dose cannot be assessed reliably. Animals which were sacrificed on or before H + 28 hours had fasted for about 36 hours and as a result had only small amounts of fluid in the gut while the animals which were sacrificed after H + 28 had been feeding and passing feces thereby diluting and removing activity.

For dogs exposed at the surface at 2500, 5000 and 8000 feet the calculated amounts of total body radioactivity were 0.998, 0.14, and 0.054 µc respectively as shown in Table 2.8. Sacrifice times for these animals were from H + 8 to H + 28 hours, the measured values having been corrected for decay to the sacrifice time of each animal. By D + 4 the activities of the tissues in dog No. 18 had decayed to undetectable amounts. Total activity in two dogs which had been exposed in foxholes at 2500 and 5000 feet were calculated to be 0.184 and 0.092 µc respectively. A lower total body internal radioactive contamination occurred at the more distant foxhole exposure. Total internal contamination for a surface exposed dog (No. 23) was about

5 times that found for a foxhole exposed dog (No. 21) although the stations were within 350 feet of each other. Within the limits of accuracy of the measurements these data indicate that the foxhole position afforded a slight protection from contamination due to airborne radioactive particulate material. This protective effect was less marked at 5000 feet where the total activity in surface (0.14 μc) and foxhole (0.092 μc) exposed dogs No. 12 and 26 respectively are comparable.

No surface exposed sheep were sacrificed before D + 4. Total body activity at D + 4 for ewe No. 18 was 0.915 μc, less than 0.005 μc per gram of body weight. Contamination found in two foxhole exposed ewes, No. 15 and No. 16 (2500 feet) was considerably higher than that found in dog No. 21 which was exposed in an adjacent foxhole. Furthermore, it may be noted that the mean gut activity of these two ewes was higher than that found for any of the animals sacrificed before H + 24. This discrepancy is consistent with the fact that the ewes, in handling larger volumes of air would obtain larger amounts of dust for a given exposure time.

A large fraction of the inhaled dust is not retained in the lungs but is removed from the bronchi to the trachea by means of ciliary activity. When the inhaled particles which have precipitated on the moist membranes of the upper respiratory tract are moved into the pharynx they are swallowed and thus enter into the digestive tract. An indeterminate amount of this material reaches the circulation through the gut walls and another fraction of it is eliminated in the feces. Gut contamination is also derived from dust on the hairs about the mouths of the animals. Dogs are mouth breathers more or less of the time and also lick themselves about the face and body frequently. Sheep on the other hand are primarily nose breathers and therefore probably derived the bulk of their gut contamination secondarily from the lungs.

From the comparison of the area of principal fall-out as determined from independent measurements it is clear that the plan of layout of animal stations was such that few of the animals were subjected to the maximum contaminating exposure. This largely accounts for the low activity found in the tissues studied and it is possible only to speculate upon the amount of radioactivity which might have been taken up had the animals been exposed at positions of maximum dust concentration during the surface test.

2.2.2 Summary - Surface Test

1. Total body internal radioactive β contamination was calculated to be less than 1 μc in surface exposed dogs sacrificed before H + 28. A foxhole exposed dog sacrificed within a comparable time had less than 0.2 μc of radioactivity.

2. By D + 4 the counts in tissues were reduced below detectable limits.

3. Amounts of radioactivity calculated for individual animals decreased with distance from ground zero.

4. Neither bone nor soft tissue samples from animals sacrificed at D + 70 contained detectable radioactivity.

2.3 DETERMINATION OF INTERNAL RADIOACTIVITY AND DOSAGE IN TEST ANIMALS FOLLOWING THE UNDERGROUND TEST

2.3.1 Limitation of Field Methods and Measurements

Larger amounts of contamination were present in many tissues obtained from animals sacrificed after exposure during this test than in the surface test. It was therefore possible to estimate with somewhat greater accuracy the total internal activity which resulted from the combined inhalation and ingestion of radioactive dust. Several assumptions have been made in converting experimental data to total activity and total internal dosage and these assumptions will be considered at appropriate places in the discussion of the results. It is unlikely that the order of magnitude of the results would have been altered even with shorter sacrifice intervals and larger numbers of animal stations. Physiological variation between test animals as well as variability in the degree of contaminating exposure accounts for some of the variability in the data about to be presented. The concentration of dust during exposure was controlled only by placing the exposure stations along the arcs indicated in Tables 2.3 and 2.4. No precautions could be taken to insure uniformity in the amount of contaminating exposure. The exposed animals were fasting at the time of exposure and were confined under conditions which might be expected to alter normal respiratory rates. Environmental temperature was low (Appendix C) at the time of exposure and probably resulted in shivering among some of the animals. Shivering may have altered the circulatory rate and in turn effected in some way the rate at which materials were carried through the gut and viscera. Since the effects of internal gamma emitters would be negligible gamma activity was not determined in tissue samples.

Recovery time for some animals was H + 6 hours while the remainder were recovered at H + 24 hours. The extended period of time and the consequent longer fast together with increased total body dosage represent variables of unknown magnitude in respect to internal distribution of activity.

2.3.2 Total Amounts of Radioactivity and Internal Dosage Due to β Activity

Total activities at sacrifice time were calculated from counts obtained on weighed tissue samples prepared as described in Appendix B. Disintegration rate for each organ selected was found as follows:

$$(d/gm/min)_{organ} = (c/min/gm)(\text{geometry correction})(\text{decay correction})$$

An average value for the disintegration rate per gram for the total soft tissues of each animal was determined from the sum of the organ rates.[1] Total body disintegration rate was then found after multiplying the average value for each animal by the total weight of soft tissues. From this value total microcuries was obtained:

$$\text{Total } \mu c = \frac{\text{Total } d/gm/min}{2.22 \times 10^6} (\text{body weight})$$

Substitution of (organ weight) and $(\text{total } d/gm/min)_{organ}$ in the preceding equation gives the total microcuries for a specific organ at sacrifice time.

Figure 2.2 gives the disintegration rate for soft tissues of a few of the animals at the time of their sacrifice. Inspection of the distribution of the experimental points in the figure shows the large amount of variation in the data. The area under a linear plot of the curve shown in Figure 2.2 represents the total disintegrations for an average test animal. Integrated internal dose for the inhaled and ingested mixture was obtained from the experimental points by averaging their extropolated values at H + 10 hours and drawing the decay curve for the earth sample β components through this average. Roentgen dosage was calculated as follows:

$$\text{Integrated internal dose, rep}^2 = \frac{(\text{Total } d/gm/min)(0.7Mev)(1.6 \times 10^{-6})}{83 \text{ ergs}}$$

and the internal dosage for individual animals was taken as proportional to the dose calculated for the average animal and assumes survival to H + 1000 hours. A similar procedure was used in obtaining roentgen dosage to lungs of test animals. Table 2.9 compares internal dose and lung dose due to β activity with external gamma dose. Total internal dose for dogs ranged from 0.10 to 0.43 rep and from 0.05 to

1. For a given test animal counts on samples of lung, spleen, liver, kidney and blood were required in order tc compute total body activity. Blood was taken as 7.2% of the body weight.
2. R.E. Lapp, and H.I. Andrews, Nuclear Radiation Physics, Prentice Hall Co; 1948, p. 435.

0.31 rep for sheep. Roentgen dose to lung tissue was higher than that for other soft tissues and for dogs had a range of 0.25 to 7.03 rep

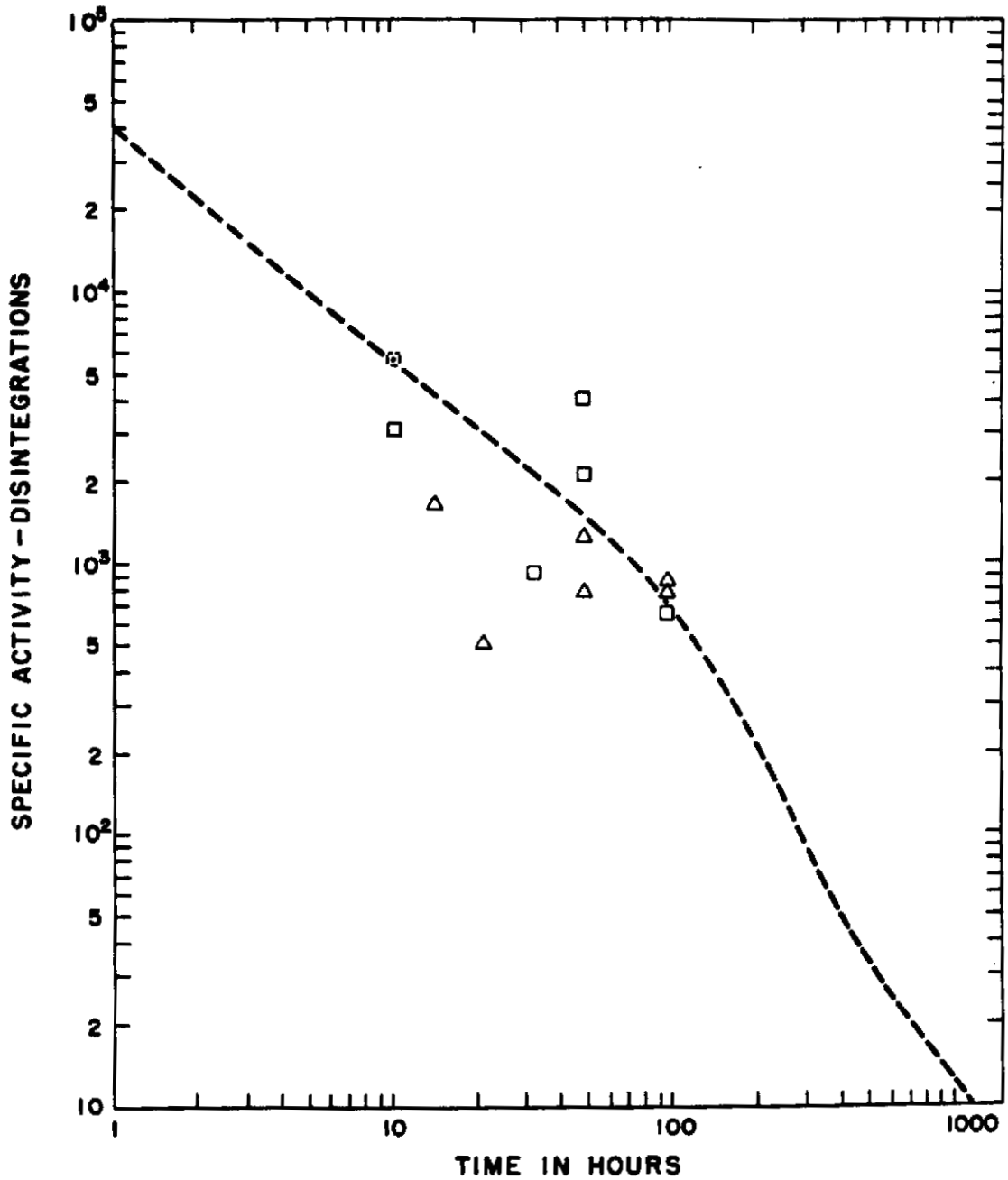

Figure 2.2. Disintegrations Per Gram Per Minute in Soft Tissues of Dogs □ and Sheep △ at the Time of Their Sacrifice Compared with the Physical Decay of the β Components in the Earth Sample (- - -)

PROJECT 2.7

TABLE 2.9

Internal Dose and Lung Dose Due to β Activity Compared to External Dose in Animals Exposed During the Underground Test

Animal No.	Time of Sacrifice Hours	Integrated Dose rep[a]	Lungs Integrated Dose rep[a]	External Dose r[b]
Dogs				
7	10	0.18	2.37	1325
27	32	0.10	0.41	12
5	48	0.43	3.14	(3100)
17	48	0.41	7.03	(360)
13	96	0.19	1.96	2740
Sheep				
1	14	0.10	0.47	1400
19	21	0.05	0.10	11
4	48	0.22	0.99	2425
12	48	0.13	4.69	(360)
20	96	0.31	8.83	133
10	96	0.25	0.19	(360)

a. Values given for test animals are obtained from calculations based on the area under a linear plot of the curve shown in Figure 2.2 and assume survival to H + 1000 hours.
b. External dose in parentheses is estimated.

compared to 0.19 to 8.83 rep for sheep. No correlation could be found between external gamma dose and internal dose among the surface exposed animals. Dog No. 27 and ewe No. 19 were foxhole exposed animals and their internal dosage as well as lung dosage were low. On the other hand ewe No. 20 was also exposed in a foxhole position and her total internal dose as well as lung dose were the highest for the series.

Total body activity in microcuries at sacrifice time was determined when experimental data were sufficiently complete. Tables 2.10 and 2.11 summarize the data for total body and total lung activity in the test animals. Activity in the soft tissue was reduced below detectable limits in animals sacrificed after D + 9 days. Total amounts of radioactive materials (as corrected to sacrifice time) taken up were higher on the average in the ewes than in the dogs. The range for the ewes was from 2.22 to 31.12 μc and from 3.24 to 11.70 μc in the dogs. Similarly the total lung uptake was greater in the ewes, 0.05 to 7.44

PROJECT 2.7

TABLE 2.10

Radioactivity in Soft Tissues and in Lungs at the Time of Sacrifice in Dogs Exposed During the Underground Test

Group[a]	Dog No.	Sacrifice Time	Total Tissues		Integrated Dose rep[b]	Lung	
			μc	μc/gm		μc	Integrated Dose rep[b]
1	17	D + 2	11.70	0.0016	0.41	0.730	7.03
	22	D + 4				0.007	0.25
	4	D + 9				0.036	0.83
	30	D + 70	0				
2	15	D + 4				0.036	0.51
	8	D + 9				0.008	0.69
	24	D + 70	0				
	28	D + 75	0				
3	27	H + 32	4.19	0.0003	0.10	0.080	0.41
4	7	H + 10	11.60	0.0014	0.18	1.160	2.37
	5	D + 2	6.43	0.0007	0.43	0.385	3.14
	13	D + 4	3.24	0.0002	0.19	0.235	1.96
5	19	D + 4				0.217	3.83
	32	D + 70	0				

a. Groups designated as follows:
   1. 8000 foot, surface
   2. 5000 foot, surface
   3. 5000 foot, foxhole
   4. 2500 foot, surface
   5. 2500 foot, foxhole

b. Determined as explained in text, 2.3.2.

μc, than in the dogs, 0.007 to 1.16 μc. This result is in agreement with the relatively larger lungs and higher respiratory rate of sheep.

Specific activities at sacrifice time of all of the tissues examined may be compared in the data given in Tables 2.12 and 2.13. Of all the soft tissues examined lungs had the highest specific activity. Lung specific activity in the dogs was higher than in sheep at any given time of sacrifice with the exception of the two animals-ewe No. 20 and dog No. 19, both of which were sacrificed at D + 4 after exposure in foxholes. Specific activity in the lungs and other organs

TABLE 2.11

Radioactivity in Soft Tissues and in Lungs at the Time of Sacrifice in Ewes Exposed During the Underground Test

Group[a]	Ewe No.	Sacrifice Time	Total Tissues		Integrated Dose rep[b]	Lung	
			μc	μc/gm		μc	Integrated Dose rep[b]
1	12	D + 2	18.75	0.0003	0.13	3.43	4.69
	10	D + 4	2.22	0.0001	0.25	0.05	0.19
2	19	H + 21	11.80	0.0002	0.05	0.11	0.10
3	1	H + 14	31.12	0.0007	0.10	0.92	0.47
	4	D + 2	23.79	0.0006	0.22	0.52	0.99
	13	D + 4				0.15	0.47
4	20	D + 4	14.95	0.0004	0.31	7.44	8.83

a. Groups designated as follows:
   1. 8000 foot, surface
   2. 5000 foot, foxhole
   3. 2500 foot, surface
   4. 2500 foot, foxhole

b. Determined as explained in text, 2.3.2.

was highest in the animals which were sacrificed early and diminished rapidly in animals sacrificed later. Variation in the data was such as to prevent making a reliable estimate of the retention time for the radioactive mixture in the organs.

Pulmonary lymph nodes had lower specific activities than might have been anticipated in view of their function and considering the fact that histological preparations of the lymph nodes contained accumulations of dust particles. Specific activities of kidney, spleen and liver tissues were nearly similar indicating a generalized distribution of the radioactivity among these organs. Blood specific activity was less than spleen or kidney tissues (except for ewe No. 1) showing that in passing through these organs some of its radioactive burden was given up. Urine generally had a higher specific activity than the blood and frequently higher than the kidney from which it was derived.

Specific activity of gut contents in dogs, shown in Table 2.14 was 5 to 10 times higher than lung tissue activity in the

TABLE 2.12

Specific Activities in μc/gm at Sacrifice Time of Various Organs from Dogs Exposed During the Underground Test

Group[a]	Dog No.	Sacrifice Time	Lung	Lymph[b] Node	Kidney	Spleen	Liver	Blood	Urine[c]
1	17	D+ 2	0.0110	0.0049	0.014	0.0018	0.0016	0.0003	0.0065
	22	D+ 4	0.0001	0	0				
	4	D+ 9	0.0004	0.0002					
	30	D+70		0		0	0		
2	15	D+ 4	0.0003	+	+				
	8	D+ 9	0.0001	+					+
	24	D+70	0	0		0	0		0
	28	D+75	0	0		0	0		0
3	27	H+32	0.0008	0.0003	0.0002	0.0004	0.0003	+	0.0017
4	7	H+10	0.0141	0.0003	0.0012	0.0009	0.0014	0.0002	0.0001
	5	D+ 2	0.0051		0.0018	0.0013	0.0009	+	0.0002
	13	D+ 4	0.0025	0.0019		0.0005		0.0002	0.0005
5	19	D+ 4	0.0033	0.0005		0.0003		+	0.0001
	32	D+75	0	0		0			0

Note: Plus indicates that planchet counts were just detectable; 0 indicates no detectable activity; where no figure is given, the determination is lacking.

a. Groups designated as follows:
   1. 8000 foot, surface
   2. 5000 foot, surface
   3. 5000 foot, foxhole
   4. 2500 foot, surface
   5. 2500 foot, foxhole

b. Pulmonary lymph nodes.

c. 1 ml quantities of urine were sampled.

PROJECT 2.7

TABLE 2.13

Specific Activities in μc/gm at Sacrifice Time of Various Organs from Ewes Exposed During the Underground Test

Group[a]	Ewe No.	Sacrifice Time	Lung	Lymph[b] Node	Kidney	Spleen	Liver	Blood	Urine[c]
1	12	D+ 2	0.0072	0.0006	0.0005	0.0002	0.0006	0.0001	
	10	D+ 4	0.0001	0	0.0001		+	0	+
	23	D+ 9	0	0	+				
	21	D+75	0	0		0	0		0
2	6	D+ 4	0.0001	0	0			0	0.0002
	2	D+ 9	+	0	0				
	7	D+70		0		0			0
3	19	H+21	0.0002			+	+	0.0005	0.0049
	22	D+75	0	0		0	0		0
4	1	H+14	0.0019		0.0001	0.0013	0.0004	0.0014	
	4	D+ 2	0.0015		0.0003	0.0020	0.0007	0.0002	
	13	D+ 4	0.0003	0.0002		0		0	0.0003
5	20	D+ 4	0.015	0.0003		0.0003		0	0.0004
	25	D+75	0			0	0		0

Note: Plus indicates that planchet counts were just detectable; 0 indicates no detectable activity; where no figure is given, the determination is lacking.

a. Groups designated as follows:
   1. 8000 foot, surface
   2. 5000 foot, surface
   3. 5000 foot, foxhole
   4. 2500 foot, surface
   5. 2500 foot, foxhole

b. Pulmonary lymph nodes.

c. 1 ml quantities of urine were sampled.

PROJECT 2.7

TABLE 2.14

Specific Activity in μc/gm of
Gut Contents of Dogs Exposed During the Underground Test

Group[a]	Dog No.	Sacrifice Time	Stomach	Small Intestine	Feces[b]
1	17	D + 2	0.020	0.106	0.066
	4	D + 9		0.002	
2	27	H + 32	0.003	0.010	0.004
3	7	H + 10	0.140		2.962
	5	D + 2		0.087	0.067

TABLE 2.15

Specific Activity in μc/gm of
Gut Contents of Ewes Exposed During the Underground Test

Group[a]	Ewe No.	Sacrifice Time	Stomach	Small Intestine	Feces[b]
1	12	D + 2		0.0059	0.0032
	10	D + 4	0.0076	0.0002	
	23	D + 9		0.0001	
2a	6	D + 4		0.0013	
3a	19	H + 21	0.0032	0.0017	
4	1	H + 14	0.0019		0.0012
	4	D + 2	0.0003	0.0003	0.0004

a. Groups designated as follows:
   1. 8000 foot, surface
   2. 5000 foot, foxhole
   2a. 5000 foot, surface
   3. 2500 foot, surface
   3a. 5000 foot, foxhole
   4. 2500 foot, surface

b. Feces were taken from the colon during autopsy.

corresponding animal. This greater amount of activity may partly be due to the fact that the dogs tended to lick themselves and thus ingest radioactive materials collected by the pelt during exposure. Table 2.15 shows that sheep gut contents had only slightly greater specific activity than did the lung tissue of the corresponding animal. No correlation between distance from ground zero and gut activity was evident from the data obtained, nor was there evidence that gut contents of foxhole exposed animals had lower specific activities than surface exposed animals.

The contribution of the contamination in the gut contents to the total internal dose was not evaluated because of the difficulties inherent in the field operations. Animals which had been sacrificed at early times after the shot had fasted for about 36 hours and consequently had only small amounts of fluid in the gut. Animals sacrificed later had taken food and passed feces so that it was felt that estimated quantities of radioactivity would not be realistic.

2.3.3 Comparison of Decay of Contaminating Materials with Earth Sample β Decay[1]

Quantitative and qualitative radiochemical analysis of the radioactive components in the tissues of sacrificed animals was impractical because of the minute amounts of activity present. It was therefore decided to assume identity of internal contamination with earth sample activity. Evidence that fractionation of the inhaled and ingested materials had occurred by the time of sacrifice is shown in Figures 2.3, 2.4 and 2.5. Two animals, dog No. 7 and ewe No. 1 were found to have acquired sufficient activity to permit decay curves to be made of the activity in some tissues. Figure 2.3 shows β decay curves for gut contents and for blood, kidney, lung and spleen of dog No. 7 and allows a comparison of the individual slopes with that found for earth samples. Contamination in stomach contents and lung tissue decays along a slope which appears nearly parallel with the earth sample β decay. Contents of the large intestine have a somewhat steeper slope during the period studied. This lack of correspondence indicates that chemical fractionation of the radioactive materials had taken place during the passage along the gut and is evidence that at least some of the activity measured in the tissues must have been derived from gut contents. The blood and kidney slopes, -1.41 and -1.46 respectively, are nearly linear on a log-log plot and therefore different from the lung and gut contents slopes. On the other hand the spleen contamination decays at a rate which is similar to that

---

1. Crater and lip sample measurements and radiochemical analyses were provided by Dr. Charles R. Maxwell and Capt. Saul J. Abraham of Project 2.6 and the authors wish to express their appreciation for these data.

found for the earth samples.

Figure 2.4 gives decay curves of the contamination found in some of the tissues and gut contents of ewe No. 1. In this case the similarity between decay curves of stomach contents and the earth sample is less striking than that shown in Figure 2.3 for the dog. Decay slope for the blood is -1.48 compared to -1.24 for spleen.

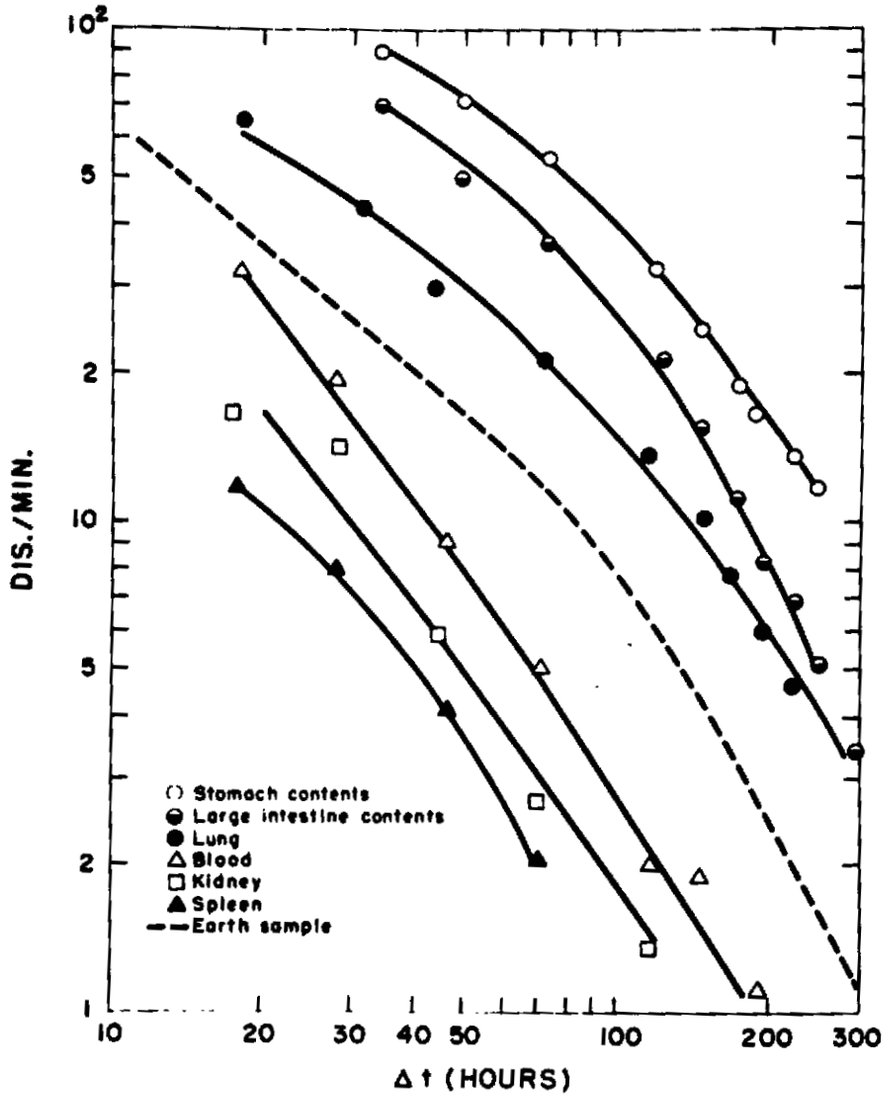

Figure 2.3. Comparison of the β Decay Curves of the Activity in Tissues from Dog No. 7 With Those of Its Gut Contents and Earth Sample

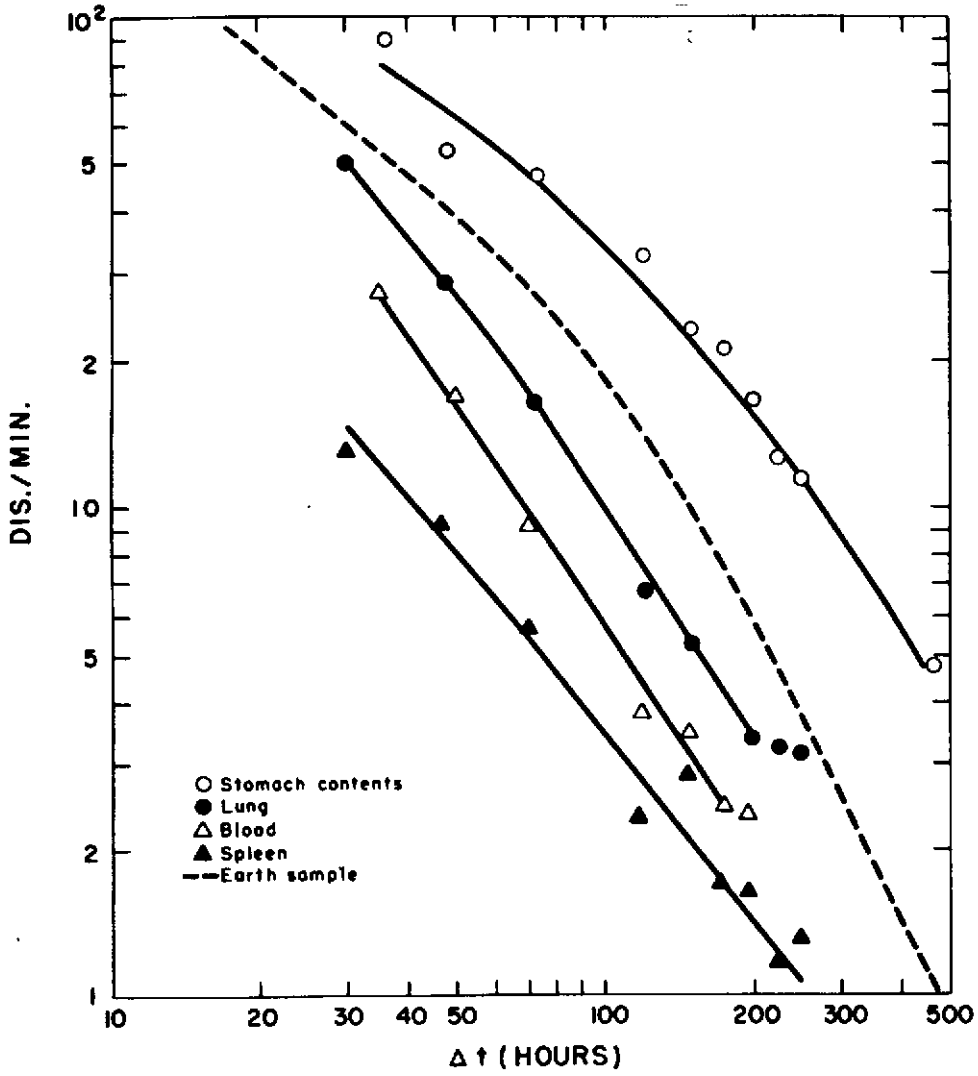

Figure 2.4. Comparison of the β Decay Curves of Activity in Tissues of Ewe No. 1 With Those of Its Gut Contents and Earth Sample

Decay of lung activity is not linear on a log-log plot and corresponds roughly to the earth sample and stomach contents decay curves.

A third illustration of the fractionation which has occurred is shown in Figure 2.5 which compares the earth sample decay with stomach contents, blood, amniotic fluid, placenta and fetal liver. The amniotic fluid β decay slope is -1.27 compared with a slope of

-1.48 for the blood of the same animal. Placental tissue decay parallels stomach contents. Too few points could be obtained for fetal liver to describe a slope accurately, however, if the points be taken to represent a straight line then the slope of the line is -1.26 and therefore similar to that found for the amniotic fluid. This latter assumption implies that chemical fractionation is complete by the time the activity has reached the amniotic fluid. The maternal tissue, represented by the placental curve in Figure 2.5 obviously contained a different mixture of radioactive materials than the fetal liver or amniotic fluid. The residue of activity to which the developing fetus was subjected was therefore different from that which was contained in the closely associated maternal tissue. Furthermore the specific activity was lower in fetal tissues, suggesting that by successive dilution and fractionation in maternal tissues the fetus was subjected to a lower total dose than might have been expected with a completely uniform distribution of activity.

Specific identification of the contamination detected in the tissues could not be undertaken and it has been shown that the internal distribution of the inhaled and ingested radioactive mixture was not uniform quantitatively or qualitatively. It was found possible to make β absorption curves (from H + 148 hours) for the stomach contents of dog No. 7 and for the urine from sheep No. 19. Analysis of these curves indicates that the energy spectra for the activity in the two samples were different thus emphasizing that in its passage through the tissues the inhaled and ingested mixture is fractionated.

2.3.4 Estimation of Amounts of Activity in Fetal Tissues from Pregnant Ewes Exposed During the Underground Test

Radioactivity in amniotic fluid ranged from 1×10^{-4} to 9×10^{-4} μc per gram and in placental tissue from 1×10^{-4} to 5×10^{-4} μc per gram. In Figure 2.5 it was shown that the composition of the activity in the amniotic fluid was not identical with that in the placenta.

Activity per ml. of amniotic fluid in one instance (ewe No. 1) was 9×10^{-4} μc/gm compared to only 5×10^{-4} μc/gm of placental tissue. Total activity in the amniotic fluid[1] in this case was estimated to be of the order of 0.35 μc or just over 1% of the total μc of activity occurring in the mother. Spleen tissue taken from the fetus in this ewe contained as much activity per gram as did the placenta whereas the liver had 1×10^{-4} μc per gram.

No significant activity was found in any fetal tissue from ewes sacrificed after 48 hours after exposure. Data were not

1. This calculation assumes a total volume of 1500 ml.

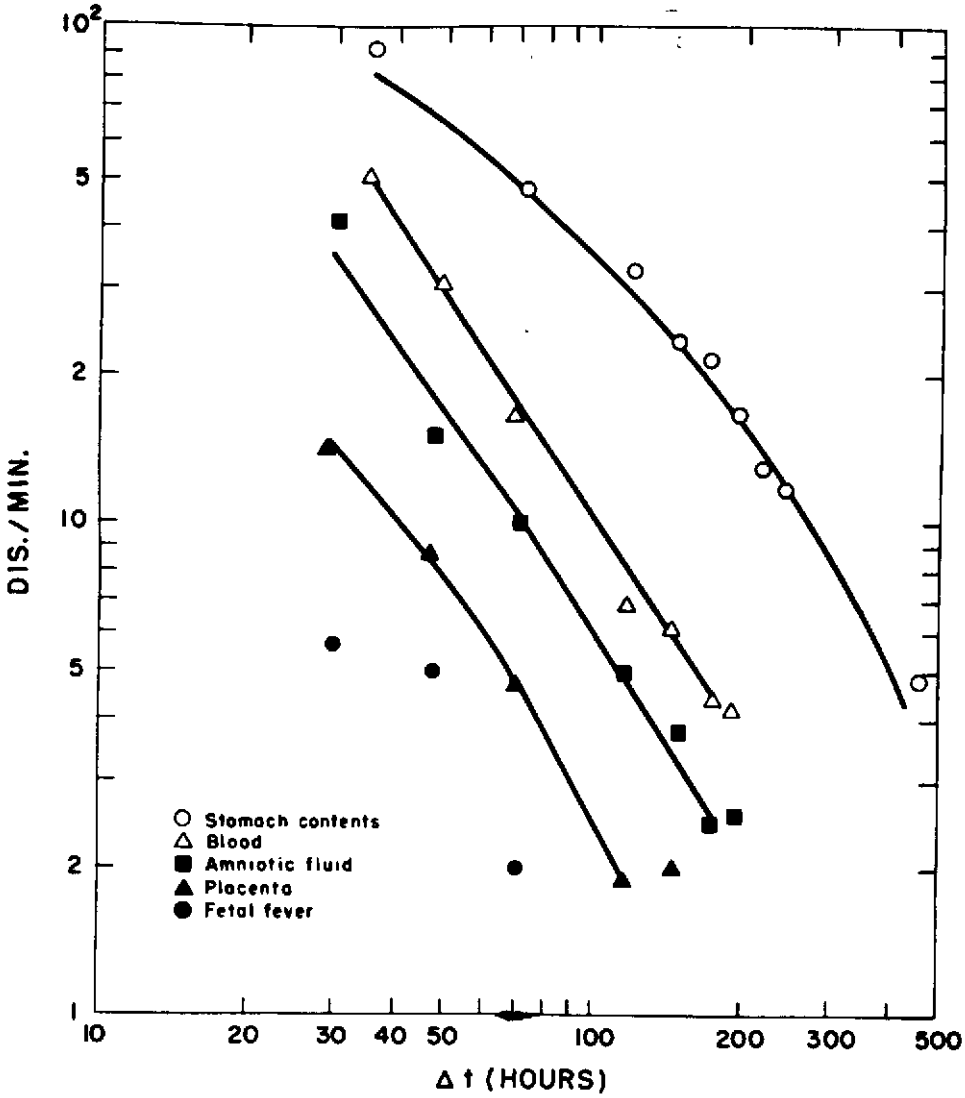

Figure 2.5. Decay Curves of β Activity in Stomach Contents and Blood Compared with Amniotic Fluid, Placenta and Fetal Liver in Ewe No. 1

obtained which would permit a calculation to be made of integrated dose for the developing fetuses. It is estimated from the data available that activity was so low that the dose was below physiological significance. No evidence of radioactivity in fetal bones could be found, thus indicating that neither Ba^{140} nor Sr^{90} passed the placental barrier in detectable amounts.

One ewe (No. 7) gave birth to two normal lambs on D + 69.

External gamma dose to this animal was 350 r, a dose which had been lethal to several ewes as indicated in Table 2.3. Under the conditions of exposure in the underground test some developing sheep fetuses had quantities of radioactivity which were just physically detectable. From the fact that no fetal radioactivity could be detected after H + 48 hours and from the fact that one ewe carried her lambs to normal birth, it is assumed that normal development and parturition could have followed in all the pregnant ewes which would have survived the external dose.

2.3.5 Deposition of Radioactive Material in Bones of Test Animals

Radiochemical analysis of material from the bones of pup C[1] and dog No. 17 strongly indicated that the activity was due to radioactive barium and strontium. The calculated decay curve[2] of Ba^{140} and Sr^{90} compares favorably with experimental determinations of decay of the activity in several bone samples as shown in Figure 2.6. These facts do not exclude the possibility that the bone activity may have been due to additional materials besides these two components. However, the data are taken as evidence that deposition of both Ba^{140} and Sr^{90} had occurred in the bones of some of the dogs. Activity in the bones of the several dogs indicated in Figure 2.6 was qualitatively uniform.

Bone samples were prepared by wet ashing with nitric acid and Table 2.16 presents data showing the specific activity of the bone at the time of their sacrifice or death in the animals exposed to the underground detonation. Roentgen dosage to the bone could not be calculated because of differences in uptake and wide variability among determinations. There is a correlation between bone activity and exposure position during the test. Femurs of most of the dogs exposed at 2500 feet contained appreciable amounts of activity while few of the femurs of dogs exposed at 5000 or 8000 feet contained enough activity to be significant in counting. Femurs of three pups exposed at each of the three distances had the highest specific activity due probably to the greater rate of bone growth in the juveniles. Sheep femurs did not contain sufficient activity for reliable measurement. The nearly complete absence of detectable radioactivity in sheep bones may be due to sampling error if it is assumed that the metabolism of the bone-seeking mixture which was taken up was similar in sheep and dogs. A smaller quantity would have been deposited per gram of bone in the sheep than in the dogs because of the greater total quantity of bone in the sheep. Dilution in this way may have obscured the detection of activity in 0.5 gm. samples of bone even though the total activity was somewhat

1. Pup C and dog No. 17 were placed together in a cage during exposure at 8000 feet.
2. This calculation assumes an initial ratio of 1 Sr^{90}: 5 Ba^{140}.

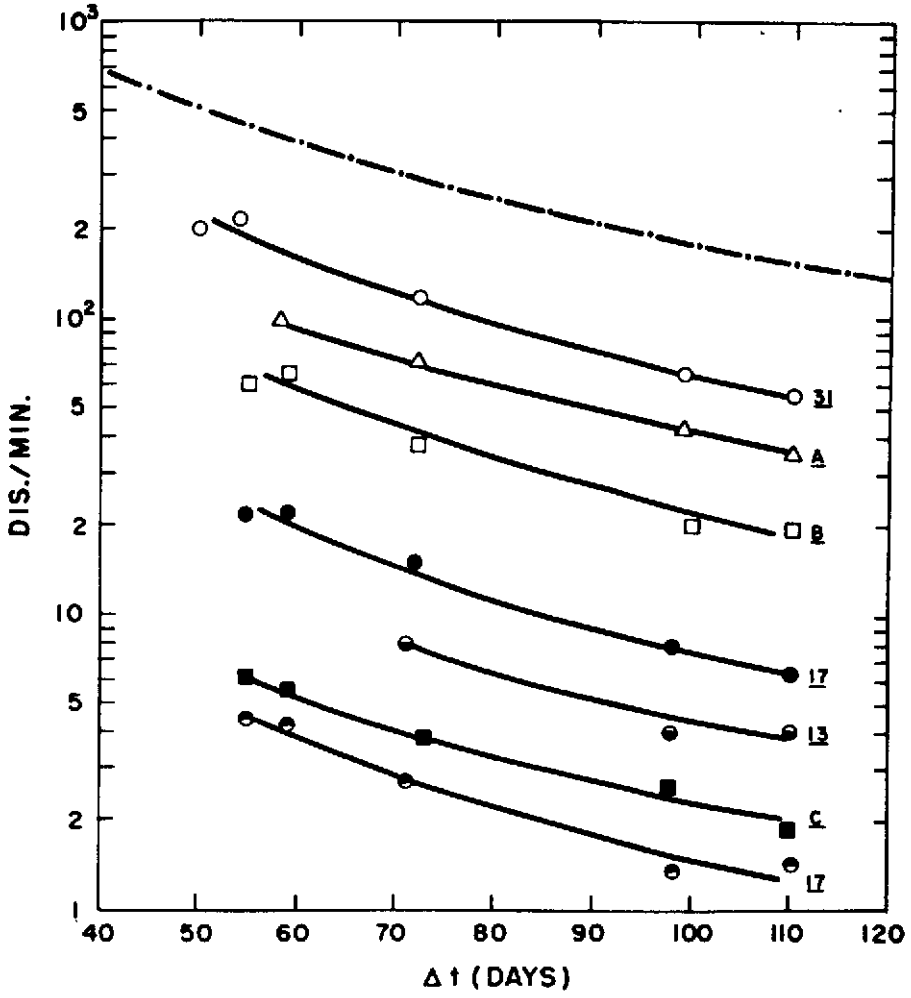

Figure 2.6. Comparison of the Decay of Radioactivity Deposited in the Femurs of Adult Dogs Nos. 31, 16, and 13, and Three Pups, A, B, C, (solid lines) With a Calculated Curve of Ba^{140} and Sr^{90} (broken line). The calculated curve assumes an initial ratio of 1 Sr^{90}: 5 Ba^{140}.

higher in sheep than in dogs.

Figure 2.7 shows the distribution of the activity in the bones of the 3 pups and one adult dog (No. 17). Pup bones show deposition of activity in epiphysial cartilage and an almost equally heavy deposition in the spongiosa and shaft. The portion of the head of the femur of the adult dog shows a faint shadow along the shaft and the contour of the proximal end of the bone is just visible.

TABLE 2.16

Specific Activities in μc/gm at Time of Death in Samples of Femurs from Sheep and Dogs Exposed During the Underground Test

Group[a]	Animal Number	Time of Death or Sacrifice	μc/gm[b]
1	Dog 17	D + 2	0.0023
	" 22	D + 4	+
	" 16	D + 8	0.0007
	" 4	D + 9	+
	" 11	D + 9	+
	" 30	D + 70	0
	Pup C	D + 3	0.0169
	All Ewes (5)	D + 2 - D + 75	0
2	Dog 10	D + 4	+
	" 15	D + 4	0
	" 2	D + 8	+
	" 8	D + 9	+
	" 20	D + 10	+
	" 24	D + 70	0
	" 28	D + 75	0
	Pup B	D + 7	0.0012
	All Ewes (4)	D + 2 - D + 70	0
3	Dog 27	H + 32	+
	Ewe 19	D + 21	+
	" 22	D + 75	0
4	Dog 5	D + 2	0
	" 3	D + 4	0.0009
	" 9	D + 4	0.0008
	" 13	D + 4	0.0017
	" 31	D + 4	0.0012
	" 1	D + 10	0
	Pup A	D + 3	0.0074
	Ewe 13	D + 4	+
	" 24	D + 8	+
	Other Ewes (3)	D + 2 - D + 6	0
5	Dog 19	D + 4	+
	" 32	D + 70	0
	Ewe 20	D + 4	0
	" 25	D + 70	0

a. Groups designated as follows: 1. 8000 foot, surface exposed; 2. 5000 foot, surface exposed; 3. 5000 foot, foxhole exposed; 4. 2500 foot, surface exposed; 5. 2500 foot, foxhole exposed.

b. + indicates that planchet counts were detectable but below statistical significance; 0 indicates no detectable counts in the planchet.

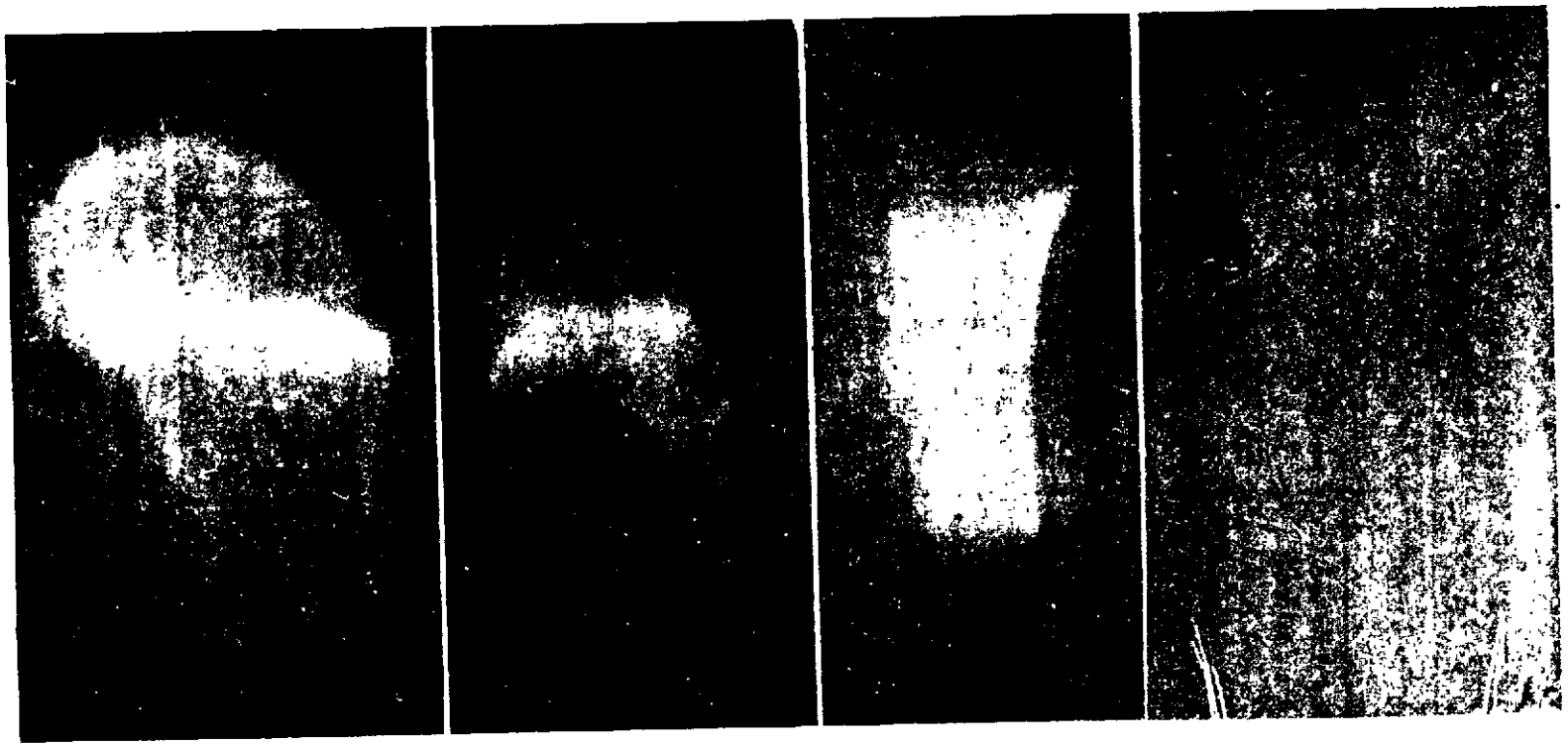

a b c d

Figure 2.7. Autoradiographs Produced by Pieces of Femurs of Dogs Exposed During the Underground Test; a, b, c, Proximal Ends of Femurs of Pups A, B, C Exposed at 2500, 5000 and 8000 Feet; 38-day Exposure on Emulsion, 3 X; d, Head of Femur of Dog No. 17, 29-day Exposure on Emulsion, 3 X

2.3.5 Summary - Internal Radioactivity and Dosage Following the Underground Test

1. Total internal dosage assuming survival to H + 1000 hours for test animals was calculated to be less than 1 rep. Dose to lung tissue calculated in the same way varied from 0.10 to 8.83 rep.

2. Total quantities of radioactivity exclusive of bone and gut contents at sacrifice time were between 2.2 and 31.2 μc with a range in specific activities of 0.0001 μc/gm to 0.0016 μc/gm. At the same time total amounts of activity in lung tissue ranged from 0.007 μc to 7.44 μc with specific activities of lung tissue in the range of 0.0001 μc/gm to 0.0141 μc/gm.

3. There was no evidence that foxhole exposure positions afforded an appreciable alteration in total uptake of radioactive materials over surface exposure positions.

4. Radioactivity had diminished to undetectable amounts in many tissues by D + 9 and by D + 75 days had dropped below detectable levels in all tissues.

2.4 DEPOSITION OF PARTICULATE MATTER IN LUNGS AND OTHER TISSUES- AUTORADIOGRAPHIC EVIDENCE

Autoradiographic evidence of the deposition of radioactive contaminants was sought for both in the lungs and in other soft tissues. Since the total body quantities of radioactivity were of such low order in the tissues of animals exposed during the surface test no autoradiographs were made. Ten μ sections of soft tissues from animals which had relatively large amounts of activity following exposure in the underground test were exposed on Ilford G-5 nuclear track plates (see Appendix B for methods). After exposure times beginning at D + 7 days of from 27 days to 71 days duration all tissues except those of the lungs and bones were considered to be at background level. Attempts to find evidence of localized activity by means of differential grain counts were unsuccessful because of the extremely small amounts of radioactivity and the consequent small differences between background grain counts and grain counts underlying the tissue. Examination of samples of lung tissue was only mildly rewarding in that an occasional section revealed concentrations of activity as evidenced by clusters of activated grains.

PROJECT 2.7

Evidence of three types of particles, based on the reaction in the emulsion, could be distinguished beneath the lung tissue sections. In the examination under high dry and oil of 107 sections of lung tissues of both sheep and dogs a single specimen of a pure α emitting particle was found. Figure 2.8a and b are dark-field and bright field illustrations of the tracks originating from this particle. The mean track length, 20 μ, corresponds to the emission of α particles of 5 mev energy, therefore the particle is probably Pu^{239}, although Po^{210} can not be excluded. Total exposure time for the particle illustrated in Figure 2.8 was 47 days and about 400 tracks were produced in the emulsion during that time. The total number of disintegrations and the mass of the original particle were calculated as follows:

$$n = \frac{2\,C^{1}}{\lambda \cdot t} \qquad (2.1)$$

where: n = number of atoms
C = observed track count
λ = disintegration constant for Pu^{239}
t = exposure time

substituting experimental values in (2.1) (2.2)

$$n = \frac{800}{(9.13 \times 10^{-13})\,(8.64 \times 10^{4})\,(47)}$$

$$= 2.164 \times 10^{8}$$

and this number of atoms represents a mass of

$$\text{gms.} = \frac{2.164 \times 10^{8}}{6.023 \times 10^{23}}\,(239) \qquad (2.3)$$

$$= 8.58 \times 10^{-14}$$

It is not possible to state whether the entire particle was made up of Pu^{239} or whether the mass calculated above was carried on a radio-inert fragment. A similar calculation may be made in the case of Po^{210}.

A second type of particle illustrated in Figure 2.9 was found only once after careful examination of the lung sections. This particle carried both β and α activity as evidenced by the presence of numerous granules and several α tracks in the underlying emulsion. Because of the proximity of the grains and the tracks it was assumed that both types of activity were carried together on a single particle although the dust grain was not seen.

1. Yagoda, H., Radioactive Measurements with Nuclear Emulsions, J. Wiley and Sons, N.Y. (1949), p. 215.

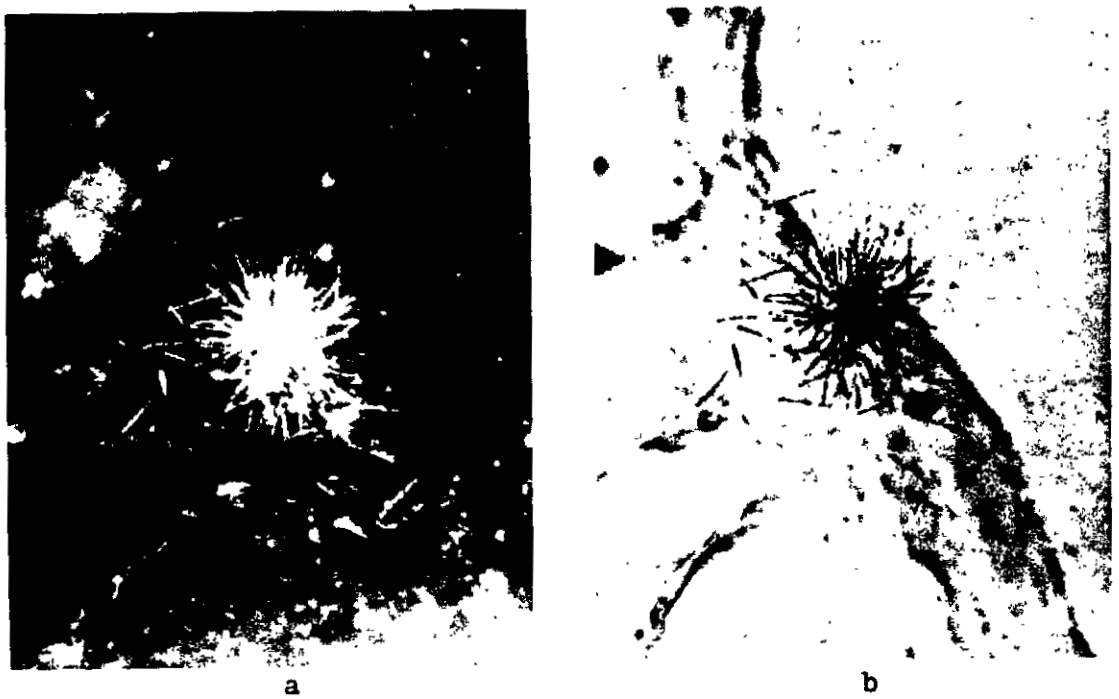

a b

Figure 2.8. Tracks From a Pure α Emitting Particle Found in Lung of Ewe No. 4 Exposed at 2500 Feet During the Underground Test; a, Dark Field Illimination; b, the Same Track in Bright Field, 430 X

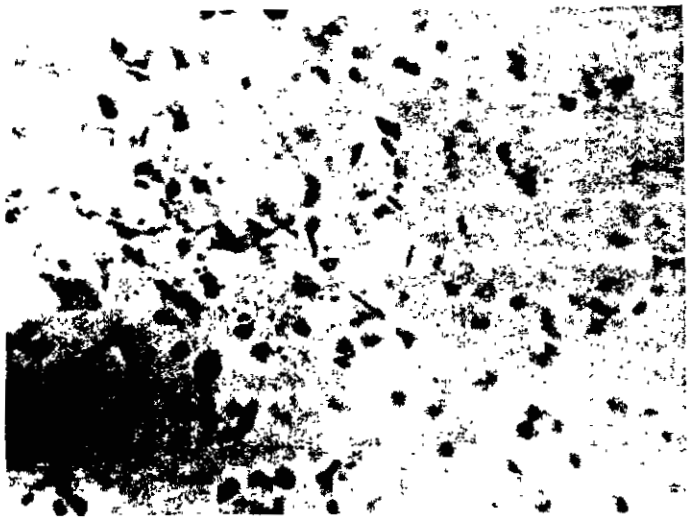

Figure 2.9. Tracks and Grains from a Mixed α and β Emitting Particle Found in Lungs of Dog No. 17, Exposed at 8000 Feet During the Underground Test, 430 X

The third type of particle found much more frequently in lung sections, is illustrated in Figure 2.10. The concentrations of grains were caused by pure β particle emission from sources which may differ in magnitude energy or half-life. The concentration of grains shown in Figure 2.10-b originate from a source which was either nearly spent by the time the preparation was made or which contained much less activity than was contained in the particle whose grain concentration is illustrated in Figure 2.10-c and d. In 107 lung tissue sections examined evidence of this third type of particle was encountered 55 times in the underlying emulsion.

Since careful study of autoradiographs was unrewarding generally even in the face of the fact that the lung tissue contained the largest amount of activity per gram when assayed by counting techniques, some explanation was sought for the discrepancy. Examination of lymph nodes, alveolar spaces and lung tissue revealed accumulations of debris containing crystalline particles 2 μ and less in diameter which could not be attributed to technique and which did not blacken the underlying silver grains. Particulate material of this sort must have been inhaled and must be either (1) particles which were no longer sufficiently active to produce a detectable image on the film or (2) those which had never carried radioactive components. It seems possible to explain the absence of a larger number of highly active particles in lung and lymph node radioagraphs on the basis of the following considerations. During an early phase following the detonation nearly all the components of the bomb are in a gaseous state. Shortly thereafter, as the mass cools, molten matter takes up a share of the radioactive debris. Somewhat later more radioactive material condenses out on the mass of fines which are in the vicinity and thereupon come into a somewhat loose association with these substrate particles. Thus it is possible for a flake of mica or other mineral to carry on its surface loosely associated radioactive particles, perhaps of molecular dimensions. If such particles reach the alveoli, the finely divided radioactive components might become dissolved off in the body fluids and be redistributed, leaving the inert residue. Studies of air-born particles[1] show that over 90% of the activity resides in particles above 10 μ in diameter. Such particles would not reach the alveoli in healthy lungs although they could be taken into the gut by swallowing. These considerations are of importance in dealing with the overall inhalation hazard. In addition it is estimated that the cloud may have contained an amount of air borne inert crater material of the order of 10^{10} grams while the fission product content was of the order of 10^{3} grams.

If the type and condition of detonation were such as to raise either the total number or specific activity of the condensation-

1. Final report N.R.D.L. Project 2.5a-2.

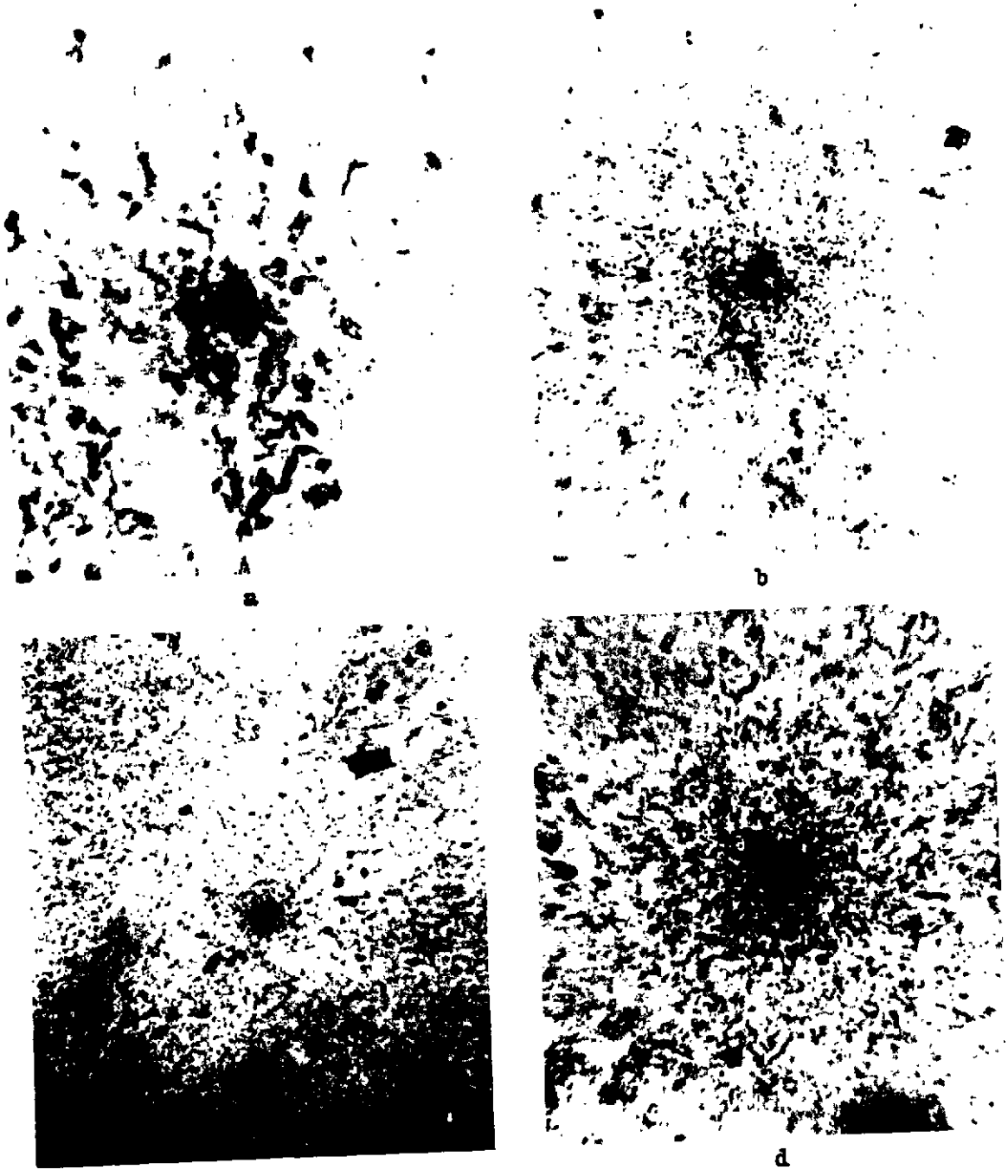

Figure 2.10. Autoradiograph Produced by a Pure β Emitting Particle in the Lung of Dog No. 7; a, Tissue Level; b, Emulsion at 10 μ Below Tissue, 430 X; c and d Autoradiograph Produced by β Emitting Particle in Lung of Dog No. 4, a-100 X, b-430 X

substrate type of particle between 8 μ and 0.5 μ in diameter, it is predicted that the inhalation hazard would increase. Condensation-substrate types of particles might be dealt with promptly by solution in the body fluids and thus result in a prompt redistribution of their radioactive components.

CHAPTER 3

DISCUSSION

Exposure of sheep and dogs during a surface or underground nuclear detonation was associated with the accumulation of a mixture of radioactive products within their bodies. The amount of such materials which may be taken up during an acute exposure is markedly dependent upon the concentration of radioactivity-bearing particles in the cloud and therefore the position of the animal during exposure. Wider distribution of airborne particles bearing radioactivity were associated with the underground shot than with the surface shot and the chances for the exposed animal to inhale contaminated materials were much greater at least up to 8000 feet from zero during the underground detonation.

Total activity in microcuries which theoretically could have been taken up in inhalation by an 8 kg dog (180 μc) during a 30 minute acute exposure and by a 45 kg sheep (900 μc) under identical conditions were 10 to 100 times the amounts which were found experimentally. This discrepancy results from the operation of several factors, among which the most important may be related to the concentration of the radioactivity in the inhaled debris during exposure. Differential fall-out data indicate that periods of high concentration of short duration occurred and therefore during 30 minutes the concentration of activity fluctuated. Experimental values for total activity given in Tables 2.10 - 2.11 do not include total activity within the gut.

Physiological response during the period of exposure might have been different from that postulated for a normal dog and sheep. No data are available relating to the respiratory response of an animal subjected to fluctuating concentrations of dust such as were prevalent during the underground test. It seems possible that the normal respiratory pattern would be greatly different under these conditions than when breathing normal air. Minor interruptions in the breathing response could effect appreciable changes in the total uptake during acute exposure. In the data presented it is felt that such factors as these could account for some of the variability.

Tissue sampling error and radio-assay may have resulted in calculations for total uptake that are too low. In defense of the method of tissue sampling employed it is pointed out that a more complete sampling per animal could only have been conducted at the cost of a reduction in the total number of animals exposed as well as reduction in sacrifice schedule. Radio-assay was carried on in the generally accepted manner and losses from the evolution of activity due to heating

the tissue samples to 500°C. could account for some of the indicated discrepancy. Generally, counting had to be conducted at near background levels due to the low activities.

Prediction of the biological effect of more powerful detonations than occurred in the surface and underground JANGLE tests may be made if due consideration is given to the assumptions and extrapolations which have been made in the results of the tests under discussion. A simple scaling factor cannot be found because of the complexity both of the respiratory process and the physical results of the detonation. The amount of earth moved into the air may be considered roughly proportional to the yield while the amount of residual activity will be closely proportional to the yield. If these assumptions are reasonable then the concentration in the cloud in microcuries per gram of particulate matter should not vary greatly with yield. The biological consequences of the higher yield detonation, aside from higher external radiation dose, will be due only to a larger cloud and the resultant increased exposure time. If it is assumed that the cloud diameter is proportional to the cube root of the yield a 20 fold increase would raise the inhaled activity by a factor of only 2.76.

In Tables 2.10 and 2.11 it was shown that the total radioactivity taken up averaged about 10 μc in dogs and 15 μc in sheep at the time of early sacrifice. If these values be raised to 15 μc and 20 μc respectively allowing a factor for error in sampling it remains that these quantities of material were retained in test animals during a 30 minute exposure. In the case of the higher yield detonation and assuming comparable conditions of exposure the inhaled activity in the average dog (8 kg.) would total about 41.4 μc while the sheep (45 Kg) might inhale as much as 55.2 μc. If the retention was comparable to that which prevailed in the JANGLE underground test this amount of radioactivity is estimated to correspond to about 0.9 rep (assuming an average of about 0.33 rep in the JANGLE test) while the dose to the lung tissue (assuming lung dosage to be about 3.62 rep in the JANGLE test) from inhaled materials would be of the order of 10 rep. The external dose, being correspondingly greater in the scaled test would be the dominant harard. The internal dose in the scaled test would be higher but insufficient to produce tissue damage over a short period of time. The possibility of a long delayed injury such as cancer resulting from a small amount of sharply localized irradiation from inhaled radioactive particles cannot be overlooked, although there are no data in the literature relating to such effects.

CHAPTER 4

CONCLUSIONS AND RECOMMENDATIONS

4.1 CONCLUSIONS

Biological injury resulting from a ~~1.2 KT~~ surface or underground nuclear detonation is predominantly due to total body external radiation. Sheep and dogs exposed at 2500, 5000 and 8000 feet from the zero points in both tests did not acquire by inhalation and ingestion physiologically significant quantities of radioactivity. Total internal dose due to the emission of β particles in animals exposed to the dust following the underground detonation was less than 1% of the external dose.

Estimates indicate that in the case of an underground detonation having a yield of 20 KT, the total internal activity in microcuries would be of the order of 2.76 times greater than in an underground detonation ~~having a yield of 1.2 KT, and therefore would give an internal dose of about 0.9 rep~~. However, the external radiation dose produced by contaminating detonations of the type in Operation JANGLE is overwhelmingly more important biologically up to 8000 feet from the zero point than the internal dose resulting from inhalation and ingestion of residual activity.

4.2 RECOMMENDATIONS

Long term survival studies on dogs or other large animals which have been exposed to the dust cloud following a contaminating detonation are required in order to evaluate the inhalation effects more completely. Repeated analyses of blood and urine during a long post-exposure period are necessary. Animals sacrificed after 12 to 24 months after exposure should be examined for evidence of pathology especially to lung, kidney and gut tissues.

Considerably more data are required on the early internal distribution of the inhaled and ingested radioactive mixture, which, when compared with radiochemical analyses of the contamination in specific organs will add greatly to an evaluation of the biological effects to be anticipated.

Additional experiments should be conducted in such a way as to permit an evaluation of the inhalation hazard independently from the external dose, since the latter may influence the degree of physiological response to inhaled radioactive contamination. Furthermore a clear separation of the contribution of the contamination in gut contents to

the total internal dose is needed.

In order to evaluate accurately the biological injury resulting from the inhalation of mixtures of fission products under the conditions existing in the JANGLE tests additional studies are needed in which activity and particle size measurements are closely correlated with biological data. These studies are particularly important for particles in the size range of 0.5 μ to 8 μ.

APPENDIX A

TEST ANIMALS, EXPOSURE PROCEDURES AND AUTOPSY PROCEDURES

A.1 TEST ANIMALS

Sheep and dogs were selected as test animals during the JANGLE tests. Mongrel dogs of both sexes, approximately 1 year old were procured from a dealer at Bethesda, Maryland. Each was vaccinated against distemper, treated for ectoparasites and held in the laboratory for observation for about 10 weeks prior to the tests. The animals were healthy and apparently free of pulmonary disease prior to exposure. Attempts to have several pregnant female dogs in time for the test failed. Only one dog, No. 12, was pregnant at the time of exposure and since she was exposed during the surface test little could be learned about the uptake of activity by the fetus. Range in weight of the dogs at the time of exposure are shown in text Table 2.6.

Three puppies ranging in age from 3 to 8 weeks were exposed during each test in an attempt to compare the total internal activity with that of adult dogs. The results of this experiment are discussed in the text.

Two-year old ewes were purchased from a dealer in Utah. At least 20 of the 25 which were procured were apparently pure Suffolk while 2 appeared to be Rambouillet and 3 Suffolk crossed with Rambouillet. It turned out that many of the ewes were pregnant upon arrival and this was turned to advantage in obtaining data upon the uptake of activity by the fetal and maternal tissues. The range in weights of the sheep at the time of exposure as well as estimated length of pregnancy are given in Table 2.7.

A.2 ANIMAL EXPOSURE PROCEDURES

Three types of cages were developed for use in both the surface and underground test. The first type of cage, designed for use with dogs at 2500 foot arc is illustrated in Figure A.1. This type of cage consisted simply of a pair of wood "A" frames securely joined and braced. The bottom of the wire cage was at 30 inches above the ground and the top at 4 feet. Entrance was secured through a wire screen flap at the rear of the cage. Two by 4 inch by 6 foot base plates were secured at the ground by 30 inch steel stakes. A system of guy wires arranged as shown in the illustration guaranteed that the cage would not give way in the blast. A large safety factor was obtained with this arrangement because no blast effects could be found at any animal station. In some cases, cages placed at 2500 feet from under-

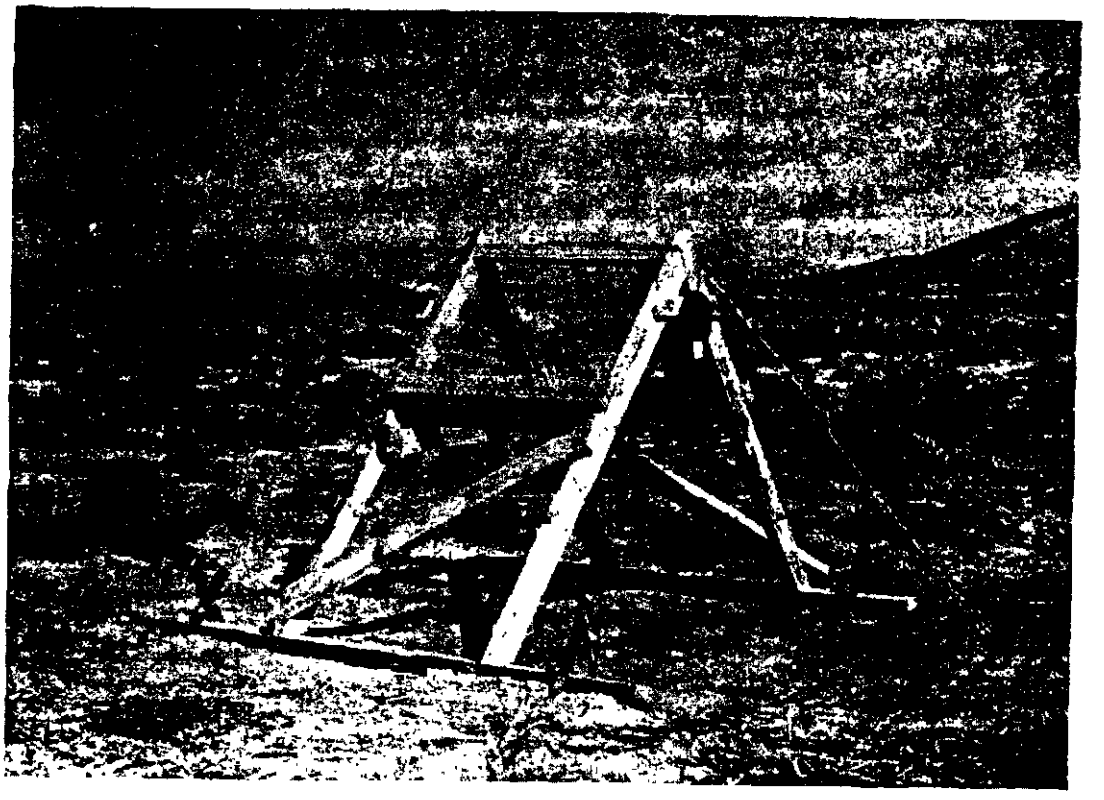

Figure A.1. Dog Exposure Cage As Used at 2500 Feet From Ground Zero in Both the Surface and Underground Tests

ground zero were not staked to the ground yet no evidence of blast effect could be found at the time of recovery. The second type of cage, used for dogs along the 5000 and 8000 foot arcs, consisted of braced wood "A" frames supporting the wire mesh cage at 30 inches off the ground level. Entrance to the cage was gained through a hinged door at one side.

Cages for sheep as shown in Figure A.2 were made from wood frames covered with screen wire and were 4 feet long, 28 inches wide and 30 inches high. A door at one end allowed access to the cage. Steel stakes and guys were used to secure the cage to the ground.

Modifications were made in the standard plywood lined foxholes in order to accommodate the animals. Figure A.3 illustrates the standard 2 by 4 by 6 foot foxholes with a ewe in place. Screen ends and top were added to the foxholes in order to prevent predators from entering as well as to reduce the amount of space in which the test animals could move about.

Prior to their being placed at their exposure stations, each animal was fitted with a harness made from 3/8 inch manila line. This

provided a useful sling with which to handle the animals in loading. In addition each animal was fitted with a blanket made from unbleached muslin. The purpose of the latter was to protect the pelt from fallout as much as possible. The blankets were discarded at the time of the recovery of each animal. Each of the dogs was fitted with a wire muzzle in order to reduce the amount of ingested materials by preventing the dogs from licking themselves.

Test animals were distributed to their respective exposure stations as shown in Tables 2.1 through 2.4 at approximately H minus 8 hours for both tests. Total time during which the animals were in the forward area was about 12 hours for the surface test. Some of the animals (Tables 2.3 and 2.4) were recovered after 14 hours (H + 6) following the underground shot while the remaining animals were recovered at 26 hours (H + 24). Neither food nor water were furnished the test animals while they were at their exposure stations and those which were sacrificed during the first day after each test received no food between the time they were placed on test and their sacrifice.

A.3 AUTOPSY PROCEDURES

Both the ewes and the dogs were sacrificed by administering a lethal dose of phenobaribital sodium (50 mg per kg). The barbiturate

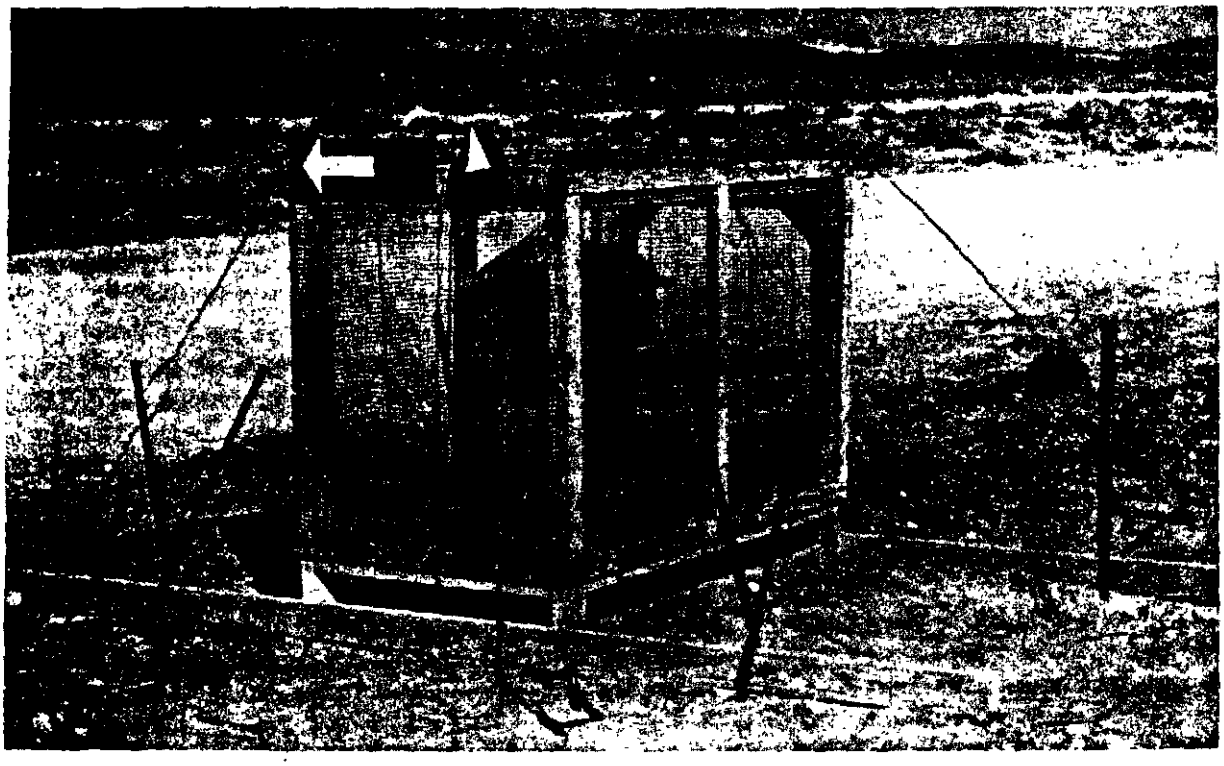

Figure A.2. Sheep Exposure Cage Used During the Surface and Underground Tests

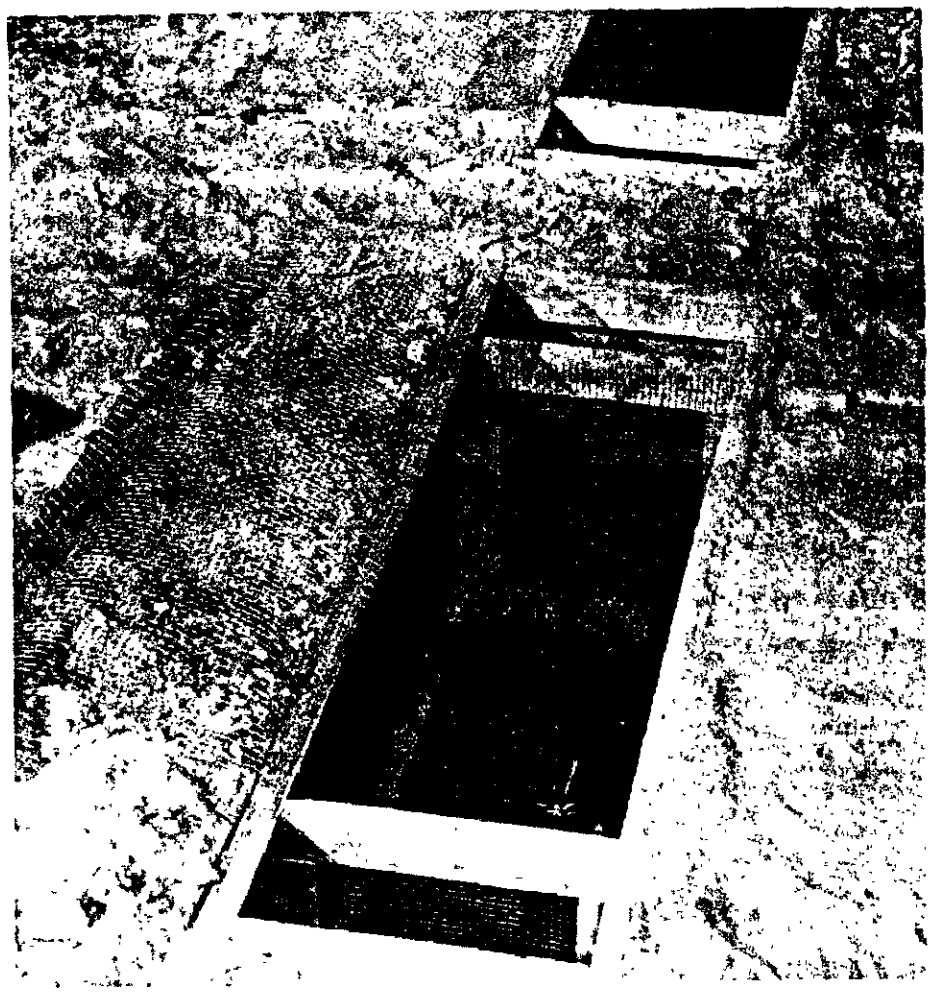

Figure A.3. Standard Foxholes Modified for Animal Exposures

was given intravenously and the dose proved to be very prompt in action. Upon the cessation of respiration a 5 ml blood sample was obtained and the animal was quickly exsanguinated. The autopsy followed immediately by opening the thorax and abdomen. Care was taken to avoid contaminating the underlying tissues with the pelt. The lungs were removed and dissected free of allied structures and weighed as promptly as possible. Several pulmonary lymph nodes were next obtained. Particular effort was made to remove the lymph nodes lying at the branching of the trachea. Other organs including the liver, spleen and kidneys were removed in turn and weighed. Wherever possible urine was taken as well as placental tissue and amniotic fluid. Fetuses were also taken when present. A portion of the femur was dissected free of musculature and allowed to dry for later study. When the autopsy was completed the carcasses were disposed of by burial under 4 feet of earth in a slit trench.

APPENDIX B

PREPARATION OF TISSUE SAMPLES FOR COUNTING AND AUTORADIOGRAPHY

B.1 PREPARATION OF TISSUE FOR COUNTING

Fresh pieces of tissue weighing from 0.5 gm to 1 gm were minced, placed in tared crucibles and heated to 500°C for 1 hour, in order to reduce their volume. Ashed tissues were removed from the crucibles by rinsing out with small quantities of absolute alcohol. Careful monitoring of the filtrate revealed no loss of activity to the alcohol. The ashed tissue was rinsed into specially constructed funnels provided with discs of filter paper upon which the tissue precipitated. Standardized planchets were made up from the charred samples and these were weighed in order to determine the quantity of material on each planchet. Bone samples were wet ashed with concentrated nitric acid.

B.2 CONSTRUCTION AND USE OF FREEZING-DEHYDRATION APPARATUS[1]

In preparing tissues for autoradiographs and pathological study it was felt that standard tissue techniques would not be reliable in the preparation of tissues suspected of containing contaminants. The strong possibility of displacement, solution and leaching during the course of preparation of sections by standard procedures gave rise to the design and application of the apparatus described here. Figure B.1 gives the specifications of the apparatus designed for use at the field laboratory.

In practice the tissue samples are quick frozen in the brass cups by immersion in a mixture of acetone and dry ice. Sufficient paraffin, to cover the piece of tissue is poured into the cup, allowed to solidify and fresh tissue added before the cup and tissue are placed in the chamber. The apparatus is then assembled and the vacuum pump[2] started. During the dehydration the inner thin walled chamber is maintained as near dry ice temperature as possible by means of a mixture of trichlorethylene and dry ice, while the plate on which the tissue cups are resting is maintained at -10°C. The latter is accomplished by placing the brass conducting legs in a dry ice alcohol mixture contained in 3 liter Dewar flask. Dehydration proceeds promptly because of the differential temperature between tissue and colder baffle; the short mean free path for the water molecules; leaving the tissue and

---

1. For details of a more elaborate apparatus and technique see Gersch, I, The Altman Technique for Fixation by Drying While Freezing. Anat. Rec. 53: 309, 1932.
2. Cenco-megavac capacity, 57 l/min.

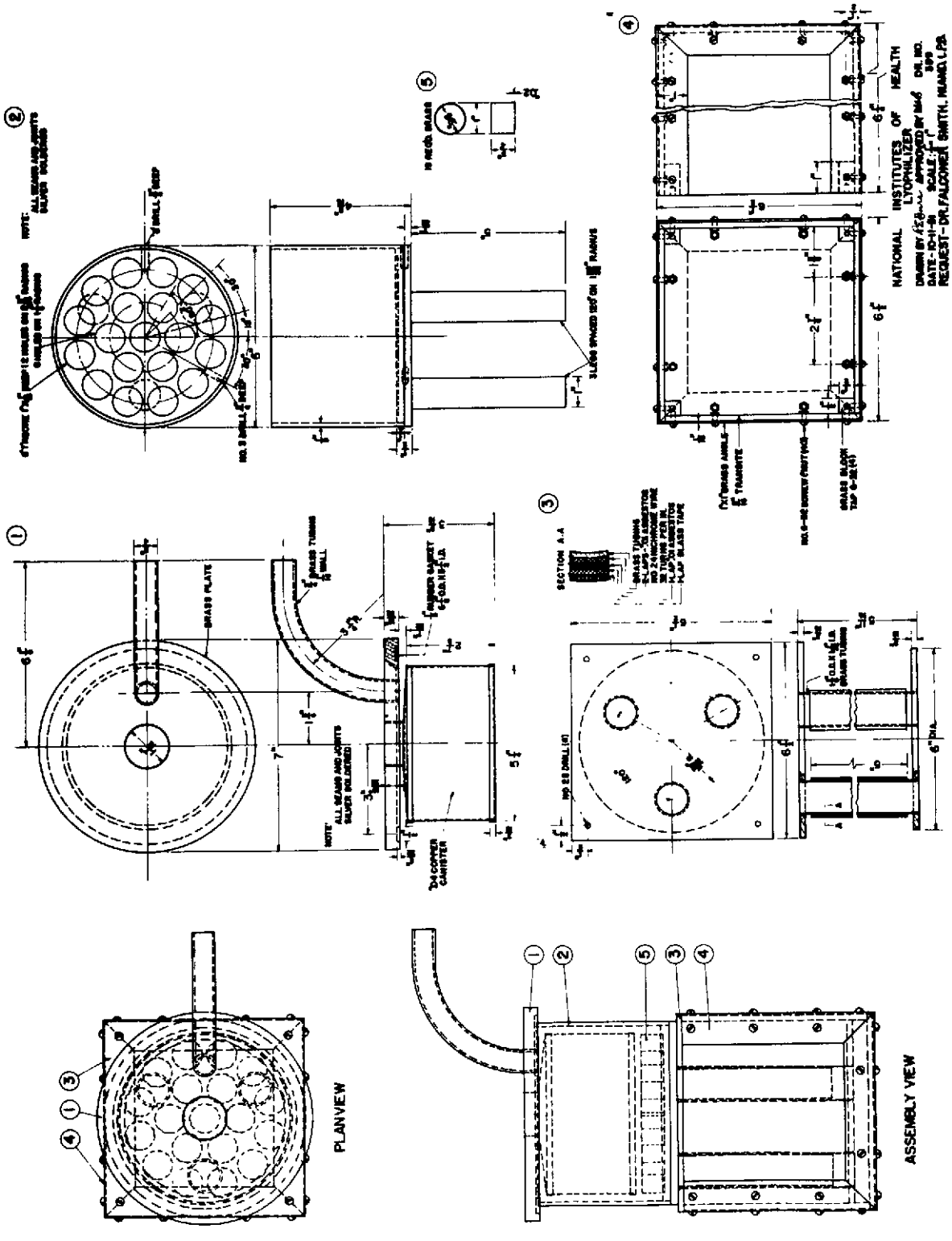

Figure B.1. Specifications of the Apparatus Designed to Fix and Embed Tissues by Means of a Freezing-dehydration Method

because of the continuous high vacuum in the dehydration chamber.

Experience has shown that under the above conditions even the most resistant tissues are thoroughly dehydrated in 6 hours. The infiltration and embedding is carried on by removing the apparatus from the alcohol-dry-ice bath and inserting the legs in a tube furnace (Figure B.1) and slowly bringing the temperature of the heavy brass plate to 70°C while continuing the high vacuum.

Well embedded paraffin blocks may thus be obtained about 8 hours from the time the fresh tissue is secured. Sections prepared from blocks made as described show excellent staining characteristics and minimal distortion. Tissue sections for pathological study were cut at 10 μ, stained with iron hematoxylin and counterstained with eosin. Autoradiographs were prepared from paraffin ribbons cut at 10 μ. Ribbons were floated directly on the emulsion out of warm absolute alcohol. After exposure the tissue sections were stained with metanil yellow and lightly counterstained with hematoxylin as described by Simmel. Autoradiographs were prepared at Bethesda where the possibility of extraneous radioactive contaminants was minimized.

APPENDIX C

Tabular Summary of Weather Data Pertinent to Animal Exposure During the Surface and Underground Tests

Date	Time	Temp. °C	Wind Direction	Wind Rate, mph
	Surface Test			
~~9 Nov.~~[a]	0930	2.78	Calm	
	1030	2.78	160	3.5
	1130	6.10	160	4.6
	1230	10.55	140	6.9
	1330	12.78	140	5.7
	1430	13.30	140	14.9
	Underground Test			
~~29 Nov.~~[b]	0530	-1.1	000	5
	0630	0	000	4
	0730	3.88	045	6
	0830	6.66	045	6
	0930	9.42	045	6
	1030	12.78	045	3
	1130	13.90	045	2
	1200	14.45	225	3
	1230	14.45 est.	225 est.	4 est.
~~30 Nov.~~[a]	0430	0	Calm	
	0830	2.78	Calm	
	1230	12.23	SE	6

a. Weather data from control point.
b. Observations made at underground zero.

PROJECT 2.7

BIBLIOGRAPHY

1. Van Wijk, A. M. and H. S. Patterson, "Percentage of Particles of Different Sizes Removed from Dust Laden Air by Breathing", Jour. Indust. Hyg. and Tox., XXII (1940), p. 31.

2. Hatch, T. F. and W. C. L. Hemian, "Influence of Particle Size in Dust Exposure", Jour. Indust. Hyg. and Tox., XXX (1948), p. 30.

3. Dygbert, H. P. et al. Pharmacology and Toxicology of Uranium Compounds, National Nuclear Energy Series IV (New York: McGraw Hill, 1949). Vol. I, p. 423.

4. Taplin, George V., et al. "Pulmonary Distribution of Radioactive Particles After Inhalation and Intravenous Injection", University of California School of Medicine. AEC Report 132 (1951).

5. Landahl, H. D., T. N. Tracewell, and W. H. Lassin, "On the Retention of Air-borne Particulates in the Human Lung". University of Chicago Tox. Lab. Quart. Prog. Report, 10 (1951), p. 61.

6. Morgan, Donald P., and Fred S. Grodins, "Regulation of Breathing During Electrically Induced Muscular Work in the Intact Anaesthetized Dog". Am. Jour. Physiol. CL XII (1950), p. 54.

7. Grodins, Fred S., Donald P. Morgan, "Regulation of Breathing During Electrically Induced Muscular Work in Anaesthetized Dogs Following Transection of the Spinal Cord". Am. Jour. Physiol., CLXII (1950), p. 54.

8. Comroe, J. H. Jr., and C. F. Schmidt, Am. Jour. Physiol., CXXXVIII (1943), p. 536.

9. Gardner, E. and J. Jacobs, Am. Jour. Physiol. CLIII (1948), p. 567.

10. Kibler, H. H. Personal communication. (1952).

11. Lee, Douglas H. K. Personal communication. (1952).

12. Brown, J. H., K. M. Cook, F. G. Ney and Theodore Hatch, "Influence of Particle Size Upon the Retention of Particulate Matter in Human Lung", Am. Jour. Public Health, XL (1950), p. 450.

13. Stokinger, H. E., H. B. Wilson, G. E. Sylvester and S. P. Dzuiba, "Lobar Partition of Inhaled U_3O_8 Particles," University of Rochester AEC Quarterly Technical Report, UR-127, 1950.

PROJECT 2.7

BIBLIOGRAPHY (Continued)

14. Dukes, H. H., The Physiology of Domestic Animals, Comstock Co., Ithaca, New York, (1943), p. 341.

15. Drinker, Phillip, et al., "Quantitative Measurements of the Inhalation, Retention and Exhaustion of Dusts and Fumes by Man". Jour. Ind. Hyg. and Toxicol., X (1928), p. 10.

16. Simmel, Eva B., Patrick J. Fitzgerald and John T. Godwin, "Staining of Radioautographs with Metanil Yellow and Iron Hematoxylin". Stain Technology XXVI (1951), p. 25.

DISTRIBUTION

	Copy No.
ARMY ACTIVITIES	
Asst. Chief of Staff, G-1, Department of the Army, Washington 25, D. C.	1
Asst. Chief of Staff, G-2, Department of the Army, Washington 25, D. C.	2
Asst. Chief of Staff, G-3, Department of the Army, Washington 25, D. C.	3- 6
Asst. Chief of Staff, G-4, Department of the Army, Washington 25, D. C.	7- 11
Chief of Ordnance, Department of the Army, Washington 25, D. C.	12- 14
Chief Chemical Officer, Temp. Bldg. T-7, Room G-522, Gravelly Point, Va.	15- 18
Chief of Engineers, Temp. Bldg. T-7, Room G-425, Gravelly Point, Va.	19- 21
The Quartermaster General, Second and T Sts. SW, Room 1139A, Washington 25, D. C.	22- 26
Chief of Transportation, Temp. Bldg, T-7, Room G-816, Gravelly Point, Va.	27- 28
Chief Signal Officer, Department of the Army, Washington 25, D. C.	29- 31
The Surgeon General, Main Navy Bldg., Room 1651, Washington 25, D. C.	32- 34
Provost Marshal General, Main Navy Bldg., Room 1065, Washington 25, D. C.	35- 37
Chief, Army Field Forces, Fort Monroe, Va.	38- 41
President, Army Field Forces Board No. 1, Fort Bragg, N. C.	42
President, Army Field Forces Board No. 2, Fort Knox, Ky.	43
President, Army Field Forces Board No. 3, Fort Benning, Ga.	44
President, Army Field Forces Board No. 4, Fort Bliss, Tex.	45
Commandant, The Infantry School, Fort Benning, Ga.	46- 47
Commandant, The Armored School, Fort Knox, Ky.	48- 49
President, The Artillery School Board, Fort Sill, Okla.	50- 51
Commandant, The AA&GM Branch, The Artillery School, Fort Bliss, Tex.	52- 53
Commandant, Army War College, Carlisle Barracks, Pa.	54- 55
Commandant, Command and General Staff College, Fort Leavenworth, Kans.	56- 57
Commandant, Army General School, Fort Riley, Kans.	58

DISTRIBUTION (Continued)

	Copy No.
Commanding General, First Army, Governor's Island, New York 4, N. Y.	59- 60
Commanding General, Second Army, Fort George G. Meade, Md.	61- 62
Commanding General, Third Army, Fort McPherson, Ga.	63- 64
Commanding General, Fourth Army, Fort Sam Houston, Tex.	65- 66
Commanding General, Fifth Army, 1660 E. Hyde Park Blvd., Chicago 15, Ill.	67- 68
Commanding General, Sixth Army, Presidio of San Francisco, Calif.	69- 70
Commander-in-Chief, European Command, APO 403, c/o Postmaster, New York, N. Y.	71- 72
Commander-in-Chief, Far East, APO 500, c/o Postmaster, San Francisco, Calif.	73- 74
Commanding General, U. S. Army, Pacific, APO 958, c/o Postmaster, San Francisco, Calif.	75- 76
Commanding General, U. S. Army, Caribbean, APO 834, c/o Postmaster, New Orleans, La.	77- 78
Commanding General, U. S. Army, Alaska, APO 942, c/o Postmaster, Seattle, Wash.	79- 80
Director, Operations Research Office, 6410 Connecticut Ave., Chevy Chase, Md.	81- 83
Commanding Officer, Ballistic Research Laboratories, Aberdeen Proving Ground, Aberdeen, Md.	84- 85
Commanding Officer, Engineer Research and Development Laboratory, Fort Belvoir, Va.	86- 87
Commanding Officer, Signal Corps Engineering Laboratories, Fort Monmouth, N. J.	88- 89
Commanding Officer, Evans Signal Laboratory, Belmar, N. J.	90- 91
Commanding General, Army Chemical Center, Md. ATTN: Chemical and Radiological Laboratory	92- 93

NAVY ACTIVITIES

Chief of Naval Operations, Department of the Navy, Washington 25, D. C. ATTN: Op-36	94- 95
Chief, Bureau of Ships, Department of the Navy, Washington 25, D. C.	96- 99
Chief, Bureau of Ordnance, Department of the Navy, Washington 25, D. C.	100
Chief, Bureau of Medicine and Surgery, Department of the Navy, Washington 25, D. C.	101-102
Chief, Bureau of Aeronautics, Department of the Navy, Washington 25, D. C.	103-104
Chief, Bureau of Supplies and Accounts, Department of the Navy, Washington 25, D. C.	105-106
Chief, Bureau of Yards and Docks, Department of the Navy, Washington 25, D. C.	107-109

DISTRIBUTION (Continued)

	Copy No.
Chief of Naval Personnel, Department of the Navy, Washington 25, D. C.	110
Commandant of the Marine Corps, Washington 25, D. C.	111-113
Commander-in-Chief, U. S. Pacific Fleet, Fleet Post Office, San Francisco, Calif.	114
Commander-in-Chief, U. S. Atlantic Fleet, Fleet Post Office, New York, N. Y.	115
President, U. S. Naval War College, Newport, R. I.	116
Commandant, Marine Corps Schools, Quantico, Va.	117-118
Chief of Naval Research, Department of the Navy, Washington 25, D. C.	119-120
Commander, U. S. Naval Ordnance Laboratory, Silver Spring 19, Md.	121
Commander, U. S. Naval Ordnance Laboratory, Silver Spring 19, Md. ATTN: Aliex	122
Director, U. S. Naval Research Laboratory, Washington 25, D. C.	123
Commanding Officer and Director, U. S. Naval Electronics Laboratory, San Diego 52, Calif.	124
Commanding Officer, U. S. Naval Radiological Defense Laboratory, San Francisco 24, Calif.	125-128
Commanding Officer and Director, David Taylor Model Basin, Washington 7, D. C.	129
Commander, Naval Material Laboratory, New York Naval Shipyard, Naval Base, New York 1, N. Y.	130
Officer-in-Charge, U. S. Naval Civil Engineering Research and Evaluation Laboratory, U. S. Naval Construction Battalion Center, Port Hueneme, Calif.	131-132
Commanding Officer, U. S. Naval Medical Research Institute, National Naval Medical Center, Bethesda 14, Md.	133
Commander, U. S. Naval Ordnance Test Station, Inyokern, China Lake, Calif.	134

AIR FORCE ACTIVITIES

Assistant for Atomic Energy, Headquarters, United States Air Force, Washington 25, D. C.	135-136
Director of Operations, Headquarters, United States Air Force, Washington 25, D. C. ATTN: Operations Analysis Division	137-138
Director of Plans, Headquarters, United States Air Force, Washington 25, D. C. ATTN: AFOPD-P1	139
Director of Requirements, Headquarters, United States Air Force, Washington 25, D. C.	140
Director of Research and Development, Headquarters, United States Air Force, Washington 25, D. C.	141-142
Director of Intelligence, Headquarters, United States Air Force, Washington 25, D. C. ATTN: Phys. Vul. Branch, Air Targets Division	143-144

DISTRIBUTION (Continued)

	Copy No.
Director of Installations, Headquarters, United States Air Force, Washington 25, D. C.	145
Asst. for Development Planning, Headquarters, United States Air Force, Washington 25, D. C.	146
Asst. for Materiel Program Control, Headquarters, United States Air Force, Washington 25, D. C.	147
The Surgeon General, Headquarters, United States Air Force, Washington 25, D. C.	148
Commanding General, Strategic Air Command, Offutt Air Force Base, Nebr.	149-151
Commanding General, Air Research and Development Command, P.O. Box 1395, Baltimore 3, Md.	152-161
Commanding General, Air Materiel Command, Wright-Patterson Air Force Base, Dayton, Ohio	162-163
Commanding General, Air Materiel Command, Wright-Patterson Air Force Base, Dayton, Ohio. ATTN: Air Installations Division	164-165
Commanding General, Tactical Air Command, Langley Air Force Base, Va.	166-168
Commanding General, Air Defense Command, Ent Air Force Base, Colo.	169-171
Commanding General, Air Proving Ground, Eglin Air Force Base, Fla.	172-173
Commanding General, Air Training Command, Scott Air Force Base, Belleville, Ill.	174-176
Commanding General, Air University, Maxwell Air Force Base, Montgomery, Ala.	177-179
Commanding General, Special Weapons Center, Kirtland Air Force Base, N. Mex.	180-182
Commanding General, 1009th Special Weapons Squadron, 1712 G St. NW, Washington 25, D. C.	183
Commanding General, Wright Air Development Center, Wright-Patterson Air Force Base, Dayton, Ohio	184-187
Commanding General, Air Force Cambridge Research Center, 230 Albany St., Cambridge 39, Mass.	188-189
Commanding General, U. S. Air Forces in Europe, APO 633, c/o Postmaster, New York, N. Y.	190-191
Commanding General, Far East Air Forces, APO 925, c/o Postmaster, San Francisco, Calif.	192-193
Commanding General, Air Force Missile Center, Patrick Air Force Base, Cocoa, Fla.	194
Commandant, USAF School of Aviation Medicine, Randolph Air Force Base, Randolph Field, Tex.	195
Asst. to the Special Asst., Chief of Staff, United States Air Force, Washington 25, D. C. ATTN: David T. Griggs	196
The RAND Corporation, 1500 Fourth St., Santa Monica, Calif.	197-198

DISTRIBUTION (Continued)

No. | Copy No.

AFSWP ACTIVITIES

5 | Chief, Armed Forces Special Weapons Project, P.O. Box 2610, Washington 13, D. C. — 199-207
5 | Commanding General, Field Command, Armed Forces Special Weapons Project, P.O. Box 5100, Albuquerque, N. Mex. — 208-213

OTHER ACTIVITIES

Chairman, Research and Development Board, Department of Defense, Washington 25, D. C. — 214
Director, Weapons System Evaluations Group, Office of the Secretary of Defense, Washington 25, D. C. — 215
Executive Director, Committee on Atomic Energy, Research and Development Board, Department of Defense, Washington 25, D. C. ATTN: David Beckler — 216
Executive Director, Committee on Medical Sciences, Research and Development Board, Department of Defense, Washington 25, D. C. — 217
U. S. Atomic Energy Commission, Classified Document Room, 1901 Constitution Ave., Washington 25, D. C. ATTN: Mrs. J. M. O'Leary — 218-220
Los Alamos Scientific Laboratory, Report Library, P.O. Box 1663, Los Alamos, N. Mex. ATTN: Helen Challenger — 221-223
Sandia Corporation, Classified Document Division, Sandia Base, Albuquerque, N. Mex. ATTN: Wynne K. Cox — 224-243

AEC, Oak Ridge, Tenn., A31930